2015

Studies on the Maturation of Secreted Quorum Sensing Peptides That Regulates S. Aureus Virulence

Jeffrey Grant Johnson

STUDIES ON THE MATURATION OF SECRETED QUORUM SENSING PEPTIDES THAT REGULATE *S. AUREUS* VIRULENCE

A Thesis Presented to the Faculty of

The Rockefeller University

in Partial Fulfillment of the Requirements for

the degree of Doctor of Philosophy

by

Jeffrey Grant Johnson

June 2015

STUDIES ON THE MATURATION OF SECRETED QUORUM SENSING PEPTIDES THAT REGULATE *S. AUREUS* VIRULENCE

Jeffrey Grant Johnson, Ph.D.

The Rockefeller University 2015

The *accessory gene regulator* (*agr)* locus in the commensal human pathogen, *Staphylococcus aureus,* is a two-promoter operon with allelic variability that encodes a quorum sensing circuit involved in regulating virulence in the bacterium. Secretion of unique autoinducing peptides (AIPs) and detection of their concentration via AgrC, a transmembrane receptor histidine kinase, coordinates local bacterial population density with global changes in gene expression. In order for *S. aureus* to produce AIP, three proteolytic transformations involving the proteins AgrB and SpsB are required. However, despite our current understanding of AIP peptide processing, the actual manner in which the AIP crosses the cellular membrane, and specifically the role of AgrB in this process, has not been examined. Neither is it clear whether SpsB cleaves all four variants of the AgrD precursor peptide. Initially, the aims of this thesis were to: 1) determine the role of AgrB in secreting the AgrD(1-32)-thiolactone and 2) confirm that SpsB is the protease responsible for the final cleavage step of AgrD in AIP biosynthesis. To achieve these goals, an *in vivo* secretion assay using intein chemistry to produce AIP in the absence of AgrB was developed to examine whether AgrB facilitates AIP secretion. Also, SpsB biochemical assays were used to provide a thorough investigation of the final cleavage step in AIP biosynthesis for AgrD-I and AgrD-II. The findings of this work indicate that AgrB does not facilitate secretion, and SpsB can only cleave AgrD-I correctly but not AgrD-II. Taken together, these observations suggest that AgrB and SpsB are two proteins

associated with AIP biosynthesis, but there are likely other proteins that need to be identified. The final aim of this work was to investigate the effect of AIP macrocycle size on AgrC activation. Since staphylococcal virulence can be inhibited through antagonism of its quorum sensing system, there has been tremendous interest in understanding the structure-activity relationships underlying the AIP-AgrC interaction. The defining structural feature of the AIP is a 16-membered, thiolactone-containing macrocycle. However, the importance of ring size on *agr* activation or inhibition has not been explored. This deficiency is addressed through the synthesis and functional analysis of AIP analogs featuring enlarged and reduced macrocycles. This study is the first to interrogate AIP function using both established cell-based reporter gene assays and newly developed *in vitro* AgrC-I binding and autophosphorylation activity assays. Based on our data, we present a model for robust *agr* activation involving a cooperative, 3-points-of-contact interaction between the AIP macrocycle and AgrC.

Acknowledgements

I owe a great amount of gratitude to my mentors, Tom Muir and Richard Novick. Richard was very helpful, as I started working with *S. aureus* cells, and he was always willing to advise and guide me when I needed it. To Tom, I am grateful that he took a chance on a 3-week TPCB rotation student in January of 2009. He was always quick to give advice when sought but patient enough to let me develop my own ideas in pursuing scientific knowledge. I am a better scientist because of his guidance.

I appreciate the many labmates and collaborators who helped me along the way to this accomplishment: Beth George Cisar guided me as I took on an *agr* project. Boyuan Wang was a great member of Team *agr* and provided many important tools for this study. Aishan Zhao was always willing to help when asked. Connie Wang was a Princeton student researcher, who I enjoyed mentoring. It was great to help with her thesis. Hope Ross of the Novick lab was a great resource for all things related to *S. aureus*. Galia Debelouchina was very helpful in running and analyzing my NMR spectra.

Besides those that helped with this work, there are many labmates who were helpful and great scientists. Miquel Vila-Perello and Peter Moyle are great scientists who tried to teach me all they knew about peptide synthesis and protein expression. Neel Shah was an amazing grad student and always willing to answer a question. Rob Oslund, Glen Liszczak, and Uyen Nguyen provided great suggestions and support in the lab. Lenka Bittova deserves many thanks for managing the lab and making sure that equipment was always working. To all the other members of the Muir lab, many thanks for your generosity and help. Thanks for making the lab a great workplace.

I thank my committee members, Sean Brady, Erec Stebbins, and Vincent Fischetti of Rockefeller University and Frederick Maxfield of Weill Medical College-Cornell University, for their advice and perspective throughout the development of this project. I also thank Martin Semmelhack of Princeton University for joining my thesis defense.

I am grateful to have been part of the outstanding Tri-institutional Training Program in Chemical Biology, which provided the opportunity to pursue a Ph.D.

However, the greatest acknowledgement needs to go to my family, starting with my parents, Randy and DiAnn Johnson. They are not college graduates, but that did not stop them from instilling in me a desire to learn and gain knowledge from my youth. I know that they take great pride in this accomplishment, if not more than I do. Thanks, mom and dad! I want to thank my brothers, Jared and Jacob, and their families for their support and love.

Finally, to my wife, Malorie, thank you for all your support and understanding through this challenging and enlightening process. It's a good thing the Muir lab moved to Princeton. Otherwise, we may never have met, and I would be much worse off if that were the case.

Table of Contents

List of Figures

List of Tables

List of Abbreviations

agr	accessory gene regulator
AgrA	*agr* protein A, TCS response regulator
AgrB	*agr* protein B, cysteinyl membrane peptidase
AgrC	*agr* protein C, TCS membrane receptor histidine kinase
AgrD	*agr* protein D, AIP propeptide
AIP	autoinducing peptide
Boc	tert-butoxycarbonyl
CA	catalytically active kinase subdomain of the HK domain
CI	confidence interval
DDM	*n*-Dodecyl β-D-maltoside
DHp	dimerization/phosporylation site subdomain of the HK domain
DIPEA	diisopropylethylamine
DMF	N, N-dimethylformamide
DMSO	dimethyl sulfoxide
EC_{50}	half maximal effective concentration
EPL	expressed protein ligation
FLAG	a polypeptide protein tag with the sequence DYKDDDDK
fl-SpsB	His_5-tagged full-length SpsB
Fmoc	9-fluorenylmethoxycarbonyl
HBTU	2-(1H-Benzotriazole-1-yl)-1,1,3,3-tetramethyluronium Hexafluorophosphate
hβ-AA	L-β-homo-amino acid
HF	hydrogen fluoride
HK	histidine kinase domain
HPK	histidine protein kinase
HPLC	high pressure liquid chromatography
IC_{50}	half maximal inhibitory concentration
MAD	membrane association domain of AgrC
MRSA	methicillin-resistant *S. aureus*
MS	mass spectrometry
NMR	nuclear magnetic resonance spectroscopy
PSM	phenol-soluble modulin
SDS-PAGE	sodium dodecyl–protein acrylamide gel electrophoresis
SEM	standard error measurement
SID	secretion inhibition domain of AgrD
SpsB	type I signal peptidase of *S. aureus*
TCS	two-component system
TFA	trifluoroacetic acid
tr-SpsB	His_6-tagged SpsB Δ1-21 deletion mutant

Chapter 1. Introduction

1.1 Regulation of Virulence in *Staphylococcus aureus*

1.1.1 Emergence of Antibiotic-Resistant Strains of *S. aureus*

Staphylococcus aureus is part of the commensal microbial flora of ~30% of the adult population. In spite of its normal, beneficial nature, *S. aureus* is an opportunistic pathogen and a major health threat worldwide when it is capable of invading mucous membranes or soft tissue.[1] Once invasion occurs, the bacterium is a remarkable, dynamic pathogen that is known to cause both acute and chronic illnesses such as bacteremia, sepsis, endocarditis and toxic shock syndrome.[2, 3] Although the immune system and treatment with antibiotics can clear these infections, there are several risk factors that include a weakened immune system, surgery, and/or implanted medical devices that can lead to fatal infections.[4] Noticeably, these risk factors often persist in a hospital environment, and virulent *S. aureus* strains can thrive in hospitals, where vulnerable patients being treated for an unrelated problem may become infected with a commensal strain or with a strain spread in the hospital.[5] Such infections have only become more lethal with the emergence of antibiotic resistant strains of *S. aureus* (e.g. MRSA and VRSA). In 2005, there were over 278,000 MRSA-related hospitalizations, and estimates place MRSA-related deaths of at least 18,000 per year in the United States, which is nearly as many deaths as AIDS, tuberculosis and viral hepatitis combined.[6, 7]

Researchers have been trying to understand the emergence of antibiotic resistant *S. aureus* strains starting with penicillin resistance in the 1940s.[8, 9] As these new resistant strains emerged, new antibiotics were used to combat infections, resulting in several

waves of antibiotic resistant strains of *S. aureus*.[3] Methicillin, the first semisynthetic penicillin (Figure 1), was introduced in October 1960 and within 6 months the first methicillin-resistant *S. aureus* (MRSA) strains had been isolated.[6, 10] Between 1998 and 2007, hospital-acquired MRSA (HA-MRSA) infections increased from 3.2 hospital discharges to 4.8 discharges per 1000.[11] While this increase was statistically significant, even more significant was the increase in community-acquired MRSA (CA-MRSA) infections. During the same time period, CA-MRSA infections increased from 0.4 hospital discharges to 3.3 discharges per 1000—an 8-fold increase. Alarmingly by 2007, CA-MRSA infections accounted for 82% of all MRSA infections in children under the age of fifteen.[11] The threat of MRSA infections has, thus, left the hospital.[12, 13]

During this 4-decade evolution of MRSA infections, *S. aureus* was also under another selective pressure from vancomycin—one of the antibiotics of last resort for Gram-positive bacteria (Figure 1). By the late 1990s, the first vancomycin intermediate-resistant *S. aureus* (VISA) strains were isolated in Japan, and the first vancomycin-resistant *S. aureus* (VRSA) strain was isolated in the United States in 2002.[3, 14-17] Uncompromisingly fueled by its need for survival, this tiny organism continues to expand its arsenal and defense to dominate in a chemical war between host and pathogen. To combat the pervasive, pathogenic potential of this bacterium, research efforts to further understand *S. aureus* virulence and pathogenesis are essential.

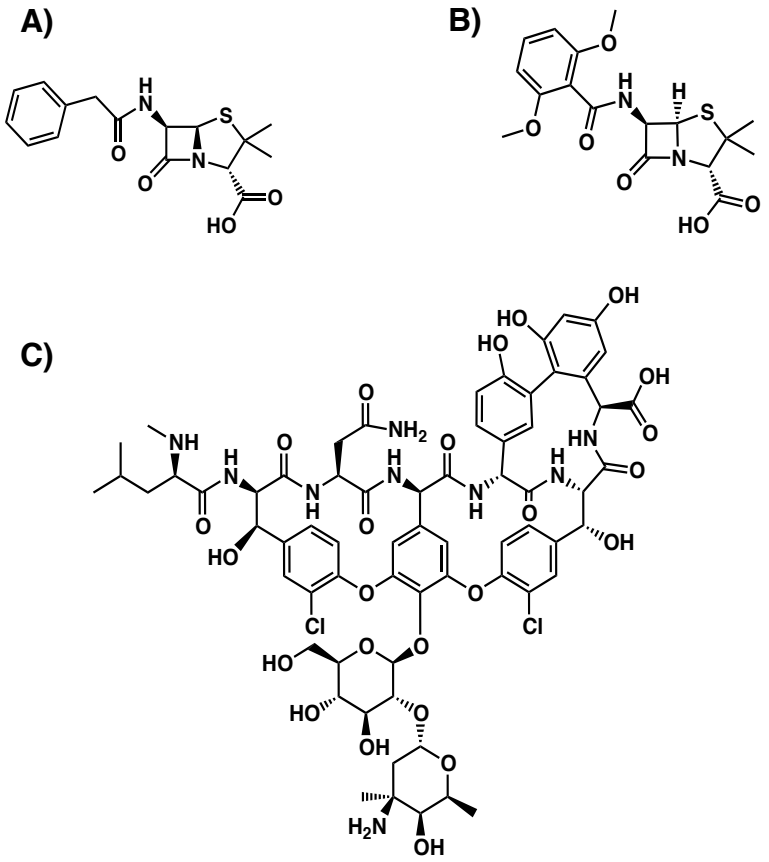

Figure 1. Chemical Structures of Several Antibiotics Used to Treat *S. aureus* Infections

A) Penicillin G or benzylpenicillin is one of the more common penicillin antibiotics. B) Methicillin is a derivative of pencillin, but it is a penicillinase-resistant β-lactam antibiotic. C) Vancomycin belongs to the glycopeptide class of antibiotics. All three of these antibiotics inhibit cell wall synthesis.[18, 19]

1.1.2 A Quorum Sensing Circuit Coordinates Virulence in *S. aureus*

In bacteria, extracellular small-molecules play a major role in cell-cell communication, which involves the production, release, and community-wide detection of such small molecules. Quorum sensing (QS) is one form of cell-cell communication that allows a bacterial strain to monitor its own population and to adjust gene expression according to bacterial population changes.[20, 21] In a QS circuit, a signaling molecule—an autoinducer—is constitutively secreted in proportion to bacterial population density. Once a threshold autoinducer concentration is achieved, the target receptor is activated resulting in a specific, coordinated response through targeted gene transcription and expression. Thus, activation of energetically demanding processes is limited to instances in which there are enough bacteria present to elicit the desired effect. Synchronized behaviors regulated by QS circuits include bioluminescence, sporulation, conjugation, pigment production, biofilm formation and production of virulence factors.[20, 22, 23] There are two general types of QS systems in bacteria: LuxIR circuits in Gram-negative bacteria and oligopeptide two-component circuits in Gram-positive bacteria. In the LuxIR circuit, the LuxI-type enzyme catalyzes the formation of a specific acyl-homoserine lactone (AHL) autoinducer that freely diffuses in and out of a cell. The LuxR-type proteins bind a specific AHL autoinducer once it reaches a threshold concentration.[24] In Gram-positive bacteria, the autoinducers are short peptides called autoinducing peptides (AIPs) that are typically detected by a classical histidine kinase two-component signaling (TCS) system.[21, 23]

In the Gram-positive bacterium, *S. aureus*, the *accessory gene regulator* (*agr*) locus encodes a quorum sensing circuit that includes a canonical TCS system.[25] In general, TCS systems are ubiquitous in bacteria, allowing them to sense and react to a variety of stimuli, including osmolarity, pH, oxygen, chemoattractants, and autoinducers.[26] Each TCS is typically composed of a receptor histidine protein kinase (HPK) that senses the signal and a response regulator (RR) transcription factor that modulates gene expression. The HPK receptor typically forms a dimer, and each receptor protomer consists of a sensory domain and an histidine kinase (HK) domain, which is further divided into two subdomains: 1) an α-helical coiled-coil region containing the dimerization interface and histidine phosphorylation site (DHp) and 2) the catalytic kinase domain (CA).[27-29] Stimulus detection by the HPK sensory domain triggers activation of the HK domain, resulting in trans-autophosphorylation of the contralateral histidine and then phosphoryl-group transfer to a conserved aspartate in the TCS-associated RR.

As part of the *agr* locus encoded QS system, there is also an AIP autoinducer that helps coordinate virulence factor production.[25, 30, 31] *S. aureus* has a diverse arsenal of virulence factors by which it evades the host immune system and then becomes very toxic in the correct host environment. The two main classes of virulence factors are associated with different phases of population growth in *S. aureus* (Figure 2).[2] During the lag and exponential phases, virulent *S. aureus* cells produce cell wall-associated factors that facilitate tissue attachment and evasion of the host immune system, allowing the bacteria to accumulate and possibly form a biofilm.[21] For example, microbial surface

components recognizing adhesive matrix molecules (MSCRAMMS) adhere to the extracellular matrix to give the bacteria an attachment point in the host. Protein A binds IgG antibodies to form a protective coat and evade the host immune system.[1, 2]

Once the *S. aureus* bacterial population size achieves the autoinducer threshold concentration, the cell wall-associated factors are down-regulated in late exponential phase and stationary phase, allowing for detachment from the original colonization site and possible establishment of an invasive infection.[32] At the same time, the bacterium secretes enzymes and toxins, termed exoproteins, to degrade host tissue and to promote spread of the infection. The degradative enzymes include proteases and hemolysins, which lyse red blood cells by creating pores in the cell membranes or by hydrolyzing membrane lipids. Enterotoxins are the causative agents of *S. aureus* food poisoning and contribute to toxic shock syndrome and other diseases by stimulating T-cells to produce proinflammatory cytokines in excessive amounts.[1, 2, 32] Such coordination of virulence factors is conserved not only in Staphylococci[33] but also within the phylum firmicutes[34] including pathogenic bacteria such as *Enterococcus faecalis*,[35] *Listeria monocytogenes*,[36] *Clostridium perfringens*,[37] and *Clostridium botulinum*[38] all showing identifiable AIP-like signals.

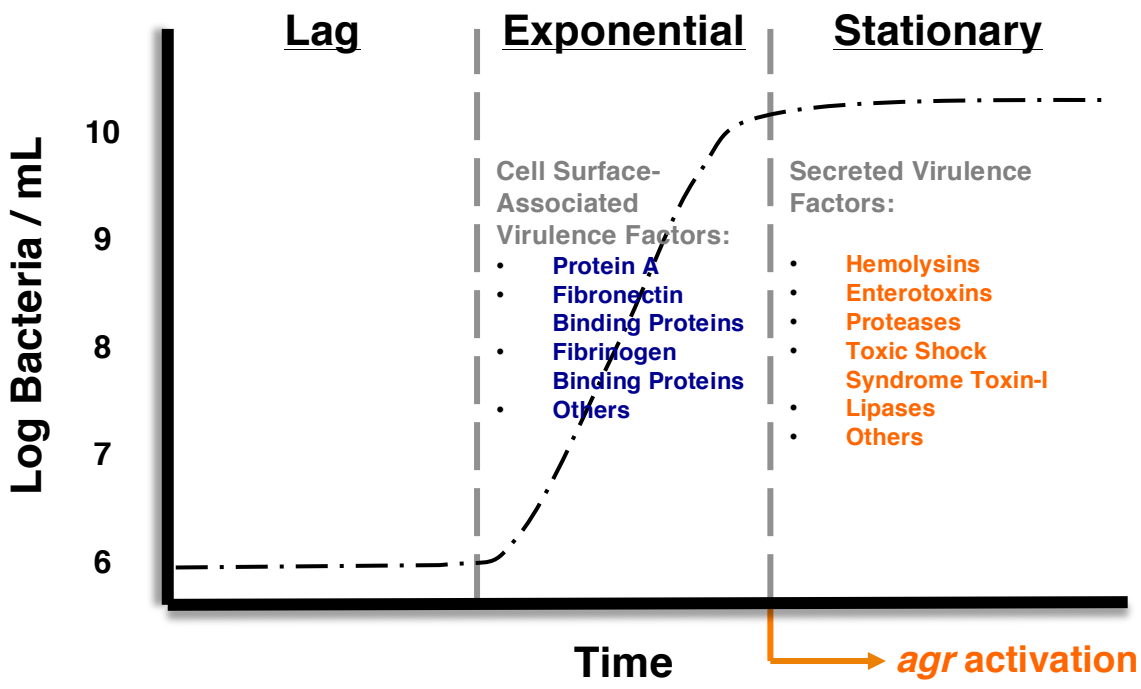

Figure 2. The Effect of *S. aureus* Population Growth on Virulence Factor Expression

Adapted from references 2 and 32. Cell surface-associated virulence factors are highly expressed during exponential growth in order to promote attachment to the host extracellular matrix and evade the host immune system. In stationary phase, the cell surface-associated virulence factors are down-regulated and expression of secreted exoproteins is induced to promote invasion of the host and impart toxicity.[1, 2, 32] Staphylococci monitor their increase in population density using the quorum sensing circuit encoded by *agr*, which regulates the transition between exponential and stationary growth phases and coordinates expression of the two classes of *S. aureus* virulence factors.[31]

While the *agr* locus is considered a global regulator of *S. aureus* virulence, it is only one of several genetic loci that produce a complex signaling network that coordinately regulate the staphylococcal virulon (Figure 3).[39-42] The *staphylococcal accessory regulator* (*sar*) and its relatives are important regulators of virulence that mediate many of their effects by influencing *agr* transcription: SarA, SarU and SarR up-regulate *agr* transcription. SarA and SarU are also repressed by SarR and SarT, which thereby indirectly down-regulate *agr* transcription. Some Sar family proteins regulate virulence factors independently of *agr*. In a variety of infection models, loss of function mutations in either *agr* or *sar* exhibit reduced virulence, and the virulence of double agr^- sar^- mutants is, in some models, further reduced.[43-47] The *mgrA* locus also appears to regulate *sar* transcription and thereby *agr* transcription.[48] It also up-regulates some efflux pumps and exoproteins in *S. aureus* among many other genes involved in virulence. Other important loci include *S. aureus exoprotein* expression (*sae*),[49] which may act downstream of *agr* to maintain hemolysin and coagulase expression;[50] *staphylococcal respiratory response* (*srr*), which is required for optimal growth in anaerobic conditions and inhibits *agr* output;[51] and *repressor of toxins* (*rot*), which counteracts many effects of *agr* but also induces expression of some exoproteins.[52-54] Because of this complex genetic network of virulence loci in *S. aureus*, it is still not precisely understood what role *agr* plays in initiating and establishing an infection.

The *agr* locus of *S. aureus* contains two divergent promoters, P2 and P3, of which the P2 transcript encodes a 4-gene operon, *agrBDCA*, whose gene products are four proteins involved in the biosynthesis (AgrB and D) and detection (AgrC and A) of the

AIP—the autoinducer of the *agr* QS system (Figure 4A).[21, 25, 55] For AIP biosynthesis, AgrD undergoes two proteolytic cleavage events: 1) AgrB cleaves off the C-terminus of AgrD and catalyzes the AIP thiolactone cyclization via an enzyme-mediated trans-thioesterification reaction,[56, 57] and 2) a signal peptidase cleaves AgrD near its newly-formed, cyclized C-terminus[58] to release the mature AIP into the surrounding, cellular environment, where it increases in concentration as bacterial growth continues. The four allelic AIPs expressed by *S. aureus* are 7-9 amino acid residues in length (Figure 4B). Structurally, they have 2-4 amino acid residues connected to a thiolactone macrocycle, which contains 5 amino acid residues and a thiolactone linkage formed by condensation of the sulfhydryl group of a conserved Cys residue and the a-carboxyl group.[45] Similar to other *staphylococci*, these AIPs also have at least two hydrophobic residues at their C-terminus.[59] AIP binding of AgrC, a membrane-bound receptor histidine kinase, results in the activation of a TCS system comprised of AgrA and AgrC. Upon AIP binding, AgrC dimers undergo autophosphorylation and then phosphoryl-group transfer to AgrA, the TCS response regulator.[21, 55] Phosphorylated AgrA binds and activates the P2 and P3 promoters completing a strong, positive feedback loop.[47] The P3 transcript encodes RNAIII, which encodes the δ-hemolysin toxin and is a regulatory RNA and effector molecule of *S. aureus* virulence factors.[25, 60]

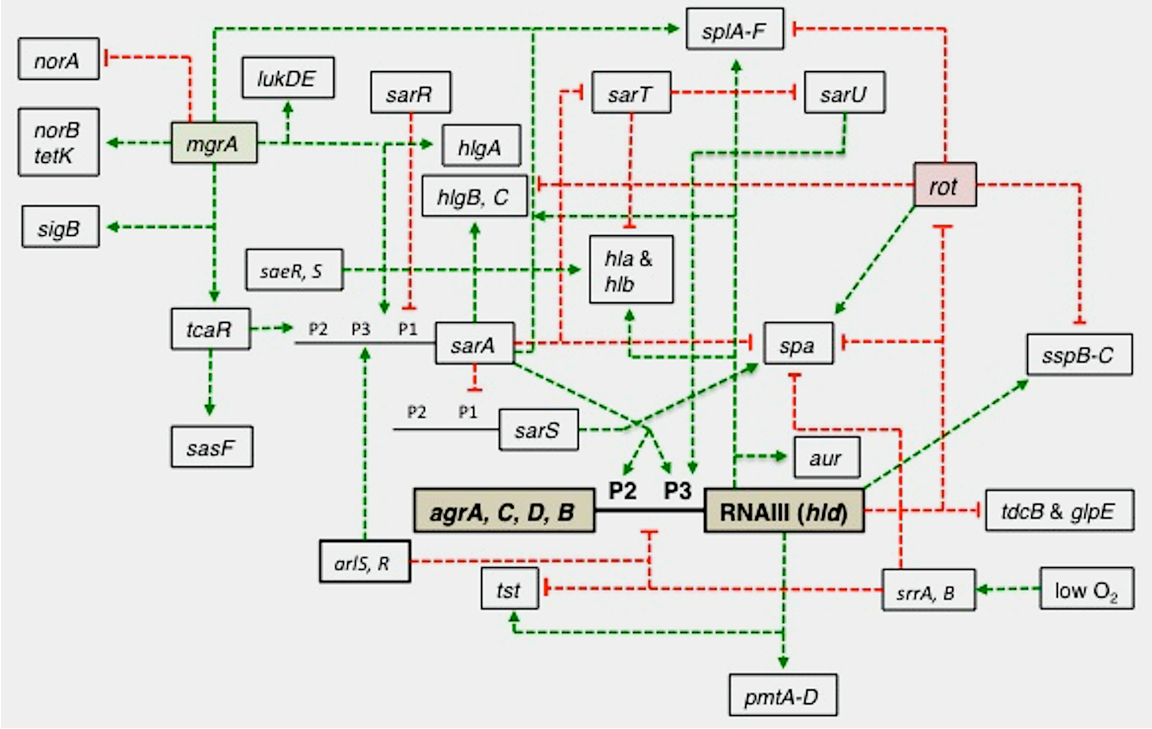

Figure 3. A Network Schematic of Some of the Genetic Loci That Control Virulence in S. aureus

The regulation and expression of virulence genes such as α-hemolysin (*hla*), δ-hemolysin (*hld*), serine proteases (*splA-F*), exotoxins (*hlgA-C* and *pmtA-D*), and Protein A (*spa*) is modulated by a complex, interactive network of many regulatory loci, including the *agr* locus, in *S. aureus*. Repressive interactions are represented in red. Activating interactions are represented in green. The *sar* locus is the *staphylococcal accessory regulator*, including SarA, SarU and SarR, which up-regulate *agr* transcription. MgrA is a transcription regulator with homology to SarA and MarR proteins. Other important TCS systems include: *arlR* and *-S*, *S. aureus exoprotein* expression (*sae*) and *staphylococcal respiratory response* (*srr)*. Genes of interest: *tst* = toxic shock toxin; *rot* = repressor of toxin; tdcB = threonine dehydratase; and aur = aureolysin. *norA*, *norB* and *tetK* are efflux pumps. *sigB* encodes an alternative sigma factor in *S. aureus*.

While the *agr* locus is conserved among the staphylococci, it has undergone an interesting evolutionary divergence, giving rise to variant specificity groups, of which there are four groups in *S. aureus* and at least two groups in several other staphylococcal species. The sequence variability of each *agr* specific group appears within the genes of *agrB*, *agrD*, and the transmembrane sensor domain of *agrC*, giving rise to the variability of the AIP and its receptor.[21, 33, 61] (It is important to note that a *S. aureus* bacterium can only express one of the four specificity groups.[61]) Meanwhile, *agrA* is identical across all four *agr* groups of *S. aureus*. Each group produces a distinct AIP with a different amino acid sequence and with differing ligand-receptor specificities with its AgrC receptor. These different ligand-receptor interactions are responsible for *agr* group identification and activation when cognate AIP and AgrC interact.[62] Interestingly, a heterologous pairing of AIP and AgrC inhibits the *agr* feedback loop while still allowing bacterial growth to continue.[61] The only exception to this intergroup interference is the cross-activation observed between groups I and IV, which is likely due to these two AIPs differing in sequence by a single amino acid.[63] Intergroup quorum sensing interference may be unique to *S. aureus*, since such a phenomenon has not been observed among the *agr* groups of *S. epidermidis*.[33] The *in vivo* relevance and therapeutic implications of this intriguing phenomenon are the subject of ongoing study in several laboratories. This cross-group antagonism has also proven a valuable tool for studying AIP structure-activity relationships (SAR) and makes *agr* an especially attractive model system for the study of quorum sensing in Gram-positive bacteria.

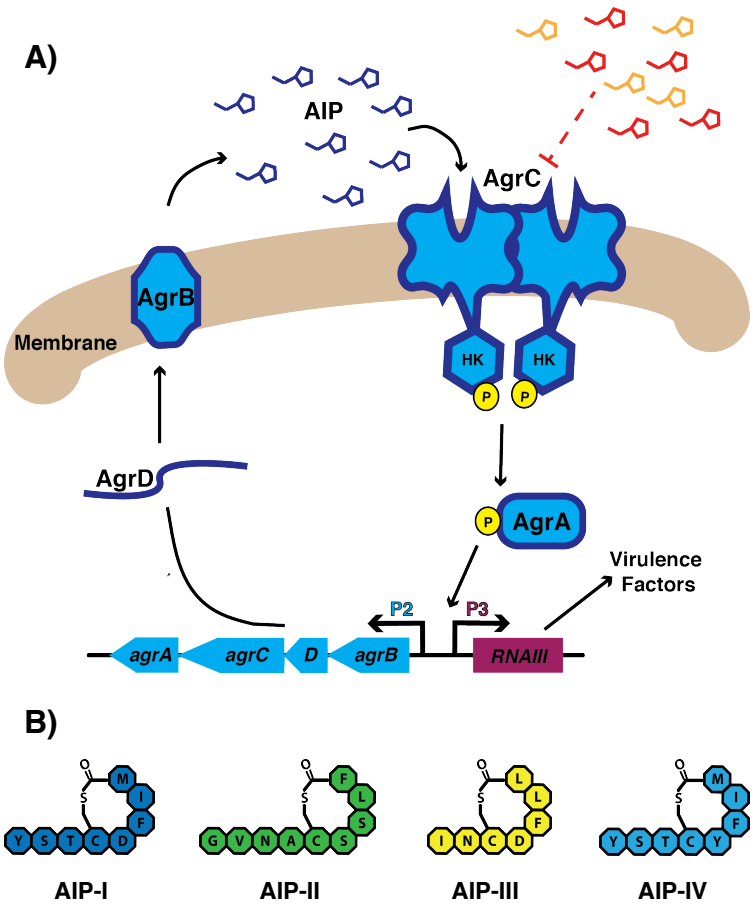

Figure 4. The *agr* Quorum Sensing Circuit

A) Schematic depicting the general *agr* QS circuit in *S. aureus* (black arrows). The P2 operon (blue) contains four genes to synthesize and detect AIP. The AgrD precursor peptide is processed into the mature AIP. (Schematic of sequence and structure of the four possible AIPs is shown in B.) Production of AIP requires an integral membrane protease, AgrB. Secretion of the AIP involves the AgrD precursor crossing the bacterial membrane and a second cleavage step that liberates AIP into the extracellular environment. AIP (dark blue) binds to homodimeric AgrC, a receptor histidine kinase (HK), which induces its autokinase activity. Activated AgrC relays the phosphoryl group to the response regulator, AgrA, which then activates transcription of both P2 and P3 (purple) operons in the *agr* locus. This results in a positive feedback on the circuit and an up-regulation of the P3 transcript, RNAIII, which controls the expression of *agr*-related virulence genes. A heterologous AIP (orange and red) suppresses *agr* expression and RNAIII production by inhibiting AgrC autokinase activity.[21, 55]

1.2 Molecular Components of the *agr* Locus

The *agr* system is one of the most extensively studied QS systems with the work of several laboratories providing a relatively detailed picture of the molecular mechanisms in this biological system. Our understanding of this system is nevertheless a work in progress, and the following sections detail what is known in the field and what questions remain to be answered.

**Note: one convention employed herein will be to designate group specificity when referring to *agr*-encoded proteins by adding the group number in roman numerals following the protein or AIP (e.g. AIP-I, AgrB-II, AgrC-III and AgrD-IV). If no specificity group is designated, it can be assumed that a general statement is being made about the referenced *agr* molecule—protein or AIP.

1.2.1 AIP Biosynthesis

The AIP sequence is embedded within the AgrD polypeptide (Figure 5A).[25, 64] In *S. aureus*, AgrD is a polypeptide chain of either 46 or 47 amino acids depending on the specificity group. (AgrD-II is the only one consisting of 47 amino acids.) Structurally, AgrD can be divided into three general domains: 1) the N-terminal 24 residues form an amphipathic helix that is capable of targeting the AgrD polypeptide to the cell membrane;[64] 2) the middle section of AgrD contains the amino acid sequence for the AIP molecule;[31, 64] and 3) the C-terminus of AgrD is highly acidic and contains key residues for recognition of and removal by AgrB.[57] These three general domains of AgrD are conserved among all staphylococcal species.[21, 40]

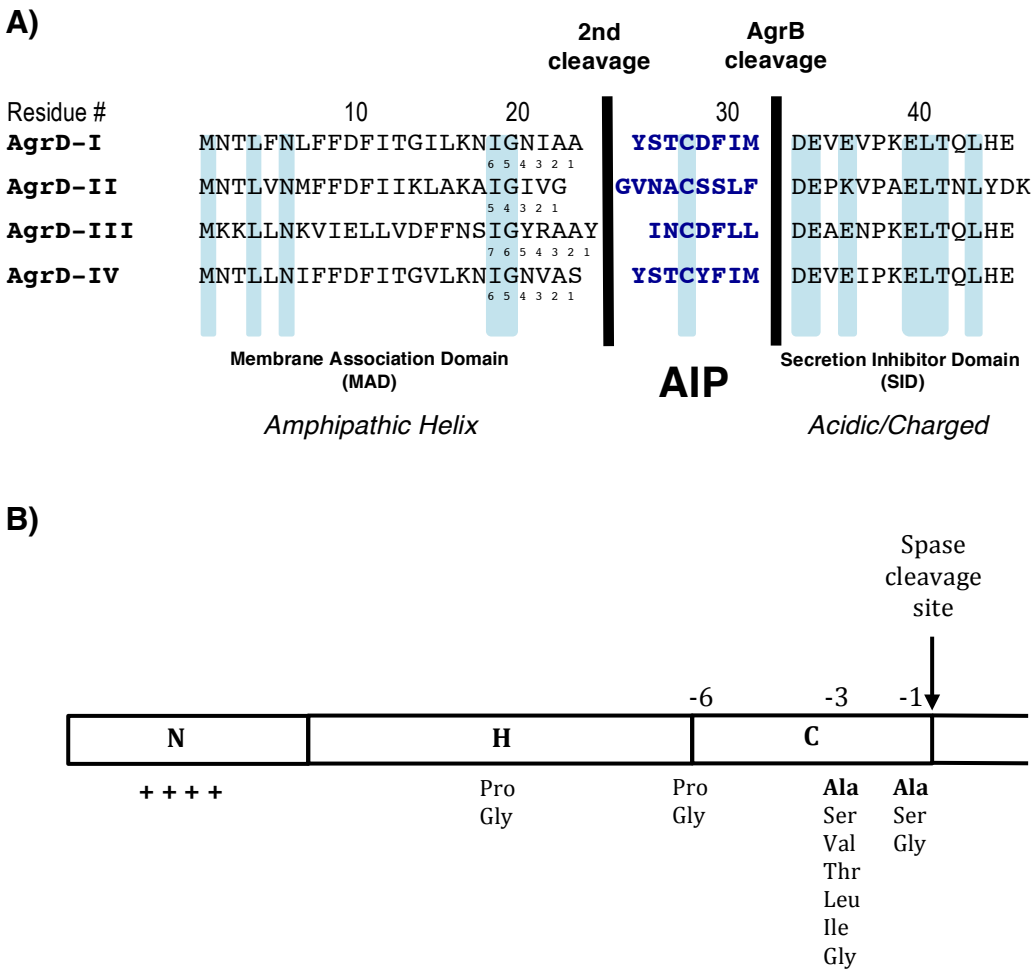

Figure 5. AgrD Sequence Alignment and Structural Characteristics

A) *S. aureus* AgrD sequences aligned with the AIP sequences colored navy blue and conserved residues shaded light blue. Domain characterization and cleavage sites are indicated, and the residues leading into the AIP N-terminal cleavage site are numbered. **B)** Schematic representation of a typical bacterial signal peptide, which usually contains a positively charged N-terminus (N), a central hydrophobic region (H), and a polar, C-terminal region (C).[65] Helix-breaking proline or glycine residues are often found in the middle of the H-region and between the H- and C-regions at the -6 position relative to the cleavage site. The signal peptidase (SPase) recognition sequence consists of small aliphatic residues at positions -1 and -3, relative to the cleavage site. The most common residue at these positions is Ala, although other common residues are listed. Compared to this schematic, the N-terminus of AgrD has some C-region characteristics.

The N-terminal helix can vary significantly in sequence with only 5 of 32 residues conserved among the AgrD polypeptides of *S. aureus*. Despite this variability, the amphipathic properties are thought to be maintained. Removal of the first 12 residues of AgrD-I is also tolerated with some AIP-I being produced, but deletion of the first 14 residues prevents AIP-I biosynthesis.[64] If these removed amino acids are replaced with an artificial amphipathic helix, AIP-I production can be rescued, suggesting the function of this section is membrane targeting, but not necessarily to mediate any specific interactions with AgrB.[64] More recently, the AgrD N-terminal leader was discovered to exist in the amyloid fibrils of *S. aureus* biofilms.[66, 67] Such behavior resembles the small peptide toxins expressed by *S. aureus* known as phenol-soluble modulins (PSMs).[68] Like PSMs, the N-terminus of AgrD forms and seeds amyloid fibrils outside the cell and displays cytolytic and proinflammatory properties, indicating that the N-terminus of AgrD might be another virulence factor directly expressed by *agr*.[66, 67] How a *S. aureus* bacterium might secrete and/or regulate this amphipathic leader peptide is not understood at all.

In other work, the N-terminus of AgrD-I was replaced with a transmembrane helix to limit the orientation of AgrD-I to the cytoplasmic side of the membrane, but this altered AgrD-I did not lead to AIP production, indicating that the N-terminal leader must be amphipathic to allow AgrB processing.[64] Additionally, the processing of AgrD results in a secreted peptide. However, the N-terminus does not resemble a canonical signal peptide typically used to target polypeptides to the secretion machinery embedded in the cell membrane (Figure 5B);[65] and using signal peptide predictive software indicates that

the N-terminus of AgrD does not include classical, recognizable elements of signal peptides.[69] Thus, the N-terminal, amphipathic helix of AgrD targets the molecule to the cell membrane, where it associates with AgrB for further processing into AIP. That is also why, herein, the N-terminus of AgrD is referred to as the membrane association domain (MAD).

The small AIP-encoding domain of AgrD also shows considerable divergence within *S. aureus*. For now, it is important to note that among the four *S. aureus* AIPs there is a conserved cysteine residue at the -5 position relative to the AgrB cleavage site (Figure 5A). This cysteine forms the thiolactone ring structure of AIP. Also, AIP-I and -IV vary by one amino acid.

The C-terminal tail is the most conserved portion of AgrD in *S. aureus*, especially the first nine residues.[33] The C-terminal portion begins with the residues aspartate and glutamate as the first two amino acids followed by two other absolutely conserved proline and glutamate residues at the sixth and eighth positions, respectively, relative to the AgrB cleavage site. The conserved proline residue at the +6 position has been used to predict the C-terminus of AIP autoinducers within several other Gram-positive bacteria that still require some experimental validation.[21] There are also two conserved leucine residues in the C-terminus of AgrD. Some elegant genetic work using alanine point mutants has shown that the first conserved glutamate (E34) and leucine (L41) residues are essential for AIP production and AgrB cleavage of AgrD.[57] It has also been reported that only a small portion of the C-terminus can be removed and still maintain AIP

production. Deleting the four most C-terminal amino acid residues is tolerated, which further confirms the importance of the E34 and L41 residues, since they are more than four amino acid residues from the C-terminus.[57] Finally, the C-terminus is highly negatively charged with at least four acidic residues within a 14-residue span. In order to biologically synthesize and secrete AIP, AgrB must remove this densely charged region of AgrD. While there is no clear secretion mechanism for AIP, secretion of this small peptide would clearly benefit from removal of this acidic patch. Therefore, the C-terminus of AgrD can be referred to as the secretion inhibitor domain (SID), which AgrB removes.

AgrB is a 22-kDa integral membrane protein and cysteinyl endopeptidase that removes the SID of AgrD and mediates the formation of the AIP thiolactone macrocycle.[56, 57, 70] In many respects, AgrB is a unique feature of the staphylococcal *agr* system since it lacks significant sequence similarity with other quorum-sensing proteins and does not share homology with other cysteine proteases or other autoinducer processing proteins in Gram-positive bacteria.[25, 56] When comparing the different AgrB sequences among *S. aureus agr* types there is a significant amount of variation between strains. Overall hydrophobic sections that make up transmembrane sections are conserved, though the sequences of these regions are diverse—a common feature of integral-membrane protein homologs. Interestingly, the N-terminal portion of AgrB is highly conserved among staphylococcal species, with the first 34 residues being absolutely conserved among the four *S. aureus agr* groups. This region is required for AgrB function.[70] However, its role in AIP production is currently unknown.

The group specificity of AgrB in the processing of AgrD is not as stringent as that of AIP-AgrC interactions. While in most cases AgrB will only process its cognate AgrD, there are exceptions. AgrB-III can process AgrD-I to form AIP-I, and AgrB-I can process AgrD-III to form AIP-III.[61] AgrB-I and -IV may also be capable of processing both AgrD-I and -IV, as the sequences of these two groups are very similar, but this possibility has yet to be tested. In trying to understand the basis for AgrB-AgrD specificity, Zhang *et al*. constructed a panel of AgrB-I/II chimeras by swapping homologous segments of the two proteins, then determined their ability to synthesize active AIPs from AgrD-I or AgrD-II.[71] The authors narrowed down the determinants of specificity in AgrB-I to amino acids 43 to 67 and to residues 126 and 141 in AgrB-II. These regions correspond to either the second and fourth transmembrane regions according to one AgrB topology map,[56] or a cytoplasmic loop and an extracellular loop in another AgrB topology map.[72] While the lack of expression and localization data for the mutant proteins is a caveat of this study, it is nonetheless interesting that the specificity determinants for AgrB-I and AgrB-II appear to be in different regions of the primary sequence. Further study will need to focus on how these patches impart specificity and how they recognize AgrD.

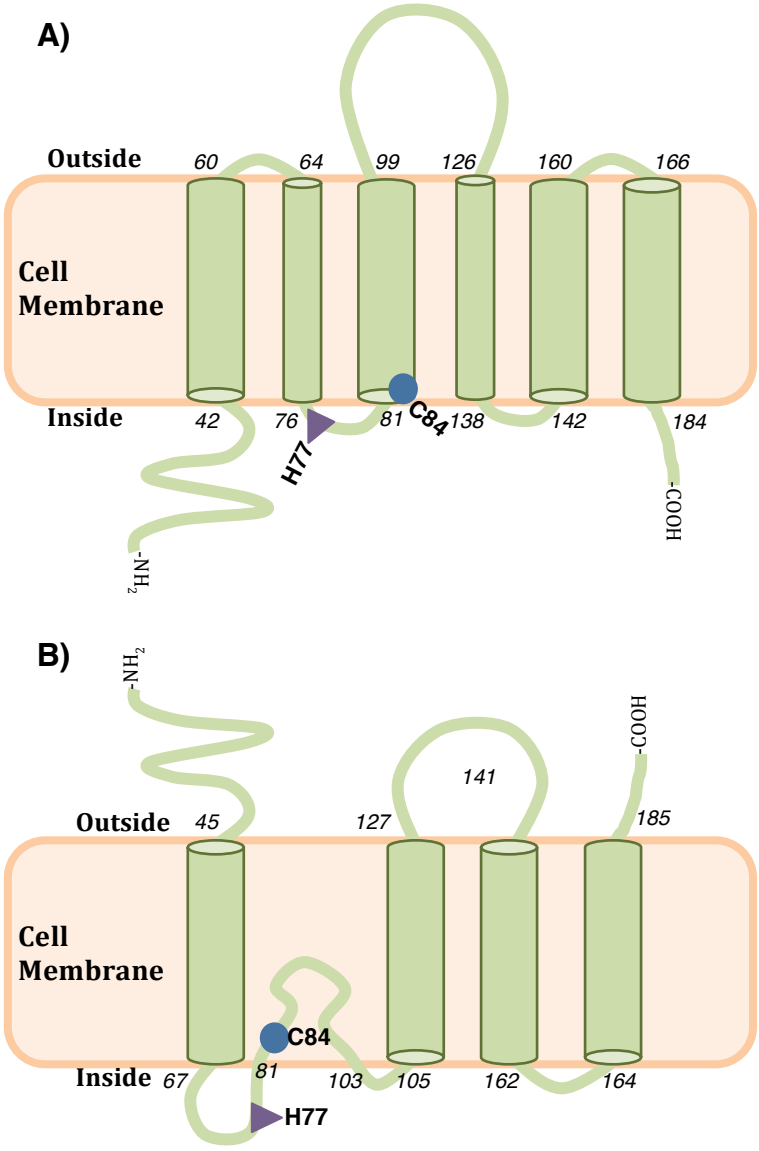

Figure 6. Topology Models of AgrB

AgrB topological studies using a **A)** PhoA-fusion protein strategy[56] or **B)** SCAM.[72] The catalytic residues C84 and H77 are indicated with either a blue circle or purple triangle, respectively, in their approximate location. The *italicized numbers* identify the residue number at the beginning or end of a proposed transmembrane domain, which are represented in the AgrB cartoons presented in A and B as cylinders within the cell membrane.

Attempts to structurally characterize AgrB have proceeded slowly. Two studies a decade apart have produced topology maps of AgrB, which have several major disagreements.[56, 72] The first study used alkaline phosphatase (PhoA) fusions of AgrB in *E. coli* to try to map the topology of AgrB in the inner membrane (Figure 6A). This method generated a topology map with six transmembrane regions, in which both the N- and C-termini are predicted to be inside the cell and a 27-residue loop located outside the cell. Topological studies indicate that the catalytic residues (H77 and C84) are located on the cytoplasmic face of the membrane.[56] The second study used the substituted cysteine accessibility method (SCAM) to investigate AgrB topology (Figure 6B). SCAM resulted in a topology map with four transmembrane regions, in which both the N- and C-termini are predicted to be outside the cell and a re-entrant loop on the cytoplasmic face positions the catalytic residues near the membrane.[72] Clearly, a crystal structure will be the only way to resolve these topological discrepancies.

Initially, progress towards elucidating the mechanism of AIP biosynthesis preceded slowly from the original report in 1995 that indicated AgrB is involved in the process.[31] Recent research, however, has helped elucidate the cleavage mechanism of AgrB. The first evidence for an AgrB-mediated removal of the AgrD SID came from Western blot analysis of crude cell lysates containing epitope-tagged AgrD, in which only AgrD intermediates corresponding to the MAD and AIP sequences were observed; and there was no intermediate detected corresponding to the AIP and SID sequences.[70] Mutagenesis experiments also revealed that residues H77 and C84 are required for production of an active AIP;[70] and later Thoendel *et al*. used Western blot analysis to

detect an AgrB-AgrD-I intermediate in membrane fractions of an *E. coli* strain that expresses AgrB-I and His_6-tagged C28A AgrD-I.[57] They were also able to prevent formation of this acyl-enzyme intermediate by using a C84S AgrB single-point mutation.[57] The C84S AgrB-I and C28A AgrD-I point mutants indicate that AIP biosynthesis requires a thioester intermediate to then undergo a thioester exchange step to form the AgrD(1-32)-thiolactone. From all of this work, a detailed AgrB-mediated cleavage mechanism can be proposed as follows (Figure 7): The SID of AgrD is removed when the sulfhydryl group of C84 in AgrB attacks the amide carbonyl of the 32^{nd} amino acid in AgrD to form an acyl-enzyme thioester intermediate. (H77 of AgrB acts as a general base to deprotonate C84.) The thiolactone macrocycle of AIP is formed when the conserved sulfhydryl group of C28 in AgrD attacks the acyl-enzyme thioester intermediate in an intramolecular trans-thioesterification reaction.[56, 57] The product of AgrB cleavage is a 32-residue polypeptide with a C-terminal thiolactone macrocycle, which includes the last five C-terminal amino acid residues (28-32).

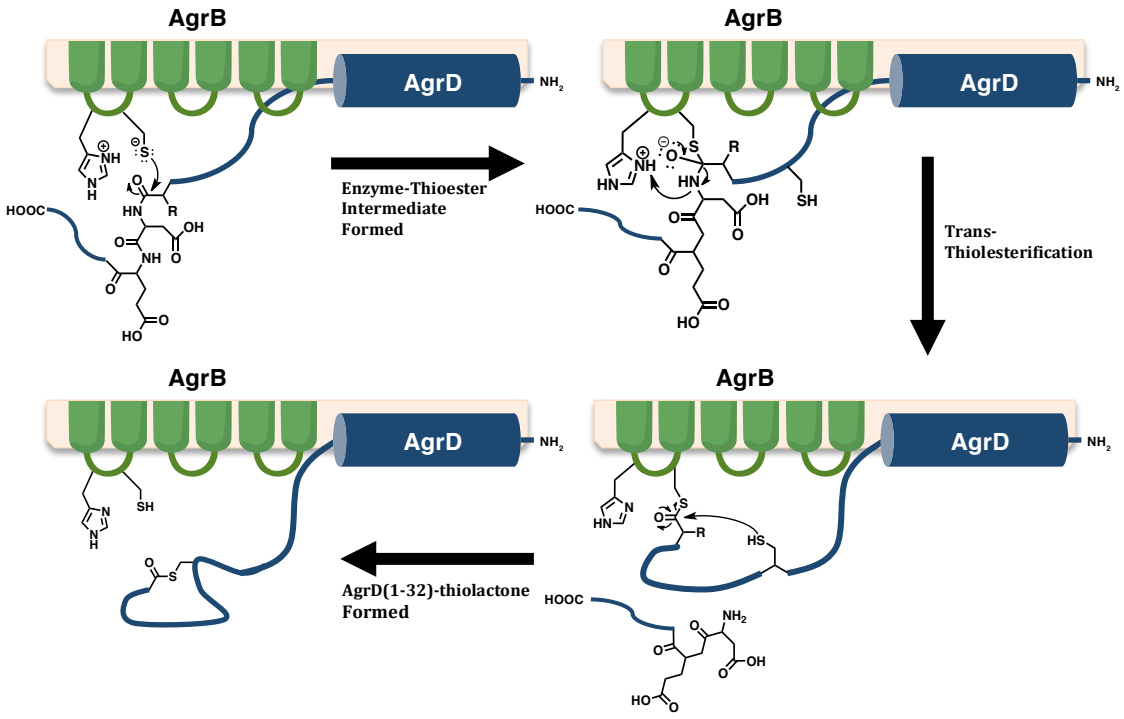

Figure 7. Proposed AgrB Cleavage Mechanism of AgrD to Form the AgrD(1-32)-thiolactone Precursor

Proposed mechanism of AgrB cleavage of AgrD. C-terminal cleavage of AgrD (dark blue) is mediated by residues H77 and C84 of AgrB to yield an acyl-enzyme intermediate,[56, 57] which is released via intramolecular trans-thioesterification with the sulfhydryl group of the conserved C28 residue of AgrD. The product of AgrB cleavage is a 32-residue polypeptide with a C-terminal thiolactone macrocycle, which includes the last five C-terminal amino acid residues (28-32). This AIP precursor will often be referred to as the AgrD(1-32)-thiolactone. The cytoplasmic proximal region of AgrB is shown in green.

The next step in AIP biosynthesis following formation of the AgrD(1-32)-thiolactone requires transport of the intermediate across the membrane in preparation for release into the external environment. There is no clear mechanism for AIP secretion. In the literature, it is assumed that AgrB is somehow involved in transporting the intermediate it forms across the membrane.[56, 57, 70-72] Only recently, has some work tried to investigate the role of AgrB in AIP secretion. After screening many AgrB mutants obtained from random mutagenesis, three point mutations were found to affect AIP production although none of the three inhibited AgrB peptidase activity. K129, K130 and K131 of AgrB form a lysine patch, and when mutated to glutamate, they inhibit secretion of an active AIP but not AgrB peptidase activity.[66] These residues are predicted to be in an extracellular loop or near the extracellular membrane face in the topology maps.[56, 72] This same study attempted to determine whether AgrB forms oligomers. Oligomerization of AgrB might indicate that AgrB forms a pore to help transport the AgrD(1-32)-thiolactone across the membrane. Expressing a T7-AgrB fusion protein and a His_6-tagged AgrB together in *E. coli*, the authors argue, based on co-immunoprecipitation data, for the existence of a complex between the two proteins.[72] However, this study did not shed light on whether this complex was a dimer or some higher oligomer, nor did it address the functional relevance of this complex for secretion. Consequently, the secretion mechanism for the AIP precursor remains poorly understood.

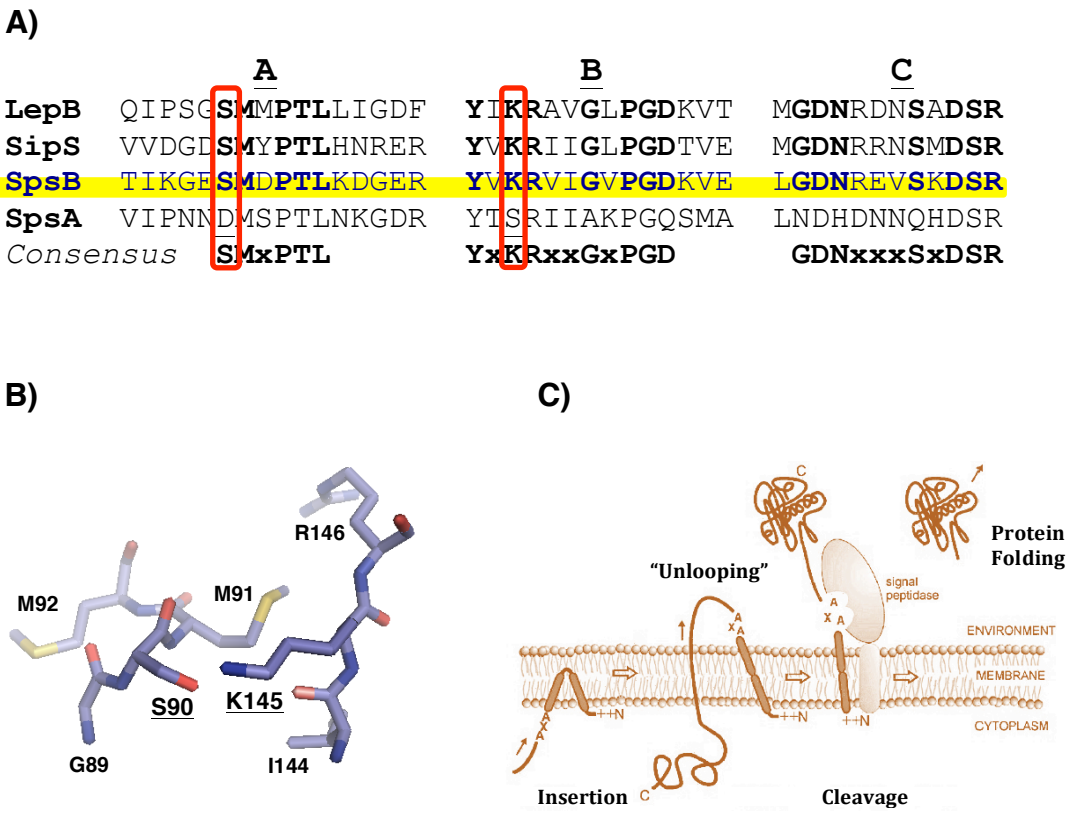

Figure 8. Type I Signal Peptidases

A) A sequence alignment of several type I SPases compares *spsB* and *spsA* to the classical Gram-negative (LepB, *E. coli*) and Gram-positive (SipS, *B. subtilis*) SPases and reveals that SpsB does have the catalytic serine/lysine dyad in the conserved regions of known SPases while SpsA does not.[73] **B)** The active site of SpsB (apoenzyme, pdb file 1KN9) is depicted in a stick model with oxygen (red), nitrogen (blue), sulfur (yellow) and carbon (blue-gray).[74] S90 is the nucleophile and K145 acts as a general base in the hydrolysis of peptide bonds. **C)** This model for signal peptide insertion into the cytoplasmic membrane and cleavage by type I SPase is adapted from van Roosmalen *et al.*[65] First, the signal peptide interacts with the membrane, inserting into the membrane and unlooping to pull part of the mature protein through the membrane. During or shortly after translocation by the protein transport machinery (not shown), the signal peptide is cleaved by type I SPase and, thereby, the mature protein is released from the membrane. Finally, the mature protein folds into its native conformation.

AIP production requires three chemical transformations: two proteolytic cleavage steps and thiolactone formation. AgrB accomplishes one cleavage step and forms the AIP thiolactone macrocycle. While it is unlikely AgrB performs all three chemical transformations to produce AIP, there are no other candidate proteins encoded in *agr*.[25] For over a decade, there was speculation that other proteins in addition to AgrB may be involved in AIP production.[56, 70, 75] In 2007, a new player in AIP processing was discovered—SpsB—the type I signal peptidase (SPase) in *S. aureus*.[58] Type I SPases utilize a Ser-Lys catalytic dyad (Figure 8A & B),[65, 74, 76-78] and they are membrane bound proteases responsible for removing N-terminal signal peptides as proteins are being secreted through the Sec or Tat secretion pathways (Figure 8C).[65, 76] In Gram-positive bacteria, SPases have an N-terminal transmembrane segment that anchors the catalytic domain to the outside of the membrane.[65, 74, 76] In *S. aureus*, SpsB is essential for cell growth and viability.[73] Proximal to the *spsB* gene is another open reading frame, *spsA*, and only 15 nucleotides separate the two genes. Alignment of these two genes with LepB (*E. coli* SPase) and SipS (*B. subtilis* SPase) indicates that SpsA is a catalytically inactive SPase, where the conserved Ser-Lys catalytic dyad is replaced by Asp and Ser, respectively.[73] Therefore, SpsB is thought to be the only active type I SPase in *S. aureus*, although many other Gram-positive bacteria may have multiple SPases.[65]

It has been reported that SpsB carries out the second cleavage event of AgrD-I, removing the N-terminal region.[58] In support of this assertion, signal-peptidase inhibitors were capable of preventing AIP production and *agr* activation in both *agr-I* and *agr-II* strains, albeit at millimolar concentrations. Also, a synthetic peptide substrate derived

from AgrD-I, NIAAYST tagged with fluorescein was added to various lysate fractions; and the correct cleavage products were identified by comparing their agarose gel retention times to synthetic standards. Through a series of fractionation and inhibition experiments, the proteolytic activity was attributed to SpsB.[58] It remains untested whether SpsB is involved in AIP production for all four specificity groups of *S. aureus* and other staphylococcal strains, so further investigation is necessary to verify the universal requirement of SPase in AIP biosynthesis.

Using all the experimental findings outlined above, a model for AIP biosynthesis has been proposed (Figure 9). First, AgrD associates with the cytoplasmic membrane via its MAD. At the membrane, AgrB catalyzes cysteine-dependent nucleophilic attack on AgrD, removing the SID through a two-step process: 1) the formation of a covalent intermediate in which AgrD and AgrB are linked through a thioester bond and 2) the conserved sulfhydryl group of C28 in AgrD exchanges with the acyl-enzyme thioester intermediate through a trans-thioesterification reaction to create the thiolactone macrocycle and to form the AgrD(1-32)-thiolactone—the AIP precursor. Finally, the precursor is transported across the membrane through an unknown mechanism, where a membrane protease such as SpsB removes the MAD sequence to release AIP into the extracellular environment. While some of the steps such as AgrD targeting to the membrane, AgrB-mediated cleavage and SpsB-mediated cleavage have been demonstrated, experimental evidence supporting the other steps is lacking.

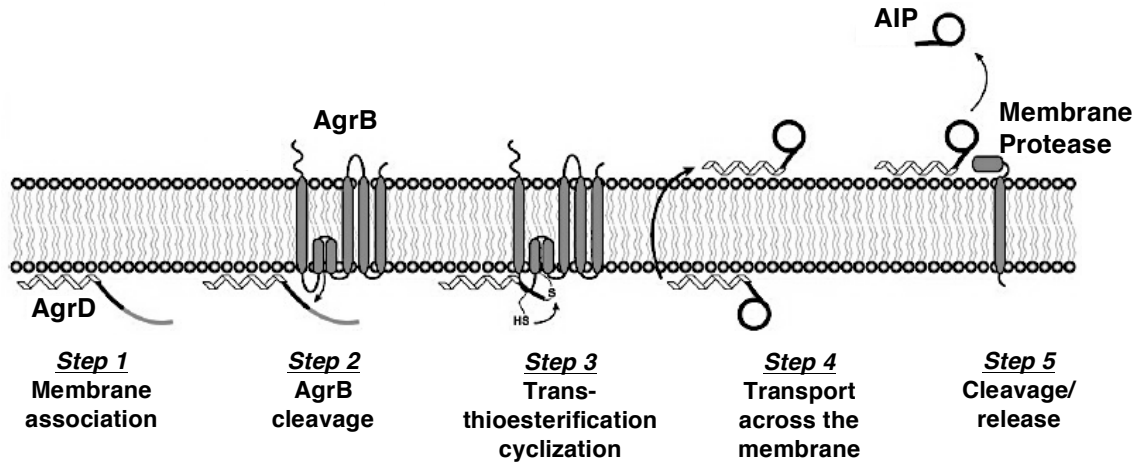

Figure 9. Proposed AIP Biosynthetic Pathway Model

A proposed AIP biosynthetic pathway model adapted from Theondel *et al*.:[72] *Step 1*, the MAD of AgrD helps target AgrD to the cytoplasmic membrane. *Step 2*, AgrB removes the SID of AgrD. *Step 3*, the acyl-enzyme thioester intermediate undergoes a trans-thioesterification reaction with the conserved Cys residue of AgrD, liberating the peptide from AgrB and forming a thiolactone macrocycle at the C-terminus of the peptide. *Step 4*, the AgrD(1-32)-thiolactone is transported to the outer face of the membrane. *Step 5*, a membrane protease such as SpsB removes the MAD of AgrD, releasing AIP from the membrane into the external environment.

Table 1. SAR of Previously Synthesized AIPs and AIP Derivatives

(Not All Synthetic AIPs Are Listed)

AIP Derivative	AIP Sequence	AgrC Activation				AgrC inhibition			
		I	II	III	IV	I	II	III	IV
AIP-I	YST**CDFIM**	+++	—	—	+	—	+++	+++	—
AIP-II	GVNA**CSSLF**	—	+++	—	—	+++	—	+++	+++
AIP-III	IN**CDFLL**	—	—	+++	—	+++	+++	—	++
AIP-IV	YST**CYFIM**	++	—	—	+++	—	+++	+++	—
AIP I-II	YST**CSSLF**	—	—	—	—	+++	++	+++	+++
AIP II-I	GVNA**CDFIM**	—	—	—	—	++	+++	++	+
AIP-II Lactone	GVNA**SSSLF**	—	—	nt	nt	+++	—	nt	nt
AIP-I Lactam	YST**(Dpr)-FIM**	+	nt	nt	nt	nt	nt	nt	nt
AIP-II Lactam	GVNA**(Dapa)-SSLF**	—	+	nt	nt	+++	—	nt	nt
tr-AIP-I"	Ac-**CDFIM**	+	—	—	—	+++	+++	+++	+++
tr-AIP-II	**CSSLF**	—	—	—	—	++	++	+++	++
tr-AIP-III^	Ac-**CDFLL**	nt	nt	nt	nt	+++	+++	—	+++
tr-AIP-IV	**CYFIM**	—	—	—	—	++	+++	+++	+
tr-AIP-I/IV 2A	**CAFIM**	—	—	—	—	+++	+++	+++	+++
Y1A AIP-I	AST**CDFIM**	++	nt	nt	nt	—	nt	nt	nt
S2A AIP-I	YAT**CDFIM**	+++	nt	nt	nt	—	nt	nt	nt
T3A AIP-I	YSA**CDFIM**	++	nt	nt	nt	—	nt	nt	nt
D5A AIP-I/IV	YST**CAFIM**	—	—	—	—	+++	+++	+++	+++
F6A AIP-I	YST**CDAIM**	+	nt	nt	nt	—	nt	nt	nt
I7A AIP-I	YST**CDFAM**	+	nt	nt	nt	—	nt	nt	nt
M8A AIP-I	YST**CDFIA**	+	nt	nt	nt	—	nt	nt	nt
M8I AIP-I	YST**CDFII**	+++	—	—	++	—	+++	+++	—
G1A AIP-II	AVNA**CSSLF**	—	+++	nt	nt	+++	—	nt	nt
V2A AIP-II	GANA**CSSLF**	—	++	nt	nt	+++	—	nt	nt
N3A AIP-II	GVAA**CSSLF**	—	—	—	—	+++	++	+++	+++
S6A AIP-II	GVNA**CASLF**	—	+++	nt	nt	+++	—	nt	nt
S7A AIP-II	GVNA**CSALF**	—	+++	nt	nt	+++	—	nt	nt
L8A AIP-II	GVNA**CSSAF**	—	—	nt	nt	—	—	nt	nt
F9A AIP-II	GVNA**CSSLA**	—	—	nt	nt	—	—	nt	nt
D5N AIP-I/IV	YST**CNFIM**	+++	—	++	—	—	+++	—	+++
D5F AIP-I/IV	YST**CFFIM**	+++	—	—	+++	—	+++	+++	—
I1A AIP-III^	AN**CDFLL**	nt	nt	nt	nt	+++	+++	++	+++
N2A AIP-III^	IA**CDFLL**	nt	nt	nt	nt	+++	+++	—	+++
D4A AIP-III^	IN**CAFLL**	nt	nt	nt	nt	+++	+++	+++	+++
F5A AIP-III^	IN**CDALL**	nt	nt	nt	nt	—	—	—	+
L6A AIP-III^	IN**CDFAL**	nt	nt	nt	nt	—	—	—	—
L7A AIP-III^	IN**CDFLA**	nt	nt	nt	nt	—	—	—	—
D-I1 AIP-III^	D**INCDFLL**	nt	nt	nt	nt	+++	+++	+++	+++
D-N2 AIP-III^	I**DNCDFLL**	nt	nt	nt	nt	+++	+++	+++	+++
D-C3 AIP-III^	IN**DCDFLL**	nt	nt	nt	nt	—	—	—	—
D-D4 AIP-III^	IN**CDDFLL**	nt	nt	nt	nt	++	+++	—	+++
D-F5 AIP-III^	IN**CDDFLL**	nt	nt	nt	nt	—	—	—	+
D-L6 AIP-III^	IN**CDFDLL**	nt	nt	nt	nt	—	—	—	—
D-L7 AIP-III^	IN**CDFLDL**	nt	nt	nt	nt	+++	+++	—	+++
AIP-III 8AA"	YIN**CDFLL**	nt	nt	—	nt	+++	+++	+++	+++
AIP-III 9AA	AYIN**CDFLL**	nt	nt	—	nt	nt	nt	++	nt
b-AIP-I	biotin-YST**CDFIM**	++	—	—	—	—	+++	+++	—
Ac-AIP-I	Ac-YST**CDFIM**	+++	—	—	—	—	+++	+++	—
fl-AIP-I	fluorescein-YST**CDFIM**	++	—	—	—	—	+++	+++	—
AIP-II acid	GVNACSSLF-OH	—	—	—	nt	—	—	—	nt
AIP-II thioester	GVNACSSLF-SR	—	—	—	nt	—	—	—	nt
AIP-I peptomers	10-20 library	—	—	—	—	++	++	++	++
AIP-I norleucyl	YST**CDFI(Nle)**	—	nt	nt	nt	—	nt	nt	nt
AIP-I methionyl sulfoxide	YST**CDFIM***	—	nt	nt	nt	—	nt	nt	nt

+, ++, +++ = weak to strong activity. The dash (—) indicates no activity detected. nt = not tested. Dapa = diaminopropanoic acid. trAIP = truncated AIP. AA = amino acids. The small D indicates a D-amino acid. Endocyclic amino acid residues are in boldface.

^The activity for these AIPs and AIP derivatives were determined using a cell-based reporter gene assay with GFP instead of β-lactamase.

"Both cell-based reporter gene assays (GFP and β-lactamase) were used to determine the activity for these AIPs and AIP derivatives.

1.2.2 AIP Structure and Activity

A large effort has been made toward determining the structure–activity relationships (SAR) of the four AIPs by employing synthetic methods and a rapid, quantitative *agrP3::blaZ* reporter assay[31, 45, 59, 62, 63, 79-83] or a similar reporter gene assay using *gfp* instead of *blaZ*.[84, 85] Efficient chemical synthesis of AIPs combines solid-phase peptide synthesis (SPPS) and solution phase chemistry.[45, 63, 80, 83, 84] In the most efficient protocol using BOC chemistry, the linear peptide is first synthesized by SPPS on an α-thioester-generating resin, then cleaved from the solid support, and the final AIP product is obtained by spontaneous trans-thioesterification of the unprotected peptide α-thioester in neutral aqueous solution.[63] Synthetic AIPs are extremely potent agonists and antagonists of cognate and non-cognate AgrC receptors, respectively, with EC_{50} and IC_{50} values in the low to sub-nanomolar range.[45, 62, 63, 80, 83, 84] The recognition determinants for agonism are much more stringent than those for antagonism, consistent with the requirement for group-specific AIP–AgrC interactions for activation but not inhibition (Table 1).[45, 62, 63, 82, 86] For example, the exocyclic "tail" residues are dispensable for inhibition but not activation.[45, 62, 84] Indeed, some truncated AIPs consisting of only the pentapeptide macrocycles inhibit all four *S. aureus* AgrC receptors, including their cognate AgrC.[83] Furthermore, replacing the thiolactone linkage of the AIP with a lactam or lactone causes a dramatic reduction in agonistic potency but has virtually no effect on antagonism.[45, 80] Linear versions of the AIPs are completely inactive, indicating that a macrocyclic structure is one requirement for inhibition as well as for activation.[45] The presence of two bulky hydrophobic residues at the C-terminus, a strongly conserved feature of the staphylococcal AIPs (Figure 10), also seems to be critical for binding and activity since

alanine substitutions at either of these positions in AIP-I, -II and -III have all resulted in a dramatic reduction in agonist and antagonist potency.[45, 59, 80, 84] Recent NMR studies produced structures of the four native AIPs that revealed a tri-residue "hydrophobic knob" essential for binding and therefore bioactivity (Figure 11).[86] Thus, the macrocycle and hydrophobic binding motif are important for bioactivity, and the thioester and tail residues are additionally required for AgrC receptor activation but not necessarily for binding or inhibition.

While all four *S. aureus* AIPs follow the general paradigm described above, determinants of specific AIP–AgrC interactions vary considerably among the different groups. Alanine scanning mutagenesis revealed that the key residues for receptor activation lie in different positions in the sequences of different AIPs. [45, 80, 84] For example, D5 of AIP-I and D4 of AIP-III are endocyclic, and N3 of AIP-II is in the tail. Each residue is a critical determinant for specific activation of its cognate AgrC receptor. Replacing these critical residues' side chain functionalities with the methyl group of alanine leads to the D5A AIP-I, D4A AIP-III and N3A AIP-II mutants that results in loss of specificity but not activity, as the AIP analogs maintain antagonism of non-cognate AgrC receptors and are converted to antagonists of their cognate receptors (Table 1). Conversely, substitution of an amide for the acid in D5N AIP-I unexpectedly converts the peptide to an AgrC-III agonist while maintaining cognate AgrC-I activation, and D5F AIP-I is also an agonist of AgrC-I.[63] Finally, nonnative appendages, such as biotin, can be conjugated to the N-terminus of AIP-I without significantly affecting its activity, but the addition of one amino acid to the N-terminus of AIP-III leads to a loss of agonism.[63]

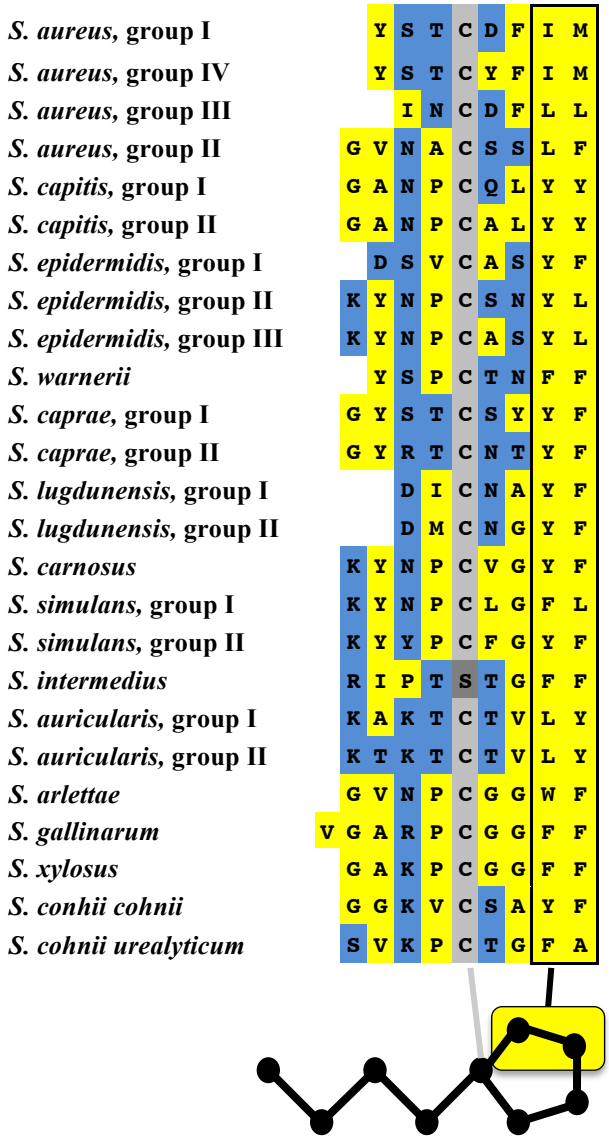

Figure 10. Sequence Alignment Indicates a Hydrophobic, C-terminal Motif in Known and Predicted Staphylococcal AIPs

Polar residues are shaded blue and non-polar residues are shaded yellow, highlighting the conserved C-terminal hydrophobic motif outlined in black. The conserved cysteine is shaded in gray, and note that the *S. intermedius* AIP contains a serine instead of a cysteine, which forms a lactone instead of a thiolactone. This figure is adapted from Wright *et al.*[59]

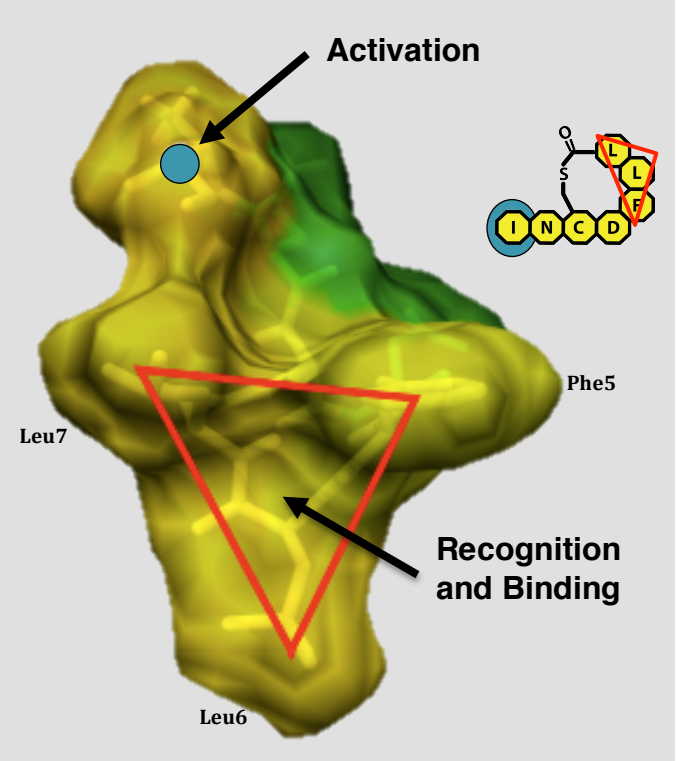

Figure 11. AIP Binding Hydrophobic Knob Motif

A space-filling model of AIP-III displaying hydrophobic residues in yellow and hydrophilic in green. This figure is adapted from Tal-Gan *et al.*[86] The model is oriented with the AIP macrocycle extending out of the plane of the paper and the AIP tail is hidden behind. The red triangle indicates the side chains of AIP-III involved in this proposed "hydrophobic knob" binding motif, which is necessary for AgrC binding. The light blue dot indicates another important interaction within AIP-III for activation—the side chain of Ile1 is required for activation.[84]

Competitive antagonism best explains the mechanism of intergroup *agr* interference of the AgrC receptor.[79] The less stringent AIP sequence requirements for antagonism suggest that an AIP binding event is sufficient for blocking activation of AgrC by a cognate AIP and that AgrC activation requires an additional, specific agonistic interaction. Wash-out and order of addition experiments indicated that both agonists and antagonists bind AgrC in a reversible manner,[79] consistent with competitive antagonism and contradictory to an earlier model involving receptor acylation by the thioester-containing AIP.[45] Inverse agonism has also been observed in constitutively active AgrC mutants, which does further support competitive binding of AgrC and raises the possibility that some non-cognate AIPs induce and/or stabilize an inactive receptor conformation.[87] Recently, AgrC-I was incorporated into nanometer-scale lipid bilayer discs (nanodiscs) for *in vitro* biochemical assays, and among other findings, AIP-II was not only confirmed as an inverse agonist of AgrC-I but also shown to stabilize AgrC-I in an inactive conformation.[88] Thus, the mechanism of intergroup *agr* interference of AgrC occurs in a competitive fashion where AIP can act as a simple, neutral antagonist or help to stabilize an inactive conformation of AgrC as an inverse agonist.[31, 79, 83, 87, 88]

1.2.3 Detecting the AIP Through a Two Component Signaling System

AgrC is an HPK that belongs to the small, unique HPK_{10} subfamily of QS receptors in Gram-positive bacteria (Figure 12A and B).[89] These receptors have a polytopic transmembrane sensor domain, a distinct sequence pattern, F[RK]HDYXN, around the histidine phosphoryl-acceptor residue (known as the H box), and catalytically important N-box and G-box residues. They lack a D-box motif, typically involved in nucleotide binding. Besides these differences, AgrC does not contain a coiled-coil HAMP (histidine kinase, adenylyl cyclase, MCP, and phosphatase) domain but instead has a putative coiled-coil in the DHp subdomain (Figure 12A),[55, 88] which likely mediates homodimerization. In order to determine whether AgrC exists as a pre-formed or ligand-induced dimer, co-immunoprecipitation of differentially tagged versions of AgrC in the absence and presence of AIP was performed. This analysis indicated that AgrC exists as a preformed dimer in the absence of AIP.[90]

The sensor domain of HPK_{10} family members is predicted to be polytopic.[89, 91] To obtain more accurate topographical description of the HPK_{10} sensory domain, [55, 92] bioinformatic analysis of sixteen HPK_{10} sequences using TOPCONS, which merges the topology predictions of five different predictive programs into a single consensus topology,[93] generated a consensus topology for an HPK_{10} sensory domain with four highly conserved TM domains within the C-terminal two-thirds of the sensory domain sequence that have the same orientation in all sixteen HPK_{10} receptors.[55] It also indicated that the N-terminus of the sensor domain is not well conserved and that the position and number of TM domains is variable among the 16 different HPK_{10} receptors, of which

AgrC was included. The AgrC sensor domain consists of the first ~205 amino acids out of 430.[94] Two different experimental studies have tried to determine the topology of the AgrC sensor domain. The first study used hydropathy analysis of AgrC along with AgrC-phoA fusion proteins, which indicated AgrC possesses six transmembrane (TM) helices and the N- and C-termini of the AgrC sensor domain on the cytosolic side of the membrane.[94] A more recent study, however, reported a topology for AgrC with seven TM helices. Wang *et al*.[95] used AgrC-GFP fusion proteins and the substituted cysteine accessibility method (SCAM) to determine AgrC's topology with a periplasmic N-terminus and a cytosolic C-terminus.[95] (Similar topological inconsistencies were observed in structural studies of another HPK_{10} family member, PlnB.[96, 97]) While the topology of the AgrC sensor domain is unresolved, experimental results and bioinformatics suggest there is some variability in its N-terminal portion.[55] What effect such variability has in the sensor domain is not fully understood, although some efforts have attempted to understand where AIP might bind and interact with AgrC.

In order to find the specificity determinants in AgrC, sensor domain chimeras were constructed by dividing the AgrC sensor domain into proximal and distal segments (Figure 12C).[59] Using the six TM helices predicted by Lina *et al*.,[94] residues 86-93 of AgrC-I are located within the third transmembrane domain and are identical in AgrC-I, -III and –IV. They were, therefore chosen as the site for splicing AgrC chimeras together (red line in Figure 12C). The resulting constructs were transduced into a β-lactamase reporter strain in order to analyze their activities.[63] In general, the functionality of each chimera was proportional to the degree of sequence conservation between the two

contributing receptors. AgrC-I and IV sensor domains share 87% sequence identity, and both AgrC-I::IV (N-terminal portion of AgrC-I fused to C-terminal portion of AgrC-IV sensor domain) and AgrC-IV::I were functional. Chimeras involving AgrC-III (~54% sequence identity with AgrC-I and IV) were functional but had unpredictable activities. Chimeras involving the most divergent receptor, AgrC-II, were not functional. Attempts to detect AgrC and the chimeras by western blot were unsuccessful in this study; thus, it was unclear whether the lack of function was due to poor expression or the inability to respond to the AIP agonist. The activities of the six functional chimeras, AgrC-I::IV, -IV::I, -I::III, -III::I, -III::IV, and -IV::III, were tested (Table 2).[59]

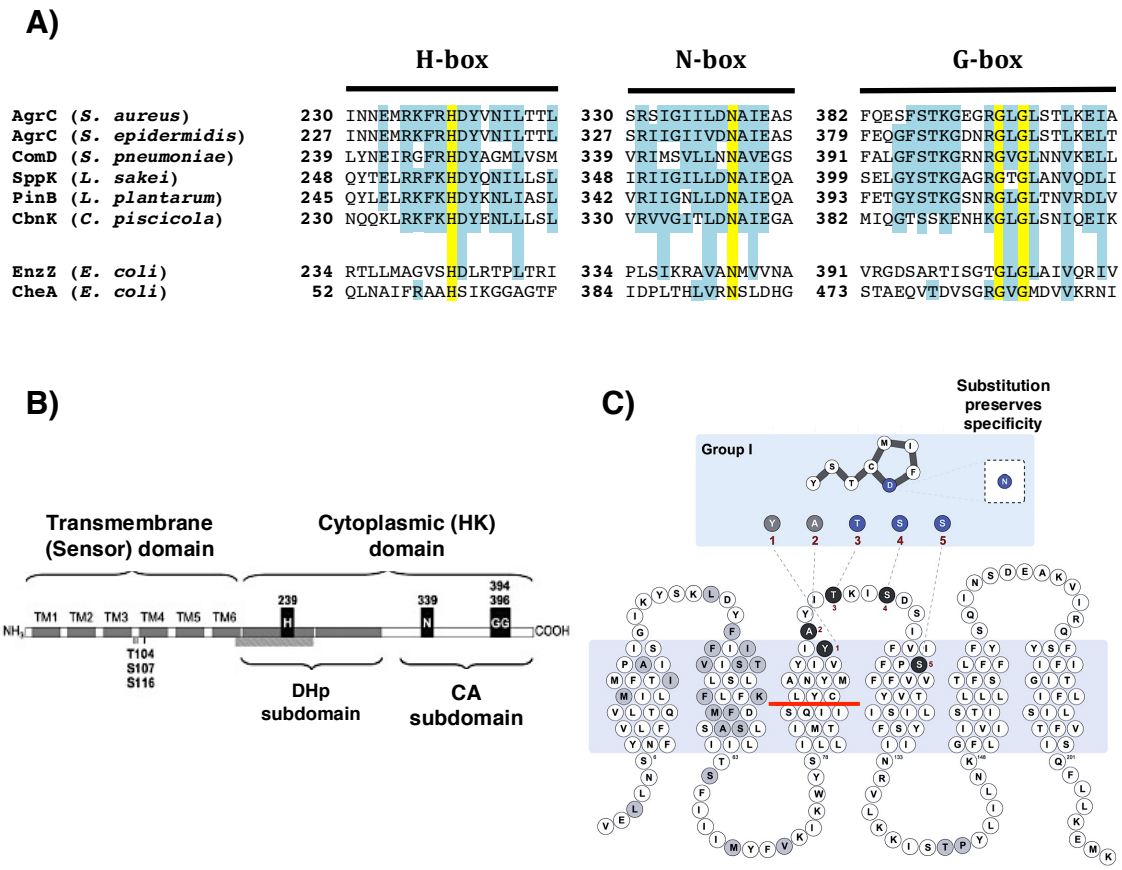

Figure 12. Histidine Protein Kinase Family 10 Alignment and AgrC Domain and Sensor Structure

A) Alignment of three conserved motifs among six HPK_{10} family members and two distantly related HPKs of Gram-negative bacteria.[89] Residues that are identical among all HPKs shown are shaded yellow and other conserved motifs are shaded turquoise. The H-box histidine is the site of phosphorylation, and the N-box and G-box asparagine and glycine residues are important for ATP binding. **B)** The domain structure of AgrC, including the positions of the residues shaded yellow in (A). The hash marks indicate a predicted coiled-coil. The transmembrane topology of AgrC-I is shown,[94] along with three residues important for recognition of AIP-I.[82] **C)** Topology of AgrC-I. The red line in the third transmembrane region represents the splicing junction for chimeras used in the study by Wright *et al*.[59] The shaded residues indicate the amino acid residues that differ with AgrC-IV. Five key residues for group I/IV specificity are highlighted (residues important for AIP-I recognition are shaded blue).[82] This figure is adapted from Geisinger *et al*.,[82] and the topology shown is based on Lina *et al*.[94]

The chimeras of the group I and IV receptors were activated by both AIP-I and -IV and inhibited by AIP-II and truncated AIP-II (trAIP-II), in line with the trends observed with the two native receptors (Table 2). However, AgrC IV::I was activated much more strongly by AIP-I than AIP-IV; whereas, the opposite was true for AgrC-I::IV (Table 2). As previously suggested by Lina *et al*.,[94] this result indicated that the major determinant of AIP recognition is in the distal, C-terminal region of the sensor, at least within *agr* group-I and -IV. In order to find the individual amino acids responsible for ligand specificity in AgrC-I and -IV, Geisinger *et al*. explored the distal, C-terminal region of the AgrC sensor domain.[82] Of the 27 amino acid differences between the AgrC-I and -IV sensor domains, only seven are located in the C-terminal region of interest; and five of those seven are located in or near an extracellular loop close to the splicing junction site, placing them nearly in the center of AgrC (Figure 12C). These five residues of interest in AgrC-IV were systematically replaced with the corresponding amino acids in AgrC-I, and reciprocal mutations were made in AgrC-I. The activities of the resulting constructs showed that the main specificity determinants between AgrC-I and -IV are indeed the five divergent residues in the second extracellular loop, which are residues 100, 101, 104, 107 and 116 (Figure 12C). Systematic mutation of these residues and testing them with synthetic AIPs revealed an interesting trend that indicated some specificity determinants of AgrC-I and -IV for their cognate AIPs. Position five of AIP-I (Asp) and positions 104, 107, and 116 in AgrC-I (Thr, Ser, Ser) are all polar amino acids, while the corresponding positions in AIP-IV (Tyr) and AgrC-IV (Val, Val, Ile) are all nonpolar. Thus, Geisinger *et al*. hypothesized that polar versus nonpolar interactions drive specificity in this case.[82]

Table 2. Activities of AIPs and AIP Derivatives against AgrC Sensor Domain Chimeras

	Activation EC_{50} (nM), (95% CI)					
AIP Derivative	**AgrC-I::IV**	**AgrC-IV::I**	**AgrC-III::I**	**AgrC-III::IV**	**AgrC-I::III**	**AgrC-IV::III**
AIP-I	+ 1220, (1050-1410)	++ 30, (15-45)	+ 1700, (1500-1900)	—	+	++
AIP-II	—	—	—	—	+ 3100	+ 640
AIP-III	—	—	—	—	++ 48	++ 4
AIP-IV	++ 6, (5-7)	++ 120, (110-125)	—	+ 340, (290-410)	++	++
D5A AIP-I	—	—	—	—	++	++
D5N AIP-I	—	+ 440, (350-530)	—	—	++	++
trAIP-II	—	—	—	—	++ 160	++ 50
Linear AIP-I	nt	nt	nt	nt	+ 3100	+ 6700
Linear AIP-II	—	nt	nt	nt	—	+
	Inhibition IC_{50} (nM), (95% CI)					
AIP Derivative	**AgrC-I::IV**	**AgrC-IV::I**	**AgrC-III::I**	**AgrC-III::IV**	**AgrC-I::III**	**AgrC-IV::III**
AIP-I	nt	nt	nt	+	nt	nt
AIP-II	+	+	+	+	nt	nt
AIP-III	—	+	+	+	nt	nt
AIP-IV	nt	nt	+	nt	nt	nt
D5N AIP-I	+	nt	+	+	nt	nt
trAIP-II	+	+	+	+	nt	nt

Chimera notation: AgrC-X::Y, referring to the *agr* group identities of the N-terminal (X) and C-terminal (Y) portions of the sensor domain. Precise EC_{50} and IC_{50} values and 95% confidence intervals are given if known. Number of plus (+) symbols indicates the approximate activity. + = EC_{50} or IC_{50} value >200 nM. ++ = EC_{50} or IC_{50} value <200 nM. nt = not tested. The dash (—) indicates no detectable activity.

The sensor domain chimeras in which the proximal region was derived from AgrC-III followed the trend of the AgrC-I/IV chimeras, but were much less sensitive to activation by the AIPs. For example, AgrC-III::I was activated by AIP-I at concentrations two orders of magnitude higher than that required to activate AgrC-IV::I and was not cross-activated by AIP-IV (Table 2). Similarly, AgrC-III::IV was activated by AIP-IV but not AIP-I or III. More surprising were the results with the AgrC-I::III and -IV::III chimeras. Just as the chimeras described above, they were preferentially responsive to AIP-III; however, both of these chimeras were also strongly activated by many other AIPs (Table 2). These included several potent inhibitors of AgrC-III, such as AIP-I, -II and -IV,[45, 61] and inhibitors of all four *agr* groups, such as D5A AIP-I and trAIP-II.[62, 63] Even linear AIP-I and -II, which are generally inert against AgrC,[45, 61] were found to weakly activate one or both of these chimeras. Moreover, no AIP or AIP derivative tested was an inhibitor of either receptor. While the requirements for activation are typically stricter than those for inhibition, AgrC-I::III and -IV::III are activated by any ligand that can bind. In other words, a distortion within these chimeras bypasses the need for any specific contacts, meaning that they are no longer regulated by group-specific determinants presumed to be responsible for activation of native AgrC receptors. Instead, all that is required for activation is the ability to bind.

It is generally accepted that AIP binding results in trans-autophosphorylation of an AgrC dimer, where an AgrC protomer within the dimer phosphorylates the opposite protomer.[90] Once trans-autophosphorylation occurs, the phosphoryl-group is transferred from AgrC to a conserved aspartate residue in AgrA.[98] Recently, there was direct

evidence of phosphoryl-group transfer from AgrC-I to AgrA. Wang *et al*. were able to purify and incorporate AgrC into nanometer-scale lipid bilayer discs (nanodiscs) for the first biochemical assays of AgrC.[88] Among many of their findings, one interaction they reported was radio-labeled phosphorelay from AgrC-I in nanodiscs and AgrA, when AgrC-I nanodiscs were incubated with AIP-I and [γ-^{32}P]ATP and then AgrA was added. Their results also indicated that AIP binds AgrC in a 2:2 stoichiometry, and they reported a binding constant of 122 nM for AIP-I. More importantly, they elucidated how the AgrC sensor domain transduces the extracellular AIP signal to trigger intracellular kinase activation (Figure 13).[88] The TMH-DHp linker of AgrC has strong helical propensity, so it was hypothesized that AgrC uses helical twisting to autophosphorylate itself. To test this model, a cysteine crosslinking strategy was used to interrogate whether this linker region undergoes conformational changes in the presence of AIP and then trap those conformations by forming a nonnative disulfide linkage. The TMH-DHp region of AgrC-I was shown to rotate in a counter-clockwise fashion in the presence of AIP-I (agonist) and in a clockwise fashion in the presence of AIP-II (inverse agonist).[88] Thus, conformational changes in AgrC lead to autophosphorylation, which enables AgrC to pass the AIP signal further onto AgrA.

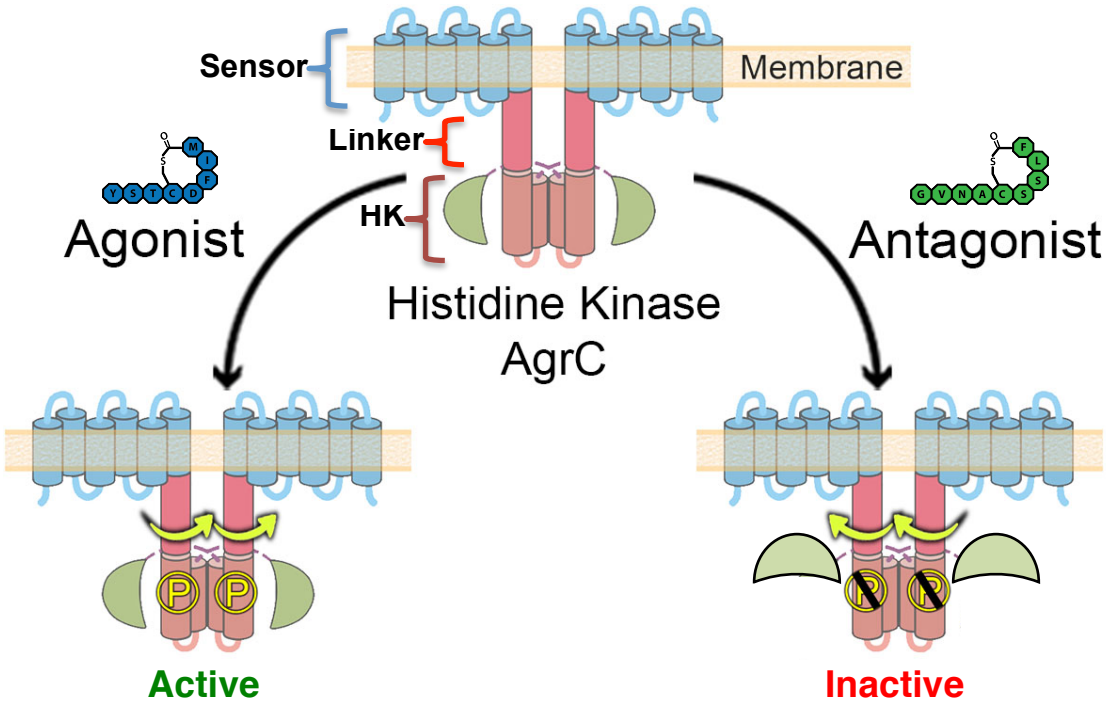

Figure 13. AgrC Signal Transduction Model

This model is adapted from Wang *et al.*[88] When the sensor domain of AgrC interacts with AIP, it induces rotational motion within the linker helix of the DHp subdomain, which connects the sensor domain and the histidine kinase domain. When the AIP is the cognate agonist of AgrC (AIP-I in the model), the linker helix rotates counter-clockwise leading to trans-autophosphorylation of AgrC and an active histidine kinase. In the event that an antagonist or inverse agonist (AIP-II in the model) binds AgrC-I, the linker helix rotates clockwise inhibiting AgrC trans-autophosphorylation and an inactive histidine kinase.

AgrA is the response regulator (RR) of the *agr* TCS system and contains 238 amino acids split into two domains, according to predictions based on homology modeling (Figure 14A).[99] It is a transcriptional regulator belonging to the LytTR family of regulators.[100] The putative phosphorylation site aspartate is in the N-terminal CheY-like receiver domain, which presumably modulates DNA binding by the C-terminal LytTR domain. The majority of RRs bind DNA via helix-turn-helix or winged helix motifs, but RRs of the LytTR family contain a novel fold.[99, 100] A crystal structure of residues 137-238 of AgrA in complex with a 15-base pair DNA duplex showed that it contains a novel 10-stranded β-fold (Figure 14B and C).[100] Residues H169 and R233 make base-specific contacts with DNA, and subsequent mutagenesis confirmed they are essential for DNA binding (Figure 14C). Addition of acetyl phosphate promotes homo-dimerization of AgrA, suggesting that the phosphorylated dimer is the active species; and electrophoretic mobility shift assay (EMSA) experiments with the *agr* P2 promoter indicate AgrA binds as a dimer with high affinity (K_d = 0.16 nM), 24-fold higher compared to un-phosphorylated AgrA (K_d = 3.8 nM).[98] A frameshift mutation in *agrA* resulting in a C-terminal amino acid sequence of KKNIIR instead of KKI causes a delay in RNAIII production and lack of δ-hemolysin activity in *S. aureus* strain RN4220.[101] Possibly, the AgrA C-terminus may be important for homo-dimerization, stability and/or other protein-protein interactions. However, the crystal structure does not provide further clarity or support for such a role of the C-terminal end in AgrA activity.[100, 101] DNaseI footprinting assays of the P2-P3 promoter region demonstrated two regions of protection, both overlapping the AgrA binding site direct repeats previously identified based on consensus LytTR binding sequences. AgrA binds to P2 with higher affinity than the P3

promoter (K_d 0.16 nM vs 1.7 nM).[98] This difference may explain why the P2 promoter is turned on before the P3 promoter when *agr* is activated. Finally, the conformational changes associated with phosphorylation and how they regulate the LytTR domain as well as AgrA's recognition of and interaction with AgrC are yet to be characterized.

1.2.4 RNAIII—the Effector Molecule of *agr*

The primary effector molecule of the *agr* response, RNAIII, acts as both a messenger and antisense RNA to carry out multiple functions.[60] RNAIII is a 514-nucleotide regulatory RNA transcribed from the P3 promoter, which is near the P2 promoter but divergent in its transcribed directionality.[25] The RNAIII secondary structure contains 14 hairpins (Figure 15), including three C-rich hairpins, which is unusual for an AT-rich organism such as *S. aureus*.[102] Near the 5'-end is a region responsible for inducing α-hemolysin toxin translation (*hla*) as well as a region containing the *hld* gene. Closer to the 3'-end are the hairpins (numbers 12-14) involved in negative regulation of translation. The high content of hairpin structures enables RNAIII to have an unusually long half-life of 45 minutes in culture.[103, 104] Nucleotides 85-165 of RNAIII encode the exotoxin δ-hemolysin (*hld* gene), which is a 26 amino acid amphipathic peptide capable of forming pores within cell membranes (Figure 15).[25, 105] A region downstream of the δ-hemolysin gene encoded in the RNAIII transcript regulates its expression; however, the mechanism of regulation is poorly understood.[102, 106] Initially, it was believed that δ-toxin was mediating much of the regulatory effects of *agr* activation. Further analysis revealed it was the mRNA itself that was responsible.[60]

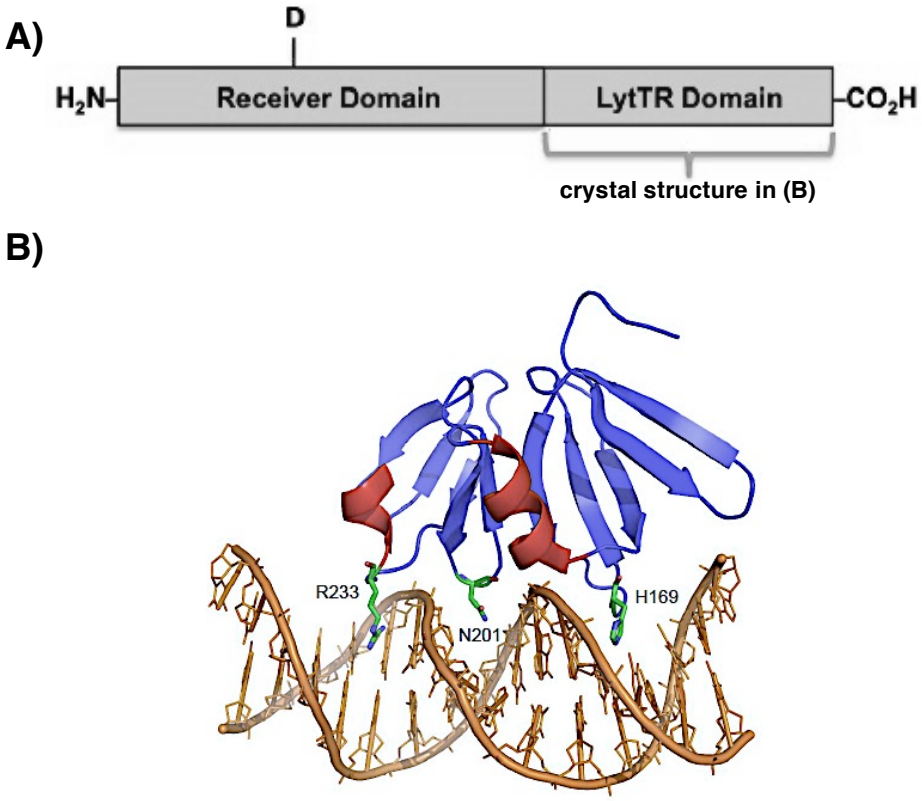

Figure 14. AgrA Domain Structure and LytTR Domain Crystal Structure

A) AgrA domain structure. The N-terminal CheY-like receiver domain is phosphorylated by AgrC, which causes a conformational change in the C-terminal DNA binding LytTR domain. The approximate position of the phosphorylation site aspartate based on sequence alignment is shown (Asp-59 in *S. aureus*). B) The crystal structure of the AgrA LytTR domain in complex with DNA (pdb code 3BS1),[100] demonstrating that AgrA has a novel ten-stranded β-fold arranged into three antiparallel β-sheets. Three key residues that interact with DNA are indicated. The β-strands are colored blue, and helices are colored red.

RNAIII regulates gene expression at the translational level by base pairing with the mRNA of numerous virulence genes as well as the Rot transcriptional regulator. RNAIII promotes translation by relieving RNAI hairpins and making a ribosome binding site (RBS) available as it does with α-hemolysin toxin.[48] Conversely, RNAIII inhibits protein translation by antisense pairing with mRNA 5' untranslated regions, often overlapping the RBS, or forming double-stranded mRNA structures unrecognizable by the translation initiation complex.[53, 103, 107-109] Formation of double-stranded RNAs has the dual effect of creating a substrate for RNase III which will cleave the targeted mRNA to remove the RBS and decrease the half-life of the mRNA.[47, 49] Inhibition of Rot translation also leads to large changes in gene regulation, resulting in upregulation of secreted virulence factors and downregulation of surface proteins.[52] Through these mechanisms RNAIII positively or negatively regulates the expression of numerous virulence factors at multiple levels (Table 3).

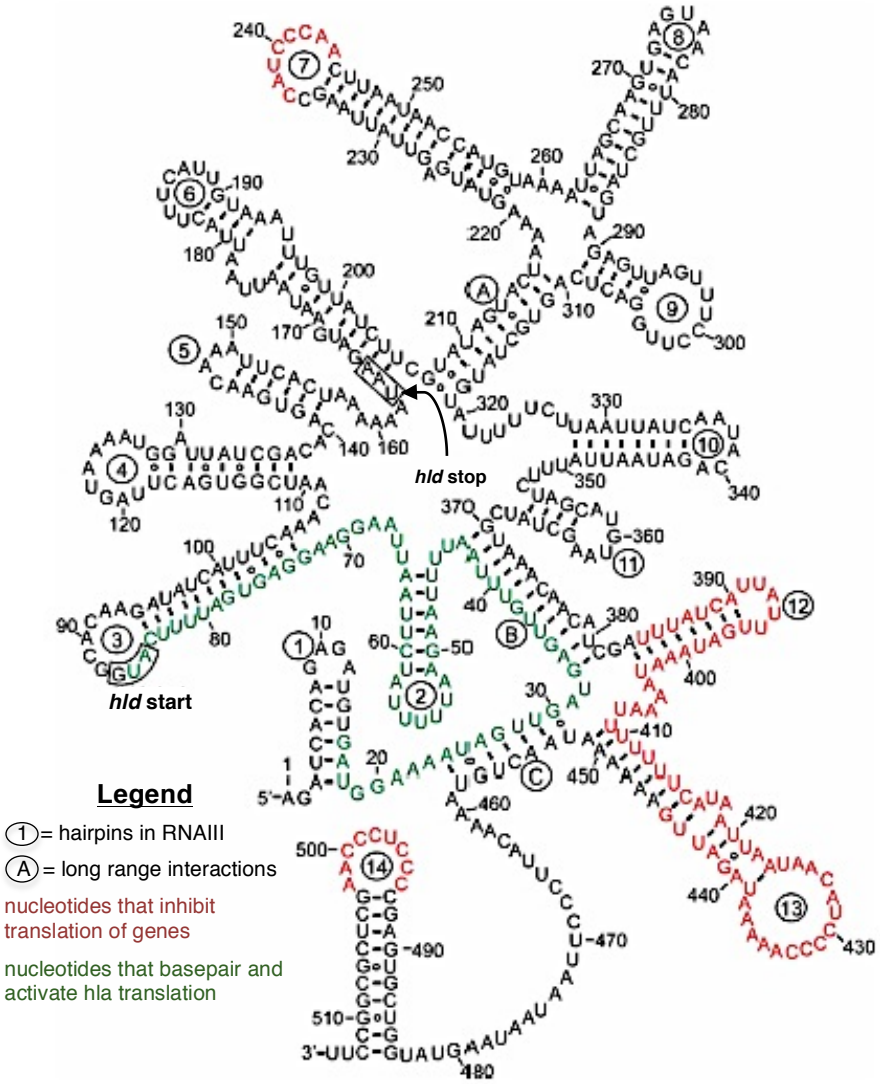

Figure 15. RNAIII Structure

Secondary structure of *S. aureus* RNAIII—the 514 nucleotide RNA that is the *agr* effector molecule.[95] RNAIII hairpins are designated with circled numbers while circled letters signify long-range interactions that establish general domains. The RNA sequence for *hld*—the δ-hemolysin toxin encoded in RNAIII— is indicated by the boxed start and stop codons within the structure. Nucleotides that basepair with and activate *hla* translation are colored green. Nucleotides demonstrated to inhibit translation of genes are red. This figure is an adaptation from Benito *et al*.[102]

Table 3. Genes regulated by *agr*

Genes upregulated by *agr*				
Gene	**Product**	**Function**	**Note**	**Reference**
Secreted Enzymes				
splA-F	Spl proteases	Serine proteases	C	[110]
sspA	V8 Protease	Serine protease	C	[111, 112]
aur	Aureolysin	Metalloprotease	C	[111, 112]
sspB	Ssp Protease	Cysteine protease	C	[111]
scpA	Staphopain	Cysteine protease	C	[111]
lip	Lipase	Fatty acid breakdown	C	
geh	Glycerol ester hydrolase	Fatty acid breakdown	C	
sak	Staphylokinase	Plasminogen activator	C	[30]
ureA-G	Urease	Urea neutralization	C	
plc	PI-Phospholipase-C	Phosphatidyl-inositol hydrolase	C	[113]
fme	Fatty acid modifying enzyme	Bactericidial fatty acid neutralization	C	[114]
Toxins				
hla	Alpha-toxin	Cytolysin, pore forming	A	[30, 60, 107]
hlb	Beta-hemolysin	Cytolysin, sphingomyelinase	C	[30]
hld	Delta-toxin	Cytolysin, pore forming	B	[30, 115]
hlgBC	Gamma-hemolysin	Cytolysin, two-component pore forming	C	[116]
lukD/E	Leukocidin	Cytolysin, two-component pore forming	C	[116]
lukS/F	Panton-Valentine leukocidin	Cytolysin, two-component pore forming	C	[116]
lukG/H	Leukocidin	Cytolysin, two-component pore forming	C	
tst	Toxic Shock Syndrome Toxin-1	Superantigen	C	[30]
seb	Enterotoxin B	Superantigen	C	[117, 118]
sec	Enterotoxin C	Superantigen	C	[119]
sed	Enterotoxin D	Superantigen	C	[120]
etaAB	Exfoliative toxins	Desmoglein cleavage (Scalded-skin syndrome)	C	[121, 122]
Other				
PSMα1-4	Alpha PSMs	Cytolysin, PMN chemotaxis, inflammatory	B	[123]
PSMβ1-2	Beta PSMs	Inflammatory	B	[123]
arcR	Transcriptional regulator	Arginine catabolism regulation	C	
rsaE	RsaE sRNA	Gene regulation	C	[124]
cap5	Polysaccharide capsule type 5	Antiphagocytic	C	[125]
cap8	Polysaccharide capsule type 8	Antiphagocytic	C	[126]
pmtA-D	Components for PSM transport	ABC transporter	B	
Genes downregulated by *agr*				
Gene	**Product**	**Function**	**Note**	**Reference**
Surface Proteins				
fnbAB	Fibronectin Binding Proteins A/B	Fibrinogen and fibronectin adhesion	A	[127]
spa	Protein A	Antibody Fc-region binding	A	[30, 60, 103]
coa	Coagulase	Plasminogen to plasmin conversion	A	[109, 128]
SA1000	Surface Protein	Fibrinogen and fibronectin adhesion	A	[108]
Other				
ssl5,8	Staphylococcal superantigen-like proteins 5 and 8	Ssl5 inhibits PMN adherence	C	[129]
rot	Repressor of toxins transcription factor	Gene regulation	A	[53, 108]

Note:

A. Post-transcriptional regulation by RNAIII.

B. Direct regulation by the AgrA transcriptional regulator

C. *agr* regulation has been demonstrated by microarray[52, 123, 130, 131] or proteomic[132] studies.

1.3 Specific Aims

Outlined below are the specific aims of the thesis project, which in part were originally submitted in November 2010. Progress toward each of these aims is reported herein.

AIM 1. Identifying the components necessary for secreting *S. aureus* AIPs

AgrD is a membrane-associated polypeptide that undergoes two proteolytic cleavage steps to release a mature AIP. While it has been shown that AgrB performs the first cleavage step to remove the SID of AgrD and form the thiolactone ring of the AIP, the role of AgrB during the secretion process is unknown. We will use intein protein chemistry in *agr* null *S. aureus* cells to express several AIP precursors and replace the known function of AgrB to investigate the role of AgrB in secreting AIP.

AIM 2. Secreting the AIP precursor across the *S. aureus* plasma membrane

As the precursor to AIP, AgrD has a unique, module-like design, which seems poised to enable AIP secretion through a series of processing events that alter its interaction with the bacterial membrane. Physicochemical, biophysical and mutational studies of AIP and AgrD will help test a hypothesized secretion mechanism.

AIM 3. Elucidating the final cleavage step to release the AIP

The final step in the AIP biosynthetic pathway is cleavage of the MAD of AgrD releasing AIP into the extracellular environment. SpsB, a type-I signal peptidase, is believed to catalyze this cleavage event, although it has only been shown to cleave an AgrD-I derived peptide. Further biochemical analysis will try to confirm the role of SpsB in AIP biosynthesis among the four *S. aureus agr* specificity groups.

AIM 4. The effect of enlarging the AIP thiolactone macrocycle on AgrC

No SAR study of AIP has investigated the effect of AIP macrocycle size on *agr* activation or inhibition. AIP-I will be used as a scaffold to investigate the effect of increasing or decreasing the size of the AIP thiolactone macrocycle on *agr* activation.

Chapter 2. The Final Steps in AIP Biosynthesis: Secreting the AgrD(1-32)-Thiolactone

2.1 Introduction

Progress towards elucidating the mechanism of AIP biosynthesis has preceded slowly since the initial 1995 report that AgrB is involved in AIP processing.[31] AIP production requires three chemical transformations of AgrD: two proteolytic cleavage steps and thiolactone formation. Research has shown that AgrB is responsible for the first cleavage step in AIP biosynthesis,[56, 57, 70-72] which removes the SID of AgrD and forms the thiolactone macrocycle of the AgrD(1-32)-thiolactone (Figures 6 and 7). AgrB accomplishes this step as a cysteinyl endopeptidase forming an acyl-enzyme thioester intermediate between AgrB and AgrD, which undergoes trans-thioesterification with the conserved sulfhydryl group of Cys-28 in AgrD to form the new thiolactone macrocycle of the AgrD(1-32)-thiolactone (Figure 7).[57, 70, 72] These steps prepare the AIP sequence of AgrD for externalization and its final chemical transformation.

The secretion mechanism of the partially processed AgrD protein is not understood. One reason AIP secretion is poorly understood involves a general uncertainty about which secretion system the cell uses. While AgrD does not have a classical signal peptide as seen in proteins meant for the Sec, Tat or Com secretion systems, it does have one element of a Sec-type signal peptide: a type I signal peptidase cleavage site (Figure 5C), which would suggest SpsB is the second enzyme involved in *S. aureus* AIP biosynthesis.[58, 73, 133] Still, AgrD does not share other common, structural elements of a protein secreted through the Sec pathway (Figure 5).[65, 133] Lacking any

clear evidence for a secretion pathway, it has been proposed that AgrB not only processes AgrD but also facilitates AgrD's partitioning into the membrane.[56-58, 72] However, AgrB is a small membrane protein (23 kDa) and has no known homology with any type of bacterial transporter.[56] Furthermore, there is no clear published evidence that AgrB forms higher order oligomers in order to form some type of pore—only dimers have been observed *in vitro*.[72] Most recently, Thoendel *et al*.[72] reported several mutants of AgrB that could cleave AgrD but did not lead to AIP production. These mutations were in the lysine patch of AgrB (K129, K130 and K131), and when any of these three residues were mutated to glutamate, AIP secretion was not observed. However, their data cannot conclusively determine whether these AgrB mutants inhibit AIP secretion or instead promote hydrolysis of the acyl-enzyme thioester intermediate, which would not produce mature AIP and explain the observed AgrB cleavage of AgrD. Clearly, there is the need for an investigation of the role, if any, of AgrB in AIP secretion.

Herein, we describe our efforts to better understand the secretion step of AIP biosynthesis. While we suspect that AgrB is not involved in secretion, there is no definitive evidence for or against AgrB facilitating transport of the AgrD(1-32)-thiolactone across the cellular membrane. We, therefore, engineered strains of *S. aureus* cells that are *agr*$^{-}$ and express an AgrD(1-32)-intein fusion protein. These cells can express the AgrD(1-32)-I-thiolactone using an intein-mediated thioester intermediate, which is independent of AgrB-I. The production of AIP by this new *S. aureus* strain was characterized using a modified version of the rapid, quantitative *agrP3::blaZ* reporter assay previously used to investigate the SAR between AIP and AgrC.[31, 45, 59, 62, 63, 79-83] We

also re-introduce AgrB into this new *S. aureus* background to examine the effect AgrB may have on AIP secretion and production.

2.2 The role of AgrB in AIP Secretion

2.2.1 Engineering the AgrD(1-32)-intein Fusion Protein for Expression in *S. aureus* Cells

Investigating the role of AgrB in AIP secretion is challenging due to the requirement of the enzyme in the first step of AIP biosynthesis. Thus, simply deleting AgrB would eliminate AgrD(1-32)-thiolactone production, precluding any studies on secretion of this molecule. In principle, producing AgrD(1-32)-I-thiolactone in an AgrB-independent fashion would make it possible to test whether AgrB is necessary for AIP secretion. To our knowledge, no other staphylococcal protein catalyzes the formation of such a cyclic peptide, so there is not another biosynthetic pathway to exploit and replace the enzymatic role of AgrB. Instead, we chose to replace the catalytic activity of AgrB using intein protein chemistry. Inteins are protein autoprocessing domains that catalyze protein-splicing events.[134, 135] Their reaction mechanism is well characterized and involves a thioester intermediate (Figure 16). In fact, Camarero *et al*. used an intein to mediate the cyclization of an SH3 protein domain in *E. coli* cells that was biologically active and adopted the native SH3 fold.[136] Initially, we tried using the same *Mxe* GyrA intein used by Camarero *et al*. to produce the AgrD(1-32)-I-thiolactone in *S. aureus* cells with a C-terminal thiolactone macrocycle. However, AIP production was not detected using a multistage MALDI-MS method developed to detect AIP molecules from cell culture medium without a liquid chromatography step.[137] Furthermore, intein-mediated cleavage

was undetectable in cell lysates using SDS-PAGE and Western blot analysis (data not shown). We suspected the slow splicing rate of the *Mxe* GyrA intein (~24 hrs) might be the problem, and as such turned our attention to a newly discovered group of inteins with ultrafast splicing kinetics.[138] These ultrafast protein splicing inteins belong to a subfamily of split inteins, where the intein exists as two separate protein domains that splice *in trans* instead of *in cis*. The split intein splicing event follows a similar mechanism for protein splicing (Figure 16), except that the first step is a binding interaction between the N- and C-inteins. Shah *et al*. characterized a modified set of split inteins that were fused together to provide a biochemical tool for generating protein α-thioester derivatives for such things as expressed protein ligation (EPL).[138] These new artificially fused split inteins have splicing rates within a few minutes as opposed to several hours for the *Mxe* GyrA intein.

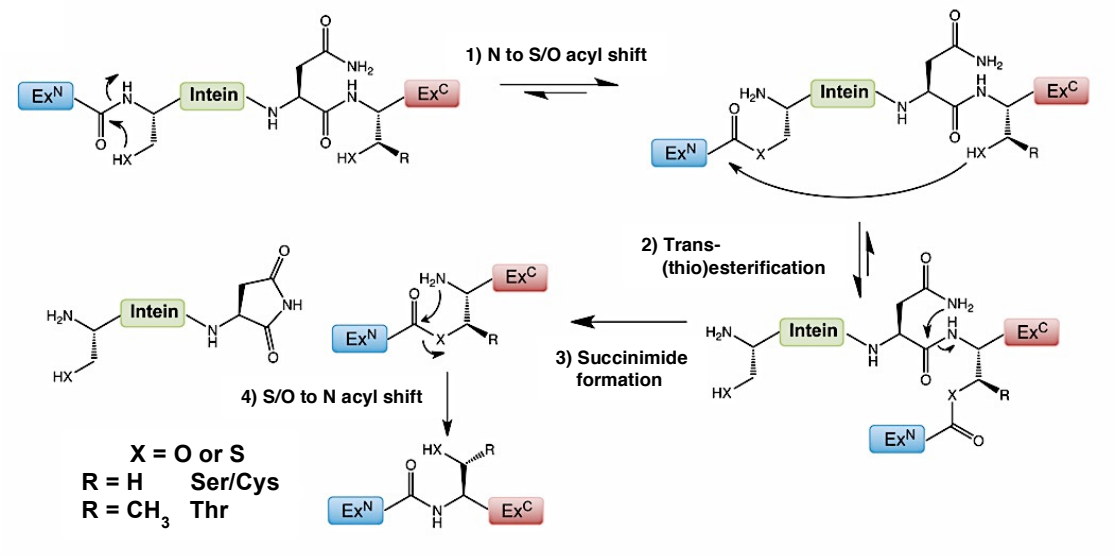

Figure 16. Intein-mediated Protein Splicing

The chemical mechanism of protein splicing using an intein is schematized. Cys-1 of the intein domain mediates an N to S acyl shift in the C-terminal residue of the N-extein. A flanking Cys residue at the C-terminal end of the intein then attacks the branched intermediate to transfer the N-extein domain near the C-extein domain via trans-thioesterification. Then, an Asn residue at the -1 positon in relation to the C-terminal Cys mediates succinimide formation, removing the intein and leaving the N-extein linked to the C-extein via a thioester bond. Finally, the thioester linkage connecting the N- and C-exteins undergoes an S to N acyl shift to form a stable amide bond within the new protein. This figure is adapted from Vila-Perello *et al*.[134]

We decided to use the fused Npu split intein (intein^{Npu}) described by Shah *et al.* [138] along with a fused Ssp split intein (intein^{Ssp}). The latter was added because it had previously been used to carry out EPL in cells.[139] In the EPL mechanism, an intein generates a recombinant protein α-thioester if the Cys residue at the C-terminal end of the intein is mutated to Ala, which traps the branched thioester intermediate formed after the first N to S acyl shift in the intein reaction mechanism (Figure 16, step 1). An exogenous thiol can then be added to release a protein α-thioester derivative. In the fused split intein constructs, the C-terminal end of the intein was mutated from CFN to AFN, and there is also a C-terminal His_6-tag for purification and/or analysis purposes. For our purposes, the sulfhydryl group of Cys-28 in AgrD is expected to attack the branched thioester intermediate formed between the fused split intein and the N-terminus of AgrD, forming the AgrD(1-32)-I-thiolactone (Figure 17A). We engineered plasmids from a shuttle vector system that contain either the gene for AgrD(1-32)-intein^{Npu} or AgrD(1-32)-intein^{Ssp} under a cadmium-inducible promoter.[140] These plasmids were incorporated into *agr-I*$^{-}$*/spa*$^{-}$ *S. aureus* cells (RN10306) for expression. We also engineered strains of *S. aureus* that only expressed the intein^{Npu} or intein^{Ssp} proteins, respectively (Figure 17B). Finally, we engineered strains of *S. aureus* that express catalytically inactive inteins by mutating the catalytic Cys to Ala, which is the 33rd residue in both of the AgrD(1-32)-intein constructs (Figure 17B). These strains, therefore, express either C33A AgrD(1-32)-intein^{Npu} or C33A AgrD(1-32)-intein^{Ssp} fusion proteins. (See *Chapter 6* for a list of all plasmids and *S. aureus* strains used and engineered.)

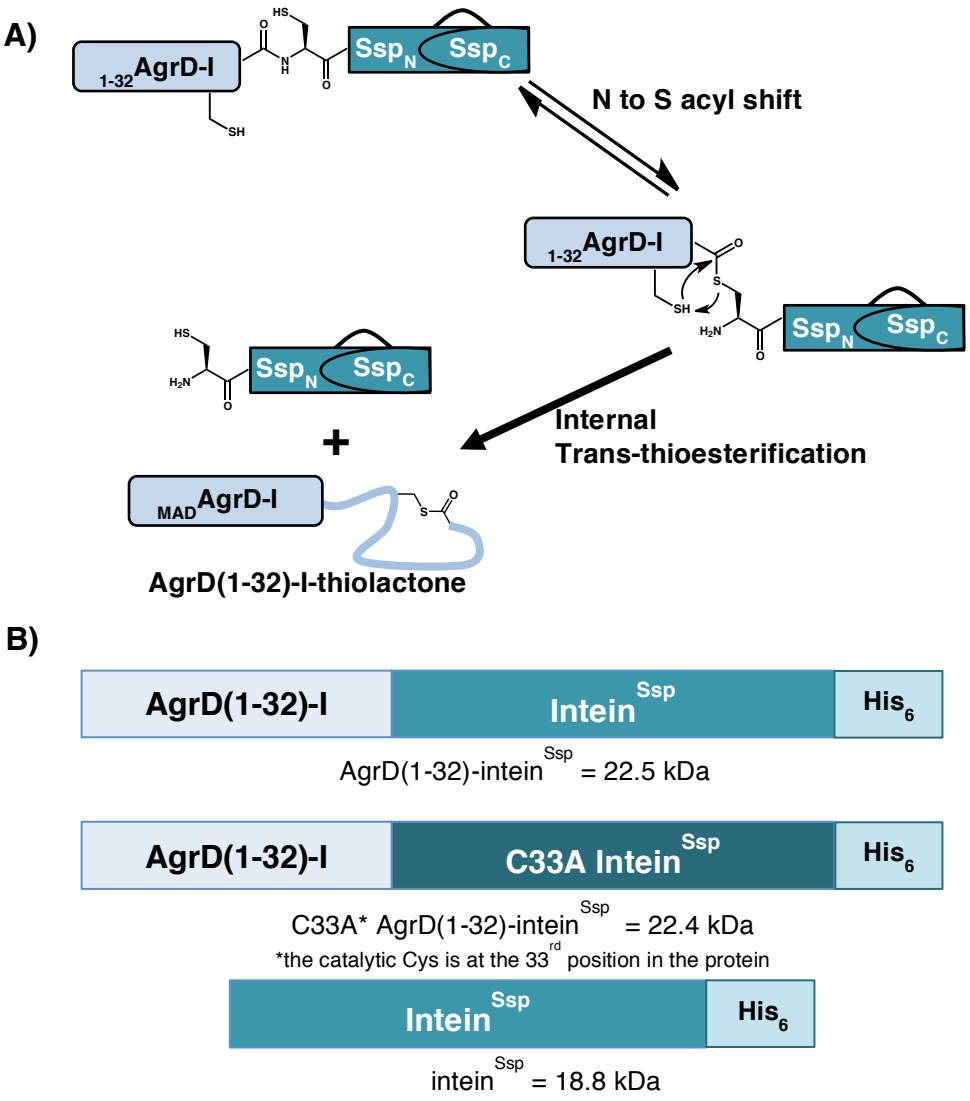

Figure 17. Generation of the AgrD(1-32)-I-thiolactone *in vivo* using a Fused Split Intein System

A) The intein-mediated *in vivo* cyclization mechanism to form the AgrD(1-32)-I-thiolactone. Like the intein splicing mechanism, the cyclization mechanism requires an N to S acyl shift within the full-length protein, which is mediated by the Cys-1 of the fused split intein domain. Divergent from intein splicing, however, the thioester intermediate undergoes trans-thioesterification with the sulfhydryl group of the conserved Cys in AIP, Cys-28 of the AgrD(1-32)-I domain. **B)** Schematics for the full-length intein^{Ssp}-containing constructs. Note the naming convention for C33A AgrD(1-32)-I-intein^{Ssp}, which indicates the point mutation in the construct is for the catalytic Cys residue of intein^{Ssp}. AgrD(1-32)-Intein^{Npu} constructs are similarly designed.

2.2.2 Expression and Characterization of the AgrD(1-32)-I-intein^{Npu} and AgrD(1-32)-intein^{Ssp} Expressing *S. aureus* Cells

To follow the intein-mediated cyclization reaction, we analyzed whole cell lysates of cells expressing AgrD(1-32)-I-intein^{Npu} and AgrD(1-32)-I-intein^{Ssp} over a 6-hour induced growth timespan with SDS-PAGE and Western blot. Using the AgrD(1-32)-I-intein^{Ssp} whole cell lysates as an example (Figure 18), the Western blot analysis detected the C-terminal His_6-tag of the intein^{Ssp} construct. Within two hours of cadmium induction, Western blot analysis detects the full-length AgrD(1-32)-I-intein^{Ssp} construct (Figure 18, lane 2). By four and six hours of induced growth, expression of the full-length construct continues and the appearance of only the intein^{Ssp} domain occurs (Figure 18, lanes 3 and 4), suggesting that a portion of the full-length AgrD(1-32)-I-intein^{Ssp} protein is lost presumably through the cyclization of the D_{1-32} domain. The uninduced AgrD(1-32)-I-intein^{Ssp} cells do not contain either of these proteins (Figure 18, lane 1). Furthermore, the inactive split intein *S. aureus* strain (C33A AgrD(1-32)-I-intein^{Ssp}) only expresses a full-length construct (Figure 18, land 5), which is expected; and the cells expressing only intein^{Ssp} are provided as a marker for the protein that accumulates over time in the Western blot analysis (Figure 18, lane 7). The cells expressing AgrD(1-32)-I-intein^{Npu} or the intein^{Npu} construct behaved similarly to the AgrD(1-32)-I-intein^{Ssp} constructs (data not shown). From this analysis, the AgrD(1-32)-I-intein expressing cells could produce the AgrD(1-32)-I-thiolactone in the absence of AgrB.

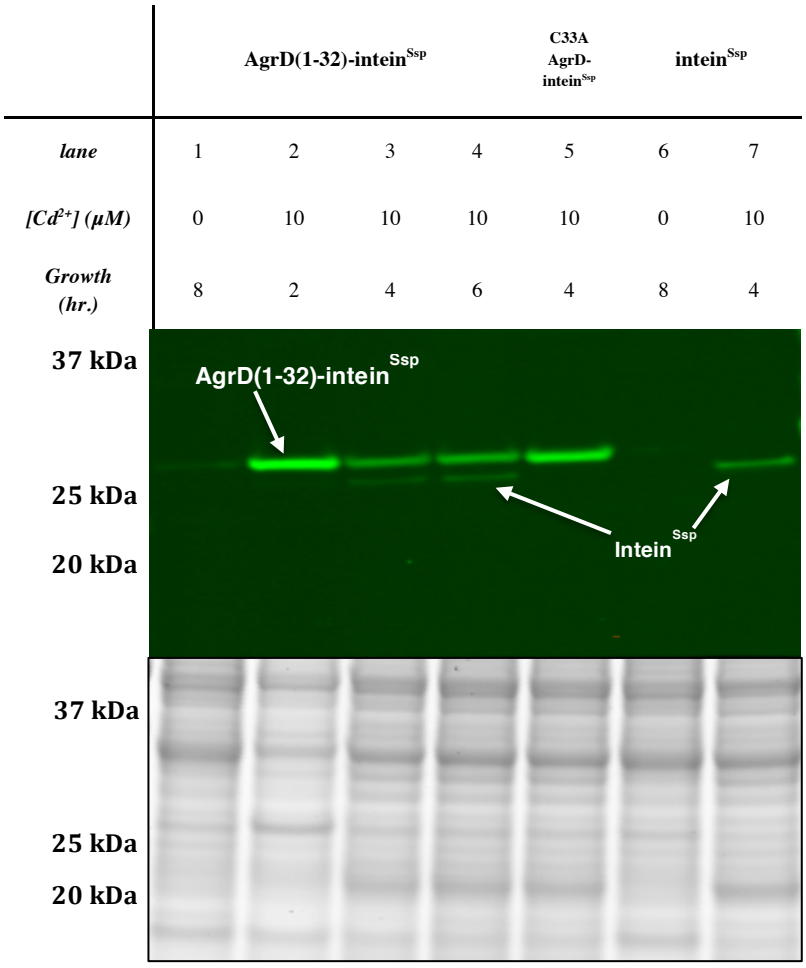

Figure 18. Western Blot Analysis of the AgrD(1-32)-intein^{Ssp} Expressing Cells

Western blot analysis of whole cell lysates from AgrD(1-32)-intein^{Ssp} over a 6-hr. Cd^{2+}-induced expression is shown (middle, lanes 1-4). Whole cell lysates from Cd^{2+}-induced C33A AgrD(1-32)-intein^{Ssp} and intein^{Ssp} expressing cells are also included (lanes 5 and 7, respectively). Since it has a low molecular weight and has no epitope tag, detection of the AgrD(1-32)-thiolactone is prohibited. Following SDS-PAGE, the proteins were transferred to a nitrocellulose membrane and probed with an Anti-His antibody. The membrane was imaged with a LI-COR Odyssey Infrared Imager. As a loading control, SDS-PAGE analysis of the cell cultures is also provided (bottom). The 12% Bis-Tris gel was stained by coomassie and imaged. Relevant molecular weight markers are indicated.

While a tagless AgrD(1-32) domain in AgrD(1-32)-intein constructs might produce the most biologically relevant molecule, it also makes detection of the AgrD(1-32)-thiolactone difficult because of its low molecular weight and lack of epitope tag. Thus, the Western blot analysis of AgrD(1-32)-intein^{Ssp} (Figure 18) does not provide any evidence for the AgrD(1-32) domain or its presumed thiolactone macrocycle, which is essential for AIP activity. It can only suggest that intein-mediated cleavage has occurred. After trying several different techniques, we used HPLC-MS to detect AIP-I from sterile-filtered cell culture supernatants of AgrD(1-32)-intein^{Npu} and AgrD(1-32)-intein^{Ssp} (Figure 19). This HPLC-MS analysis provides direct evidence that the cells expressing either AgrD(1-32)-intein constructs can produce mature AIP-I in the absence of AgrB.

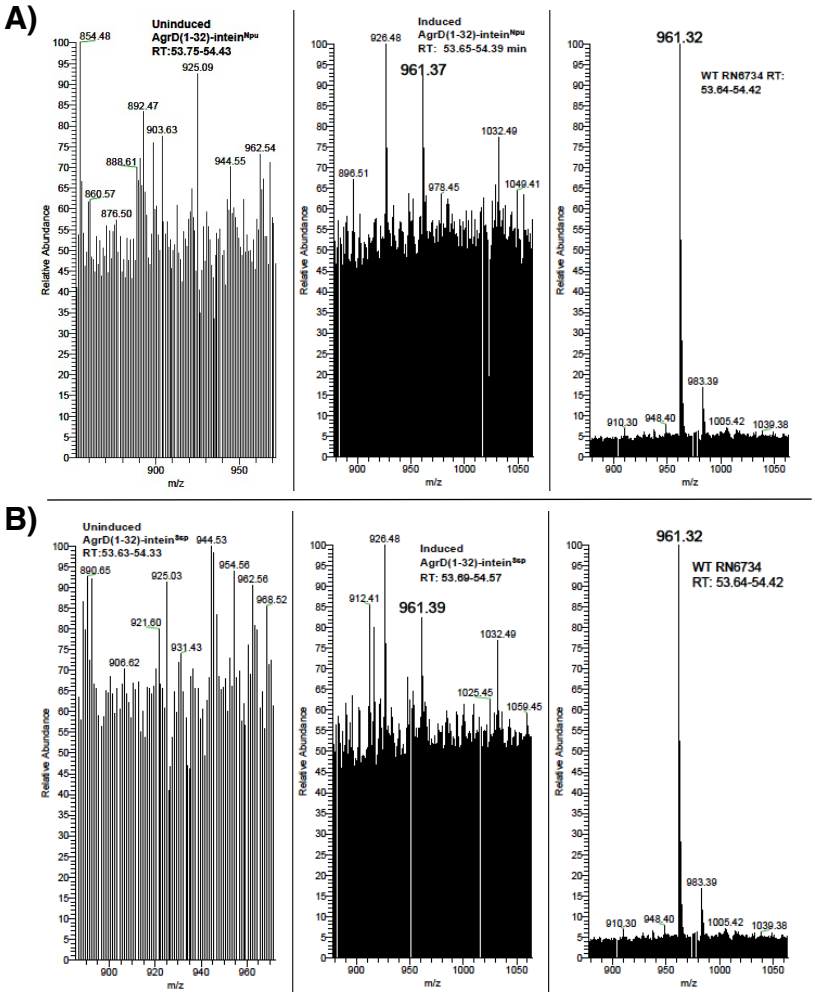

Figure 19. HPLC-MS Detection of AIP-I from AgrD(1-32)-intein Expressing Cells

A) HPLC-MS analysis of cell culture supernatants from uninduced (top left) and induced (top middle) cells expressing AgrD(1-32)-intein^{Npu} and the wild-type (WT) group I cells (RN6734, top right). The MS chromatograms were taken from similar retention times during the HPLC gradient. The AgrD(1-32)-intein^{Npu} cells secrete a small molecule with a very similar molecular weight (961.37) as AIP-I in wild-type *S. aureus* cells (961.32). **B)** HPLC-MS analysis of cell culture supernatants from uninduced (bottom left) and induced (bottom middle) cells expressing AgrD(1-32)-intein^{Ssp} and wild-type (WT) group I cells (RN6734, top right). MS chromatograms were prepared as in A, and similarly, AgrD(1-32)-intein^{Ssp} cells secrete a small molecule with a similar molecular weight (961.39) as AIP-I in RN6734 cells (961.32).

2.2.3 Cell Culture Supernatants from Cells Expressing AgrD(1-32)-intein Constructs Stimulate the TCS of *agr-I*

Having detected AIP-I from cells expressing the AgrD(1-32)-intein constructs, we wanted to further investigate their cell culture supernatants in a biological context. From our HPLC-MS analysis (Figure 19), we knew that the concentration of AIP-I was likely low (low nanomolar) in the culture supernatants, because of the low intensity of the signal. With a low concentration of AIP in the culture, any biochemical tool used to analyze the cell culture supernatants would require some AIP signal amplification. Therefore, we turned to the workhorse tool of AIP detection: the β-lactamase reporter assay, which reports on signal transduction through the entire *agr* TCS and has been used extensively for assessing AIP activity.[45, 62, 63, 80, 83, 87] It also amplifies the AIP signal by inducing expression of β-lactamase that can be monitored using a colorimetric readout like hydrolysis of nitrocefin, a β-lactam, which changes colors upon cleavage (See Appendix). Using this assay, we monitored and reported the change in OD_{490} normalized to cell density (OD_{650}) as a way to measure β-lactamase activity (Figure 20A). We observed elevated levels of β-lactamase activity in cell culture supernatants of the induced AgrD(1-32)-intein^{Npu} cells and AgrD(1-32)-intein^{Ssp} cells relative to uninduced AgrD(1-32)-intein cell culture supernatants (Figure 20A). Since expression of the AgrD(1-32)-intein^{Npu} and AgrD(1-32)-intein^{Ssp} proteins requires cadmium-induction, we also monitored the growth of the β-lactamase reporter gene assay cells to make sure the cadmium did not inhibit their growth (Figure 20B). A wild-type *agr-I* cell (RN6734) culture supernatant is included to show that the assay cells respond to a known source of AIP-I agonist.

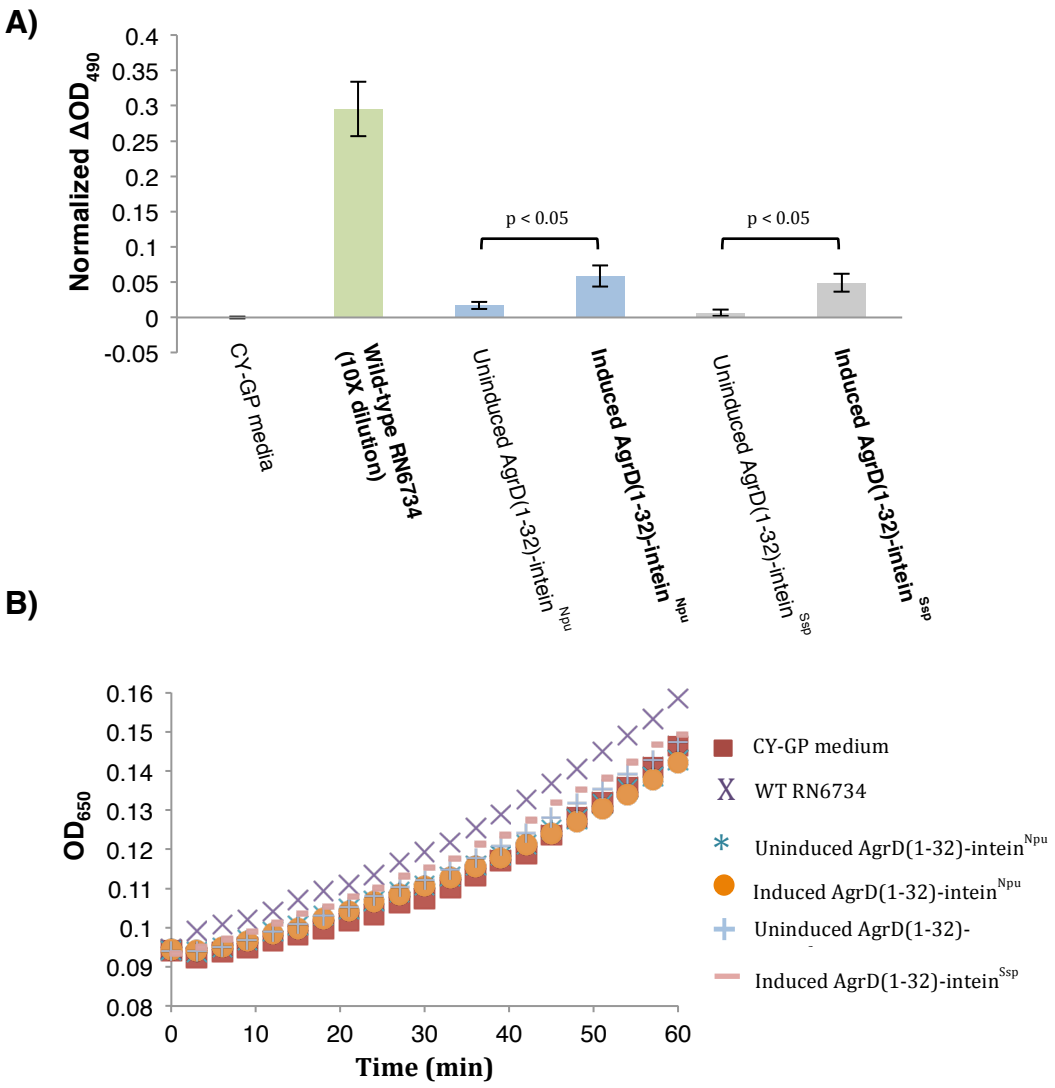

Figure 20. Biological Activity of the AgrD(1-32)-intein Cell Culture Supernatants

A) β-lactamase activity assay of cell culture supernatants from cells expressing either AgrD(1-32)-intein^{Npu} or AgrD(1-32)-intein^{Ssp} is plotted. Filtered cell culture supernatants were incubated with an exponential phase culture of group I *S. aureus* reporter strain (RN9222). Samples were removed after 60 minutes and assayed for β-lactamase activity by the nitrocefin method. After normalizing OD_{490} readings with cell density, ΔOD_{490} was calculated by subtracting an intial OD_{490} reading from the endpoint OD_{490} reading. The plot is relative to the CY-GP media normalized to zero. Errors; SD, n = 3. Important p-values are indicated with a bracket and the numerical p-value above. **B)** Monitored growth of Group I *S. aureus* reporter strain (RN9222) in the presence of cell culture supernatants presented in A. Cellular growth is plotted as raw OD_{650} readings over time.

In addition to stimulating AgrC-I and thereby β-lactamase activity, we also sought to inhibit AgrC-I activation. Previous work identified D5A AIP-I as a self-inhibitor of AgrC-I, making it a global antagonist of *agr*.[63, 80] We engineered another set of AgrD(1-32)-intein constructs with a point mutation in the AgrD(1-32) domain, changing the AIP sequence from the wild-type to the D5A AIP-I sequence (Asp-29 in the AgrD(1-32) domain). We again incorporated these constructs into *S. aureus* cells and confirmed their expression with Western blot analysis (data not shown). We then tested the D29A AgrD(1-32)-intein cell culture supernatants with the β-lactamase reporter assay (Figure 21). The D29A point mutation in the AgrD(1-32) domain abolishes β-lactamase activity in the reporter assay. We also tested the cell strains that express the catalytically inactive intein constructs, C33A AgrD(1-32)-intein^{Npu} and C33A AgrD(1-32)-intein^{Ssp}. These constructs also do not stimulate AgrC-I, as measured by β-lactamase activity. Finally, we tested the pure AgrD(1-32)-I-thiolactone (150 nM) in the growth medium to determine if it could activate the reporter gene assay cells. (AgrD(1-32)-I-thiolactone was recombinantly expressed in *E. coli* and purified by Boyuan Wang, a graduate student in the lab, who provided a small amount for this experiment.) Importantly, there was little measureable β-lactamase activity induced by the AgrD(1-32)-I-thiolactone when incubated with cells for the 60-min assay. Combining all of these observations, the cells expressing AgrD(1-32)-intein^{Npu} and AgrD(1-32)-intein^{Ssp} are producing the mature AIP-I molecule.

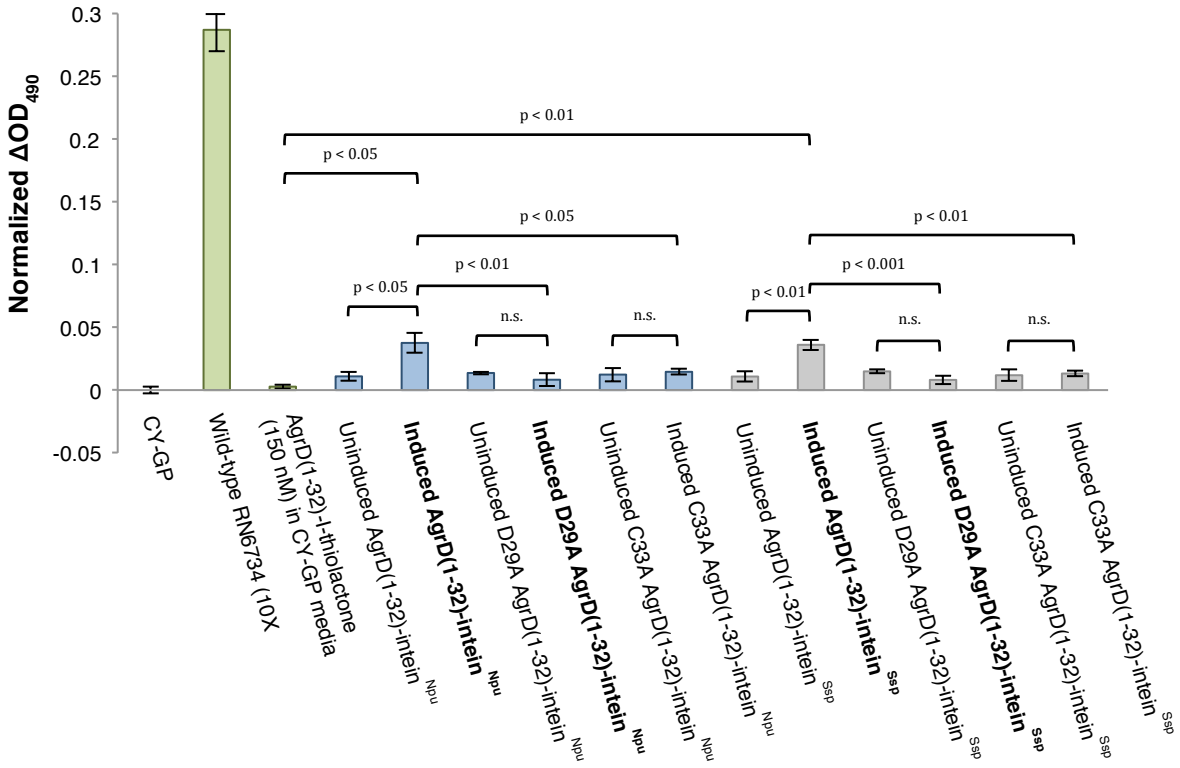

Figure 21. Cell Culture Supernatants from the D29A AgrD(1-32)-intein Expressing Cells Inhibit AIP-induced β-lactamase Activity

β-lactamase activity assay of cell culture supernatants from cells expressing the D29A AgrD(1-32)-intein constructs is plotted. Filtered cell culture supernatants from the indicated strain were incubated with an exponential phase culture of group I *S. aureus* reporter strain (RN9222). Samples were removed after 60 minutes and assayed for β-lactamase activity by the nitrocefin method. Normalized ΔOD_{490} was calculated the same as in Figure 20A. The plot is relative to the CY-GP media normalized to zero. Errors; SD, n = 3. Important p-values are indicated with a bracket and the numerical p-value above.

2.2.4 AIP-induced β-lactamase Activity is Not the Result of Cell Lysis

While *in vivo* AIP-I production in the absence of AgrB is remarkable, there is no evidence that the AIP being produced was actually secreted. It is possible that cell lysis during induced growth could release the AgrD(1-32)-I-thiolactone, AgrD(1-32)-intein^{Npu} or AgrD(1-32)-intein^{Ssp} proteins into the growth medium, where SpsB could process the AIP precursor at the outer membrane leaflet. Thus, AIP activation could result from a non-secretion pathway. To investigate whether AIP activation of AgrC results from cellular lysis, we designed a real-time assay to lyse cells and then test those cell culture lysates with the β-lactamase reporter assay. The assay involved lysing cells in the culture media via a bead-beating method. Briefly, at a certain timepoint (~5 hrs. after induction), half the cell culture was added to sterilized beads and vortexed for 10 mins. Upon bead removal, the resulting cell lysate in the growth medium was added back to the cell culture for a 30-min. incubation at 37°C to allow the possible processing of the AIP precursor by the remaining whole cells. Using this cell lysis assay, we could lyse ~40% of the cells expressing either AgrD(1-32)-intein^{Npu} or AgrD(1-32)-intein^{Ssp} in the cell cultures (Table 4), which was determined via the classical dilution method for calculating colony-forming units (CFUs).

Next, we tested the partially lysed cell culture supernatants of the cells expressing the AgrD(1-32)-intein^{Npu} or AgrD(1-32)-intein^{Ssp} proteins with the β-lactamase reporter assay. Again, using AgrD(1-32)-intein^{Ssp} as an example, we observed that the addition of cell culture lysate does not increase β-lactamase activity above the activity observed from induced AgrD(1-32)-intein^{Ssp} cell culture supernatant (Figure 22). The cell culture

supernatants from the various strains that express the AgrD(1-32)-intein^{Npu} proteins behaved similarly to the AgrD(1-32)-intein^{Ssp} in the lysis experiments (data not shown). We also analyzed the cell culture supernatants via Western blot and observed that the partially lysed cell culture supernatants contain measureable amounts of the AgrD(1-32)-intein^{Ssp} protein (Figure 22, below bars 5 and 6 of the plot). As expected, none of the unlysed cell culture supernatants have measureable amounts of their AgrD(1-32)-intein proteins, meaning that cell lysis within these cell cultures is well below ~40%. To further show that whole cells could not process the lysed culture supernatants to produce mature AIP, we included in our analysis a second lysed cell culture supernatant of the AgrD(1-32)-intein^{Ssp} cells. As previously described, cells expressing AgrD(1-32)-intein^{Ssp} were lysed by the bead-beating method but the lysed culture portion was added to and incubated with a cell culture of the uninduced inactive intein cells expressing C33A AgrD(1-32)-intein^{Ssp}, which should have produced no mature AIP up to the point of adding the lysed AgrD(1-32)-intein^{Ssp} cell culture supernatant. Thus, any increased signal in the β-lactamase assay would result from processing of the AgrD-I-thiolactone contained in the added AgrD(1-32)-intein^{Ssp} cell culture lysate supernatant (Figure 22). We observed no increase in β-lactamase activity from this hybrid cell culture supernatant, further confirming that cell lysis is not responsible for the observed mature AIP-I. The same experiment was also included in our analysis of the cells expressing AgrD(1-32)-intein^{Npu} and produced similar results.

Table 4. Colony Forming Unit (CFU) Data for Cell Lysis of Cell Cultures from AgrD(1-32)-intein^{Npu} or AgrD(1-32)-intein^{Ssp} Cells

Controlled Cell Lysis After 3 Hours of Induced Growth

Cell Strain	Induced Culture	Bead Lysis Culture	% of Induced Lysed
AgrD(1-32)-intein^{Npu}	1.58 x 10^9 cfu/ml	9.4 x 10^8 cfu/ml	59 %
AgrD(1-32)-intein^{Ssp}	2.24 x 10^9 cfu/ml	1.26 x 10^9 cfu/ml	56 %

Controlled Cell Lysis After 5.5 Hours of Induced Growth

Cell Strain	Induced Culture	Bead Lysis Culture	% of Induced Lysed
AgrD(1-32)-intein^{Npu}	3.64 x 10^9 cfu/ml	2.20 x 10^9 cfu/ml	60 %
AgrD(1-32)-intein^{Ssp}	3.76 x 10^9 cfu/ml	2.44 x 10^9 cfu/ml	65 %

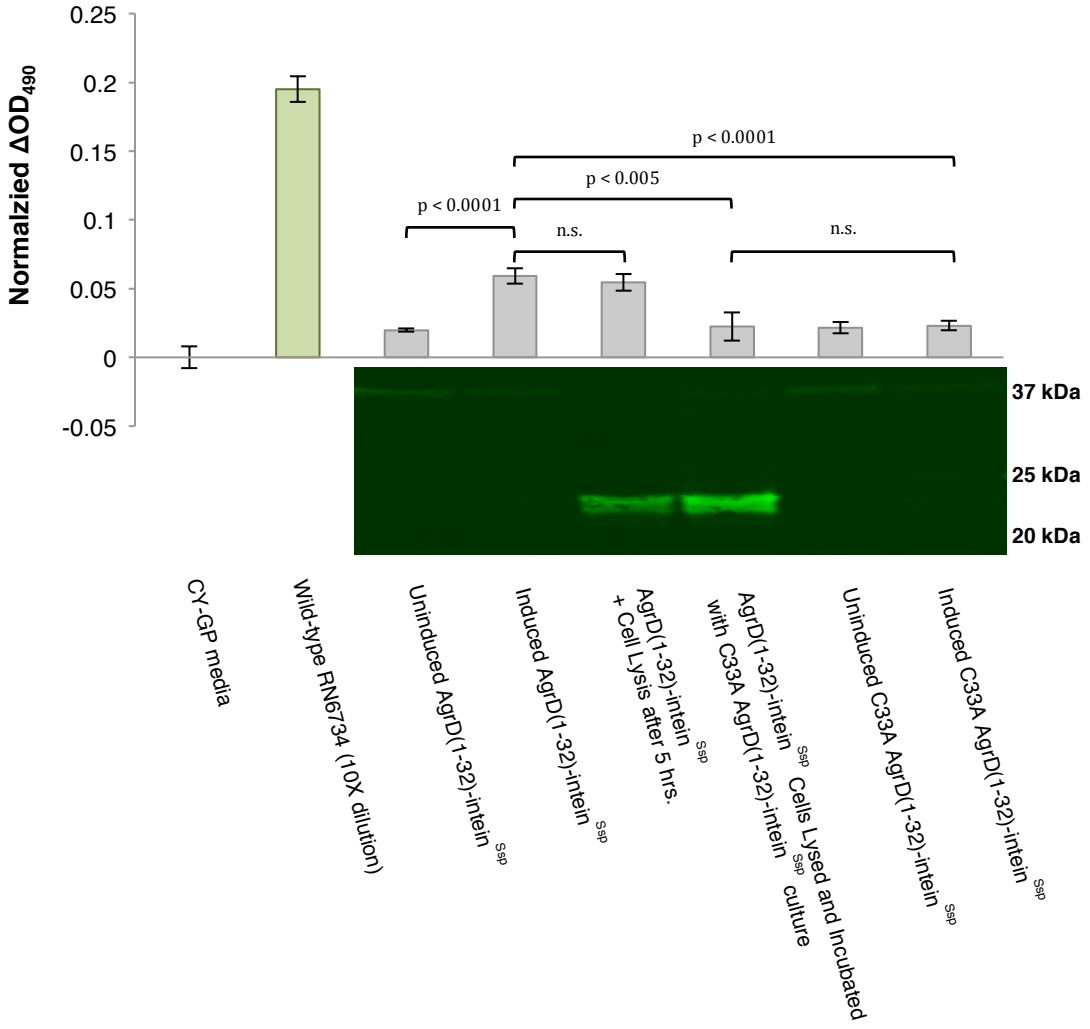

Figure 22. Cell Lysis of AgrD(1-32)-intein^{Ssp} Cells Does Not Generate AIP-I Activity

β-lactamase activity assay of cell culture supernatants from AgrD(1-32)-intein^{Ssp} expressing cells is plotted (top). Filtered cell culture supernatants from the indicated strain were incubated with an exponential phase culture of group I *S. aureus* reporter strain (RN9222). Samples were removed after 60 minutes and assayed for β-lactamase activity by the nitrocefin method. Normalized ΔOD_{490} was calculated as in Figure 20A. The plot is relative to the CY-GP media normalized to zero. Errors; SD, n = 3. Important p-values are indicated with a bracket and the numerical p-value. Western blot analysis of the AgrD-fused split intein cell culture supernatants is also provided (middle). Following SDS-PAGE, the proteins were transferred to a nitrocellulose membrane and probed with an Anti-His antibody. The blot was imaged with a LI-COR Odyssey Infrared Imager.

2.2.5 AgrB-I Does Not Facilitate an Increase in AIP-I Activity

By eliminating cell lysis as a possible cause for AIP-induced β-lactamase activity within the cells expressing AgrD(1-32)-intein constructs, we could turn our attention toward the role AgrB might play in secretion of the AgrD(1-32)-thiolactone. We engineered a new set of *S. aureus* strains that expressed either a AgrD(1-32)-intein^{Npu} or AgrD(1-32)-intein^{Ssp} construct and a variant of AgrB in *agr*$^{-}$/*spa*$^{-}$ S. aureus cells. One variant of AgrB expressed was an alanine mutation at the Cys-84 residue—the catalytic residue of AgrB. This C84A mutation would not be able to catalyze formation of the AgrD(1-32)-thiolactone, but if AgrB facilitates secretion, this mutant should be able to carry out that process. Two variants of AgrB expressed were double mutants: C84A, K129E AgrB and C84A, K131E AgrB, which were used to investigate whether the lysine patch is critical to AgrB-mediated secretion as proposed by Thoendel *et al*.[72] The wild-type AgrB was also included in this set of experiments, which made a total of eight new strains expressing either the AgrD(1-32)-intein^{Npu} or AgrD(1-32)-intein^{Ssp} with one of the four variants of AgrB. For characterization purposes, all four variants of AgrB contained a C-terminal FLAG epitope tag, and Western blot analysis of each strain confirmed expression of an AgrB variant in the whole cell lysate along with AgrD(1-32)-intein^{Npu} or AgrD(1-32)-intein^{Ssp} proteins (Figure 23). For unknown reasons, we were unable to engineer strains that expressed the C84A, K130E AgrB mutant.

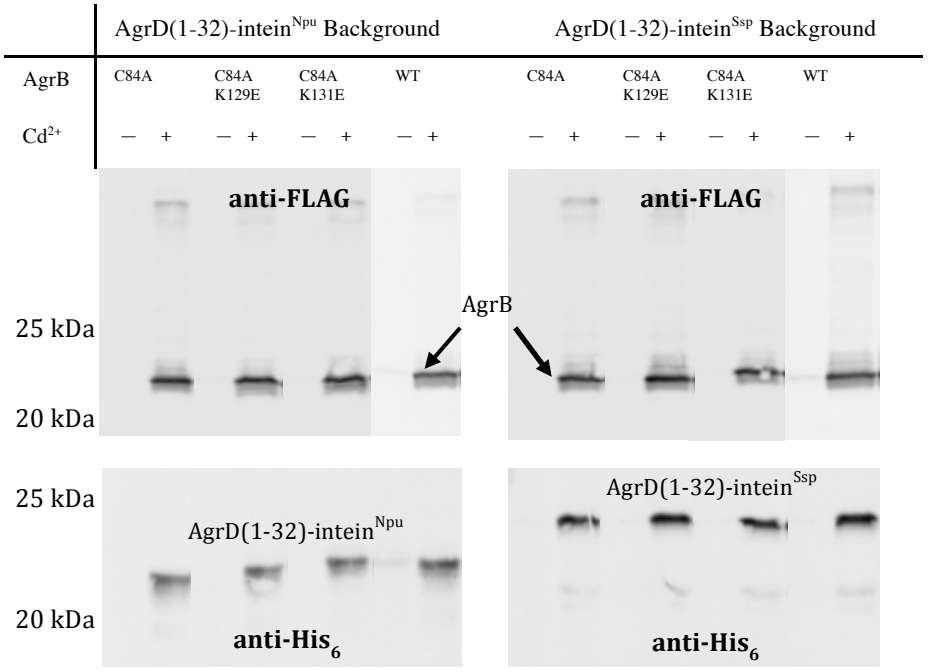

Figure 23. AgrB Mutants Co-Expressed with AgrD(1-32)-intein^{Npu} or AgrD(1-32)-intein^{Ssp}

Western blot analysis of whole cell lysates from cells expressing various AgrB mutants with either AgrD(1-32)-intein^{Npu} or AgrD(1-32)-intein^{Ssp} over a 6-hr. induced growth period is shown. AgrB mutants with a C-terminal FLAG tag are shown in the middle panel. The cells expressing WT AgrB proteins were run on a separate SDS-PAGE gel. Following SDS-PAGE, the proteins were transferred to a nitrocellulose membrane and probed with an anti-FLAG antibody. The membrane was imaged with a LI-COR Odyssey Infrared Imager. The same whole cell lysates were also checked to see whether they expressed AgrD(1-32)-intein^{Npu} (bottom left panel) or AgrD(1-32)-intein^{Ssp} (bottom right panel), respectively. Following SDS-PAGE, the proteins were transferred to a nitrocellulose membrane and probed with an Anti-His antibody. The membrane was imaged with a LI-COR Odyssey Infrared Imager.

Using the β-lactamase reporter gene assay, we tested all of the strains expressing AgrB with either AgrD(1-32)-intein^{Npu} or AgrD(1-32)-intein^{Ssp} to assay AIP-I activity and determine what effect the different variants of AgrB have on AIP-I secretion (Figures 24 and 25). When compared to the cells expressing only AgrD(1-32)-intein^{Npu} (Figure 24) or AgrD(1-32)-intein^{Ssp} (Figure 25), which produce AIP-I in the absence of AgrB, none of the cell culture supernatants from cells expressing an AgrB variant and an AgrD(1-32)-intein construct produced an increase of AIP-induced β-lactamase activity. Most of the AgrB expressing cells induced the same amount of β-lactamase activity as the non-AgrB expressing cells. Only in the instance of the cells expressing the C84A AgrB with an AgrD(1-32)-intein construct had a slight decrease in activity compared to the cells only expressing the AgrD(1-32)-intein proteins. Still, the C84A single point mutant did not induce an increase in β-lactamase activity. The C84A AgrB mutants with a lysine point mutation induced similar amounts of β-lactamase activity as the AgrD(1-32)-intein, as did the WT AgrB mutants. In all, there are six cell culture supernatants that indicate AgrB does not statistically increase AIP secretion—two of which are WT AgrB. In the other two cell culture supernatants from the cells expressing a C84A AgrB mutant, there was a slight decrease in β-lactamase activity observed.

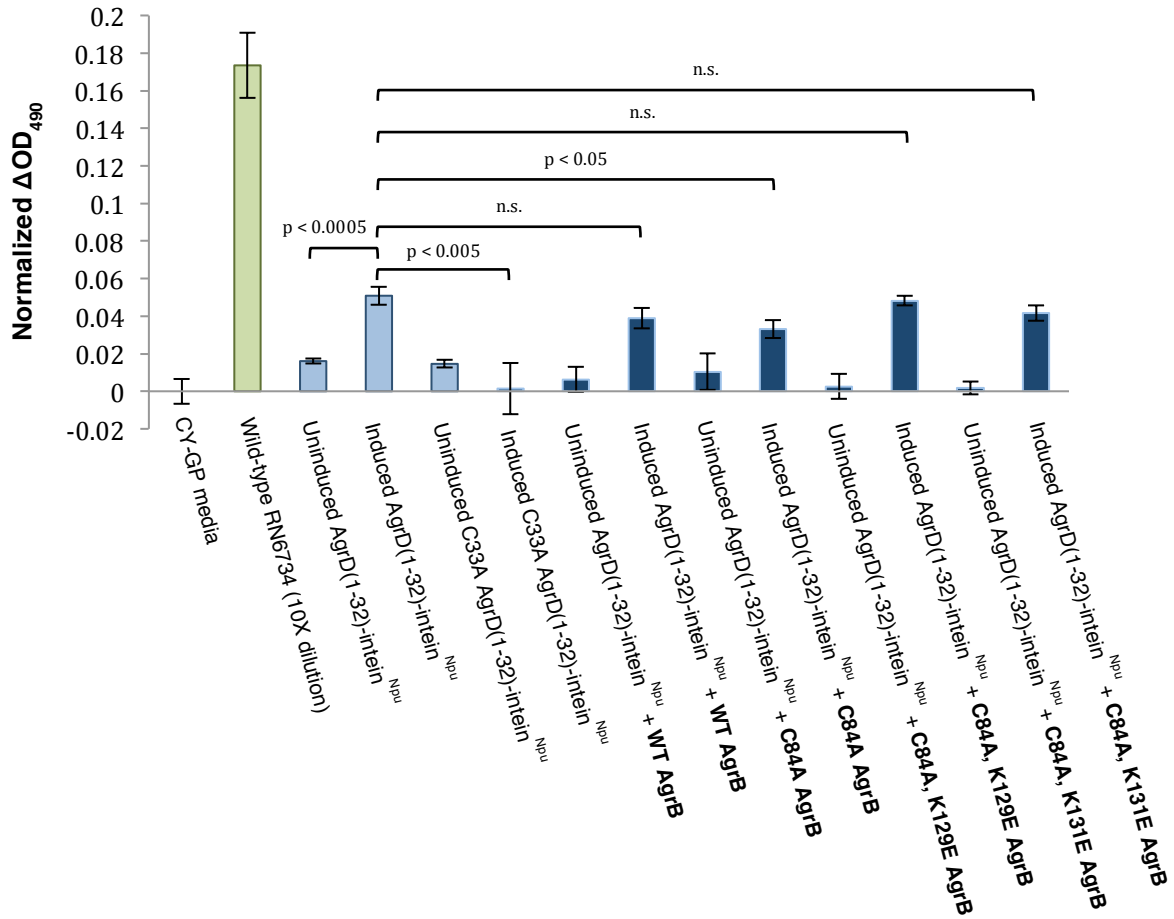

Figure 24. AgrB Does Not Increase AIP-I Activity in the AgrD(1-32)-intein^{Npu}-expressing Cell Culture Supernatants

β-lactamase activity assay of cell culture supernatants from cells expressing AgrD(1-32)-intein^{Npu} protein in the absence or presence of an indicated AgrB variant is plotted. Filtered cell culture supernatants from the indicated strain were incubated with an exponential phase culture of group I *S. aureus* reporter strain (RN9222). Samples were removed after 60 minutes and assayed for β-lactamase activity by the nitrocefin method. Normalized ΔOD_{490} was calculated the same as in Figure 20A. The plot is relative to the CY-GP media normalized to zero. Errors; SD, n = 6. Important p-values are indicated with a bracket and the numerical p-value above.

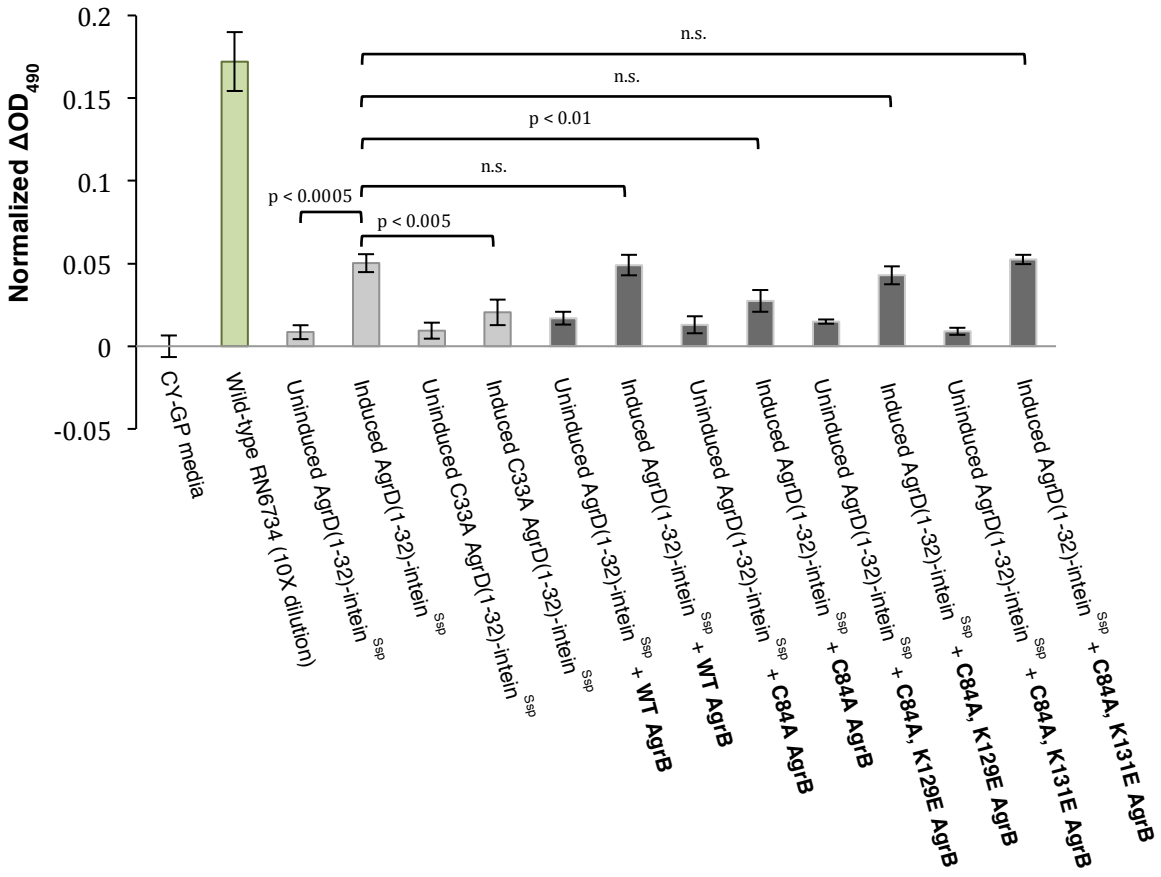

Figure 25. AgrB Does Not Increase AIP-I Activity in the AgrD(1-32)-intein^{Ssp}-expressing Cell Culture Supernatants

β-lactamase activity assay of cell culture supernatants from cells expressing AgrD(1-32)-intein^{Ssp} protein in the absence or presence of an indicated AgrB variant is plotted. Filtered cell culture supernatants from the indicated strain were incubated with an exponential phase culture of group I *S. aureus* reporter strain (RN9222). Samples were removed after 60 minutes and assayed for β-lactamase activity by the nitrocefin method. Normalized ΔOD_{490} was calculated the same as in Figure 20A. The plot is relative to the CY-GP media normalized to zero. Errors; SD, n = 6. Important p-values are indicated with a bracket and the numerical p-value above.

2.3 Characterization of AgrD Physicochemical Properties

2.3.1 The SID Sequence of AgrD Can Inhibit AIP Secretion

Previous research has shown which residues in the C-terminus of AgrD are essential for AgrB recognition and cleavage,[57] but there has been no other study to characterize the SID (secretion inhibitor domain) of AgrD. Since several *S. aureus* cell strains described in *Section 2.2.3* can produce AIP-I in the absence of AgrB-I, we designed a similar cell experiment to examine the effect that the SID sequence might have on AIP secretion and production. *S. aureus* cells were engineered to express a chimera of the MAD (membrane association domain) and SID sequence in the AgrD(1-32) domain of the AgrD(1-32)-intein constructs. We expected this chimera to inhibit secretion by interfering with the ability of AgrD(1-32) to associate with membrane. In the chimera, the 15-residue SID sequence of AgrD-II (Figures 5A and 23A, underlined sequence) is inserted into the MAD sequence of the AgrD(1-32) domain. We chose the 15-residue SID sequence of AgrD-II because its 15th amino acid residue (Lys) aligns well with Lys-17 of the D(1-32) domain (Figure 26A). Thoendel *et al*. also proposed that the SID sequence forms a α-helix,[57] so it could potentially maintain the proposed α-helix of the MAD in AgrD.[64] We then tested the cell culture supernatants of the chimera AgrD(1-32)-intein^{Ssp} using the β-lactamase reporter gene assay (Figure 26B). As expected, the SID sequence inserted into the AgrD(1-32) domain reduces the AIP-induced β-lactamase activity assay.

A)

MNTLFNLFFDFITGILKNIGNIAAYSTCDFIM
MNDEPKVPAELTNLYDKNIGNIAAYSTCDFIM

B)

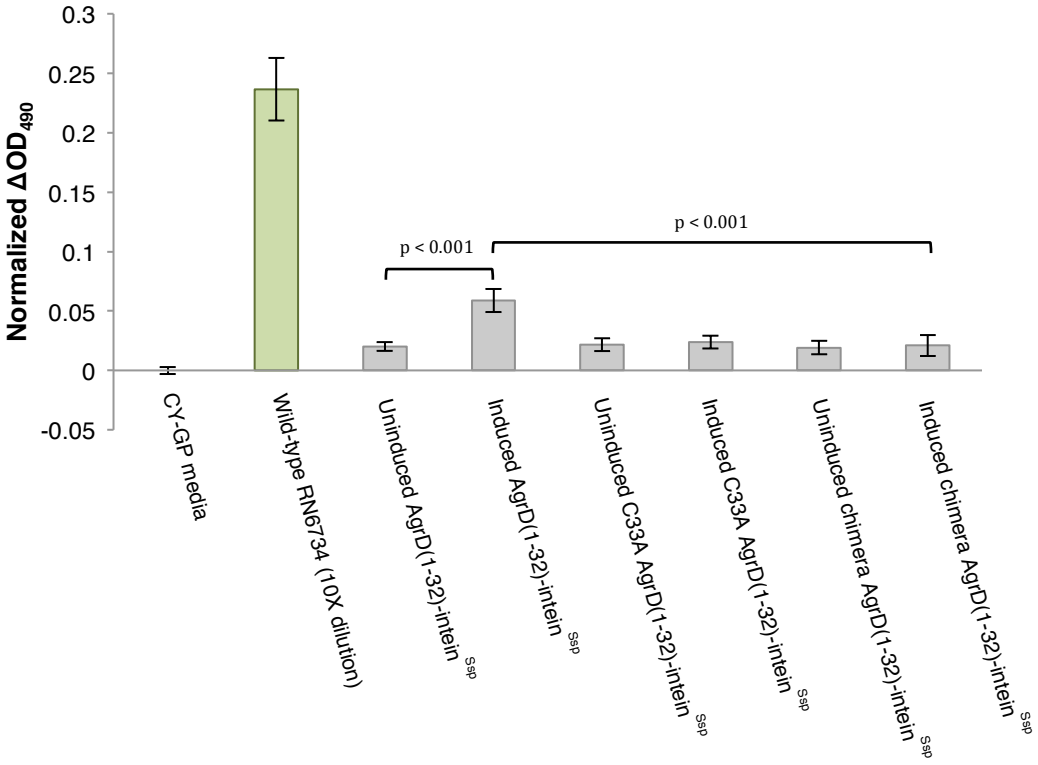

Figure 26. SID Sequence Insertion in the AgrD(1-32) Domain Stops AIP-I Activity

A) Sequence alignment of the AgrD(1-32)-I domain and the chimera AgrD(1-32)-I domain. The AgrD-II SID sequence is underlined. **B)** β-lactamase activity assay of the chimera AgrD(1-32)-intein^{Ssp} expressing cells is plotted. Filtered cell culture supernatants from the indicated strain were incubated with an exponential phase culture of group I *S. aureus* reporter strain (RN9222). Samples were removed after 60 minutes and assayed for β-lactamase activity by the nitrocefin method. Normalized ΔOD_{490} was calculated the same as in Figure 20A. The plot is relative to the CY-GP media normalized to zero. Errors; SD, n = 3. Important p-values are indicated with a bracket and the numerical p-value above.

2.3.2 Distribution-Coefficients for Several AIPs and AgrD(1-32)-thiolactone Peptides

To our knowledge, there is no published solubility data for AIP or the 1-32 AgrD Thiolactone. Previous research using SDS-PAGE and Western blot analysis has shown that the MAD anchors AgrD in the membrane and enables processing of AgrD into AIP.[64] To supplement these observations, we wanted to investigate the solubility properties of AIP and the AIP precursor. Therefore, we synthesized AIP-I, AIP-II, N-terminal acetylated AIP-I, N-terminal acetylated AIP-II, AgrD(1-32)-I-thiolactone, and AgrD(1-32)-II-thiolactone using a Boc-SPPS strategy developed by Lyon *et al*. for the synthesis of thiolactone-containing peptides.[63, 141] Briefly, the linear peptide α-thioester was generated by SPPS employing a Boc-N^{α} protection logic and using a 3-mercaptopropionamide-based linker system. Following cleavage from the support with anhydrous HF, the crude unprotected peptide was cyclized in an acetonitrile:water mixture at neutral pH via an intramolecular trans-thioesterification reaction. All of the peptides were then purified by RP-HPLC and characterized by ESI-MS (See *Chapter 6* for characterization data).

We then calculated distribution-coefficients at pH 5.9 ($LogD_{5.9}$) for all 6 of these peptides and one control compound, chloramphenicol, via the shake flask method with HPLC detection to determine the abundance of each peptide in either the aqueous buffer fraction (pH 5.9) or 1-octanol fraction (Table 5).[142] The β-lactamase reporter assay is buffered at pH 5.9, so these LogD values describe how these molecules might behave during the assay. Based on our calculated values, the AIP molecules are not lipophilic. In

the instance of AIP-II, acetylation affects solubility, while it does not affect the solubility of AIP-I. This trend is likely a result of the charged Asp residue of AIP-I, whereas, AIP-II only has a charge at its N-terminus, which is removed by the acetyl group. Finally, the trend towards insolubility continues with the AgrD(1-32)-I-thiolactone and AgrD(1-32)-II-thiolactone. As expected, they are less soluble than any of the other AIP peptides and have LogD/LogP values that suggest they are slightly lipophilic, when compared to several known LogD values (Table 5).

Table 5. Calculated $LogD_{5.9}$ Values for AIPs and AgrD(1-32)-thiolactones

Molecule	Expected Mass	Observed Mass	$LogD_{5.9}$
AIP-I	960.4	961.4[a]	-0.69 ± 0.05
Ac-AIP-I	1002.4	1003.4[a]	-0.61 ± 0.04
AgrD(1-32)-I-thiolactone	3631.2	3630.8[a]	0.41 ± 0.01
AIP-II	878.4	879.4[a]	-1.33 ± 0.04
Ac-AIP-II	920.4	921.4[a]	-0.3 ± 0.2
AgrD(1-32)-II-thiolactone	3417.1	3417.1[a]	0.6 ± 0.4

Molecule	Literature LogD[b]
Chloramphenicol[c]	1.14
Acetaminophen	0.51
L-Dopa	-2.57
Testosterone	3.29

[a]Mass observed is ($[M + H^+]$)

[b]Literature values of $LogD_{7.4}$ obtained from Kerns *et al*. [142]

[c]We characterized chloramphenicol using the same protocol as the peptides, and obtained an $LogD_{5.9}$ of 1.1 ± 0.1.

$$\mathrm{LogD_{pH}} = \mathrm{Log}\left(\frac{solute_{(oct)}}{solute_{(water)}}\right)$$

2.4 Conclusions

In this work, we investigated the role of AgrB-mediated secretion of AgrD(1-32)-thiolactone. Our data extend the current understanding of how AgrB is involved in AIP secretion. To investigate secretion of AgrD(1-32)-thiolactone, we reported the design and characterization of an AIP secretion assay, which is sensitive to low levels of AIP-I in cell culture supernatants. An important characterization of the secretion assay was to show that cell lysis of the engineered cells expressing AgrD(1-32)-intein constructs is not the source of AIP. A real-time cell lysis assay showed that cell lysis does not result in increased AIP-induced β-lactamase activity. We conclude that our AIP secretion assay can produce AIP in the absence of AgrB. To our knowledge, this assay provides the first instance of AIP production in the absence of AgrB. We, therefore, went on to examine the role that AgrB has in AIP secretion. Using this secretion assay, we showed that AIP-I is secreted in an AgrB-independent manner and that AgrB, when present, does not increase AIP-I levels in cell culture supernatants. Therefore, we find that the primary role of AgrB in AIP biosynthesis is limited to preparing AgrD for secretion by cleaving the SID and forming the thiolactone macrocycle of AIP-I. While this new AIP secretion cell-based assay can assess the role of AgrB in secretion, it cannot reveal whether another unknown protein is involved in AIP secretion. Consequently, further endeavors must focus on how the AgrD(1-32)-thiolactone crosses the membrane.

Chapter 3. The Final Steps in AIP Biosynthesis: Cleaving the AgrD(1-32)-Thiolactone

3.1 Introduction

Following our findings in *Chapter 2*, we chose to investigate the final step in AIP biosynthesis—cleavage of the AgrD(1-32)-thiolactone. Upon crossing the membrane, the AgrD(1-32)-thiolactone requires removal of the AgrD MAD (membrane association domain) in order to produce the mature AIP. This second cleavage event presumably occurs on the extracellular side of the membrane in order to liberate the mature AIP into the extracellular milieu (Figure 9). Initially, AgrB was proposed to catalyze the second cleavage event, because the P2 promoter of *agr* does not encode a second processing protein.[25, 56] Thus, AgrB could hypothetically be the only other protein necessary for AIP biosynthesis besides AgrD. However, the N-terminus of AgrD does not include the known AgrB cleavage site, which is C-terminal to the AIP sequence in AgrD (Figure 5A) which supports the idea that another protease is responsible for MAD cleavage to finish AIP biosynthesis. Indeed, the type I signal peptidase of *S. aureus*—SpsB—can correctly cleave a small peptide derivative of AgrD-I.[58] This observation not only proposes a new player in AIP biosynthesis, but also indicates that the *agr* locus of *S. aureus* may not encode all of the necessary proteins for AIP production.

The MAD cleavage event is poorly understood in comparison to the SID cleavage event mediated by AgrB, where there are conserved residues, enabling AgrB recognition and cleavage. [56-58, 72] In the only characterization of SpsB with relation to AIP biosynthesis, Kavanugh *et al*. showed that SpsB correctly cleaves a fluorescein-labeled

AgrD-I derived peptide.[58] While their findings certainly implicate SpsB, their assay showing biological relevance was done with whole cells, meaning that other peptidases were catalytically active; and they did observe nonspecific cleavage of their AgrD-I derived peptide during these assays. To determine whether SpsB correctly cleaved their peptide, they carried out *in vitro* assays with purified SpsB and a fluorescein-labeled peptide with the sequence fl-NIAAYST (AIP-I residues underlined). The agarose gel assay they developed only detected fluorescence, so they could only follow cleavage products that contained a fluorophore. Using this assay, they observed a cleavage product that they assign to fluorescein labeled NIAA based on migration, but they did not fully characterize the cleavage using RP-HPLC and/or mass spectrometry. [58] They also did not show SpsB cleavage of peptides derived from all four specificity groups of AgrD polypeptides. It should also be noted that an SpsB knockout is lethal,[73] so it has been difficult to characterize the involvement of SpsB in AIP biosynthesis using genetic tools.

A thorough investigation into the potential role of SpsB in the final step of AIP biosynthesis across the four groups is needed. Removal of the MAD produces a tail on the AIP that is biologically important—especially in the instance of AIP-II and AIP-III, where research has shown that incorrect tail length produces AIP molecules with self-inhibitory activity.[62, 63, 83] For example, the tail of AIP-III, which is the shortest among the four AIPs, could include a Tyr residue at the N-terminus (based on the sequence of AgrD-III) just like AIP-I and AIP-IV (Figures 4B and 5A). However, AIP-III with this additional Tyr residue is a self-inhibitor of its cognate AgrC-III receptor.[63] Thus, SpsB

must cleave each AIP correctly; otherwise, it could have deleterious effects on *S. aureus* virulence regulation.

Herein, we describe our efforts to better understand the role of SpsB cleavage in AIP biosynthesis. We present an investigation of the SpsB catalysis of AgrD derived peptides in biochemical and cellular assays. We surveyed several non-fluorescein labeled, AgrD derived peptides using *in vitro* SpsB cleavage assays. Using cellular assays, we then examined SpsB cleavage in the context of a membrane. We then decided to incorporate SpsB into proteoliposomes to further examine its activity in the context of a membrane. Finally, we thoroughly examine SpsB cleavage of AgrD-II—the first investigation to examine whether SpsB can cleave another specificity group AgrD polypeptide besides AgrD-I.

3.2 Biochemical Investigation of the Δ1-21 SpsB Deletion Mutant

3.2.1 Expression and Purification of the Δ1-21 SpsB Deletion Mutant

Previous research suggests that a truncated version of SpsB lacking the N-terminal membrane anchor is active in biochemical assays.[58, 143] Indeed, Kavaunagh *et al*. have shown that the purified Δ1-20 SpsB deletion mutant cleaves a fluorescein labeled AgrD-I derived peptide, albeit not to completion even after 60-hr incubations.[58] Still, this finding was a great starting point for further biochemical analysis of SpsB with other AgrD derived peptides.

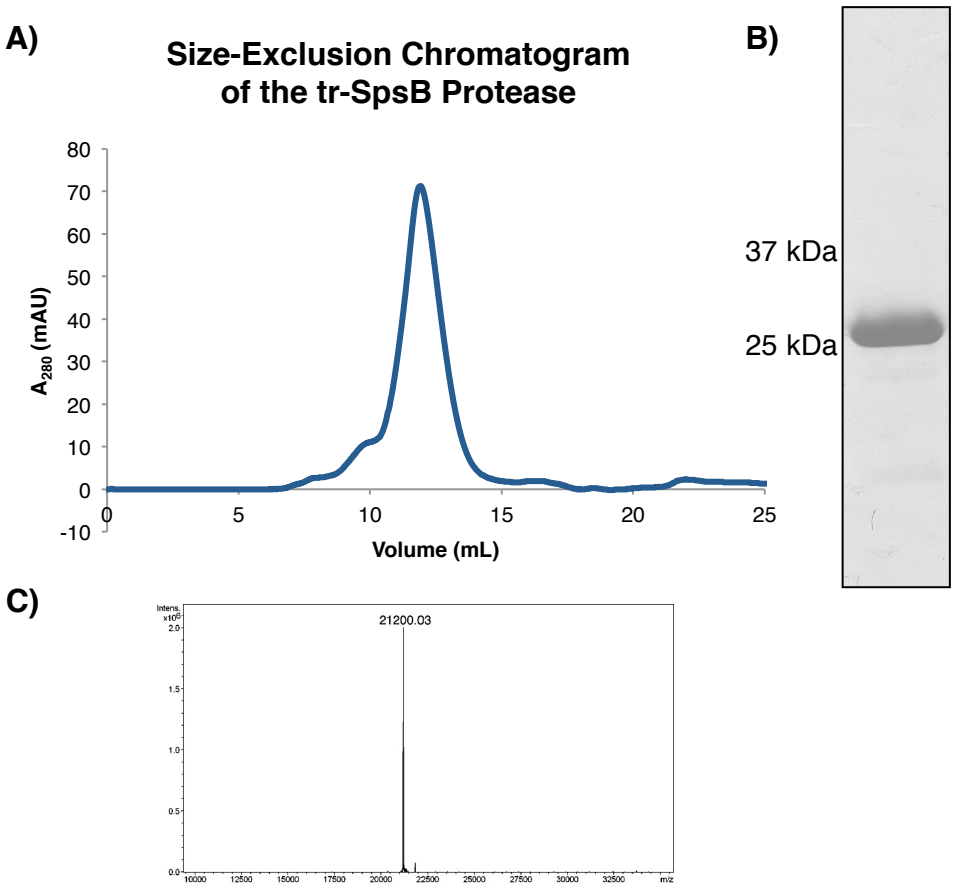

Figure 27. Characterization of the His_6-tagged $_{22\text{-}191}$SpsB deletion mutant protein

A) Size-exclusion chromatogram of tr-SpsB in a Tris-HCl (pH 7.5) and 200 nM NaCl buffer. The purified tr-SpsB is well behaved and elutes as a monomer. **B)** SDS-PAGE analysis of the purified tr-SpsB deletion mutant. Gel is stained by coomassie. The relevant molecular weight markers are represented. **C)** Molecular weight of tr-SpsB as determined by ESI-MS analysis. The MW is calculated using Bruker software with an expected mass of 21199.7.

After several unsuccessful attempts to purify recombinant SpsB, we designed an N-terminal His_6-tagged Δ1-21 SpsB deletion mutant (tr-SpsB) that also contained a TEV protease cleavage sequence between the His_6-tag and SpsB. (The TEV site is necessary, because in our hands, tr-SpsB could auto-cleave a thrombin cleavage sequence, resulting in purification problems.) tr-SpsB was expressed in *E. coli* and purified from the pellet under denaturing conditions. Upon refolding via dialysis, tr-SpsB was further purified using size-exclusion chromatography (Figure 27A and B). Finally, the identity of the purified tr-SpsB was confirmed using mass spectrometry (Figure 27C). Since tr-SpsB required refolding, we confirmed its activity using a peptide with a consensus SpsB cleavage sequence (control peptide, Table 6) generously provided by Dr. Miquel Vila-Perello, a senior researcher at Princeton University. tr-SpsB cleavage of the control peptide went to completion within 10 hours under both conditions described by Rao *et al*.[143] and Kavanaugh *et al*.[58] (Figure 28, Tables 6 and 7), which primarily differ by what aids SpsB solubility: 0.5% Triton X-100 or 25% glycerol, respectively.[58, 143] tr-SpsB cleavage was monitored via RP-HPLC and cleavage products were determined using mass spectrometry. This assay enabled quantification of the starting materials and cleavage products, which was one of the shortcomings of the fluorescent agarose gel shift peptidase assay.[58]

3.2.2 tr-SpsB Cleavage of AgrD Derived Peptides *in vitro*

With a new assay to monitor tr-SpsB activity, we synthesized several peptide amides using a standard Fmoc protocol.[144] Briefly, linear peptide α-amides were generated by solid phase peptide synthesis (SPPS) employing a Fmoc-N^{α} protection

logic and using a rink amide solid support. Following cleavage from the support with a standard TFA cocktail, the crude unprotected peptides were then purified by RP-HPLC and characterized by ESI-MS (See Table 6 and *Chapter 6* for characterization data).

After modifying the previously published assay conditions to include a low salt concentration and 20% glycerol instead of 25%,[58, 143] we re-produced the cleavage of a fluorescein-labeled peptide similar to the one previously tested, except that our peptide had fluorescein directly coupled to the N-terminus (fl-AH peptide, Figure 29, Tables 6 and 7). Using the glycerol conditions, the cleavage did not go to completion after almost 48 hours, which was previously observed.[58] In our hands, the cleavage went to ~40% completion (Table 7), which the previous assay could not determine. In contrast, the Triton conditions significantly affected SpsB with cleavage of the fl-AH peptide only going to ~7% completion (Table 7). Surprisingly, SpsB could not process the non-fluorescein labeled peptide, where the fluorescein group was replaced with an acetyl group (Table 7, AH peptide).

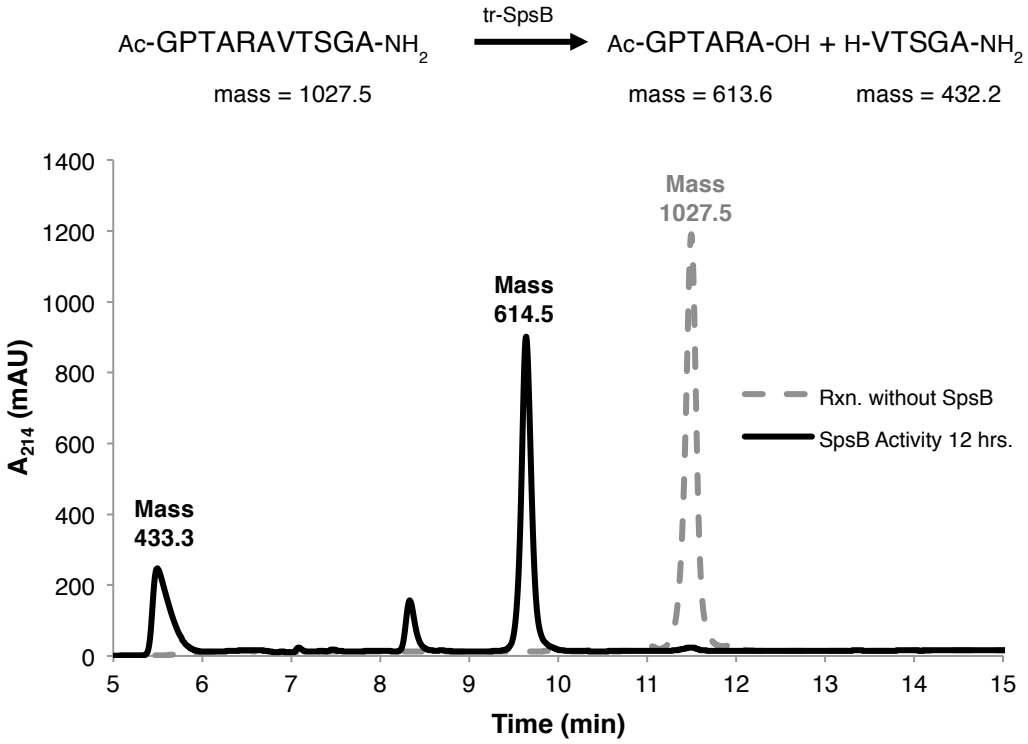

Figure 28. SpsB Cleavage of a Control Peptide

RP-HPLC analysis of the control peptide substrate in the presence or absence of tr-SpsB. After 12 hours, the control peptide (250 μM) is completely consumed and the appearance of the cleavage products is detected. Both reactions were carried out in the Triton assay conditions (See *Chapter 6*). After 12 hours, both reactions were acidified and injected for HPLC analysis (gradient of 0-73% B, over 30 mins.). Fractions from each peak were analyzed using ESI-MS, and the masses are reported as $[M + H]^+$.

Within the AgrD polypeptide sequence (Figure 5A), there is a conserved IG motif in the MAD that is located at around -6 position relative to the N-terminal cleavage site of AIP. Gly and Pro residues are presumed helix-breaking residues within signal peptides recognized by type I signal peptidases.[65] We noticed within the fl-AH and AH peptides that the conserved IG motif in AgrD was excluded (Figure 5A). We synthesized two peptides that included this sequence motif (Table 6, IG-AIP-I and IG-AIP-III), and they were tested with the SpsB activity assay. Again, we observed no cleavage of the AgrD-I derived peptide or the AgrD-III derived peptide (Table 7). Suspecting possible inhibition of SpsB by some of these peptides, we devised a competition assay where the control peptide was incubated with tr-SpsB and either the AH or IG-AIP-III peptide. tr-SpsB cleaved the control peptide, but it did not cleave either of the AgrD-I derived peptides (Figure 30A and B, respectively). We also found that there was no concentration dependence for either IG-AIP-I or AH peptide, which were tested at concentrations up to 1 mM or 400 μM, respectively (data not shown). In our hands, tr-SpsB could not cleave AgrD derived peptides unless they had fluorescein.

Table 6. Peptides used in SpsB *in vitro* assays

Peptide	Sequence	Expected Mass	Observed Mass $[M+H]^+$	HPLC R_t (min.)
Control	Ac-GPTARAVTSGA-NH_2	1027.5	1028.5	11.36
fl-AH	fl-NIAAYST-NH_2	1095.4	1096.4	17.96
AH	Ac-NIAAYST-NH_2	779.4	780.4	17.48
IG-AIP-I	Ac-KNIGNIAAYST-NH_2	1191.6	1192.6	15.30
IG-AIP-III	Ac-NSIGYRAAYIN-NH_2	1281.6	1282.6	14.26

Table 7. RP-HPLC Analysis of *in vitro* SpsB Activity Assays

Peptide	Sequence	Cleavage (Triton Rxn)^	Cleavage (Glycerol Rxn)^	Notes
Control	Ac-GPTARA/VTSGA-NH_2	Yes, 100%	Yes, 100%	within 12 hrs
fl-AH	fl-NIAA/YST-NH_2	Yes, 6.6%	Yes, 41.4%	up to 48 hrs.
AH	Ac-NIAA/YST-NH_2	None	None	
IG-AIP-I	Ac-KNIGNIAA/YST-NH_2	None	None	rxn. went 48 hrs.
IG-AIP-III	Ac-NSIGYRAAY/IN-NH_2	None	None	

Expected SpsB cleavage site is indicated with **/**. ^RP-HPLC Analysis determined % of cleavage.

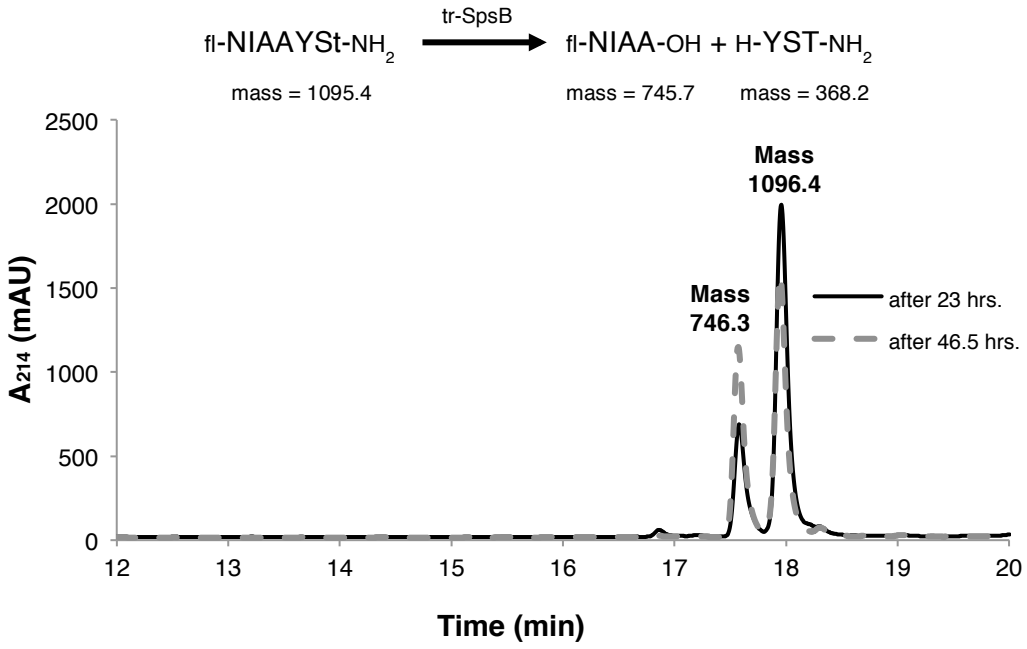

Figure 29. SpsB Cleavage of the fl-AH Peptide

RP-HPLC analysis of two reaction timepoints of the fl-AH peptide in the presence of tr-SpsB. Even after 46.5 hours, the fl-AH peptide is not consumed. Only one cleavage product was detected. Both reactions were carried out in the glycerol assay conditions (See *Chapter 6*). After the indicated time, both reactions were acidified and injected for HPLC analysis (gradient of 0-73% B, over 30 mins.). Fractions from each peak were analyzed using ESI-MS, and the masses are reported as $[M + H]^+$.

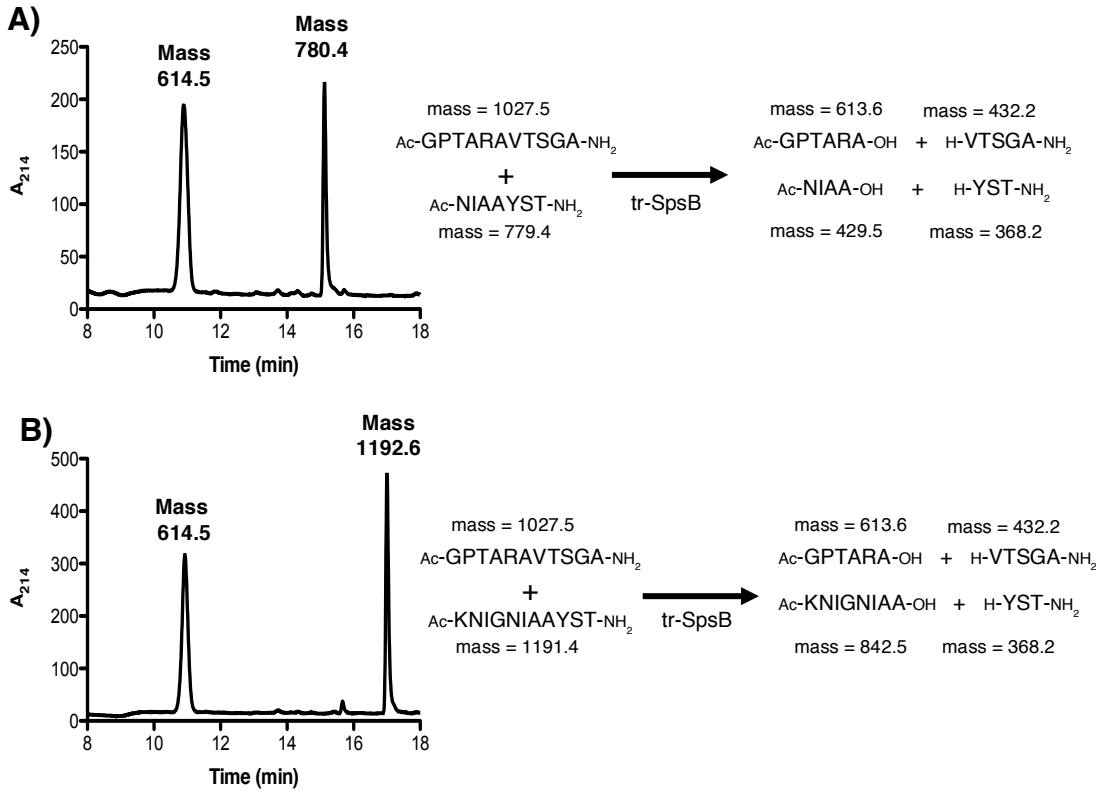

Figure 30. tr-SpsB Assays of the Control Peptide with AH or IG-AIP-I Peptides

A) RP-HPLC chromatogram is shown of the competition tr-SpsB assay with the control and AH peptides after 12 hours. Both peptides are at 100 μM, and the assay was carried out in the 20% glycerol conditions. **B)** RP-HPLC chromatogram is shown of the competition tr-SpsB assay with the control and IG-AIP-I peptides after 12 hours. Both peptides are at 150 μM, and the assay was carried out in the 20% glycerol conditions. Theoretical reaction schemes are provided to the right of the RP-HPLC chromatogram for each competition assays. After the indicated time, both reactions were acidified and injected for RP-HPLC analysis (gradient of 0-73% B, over 30 mins.). Fractions from each peak were analyzed using ESI-MS, and the masses are reported as $[M + H]^+$. Peaks are slightly shifted from R_t reported in Table 6, because the assays were analyzed on a different HPLC than the one used for the purified peptides.

3.2.3 Whole Cell Assays with the IG-AIP Peptides

Kavanaugh *et al.*[58] used whole cells to initially observe cleavage of their fluorescein-labeled peptide. Given this, we tried digesting the IG-AIP-I and IG-AIP-III (each assay at a concentration of 150 μM) peptides with whole *S. aureus* cells (RN6734), which had been washed with and re-suspended in a buffered saline solution (Tris-HCl, pH 8, and 200 mM NaCl) for the assay. After an 18-hr incubation and cell removal, the filtered supernatant was analyzed via RP-HPLC and cleavage products were characterized using ESI-MS. Using this whole cell assay, we observed cleavage of both peptides (Table 8). For the IG-AIP-I peptide, there was several cleavage products detected, of which one had a mass consistent with correct cleavage of the peptide. For the IG-AIP-III peptide, no cleavage product detected corresponded to the expected cleavage site. While the cells used in the assay were group I wild-type, SpsB is conserved among all the *agr* specificity groups,[73] so a lack of IG-AIP-III cleavage sheds doubt on the role of SpsB in AIP-III biosynthesis. Instead of increasing the evidence that SpsB is the only protease able to cleave the MAD of AgrD, these biochemical assays suggest that either SpsB is not the universal protease for AIP biosynthesis or it requires another component not present in the *in vitro* HPLC assay.

Table 8. MS Analysis of IG-AIP Substrate Peptides Incubated with *S. aureus* cells

Peptide	Sequence	Mass Observed $[M+H]^+$	Likely Fragment	Notes
IG-AIP-I	Ac-KNIGNIAA/YST-NH_2	1192.6	Ac-KNIGNIAAYST-NH_2	no cleavage
		842.5	Ac-KNIGNIAA-OH	correct cleavage
		738.4	H-NIAAYST-NH_2	non-specific cleavage[1]
		473.3	Ac-KNIG-OH	non-specific cleavage[1]
		369.2	H-YST-NH_2	correct cleavage
IG-AIP-III	Ac-NSIGYRAAY/IN-NH_2	1282.6	Ac-NSIGYRAAYIN-NH_2	no cleavage
		893.4	Ac-NSIGYRAA-OH	non-specific cleavage[1]
		822.4	Ac-NSIGYRA-OH	non-specific cleavage[1]
		550.3	H-AAYIN-NH_2	non-specific cleavage[1]
		479.3	H-AYIN-NH_2	non-specific cleavage[1]
		408.2	H-YIN-NH_2	non-specific cleavage[1]

Expected SpsB cleavage is indicated with **/**. Acetylation of the N-terminus is indicated with Ac.
[1]non-specific cleavage catalyzed by an unknown protease.

3.3 SpsB Requires a Membrane to Cleave AgrD-I (work on this section was accomplished in collaboration with Boyuan Wang and Xinhui [Connie] Wang)

3.3.1 Expression and Purification of the Proteins Required for AIP Biosynthesis

In the tr-SpsB biochemical assay, SpsB was solubilized and not incorporated into its native membrane environment. In the cell-based assay, SpsB was endogenously expressed, so it would have been incorporated into the membrane, where it could presumably cleave the IG-AIP-I substrate peptide correctly. We decided to incorporate SpsB and other AIP-related proteins into proteoliposomes (vesicles), which were reconstituted via the detergent-removal method (Figure 31).[145] Briefly, proteins and lipids dissolved in detergent are mixed together, and the detergent is removed using Bio-Beads. To accomplish this biochemical analysis, this new approach required purification of the full-length SpsB, so we designed and expressed an N-terminal His_5-tagged, fl-SpsB protein, which was solubilized from the membrane fraction of *E. coli* cell lysates with n-Dodecyl β-D-maltoside (DDM) and then purified (Figure 32A). Several constructs of AgrD were recombinantly expressed and purified as well as AgrB-I and AgrB-II (Figure 32B and C), which were also solubilized in detergents (See *Chapter 6* for detailed expression and purification protocol). (Note, we were unable to obtain AgrB-III and AgrD-III with much success, so group I and II components were employed.) To detect and analyze the cleavage products of the vesicle assays, we employed several analytical approaches, including SDS-PAGE, RP-HPLC and MS, or the β-lactamase reporter assay (Figure 31).

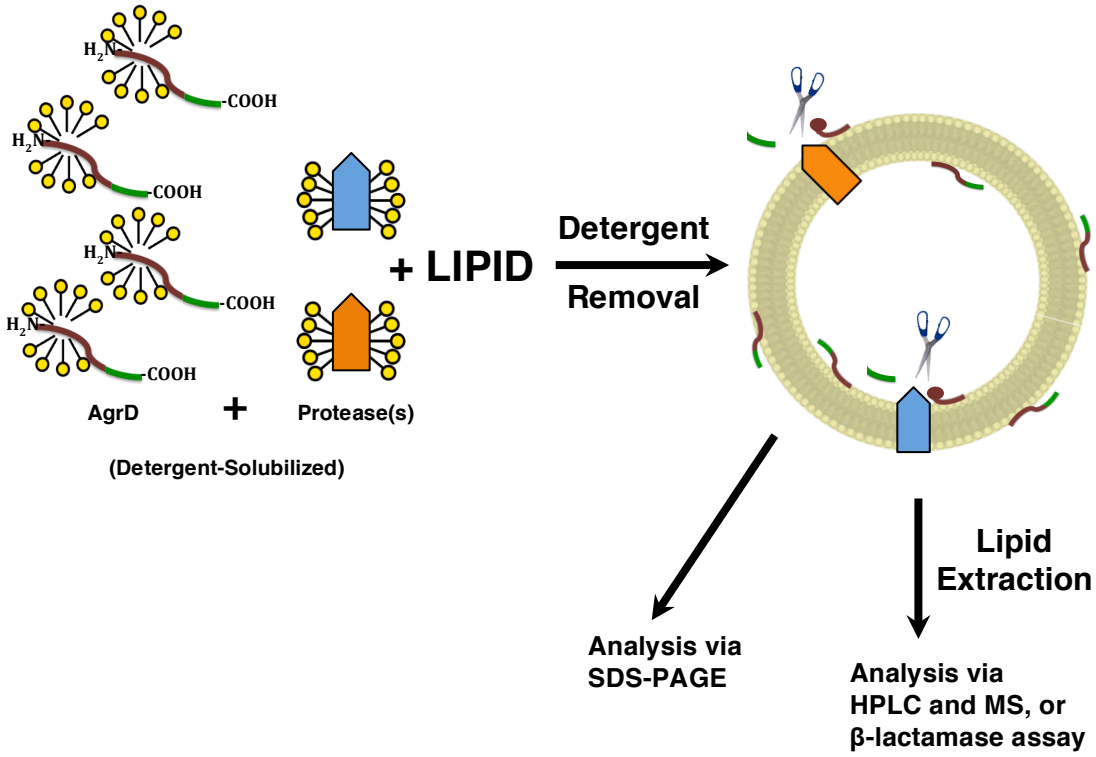

Figure 31. Liposome Assay Schematic for AgrD Cleavage

The general strategy for incorporating the proteins involved in AIP biosynthesis into proteoliposomes is illustrated. The general strategy is outlined by Rigaud *et al*.[145] Once the vesicles are prepared, they can be analyzed using SDS-PAGE, HPLC and MS, or the β-lactamase reporter assay.

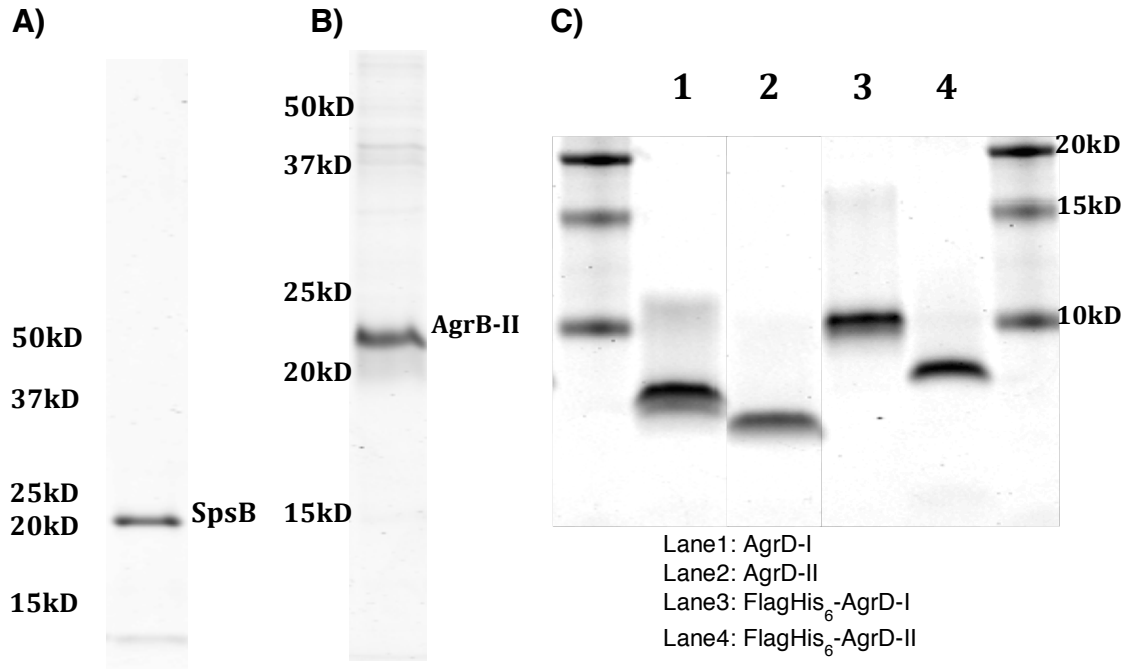

Figure 32. Purified Protein Components for AIP Biosynthesis

SDS-PAGE analysis of proteins used in proteoliposome reconstitution. **A)** fl-SpsB was analyzed using a 12% Bis-Tris SDS-PAGE gel, which was stained by coomassie. **B)** AgrB-II is shown as an example. It was analyzed using a 15% Tris-HCl gel, which was stained by coomassie. **C)** The AgrD proteins were analyzed using a 16.5% Tris-tricine gel, which was stained by coomassie. The relevant molecular weight markers are indicated for each gel.

3.3.2 Cleavage Products Produced from Proteoliposomes Containing AgrB, AgrD, and fl-SpsB

Having purified AgrD, AgrB and fl-SpsB, we decided to reconstitute them into proteolipsomes (vesicles), presumably incorporating all the essential proteins of the AIP biosynthetic pathway in a lipid bilayer. After incubating vesicles containing various combinations of AgrD with fl-SpsB and AgrB for 12 hours, we analyzed the vesicles via SDS-PAGE (Figure 33). We prepared vesicles that contained fl-SpsB and AgrD-I or AgrD-II. In the SDS-PAGE analysis of these vesicle assays, we observed fl-SpsB cleavage of AgrD-I and AgrD-II, but AgrD was not fully consumed in either reaction (Figure 33, lanes 2 and 6, respectively). We also reconstituted the group specific AgrB and AgrD proteins into vesicles to try and observe AgrB cleavage of AgrD. In the SDS-PAGE analysis of the AgrB and AgrD-containing vesicles, we also observed cleavage (Figure 33, lanes 3 and 7, group I and group II, respectively). However, SDS-PAGE analysis cannot indicate whether this cleavage product contains the thiolactone macrocycle. Finally, in the vesicles where the full AIP biosynthetic pathway was reconstituted into vesicles, SDS-PAGE analysis suggests that AgrD was cleaved twice (Figure 33, lanes 4 and 8, group I and group II, respectively). By comparing lane 2 with lane 4 and lane 6 with lane 8, the SpsB cleavage product is visible (albeit weakly) in the AgrD cleavage products (white arrows within image), although it is difficult to distinguish them in the Tris-tricine gel, where small peptides easily diffuse. While these initial attempts to reconstitute fl-SpsB cleavage of AgrD within a membrane were encouraging, SDS-PAGE analysis could not detect the small AIP molecule and cannot be used to determine, whether the correct cleavage products are produced.

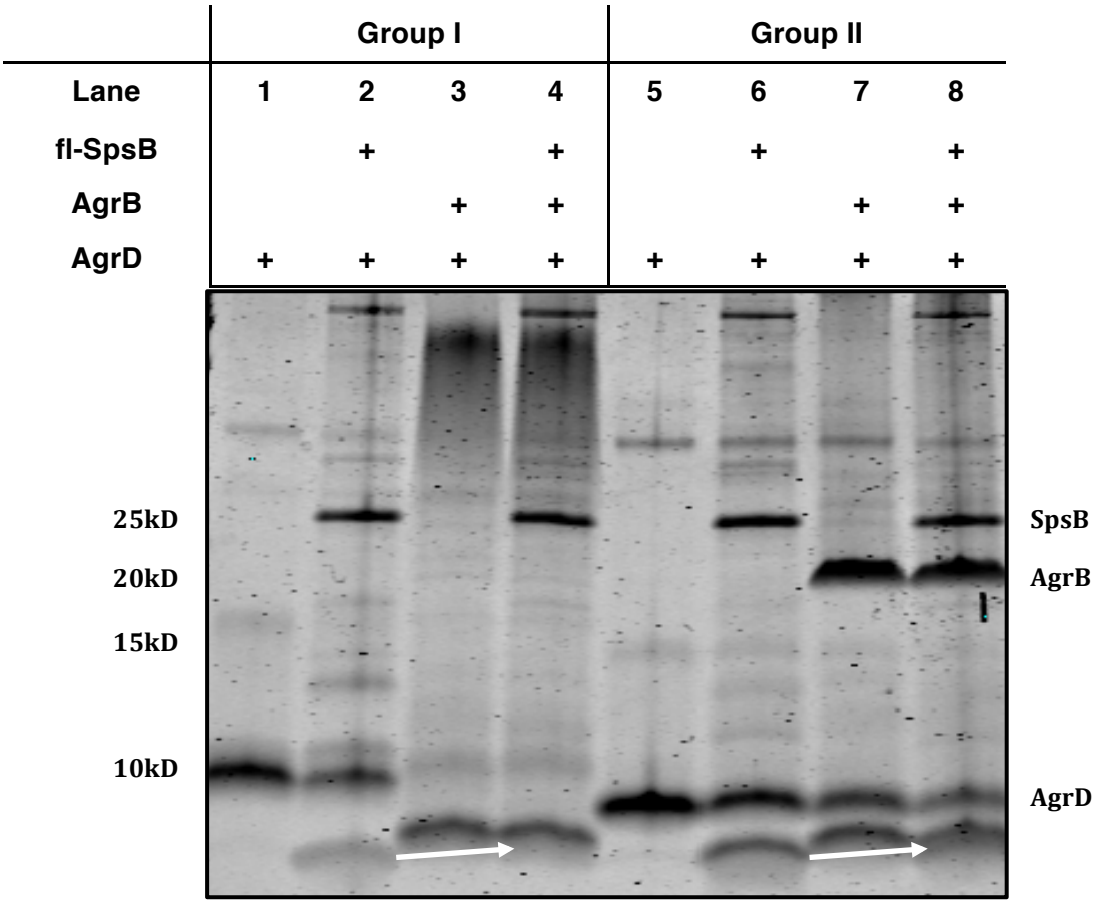

Figure 33. SDS-PAGE Analysis of AIP Biosynthesis Proteoliposomes

SDS-PAGE analysis of various AIP producing proteins in vesicles is shown. The liposomes were analyzed using a 16.5% Tris-tricine gel, which was stained by coomassie. The various vesicle components are indicated above each gel lane. The relevant molecular weight markers are also indicated. fl-SpsB is indicated. The region where AgrD and/or its cleavage products appear is also indicated. AgrB-II is a well-behaved protein in the SDS-PAGE analysis. However, AgrB-I appears as a smear in the gel. White arrows are provided to indicate where the fl-SpsB cleavage products appear in the vesicles containing the reconstituted AIP biosynthetic pathway.

To determine what AgrD cleavage products were produced in the vesicle assays, we analyzed the AgrD-containing vesicles with fl-SpsB and/or AgrB via RP-HPLC and mass spectrometry (Table 9). For solubility purposes, we reconstituted vesicles containing either N-terminal FLAG and His_6-tagged AgrD-I or AgrD-II (FLAG-AgrD-I and FLAG-AgrD-II, respectively). We also had wild-type AgrD-I available for vesicle incorporation. In order to perform this analysis, vesicle lipid removal was accomplished with solid phase extraction (SPE) columns and lyophilized elutions thereof were then dissolved and injected into the RP-HPLC. Fractions from the RP-HPLC analysis were then analyzed via ESI-MS.

In the AIP-I biosynthesis vesicles containing either FLAG-AgrD-I or AgrD-I, MS-detected cleavage products confirmed AgrB cleavage and removal of the SID of AgrD-I (Table 9, Rxn. 2 and 4). We also detected the AgrD(1-32)-I-thiolactone, when wild-type AgrD-I was incorporated into vesicles (Table 9, Rxn. 2). These vesicles also contained AgrD fragments of the hydrolyzed thiolactone molecule (Table 9, Rxn. 2 and 4). Hydrolysis of the thiolactone is not unexpected at a pH of 8, which is the optimal pH for SpsB activity.[143] In addition to containing fragments suggesting correct AgrB processing of AgrD-I, all of the reactions where fl-SpsB was reconstituted into vesicles containing AgrD-I (Table 9, Rxn. 1-4) produced fragments suggesting correct fl-SpsB cleavage. All of the vesicles containing fl-SpsB also contained fragments indicating cleavage between the Ser-26 and Thr-27 residues of AgrD-I (Table 9, Rxn. 1 and 3). This non-specific cleavage of AgrD-I would produce a truncated tail in AIP-I (Table 9, Rxn. 1-4). Finally, we did not detect the mature excised AIP-I in any of the vesicles. Taken

together, these data suggest that fl-SpsB can correctly cleave AgrD-I when reconstituted into a membrane, but it may also result in non-specific cleavage.

Having detected SpsB cleavage of AgrD-I, it was now possible to investigate SpsB cleavage of AgrD-II. In the AIP-II biosynthesis vesicles, we again confirmed correct AgrB-II cleavage and removal of the AgrD-II SID (Table 9, Rxn. 6). However, these vesicles produced no fragments that corresponded to correct SpsB cleavage of AgrD-II, although there were several fragments suggesting non-specific cleavage (Table 9, Rxn. 5 and 6). The vesicles containing fl-SpsB and FLAG-AgrD-II also only produced fragments with this non-specific cleavage (Table 9, Rxn. 5). Furthermore, the non-specific cleavage observed would produce AIP-II without the tail sequence, which is a known AgrC-II antagonist.[62, 83] As with the AIP-I biosynthesis vesicles, mature AIP-II was not detected, but more importantly, we suspected that SpsB was not the protease responsible for cleaving the MAD of AgrD-II.

Table 9. MS Data For RP-HPLC Analysis of AgrD Cleavage Vesicles

Vesicle Rxn.	Mass Observed $[M+H]^+$	Fragment	Notes
Rxn 1. ***AgrD-I + fl-SpsB***	5297	AgrD-I	unreacted
	2938	H-MNTLFNLFFDFITGILKNIGNIAAYS-OH	incorrect cleavage
	2688	H-MNTLFNLFFDFITGILKNIGNIAA-OH	**correct SpsB cleavage**
	2627	H-YSTCDFIMDEVEVPKELTQLHE-OH	**correct SpsB cleavage**
	2376.5	H-TCDFIMDEVEVPKELTQLHE-OH	incorrect cleavage
Rxn. 2 ***AgrD-I + AgrB-I + fl-SpsB***	3649	H-MNTLFNLFFDFITGILKNIGNIAAYSTCDFIM-OH	AgrB cleavage, hydrolyzed thiolactone
	3631	H-MNTLFNLFFDFITGILKNIGNIAAYSTCDFIM^	AgrD-I Thiolactone
	2938	H-MNTLFNLFFDFITGILKNIGNIAAYS-OH	incorrect cleavage
	2688	H-MNTLFNLFFDFITGILKNIGNIAA-OH	**correct SpsB cleavage**
	2376.5	H-TCDFIMDEVEVPKELTQLHE-OH	incorrect SpsB cleavage
	1666	H-DEVEVPKELTQLHE-OH	SID Sequence, AgrB cleavage
Rxn. 3 ***FLAG-AgrD-I + fl-SpsB***	7360	FLAG-AgrD-I	unreacted
	5001	FLAG-MNTLFNLFFDFITGILKNIGNIAAYS-OH	incorrect cleavage
	4751	FLAG-MNTLFNLFFDFITGILKNIGNIAA-OH	**correct SpsB cleavage**
	2376	H-TCDFIMDEVEVPKELTQLHE-OH	incorrect cleavage
	2172	H-DFIMDEVEVPKELTQLHE-OH	incorrect cleavage
Rxn. 4 ***FLAG-AgrD-I + AgrB-I + fl-SpsB***	5728	FLAG-MNTLFNLFFDFITGILKNIGNIAAYSTCDFIM-OH	AgrB cleavage, hydrolyzed thiolactone
	5001	FLAG-MNTLFNLFFDFITGILKNIGNIAAYS-OH	incorrect cleavage
	4751	FLAG-MNTLFNLFFDFITGILKNIGNIAA-OH	**correct SpsB cleavage**
	2376	H-TCDFIMDEVEVPKELTQLHE-OH	incorrect cleavage
	1666	H-DEVEVPKELTQLHE-OH	SID Sequence, AgrB cleavage
Rxn. 5 ***FLAG-AgrD-II + fl-SpsB***	7212	FLAG-AgrD-II	unreacted
	4961	H-MNTLVNMFFDFIIKLAKAIGIVGGVNA-OH	incorrect cleavage
	2269	H-CSSLFDEPKVPAELTNLYDK-OH	incorrect cleavage

	7212	FLAG-AgrD-II	unreacted
Rxn. 6	5498	FLAG-MNTLVNMFFDFIIKLAKAIGIVGGVNACSSLF-OH	correct AgrB cleavage
FLAG-AgrD-II + AgrB-II + fl-SpsB	4961	H-MNTLVNMFFDFIIKLAKAIGIVGGVNA-OH	incorrect cleavage
	4180	FLAG-MNTLVNMFFDFIIKLAKA-OH	incorrect cleavage
	2269	H-CSSLFDEPKVPAELTNLYDK-OH	incorrect cleavage
	1732	H-DEPKVPAELTNLYDK-OH	correct AgrB cleavage

^C-terminus is cyclized to form thiolactone macrocycle

Substrate	Epitope Tag	AgrD Sequence
AgrD-I		**MNTLFNLFFDFITGILKNIGNIAAYSTCDFIMDEVEVPKELTQLHE**
FLAG-AgrD-I	**MDYKDDDDKHHHHHHGG**	**MNTLFNLFFDFITGILKNIGNIAAYSTCDFIMDEVEVPKELTQLHE**
FLAG-AgrD-II	**MDYKDDDDKHHHHHHGG**	**MNTLVNMFFDFIIKLAKAIGIVGGVNACSSLFDEPKVPAELTNLYDK**

3.4 Detection of AIP from the Proteoliposomes Containing fl-SpsB and AgrD(1-32)-I Thiolactone

In an attempt to detect the AIP-I activity from the vesicle-reconstituted AIP-I biosynthesis, we developed a coupled vesicle and β-lactamase assay (See Appendix). After overnight incubation, AIP-I or AIP-II biosynthesis vesicles were buffered to pH 5.9 and then incubated with their respective group β-lactamase reporter assay strain. AIP-induced β-lactamase activity was then determined using the nitrocefin method. Initial attempts to detect AIP-I activity from vesicles containing AgrD, AgrB and fl-SpsB led to inconclusive results, possibly reflecting the very small amounts of mature AIP generated using this fully reconstituted system. In an effort to simplify our vesicle assay system to detect AIP activity, we prepared vesicles with fl-SpsB and pre-formed AgrD(1-32)-I-thiolactone, which was synthesized either using recombinant methods employing intein fusions or using Boc-SPPS as discussed previously in *Sections 2.2.3* and *2.3.2,* respectively. We then tested the buffered vesicles with the β-lactamase assay to detect activity associated with AIP-I. Excitingly, we detected AIP-I activity using this coupled vesicle and β-lactamase assay (Figure 34). As a control, AIP-I was also incorporated into vesicles to ensure the reporter gene assay cells responded to a known agonist. Importantly, we were also able to detect the generation of AIP-I from the fl-SpsB and AgrD(1-32)-I-thiolactone vesicle system using RP-HPLC-MS (Figure 35).

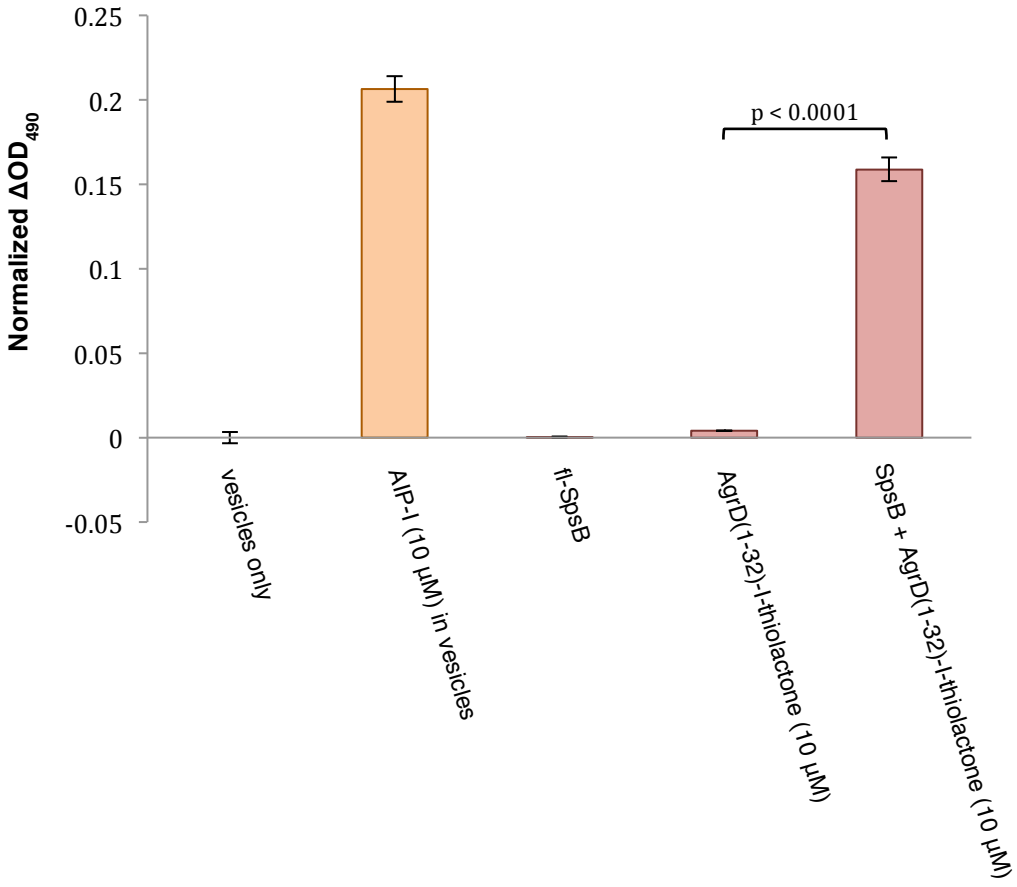

Figure 34. fl-SpsB Cleaves the AgrD(1-32)-I-thiolactone to Generate AIP-I Activity

β-lactamase activity assay of the fl-SpsB and AgrD(1-32)-I-thiolactone vesicles is plotted. The indicated vesicles were incubated with an exponential phase culture of group I *S. aureus* reporter strain (RN9222). Samples were removed after 60 minutes and assayed for β-lactamase activity by the nitrocefin method. Normalized ΔOD_{490} was calculated the same as in Figure 20A. The plot is relative to empty vesicles normalized to zero. Errors; SD, n = 3. The important p-value is designated with a bracket and the numerical p-value above.

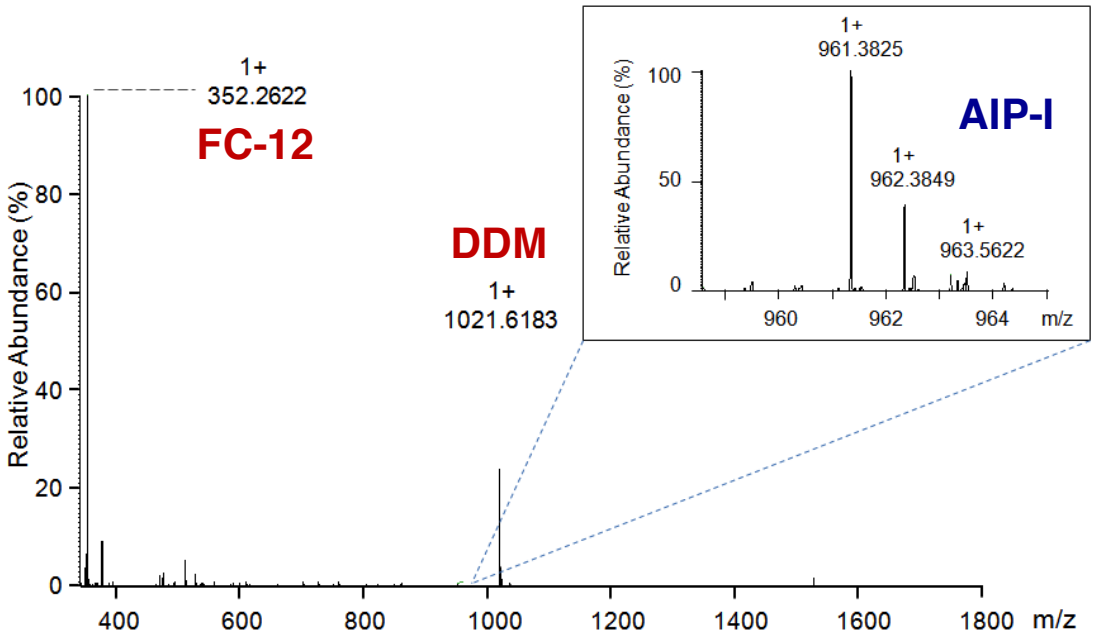

Figure 35. AIP-I Production from SpsB and AgrD(1-32)-I-thiolactone Proteoliposomes Confirmed Via RP-HPLC-MS Analysis

RP-HPLC-MS analysis of SpsB cleavage of AgrD(1-32)-I-thiolactone is shown. After lipid removal with SPE columns, the 70% elution was analyzed with RP-HPLC-MS at the Princeton University Molecular Biology MS Facility. Peaks at 352.26 and 1021.62 Daltons correspond to the detergents FC-12 and DDM (dimerized), respectively. The inset shows the presence of trace amounts of AIP-I in the sample.

3.5 fl-SpsB Does Not Cleave AgrD-II (work on this section was accomplished in collaboration with Xinhui [Connie] Wang)

3.5.1 fl-SpsB Does Not Cleave AgrD(1-32)-II-thiolactone

While we had successfully detected AIP-I production, all of our previous efforts suggested that SpsB does not cleave AgrD-II. Using the same approach to detect AIP-I production, we decided to try and reconstitute fl-SpsB and AgrD(1-32)-thiolactone into vesicles. We had previously synthesized the group II thiolactone using the general strategy of Lyon *et al*.[63] for distribution-coefficient measurements (See *Section 2.3.2* for description and *Chapter 6* for characterization data).

Since fl-SpsB cleavage of AgrD-II only produced non-specific cleavage, we wondered if SpsB required some other factor to process AgrD-II. When SpsB was first characterized in the literature, it was noted that an inactive type I signal peptidase (termed SpsA) is transcribed on the same mRNA and is separated from the SpsB gene by 15 basepairs.[73] SpsA is proposed to be structurally homologous to SpsB, but it has not been extensively characterized. Kavanaugh *et al*. purified SpsA but found it to be inactive in their peptidase assays.[58] Cregg et al. speculated that SpsA might act like some eukaryotic proteases that have mutated and become inactive but are still used as a binding partner for other proteases.[73] We decided to test whether SpsA assists SpsB cleave AgrD-II, so we purified it under the same conditions as fl-SpsB and characterized it using size-exclusion chromatography and ESI-MS (data not shown). As expected, SpsA did not cleave the control peptide in the *in vitro* HPLC assay described in *Section 2.4.1* (data not shown), which is also the same behavior observed by Kavanaugh *et al*.[58]

With fl-SpsB, SpsA and AgrD(1-32)-II-thiolactone in hand, we incorporated these three components into proteoliposomes and then analyzed these vesicles with the β-lactamase reporter gene assay (Figure 36). In the presence of only SpsA or SpsB, we observed no cleavage of the AgrD(1-32)-II-thiolactone, and when both proteins were incorporated into vesicles with the group II thiolactone, no cleavage of the AgrD(1-32)-II-thiolactone was observed. Since AIP-II could be detected when incorporated into vesicles, it was unlikely that the reporter gene assay cells were not detecting AIP-II produced in vesicles containing fl-SpsB and AgrD(1-32)-II-thiolactone. Instead, we suspected that SpsA might prevent SpsB cleavage of AgrD. Therefore, we prepared vesicles with the same fl-SpsB and SpsA stocks, but we included the AgrD(1-32)-I-thiolactone. We then analyzed these group I reaction vesicles with the β-lactamase reporter gene assay (Figure 37). From the analysis of the AgrD(1-32)-I-thiolactone vesicles, it was evident that SpsB was active in the presence of SpsA. Furthermore, SpsA did not cleave the AIP-I precursor. At the very least, these observations suggest that fl-SpsB was active in the AgrD(1-32)-II-thiolactone vesicles, and SpsA does not interact with fl-SpsB to facilitate the correct processing of AgrD-II.

In a final attempt to determine whether SpsB could cleave AgrD-II, we prepared vesicles that also incorporated AgrB-II along with SpsA, fl-SpsB and the group II thiolactone. We then analyzed these group II reaction vesicles with the β-lactamase reporter gene assay (Figure 38). Once again, there was no cleavage of the AgrD-II-thiolactone as indicated by a lack of detectable AIP-II activity.

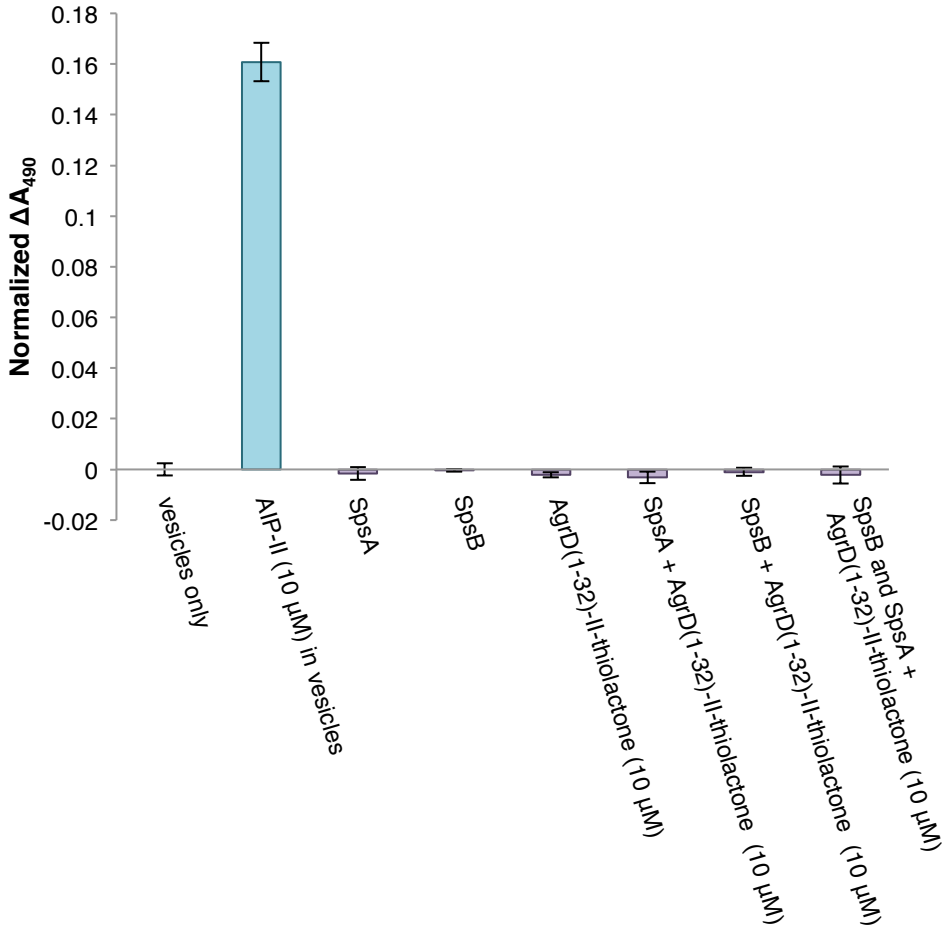

Figure 36. SpsA Does Not Promote SpsB Cleavage of the AgrD(1-32)-II-thiolactone

β-lactamase activity assay of the fl-SpsB, SpsA and AgrD(1-32)-II-thiolactone vesicles is plotted. The indicated vesicles were incubated with an exponential phase culture of group II *S. aureus* reporter strain (RN9367). Samples were removed after 60 minutes and assayed for β-lactamase activity by the nitrocefin method. Normalized ΔOD_{490} was calculated the same as in Figure 20A. The plot is relative to empty vesicles normalized to zero. Errors; SD, n = 3.

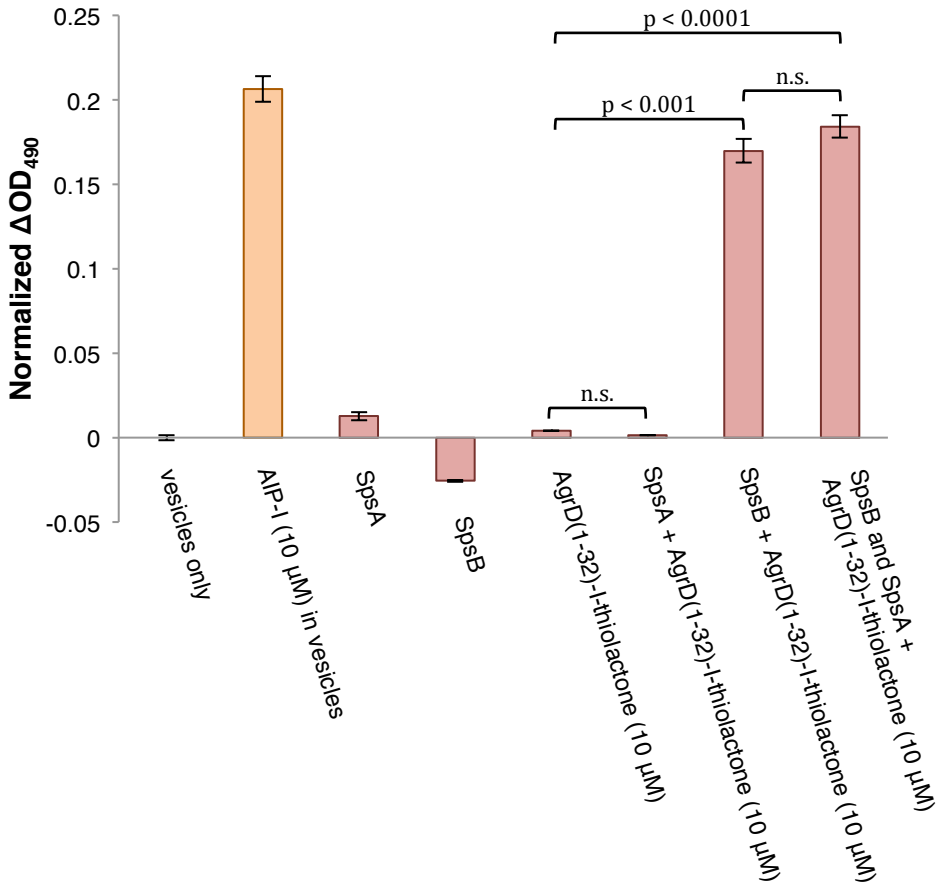

Figure 37. SpsB Cleaves the AgrD(1-32)-I-thiolactone in the Presence of SpsA

β-lactamase activity assay of the fl-SpsB, SpsA and AgrD(1-32)-I-thiolactone vesicles is plotted. The indicated vesicles were incubated with an exponential phase culture of group I *S. aureus* reporter strain (RN9222). Samples were removed after 60 minutes and assayed for β-lactamase activity by the nitrocefin method. Normalized ΔOD_{490} was calculated the same as in Figure 20A. The plot is relative to empty vesicles normalized to zero. Errors; SD, n = 3. The important p-values are designated with a bracket and the numerical p-value above.

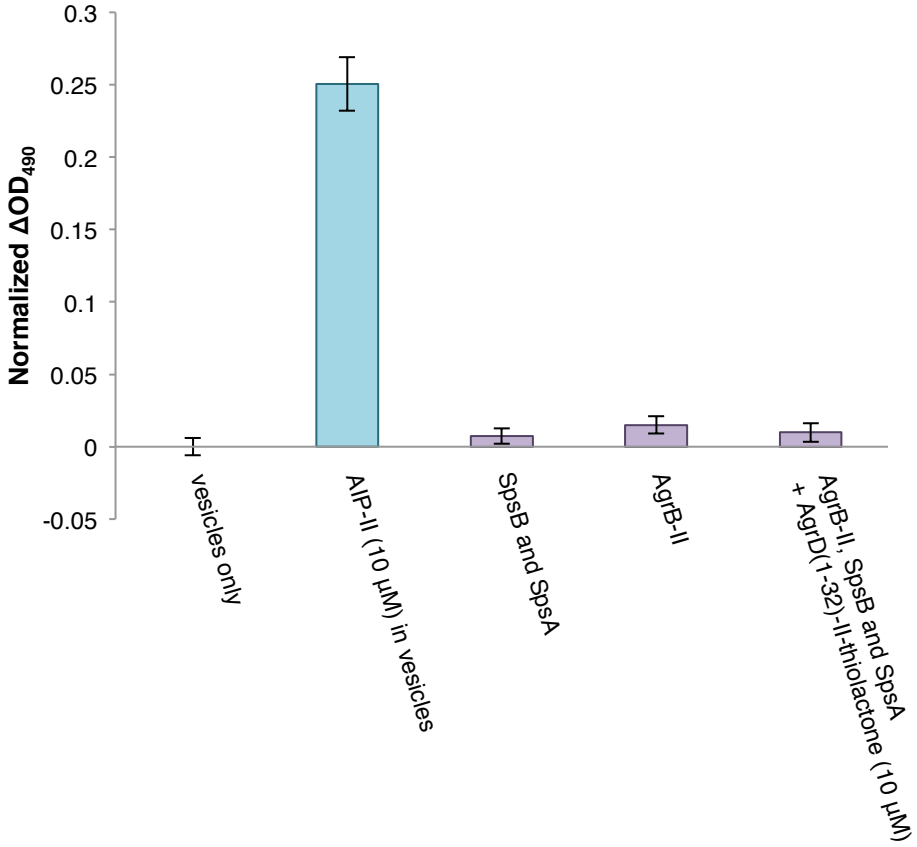

Figure 38. AgrB-II Does Not Interact with fl-SpsB to Correctly Cleave the AgrD(1-32)-II-thiolactone

β-lactamase activity assay of the fl-SpsB, SpsA, AgrB-II and AgrD(1-32)-II-thiolactone vesicles is plotted. The indicated vesicles were incubated with an exponential phase culture of group II *S. aureus* reporter strain (RN9367). Samples were removed after 60 minutes and assayed for β-lactamase activity by the nitrocefin method. Normalized ΔOD_{490} was calculated the same as in Figure 20A. The plot is relative to empty vesicles normalized to zero. Errors; SD, n = 3.

3.5.2 A *S. aureus* Membrane Protein Can Cleave The AgrD(1-32)-II-thiolactone

With no clear alternative to SpsB, we wanted to confirm that *S. aureus* whole cells could process the AgrD(1-32)-II-thiolactone. Therefore, we incubated the group II thiolactone with *agr-II* null cells (RN9120), where a tetracycline resistance gene replaced the *agr-II* locus. Therefore, these cells provided a membrane that would contain any accessory proteins necessary for AIP-II production except for AgrB-II and AgrD-II. As part of the experiment, we also prepared a cell culture supernatant where a pre-grown RN9120 culture was filtered and the AgrD(1-32)-II-thiolactone was added to the filtered supernatant. The analysis of this cell culture supernatant could indicate whether a secreted protein might process the AIP-II precursor. After a 4-hr incubation period in the cell culture, the cells were removed via centrifugation, if necessary, and the culture supernatants were filtered. These supernatants were then analyzed with the β-lactamase reporter gene assay (Figure 39). In this case, we observed correct cleavage of the AgrD(1-32)-II-thiolactone as indicated by the emergence of AIP-II activity. Moreover, the cleavage apparently occurs at the membrane, since there was no AIP-II activity detected in the filtered, cell-free RN9120 culture supernatant. Thus, the cleavage is likely not the result of a secreted factor, although it remains unclear what protein cleaves the MAD of AgrD-II to produce AIP-II.

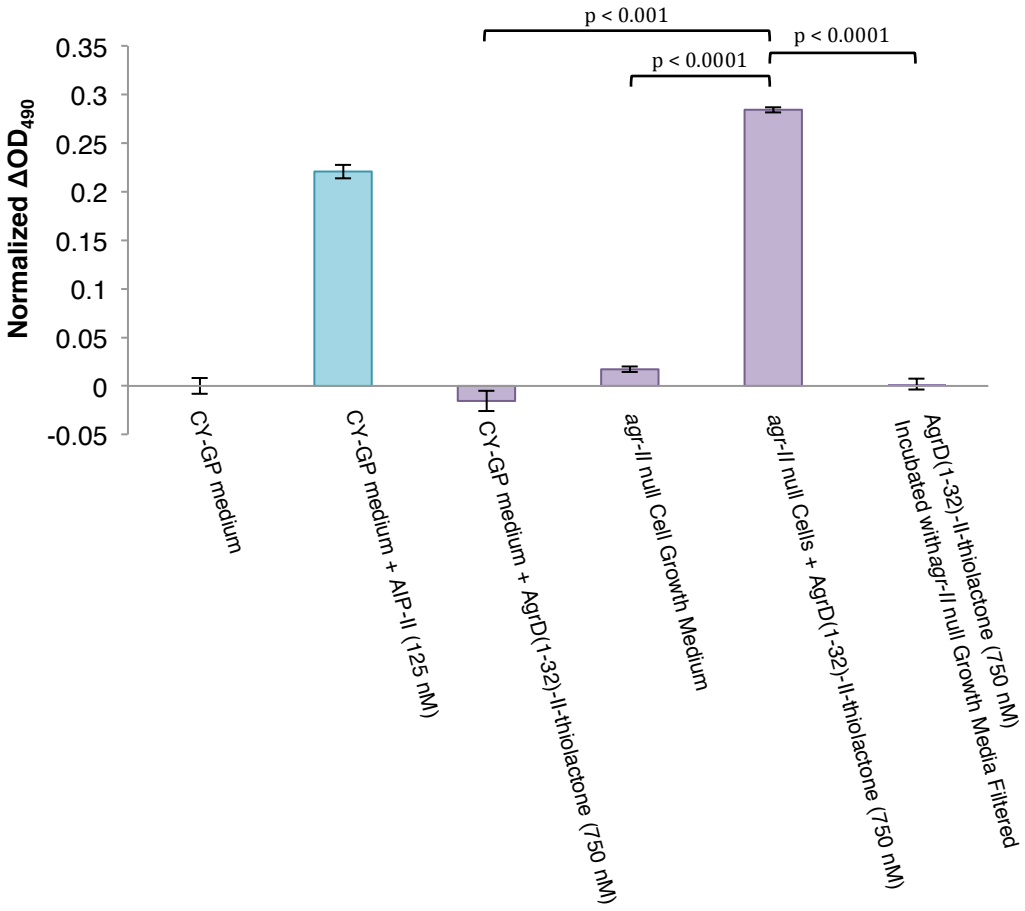

Figure 39. A Membrane Protein Can Cleave the AgrD(1-32)-II-thiolactone

β-lactamase activity assay of cell culture supernatants from *agr-II* null cells incubated with the AgrD(1-32)-II-thiolactone is plotted. Filtered cell culture supernatants were incubated with an exponential phase culture of group II *S. aureus* reporter strain (RN9367). Samples were removed after 60 minutes and assayed for β-lactamase activity by the nitrocefin method. Normalized ΔOD_{490} was calculated the same as in Figure 20A. The plot is relative to the CY-GP media normalized to zero. Errors; SD, n = 3. Important p-values are indicated with a bracket and the numerical p-value above.

3.6 Conclusions

In this chapter, we investigated the role of SpsB in AIP biosynthesis. Our findings extend the current understanding of how SpsB is likely only one of several proteases capable of processing AgrD(1-32)-thiolactone. To investigate the final cleavage step in AIP biosynthesis, we employed several *in vitro* SpsB biochemical assays to elucidate some of the requirements for SpsB cleavage of AgrD. We found that small, non-fluorescein labeled peptides are poor substrates for SpsB and that correct cleavage of AgrD-I requires a membrane. Once SpsB is incorporated into a lipid bilayer environment, it can correctly process AgrD-I and the AgrD(1-32)-I-thiolactone. To our knowledge, this is the first study with direct evidence that SpsB is involved in AIP-I biosynthesis. We detected AIP-I from SpsB-containing vesicles using a biological cell-based assay and directly by RP-HPLC-MS. Our study is also the first to investigate the possible SpsB cleavage of AgrD-II. We found that SpsB does not correctly cleave AgrD-II or AgrD(1-32)-II-thiolactone. Importantly, we found that *S. aureus* cells are able to correctly process the AgrD(1-32)-II thiolactone to give robust AIP-II activity implying an unknown protease. These studies also suggest that this unknown protease is associated with the cell membrane or peptidoglycan. Interestingly, our data suggests that multiple proteases are used in the final step of AIP biosynthesis and that these proteases may be group-specific. Consistent with previous models, we propose that the final proteolysis of AgrD occurs at the outer leaflet of the membrane enabling release of the AIP into the cellular mileau.

Chapter 4. Increasing AIP Macrocycle Size Reveals Key Features of *agr* Activation

4.1 Introduction

In the last two decades, a number of SAR studies have explored the importance of amino acid sequence in the four AIP groups using alanine-substitution, D-amino acid substitution and other native and non-native amino acid mutations.[45, 59, 62, 63, 79, 80, 83-86, 146] These studies have identified key amino acid residues, side-chain orientations and backbone interactions within AIPs required for activation and inhibition.[45, 59, 61-63, 79, 80, 83-86] Moreover, this work has led to the discovery, and in a few cases rational design, of *agr* inhibitors active against all four groups.[45, 62, 80, 83, 84] Examples of these global inhibitors include a truncated version of AIP-II lacking the tail region[63, 83] and, of relevance for this study, an analog of AIP-I in which the second endocyclic residue (Asp-5 in the primary sequence of AIP-I) is replaced by alanine.[63, 80] Note, this same residue in AIP-I can also be replaced with Asn or Phe to produce two agonists with activity comparable to that of the native peptide (Table 1).[63] While some specificity determinants important for recognition of the AIP with its receptor are understood, particularly for the AIP-I/AgrC-I pair (Figure 12C),[82] the molecular recognition principles underlying receptor agonism versus antagonism by a given AIP are incomplete. In order to better understand the relationship between AIP structure and function, we wanted to investigate the defining structural feature of the AIP: its thiolactone macrocycle (Figure 40). The effect of changing the thiolactone linkage to a lactone or lactam on AIP activity has been previously explored,[45] and alanine scanning of AIP-I indicated which residues within the macrocycle are essential for *agr* activation.[80] However, the importance of ring size on activity remains unclear. Exploiting AIP-I as a scaffold to investigate this question, we

used L-β-homo-amino acid (hβ-AA) substitution, proline substitution and amino acid deletion mutants as a means to systematically vary the size and backbone conformation of the AIP macrocycle (Figure 40, Table 10). We also substituted homocysteine (Hcy) for cysteine in AIP-I, -II and -III to see whether extending the thioester linkage effects *agr* activity. Notably, the activity of these analogs was studied using both cell based and biochemical assay systems, the first time such a comparative analysis has been possible on AIP analogs.

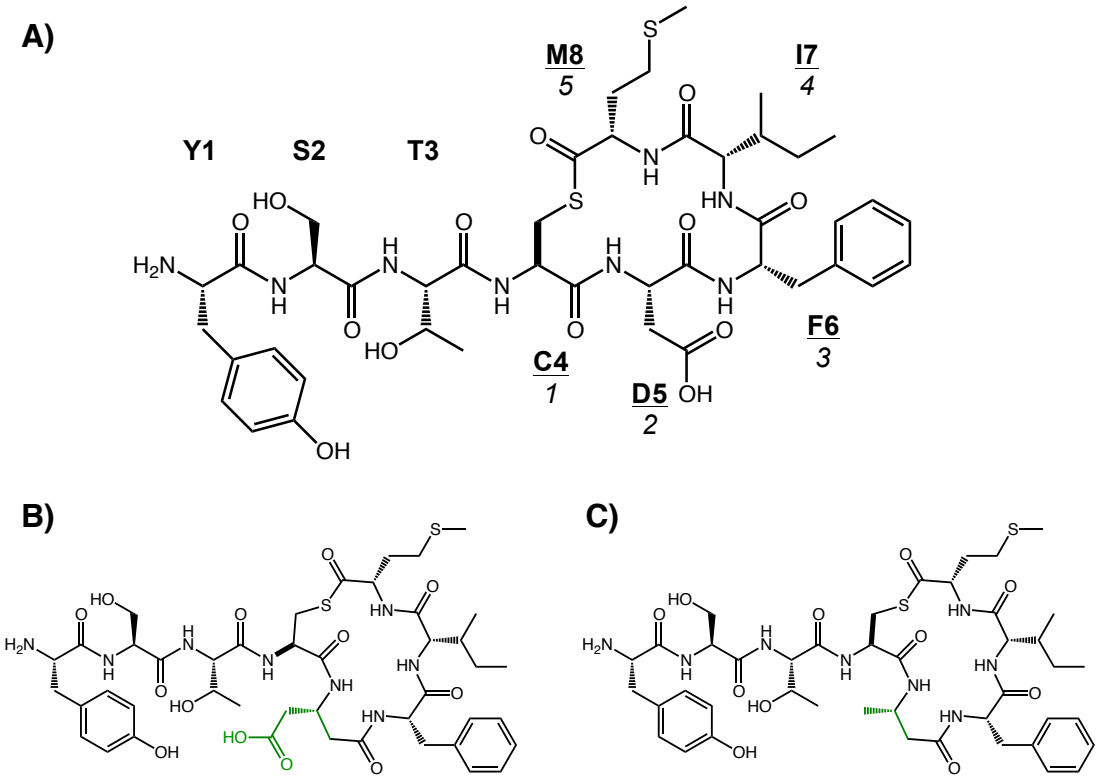

Figure 40. AIP-I Structure and Some Examples of Enlarged AIP-I Analogs

A) The AIP-I chemical structure is shown. The native AIP-I amino acid residues are numbered, with the macrocycle residues underlined and their ring position italicized. Inserting a methylene group into the macrocycle of most AIP-I analogs was accomplished using L-β-homo-amino acids as in **B)** hβ-Asp AIP-I and C) D5A hβ-Ala AIP-I (the inserted methylene group and shifted sidechain in the hβ-AA analog is indicated in green). Homocysteine was also used to enlarge the macrocycle of AIP-I, -II and -III.

4.2 Design, Synthesis and Functional Analysis of AIP Analogs Featuring Enlarged, Reduced or Constrained Macrocycles

4.2.1 Design and Synthesis of AIP Analogs

Several SAR studies[45, 63, 80] and AgrC mutant studies[82, 87] have focused on the group I system in their investigation of *agr* activation and inhibition. This information and data provides helpful insight for additional structural studies and makes AIP-I a model scaffold to study the effect of macrocycle size on function (Figure 40). This decision was also guided by the recently reported biochemical characterization of its cognate receptor, AgrC-I, providing new biochemical tools to enhance this SAR study. To enlarge the AIP macrocycle, we elected to substitute the canonical L-amino acids in the endocyclic region of the molecule with the corresponding L-β-homo-amino acids (hβ-AAs), thereby inserting a main-chain atom whilst maintaining the size and stereochemistry of the side-chains. We also expanded the ring by substituting L-cysteine with L-homocysteine. Note, for comparative reasons, this change was also made in AIP-II and AIP-III. To reduce the ring size, we decided to prepare two deletion analogs of AIP-I in which either Phe-6 or Ile-7 was removed. The design of these peptides was guided by previous alanine-scanning studies that showed neither of these amino acid sidechains is absolutely essential for activity.[80] In contrast, Asp-5, corresponding to the second endocyclic position, was found to be important for AIP activity and hence was not deleted. Finally, to explore the effect of perturbing the backbone conformation, we generated AIP-I analogs in which Phe-6 or Ile-7 were replaced by proline.

All AIP analogs were generated according to the general strategy of Lyon *et al*.[63] Briefly, linear peptide α-thioesters were generated by solid phase peptide synthesis (SPPS) employing a Boc-N^{α} protection logic and using a 3-mercaptopropionamide-based linker system (Figure 41). Following cleavage from the support with anhydrous HF, the crude unprotected peptides were cyclized in water at neutral pH via an intramolecular trans-thioesterification reaction. AIP analogs were then purified by RP-HPLC and characterized by ESI-MS and ^{1}H NMR (See Table 10 and *Materials and Methods* for characterization data).

4.2.2 Functional Analysis of AIP Analogs Featuring Enlarged, Reduced or Constrained Macrocycles (work on this section was accomplished in collaboration with Boyuan Wang)

We first assessed the activity of our AIP analogs using a β-lactamase reporter assay (See Appendix), which can be used to test the ability of each AIP analog to activate or inhibit the *agr* response in *S. aureus* cells (Table 11, Figure 42). This assay reports on signal transduction through the entire *agr* TCS and has, over many years, been the workhorse tool for assessing AIP activity.[45, 62, 63, 80, 83, 87] All of the peptides were tested against their cognate AgrC for self-activation or inhibition, and they were tested against non-cognate AgrC-II.

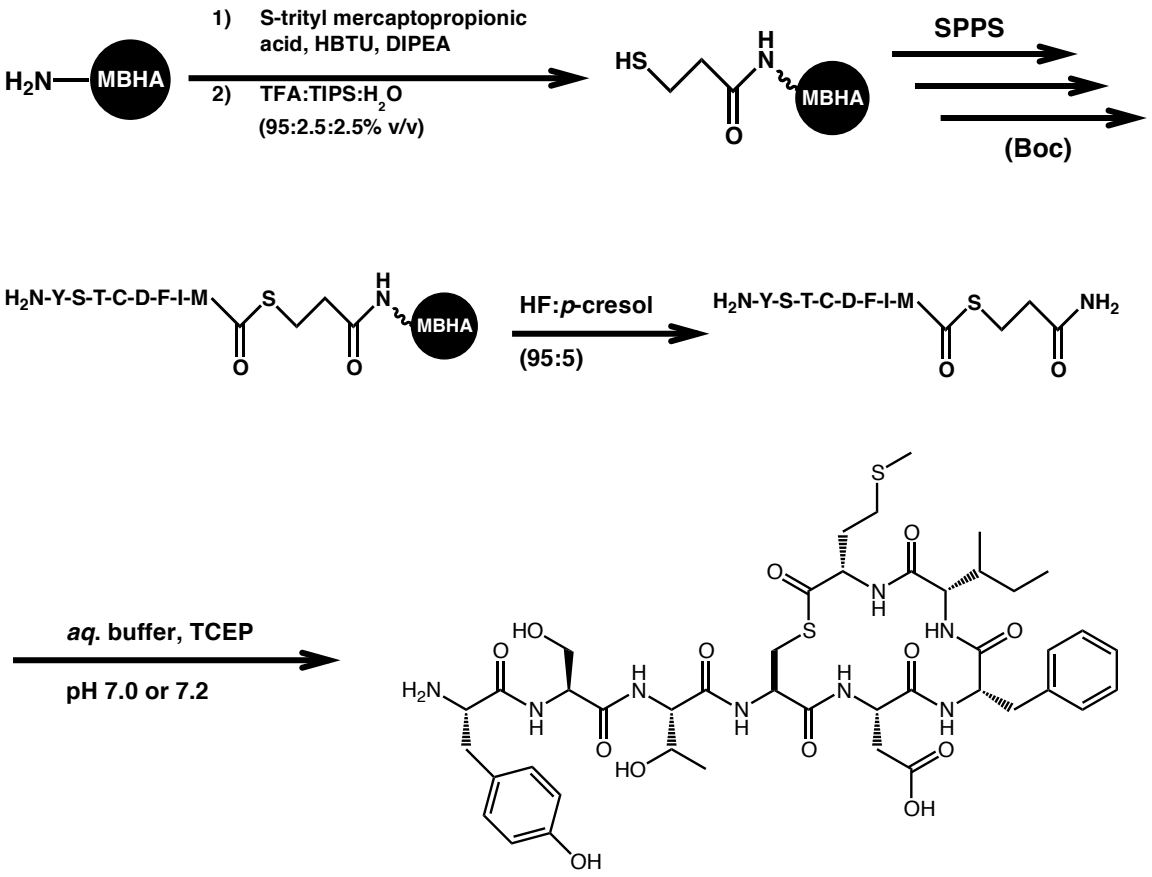

Figure 41. Synthetic Route for Boc-SPPS of AIP-I

The 3-mercaptopropionamide-based linker is synthesized on resin whereupon coupling the C-terminal amino acid results in formation of a linear thioester. Chain elongation is achieved with standard Boc-based solid phase peptide synthesis (SPPS) conditions. The peptide is cleaved from the resin with anhydrous HF and cyclized via intramolecular trans-thioesterification upon addition of aqueous buffer at neutral pH. The synthesis of AIP-I is shown as an example. For some of the enlarged AIP-I analogs, the aqueous buffer was at pH 7.2.

Table 10. Analytical Characterization of Altered Macrocycle AIP Analogs

AIP Analog	Sequence	Expected Thioester Mass	Observed Thioester Mass	Expected Thiolactone Mass	^Observed Thiolactone Mass	*HPLC R_t (min.)
Hcy AIP-I	YSTC[1]DFIM	1079.4	1079.44	974.4	975.4	19.21
Hcy AIP-II	GVNAC[1]SSLF	997.4	997.44	892.4	893.4	17.28
Hcy AIP-III	INC[1]DFLL	937.4	937.45	832.4	833.4	20.34
hβ-Met AIP-I	YSTCDFIM[2]	1079.4	1079.42	974.4	975.4	18.78
hβ-Ile AIP-I	YSTCDFI[2]M	1079.4	1079.42	974.4	975.4	18.11
hβ-Phe AIP-I	YSTCDF[2]IM	1079.4	1079.41	974.4	975.4	18.35
hβ-Asp AIP-I	YSTCD[2]FIM	1079.4	1079.41	974.4	975.4	18.51
F6P AIP-I	YSTCDPIM	1015.4	1015.4	910.4	911.4	16.76
I7P AIP-I	YSTCDFPM	1049.4	1049.4	944.3	945.3	16.35
ΔF6 AIP-I	YSTCDIM	918.3	918.33	813.3	814.3	16.27
ΔI7 AIP-I	YSTCDFM	952.3	952.33	847.3	848.3	16.92
D5A β-Ala AIP-I	YSTCA[3]FIM	1021.4	1021.41	916.4	917.4	18.08
D5A hβ-Ala AIP-I	YSTCA[2]FIM	1035.4	1035.43	930.4	931.2	18.98

^Observed thiolactone mass is equal to $(M + H^+)$

*HPLC Retention time of the final, cyclized AIP analog.

Endocyclic residues of the AIP macrocycle are underlined in the "Sequence" column of the table.

[1]Hcy, homocysteine replaces native cysteine residue within the indicated AIP analog

[2]hβ, L-β-homo-amino acid replaces indicated residue within the native AIP-I or D5A AIP-I sequence

[3]β, β-Alanine replaces indicated residue within the D5A AIP-I sequence

One mutation at endocyclic position 2 preserves self-activation: Asp-5 could be replaced with hβ-Asp (Table 11, Figures 40A and 42A). The hβ-Asp AIP-I analog has an EC_{50} value ~30-fold weaker than the native AIP-I (Table 11, Figure 42A), which makes it a moderate, nanomolar AIP-I activator similar to Y1A and T3A AIP-I analogs.[80] It also has a weaker inhibitory effect on AgrC-II with an IC_{50} value above 2 μM (Figure 42A). For the most part, however, replacing native amino acid residues with hβ-AAs in the AIP-I macrocycle produced inactive AIP-I analogs, and the constrained and smaller macrocycle AIP-I analogs showed no activity in the cell-based assays (Table 11). Evidently, the AIP-I macrocycle must have a particular size and some conformational flexibility in order for AgrC-I to bind AIP-I.

We were also keen to see the effect of increased AIP macrocycle size on antagonism of the AgrC receptor, which has previously been more resilient to changes in the AIP macrocycle.[45, 62, 63, 79, 80, 83] This indeed appears to be the case (Table 11). Thus, while some trends observed for activation of the response were also seen for inhibition (e.g. among the L-β-homo-amino acid substitutions only the hβ-Asp analog retained measureable, albeit weakened, activity); a few of the analogs that were inactive as agonists were active as antagonists. Specifically, the Hcy containing AIP analogs all had the expected cross- group inhibitory activity (Table 11, Figure 42B). The Hcy AIP-III analog was a relatively potent inhibitor of AgrC-II (only ~40-fold less than wild-type AIP-III), but a weak inhibitor of AgrC-I. Likewise, Hcy AIP-I was a potent inhibitor of AgrC-II (only ~5-fold less than wild-type AIP-I), while inactive against AgrC-I.

Table 11. Activity of AIP Analogs

	Cell-based β-lactamase reporter gene assays			*in vitro* assays using AgrC-I incorporated into nanodiscs	
AIP Analog	**Self-activation EC_{50} (95% CI)**	**Group I Inhibition IC_{50} (95% CI)**	**Group II Inhibition IC_{50} (95% CI)**	**AgrC-I Binding***	**Autokinase Activity^**
AIP-I	28 nM[5] (18-46)	—	25 nM[5] (14-45)	+++	5.0 ± 0.3
AIP-II	30 nM[5] (10-90)	40 nM[5] (12-140)	—	+++	0.59 ± 0.05
AIP-III	26 nM[5] (22-31)	70 nM[5] (30-150)	6 nM[5] (5-6.5)	+++	1.51 ± 0.09
Hcy AIP-I[1]	—	—	123.3 nM (90-163)	+	1.04 ± 0.07
Hcy AIP-II[1]	—	>2 μM	—	+	0.95 ± 0.06
Hcy AIP-III[1]	—	>2 μM	234.0 nM (185-296)	++	1.00 ± 0.06
hβ-Met AIP-I[2]	—	—	—	—	nt[4]
hβ-Ile AIP-I[2]	—	—	—	—	nt[4]
hβ-Phe AIP-I[2]	—	—	—	—	nt[4]
hβ-Asp AIP-I[2]	809.1 nM (741-883)	—	>2 μM	+++	2.8 ± 0.3
F6P AIP-I	—	—	—	—	nt[4]
I7P AIP-I	—	—	—	—	nt[4]
ΔF6 AIP-I	—	—	—	—	nt[4]
ΔI7 AIP-I	—	—	—	—	nt[4]
D5A AIP-I	—	5 nM[5] (3-7)	8 nM[5] (4-17)	+++	3.3 ± 0.3
D5A hβ-Ala AIP-I[2]	344.5 nM (316-375)	—	970.5 nM (590-1595)	+++	4.1 ± 0.7
D5A β-Ala AIP-I[3]	—	—	—	+	1.63 ± 0.09

The dash (—) indicates no activity observed with AIP analogs at concentrations up to 10 μM. [1]Hcy, homocysteine, replaces native cysteine residue within the indicated AIP. [2]L-β-homo-amino acid replaces indicated residue within the native AIP-I or D5A AIP-I sequence. [3]β-Alanine replaces D5 in the AIP-I sequence. [4]nt, not tested. [5]These values are previously reported,[63] and our data (not shown) confirms them. *AgrC-I Binding assay: +++ strong binding, ++ moderate binding, + weak binding and — no binding (Figure 46) ^AgrC-I Autokinase assay: reported as a fold-increase (± SD) to the basal level of AgrC-I autophosphorylation (Figure 43)

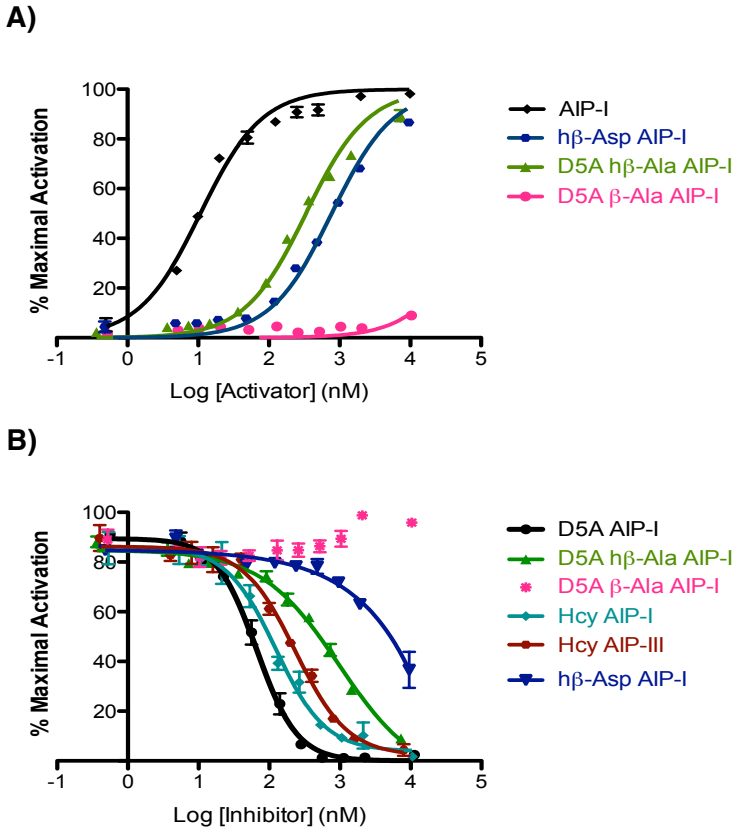

Figure 42. Cellular activity of AIP Analogs.

A) Activation dose-response curves for indicated AIP-I analogs. AIPs were added in increasing concentrations to an exponential phase culture of a group I *S. aureus* reporter strain (RN9222). Samples were removed after 60 minutes and assayed for β-lactamase activity by the nitrocefin method. Data is plotted bas % maximal activation, normalized for cell density, versus peptide concentration. Errors; SEM, n = 3. **B)** Inhibition dose response curves for AIP analogs. Group II reporter cells (RN9367) were treated with a fixed concentration of AIP-II (125 nM) and varying concentrations of the indicated analogs. β-lactamase activity was measured and the normalized data presented as in panel A. The dose-response for the D5A β-Ala AIP-I analog does not fit an inhibition curve. Errors; SEM, n = 3.

Previously, the mutation of Asp-5 in AIP-I to an Ala converted the peptide from an agonist of its cognate receptor, AgrC-I, into an antagonist,[80] a result that we reproduced using the cell-based assay (Table 11, Figure 42B). Thus, we were curious to see the effect of replacing Ala with hβ-Ala at this position. Remarkably, this substitution converted the peptide back into an activator of the group I *agr* response, while leaving it as a cross-group inhibitor (Table 11, Figure 42A). Indeed, the analog is a more potent activator and inhibitor of group I and II cells, respectively, than the corresponding hβ-Asp AIP-I analog. To our knowledge, this is the first time that an AIP analog with global inhibitory activity has been converted back to intra-group activator through the incorporation of second, compensatory modification, in this case the addition of a methylene group in the backbone. To explore this unexpected reversion phenomenon further, we prepared an additional AIP-I analog in which β-Ala was incorporated at position 5, i.e. removal of the methyl side-chain whilst keeping the extra methylene in the mainchain. Surprisingly, the β-Ala analog had no detectable agonism or antagonism activity in our cell-based assay (Table 11, Figure 42).

While the cell-based β-lactamase reporter assay can provide a way to understand some structure-activity relationships between AIP and AgrC, such assays provide no information on the strength of the interaction between the AIP and its receptor, AgrC, nor does it provide a direct readout of the extent to which this interaction activates the kinase activity of the receptor. This information is critical for a full understanding of the functional consequences of altering AIP structure, particularly since AIP binding and AgrC autophosphorylation may be uncoupled events.[88] With this in mind, we tested the

enlarged AIP analogs for cell-based activity in a recently developed *in vitro* AgrC autophosphorylation assay (Figure 43) that uses AgrC-I dimers reconstituted into nanometer-scale lipid bilayer discs (AgrC-I nanodiscs).[88] Briefly, Wang *et al*.[88] designed and characterized a protocol to incorporate AgrC-I into a lipid bilayer that is enclosed by two copies of a scaffold protein used to determine the size of the nanodisc and maintain its shape. AIP-induced activity of AgrC can be determined using autoradiography and/or scintillation counting. Working with Boyuan Wang, we were able to prepare AgrC-I nanodiscs and test the AIP analogs. This SAR study is the first to use such a biochemical tool to directly interrogate the AIP-AgrC interaction, and it provides a direct readout of the extent to which our enlarged AIP analogs activate AgrC-I (Figure 43).

Consistent with the cellular activity, the hβ-Asp and D5A hβ-Ala AIP-I analogs stimulate AgrC-I autophosphorylation *in vitro* (Table 11, Figure 43). However, the extent of that activation was not as robust as AIP-I, which also corresponds with the higher EC_{50} values determined for these enlarged AIP-I analogs. The behavior of the AgrC-I nanodiscs was further confirmed by testing the activity of AIP-II and AIP-III, which are known to act as an inverse agonist and a neutral antagonist, respectively.[87, 88] AIP-II induced less AgrC-I autophosphorylation than the basal level seen when no AIP was incubated with AgrC-I nanodiscs, which demonstrates AIP-II clearly acts as an inverse agonist of AgrC-I. Likewise, the D5A β-Ala AIP-I analog only weakly activates the AgrC-I receptor at high concentrations (10 μM) above basal level autophosphorylation, displaying similar activity to the cross-group inhibitor AIP-III

(Figure 43). The Hcy containing AIP analogs induced no significant autophosphorylation activity in AgrC-I.

In the course of our investigations we encountered one highly unexpected result. The D5A AIP-I analog, which as already noted is a global inhibitor of the *agr* response in cells,[63, 80] was found to activate AgrC-I autophosphorylation *in vitro* (Figure 43). None of the other analogs investigated in this study exhibited such discordant behavior in the *in vitro* and *in vivo* assays. In an effort to explain this contradictory result, we first turned our attention to the phospho-relay step in the *agr* TCS, i.e. phosphoryl-group transfer from AgrC to AgrA. Conceivably, the D5A AIP-I analog might inhibit the phospho-relay process, rather than AgrC autophosphorylation, thereby explaining the data. In the assay, AgrA was incubated with AgrC-I discs labeled with [γ-^{32}P]ATP and mixed with an AIP or AIP analog. Over a time-course, aliquots were removed and analyzed by SDS-PAGE followed by autoradiography. However, we saw no direct or indirect inhibition of phospho-transfer from AgrC-I to AgrA by the D5A AIP-I analog—especially when compared to AIP-II (Figure 44).

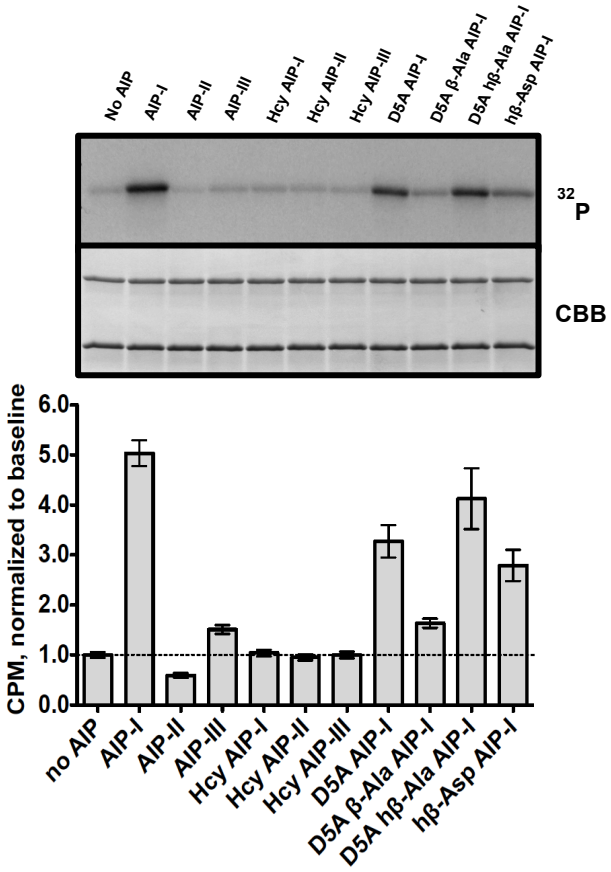

Figure 43. Stimulation of AgrC-I autokinase activity *in vitro* by AIP analogs

AgrC-I nanodiscs were treated with the indicated AIP analog (10 μM) in the presence of [γ-^{32}P]-ATP. Phosphorylation levels were analyzed by autoradiography (top) or quantified by scintillation counting (bottom). Reactions were also analyzed by SDS-PAGE with CBB-stain as a loading control (middle). Error bars = SD (n = 3).

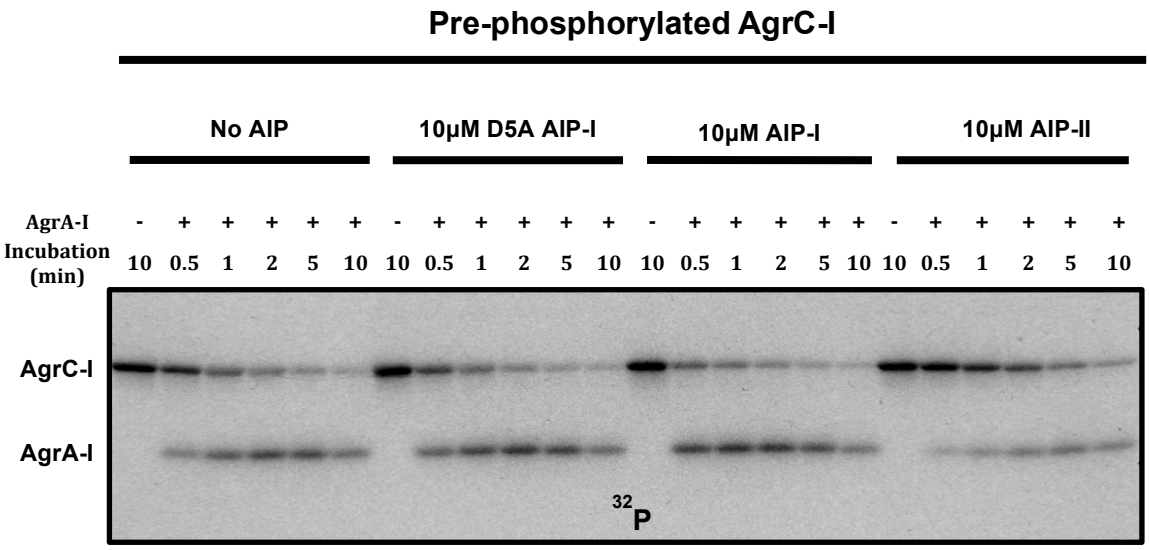

Figure 44. AgrC-I to AgrA Phospho-relay Assay

Phospho-relay assays show the phosphoryl-group transfer from AgrC-I to AgrA. AgrA was incubated with AgrC-I discs labeled with [γ-^{32}P]-ATP and the indicated AIP analogs. Aliquots were then removed at various time points and analyzed by SDS-PAGE followed by autoradiography. D5A AIP-I does not directly or indirectly inhibit phosphoryl-group transfer to AgrA—especially upon comparison to AIP-II, which is an inverse antagonist of AgrC-I.

Next, we turned our attention back to the AgrC-I autokinase activation step. Our initial *in vitro* AgrC-I autophosphorylation assay employed a single concentration of AIP (10 μM). Such a high AIP concentration may not be achievable locally at the AgrC receptor in the context of a cell due to the presence of the peptidoglycan. Hence, we decided to check whether there was a concentration-dependence of D5A AIP-I activation of AgrC-I in the autokinase activity assay. Accordingly, two separate AgrC-I activation assays, using AgrC-I nanodiscs at a concentration of either 2.8 μM or 500 nM, were tested in a dose-response manner by increasing the D5A AIP-I analog concentration. The assays were quantified using scintillation counting, and normalized AgrC-I autokinase activity is reported relative to basal activity (no AIP added). We observed a striking difference in the behavior of AIP-I and the D5A analog in the dose-response assays (Figure 45A); the former activates the receptor even at sub-stoichiometric concentrations relative to AgrC-I nanodiscs, whereas the latter only has a stimulatory effect once the ligand/receptor ratio exceeds 2:1. In the high AgrC-I concentration assay (2.8 μM), the AgrC-I dimer concentration is substantially higher than the IC_{50} value for the D5A AIP-I analog on group I cells (6 nM, Table 1), suggesting that the absence of response at low D5A AIP-I peptide concentrations is not due to a lack of receptor binding (Figure 45A). Still, there was no observed inhibitory effect by D5A AIP-I at a high concentration of AgrC-I dimers.

In the low AgrC-I concentration assay (500 nM), D5A AIP-I again had a stimulatory effect once the ligand/receptor ratio exceeded 2:1 (Figure 45B). However, in this case we observed some inhibitory effect by D5A AIP-I at a sub-stoichiometric

concentration relative to AgrC-I nanodiscs before a strong stimulatory effect began at the ligand/receptor ratio of 2:1. Furthermore, the D5A AIP-I analog did not stimulate AgrC-I to similar levels as AIP-I in either assay (Table 11, Figure 45). Using these two additional AgrC-I autophosphorylation assays combined with the known cell-based assay data indicated that the D5A AIP-I analog might access multiple binding sites within the AgrC-I nanodiscs (discussed further later).

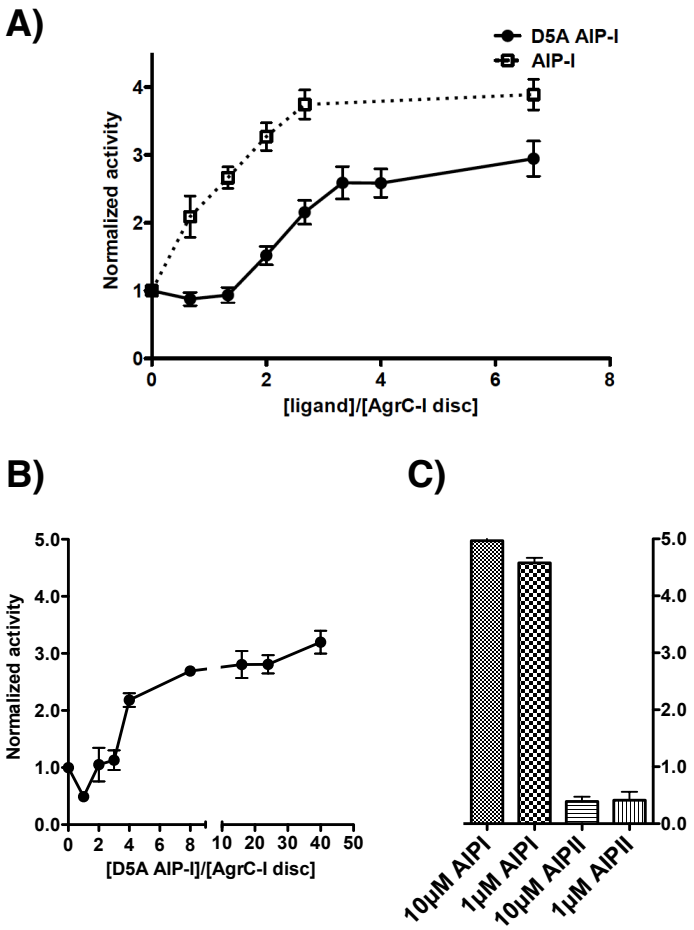

Figure 45. Further Characterization of D5A AIP-I Activation of AgrC-I

A) Dose response curves for AgrC-I autokinase activity assays at varying concentrations of AIP-I and D5A AIP-I. AgrC-I is at a concentration of 2.8 μM in each assay. The normalized activity for both AIP-I and D5A AIP-I are relative to the baseline level of phosphorylation in the absence of any ligand. ^{32}P-labeled AgrC-I in each reaction was quantified through scintillation counting. Error bars = SD (n = 3). **B)** Dose-response curve for AgrC-I autokinase activity assays at varying concentrations of D5A AIP-I. Assays were performed and analyzed as described in A, except that AgrC-I is at a concentration of 500 nM in each assay. **C)** AgrC-I autokinase activity assays at concentrations of 10 μM and 1 μM of AIP-I and AIP-II. These assays were analyzed as described in A, and the concentration of AgrC-I was 500 nM. They are provided for comparative purposes for the AgrC autokinase assay in B.

4.3 Receptor Binding and NMR Characterization of AIP Analogs (work on this section was accomplished in collaboration with Boyuan Wang and Dr. Galia Debelouchina)

4.3.1 AgrC-I Binding Assay for AIP Analogs

Since many of the AIP-I analogs showed little or no activity in the cell-based and AgrC-I autokinase activity assays, we developed an AIP-AgrC binding assay to gauge the relative affinities of the AIP analogs for the receptor. This assay is based on changes in steady-state anisotropy (SSA) that occur upon competitive displacement of fluorescein-labeled AIP-I (FAM-AIP-I) from AgrC-I nanodiscs (Figure 46A). In the binding assay, a high concentration of AIP analog (10 μM) was added to displace FAM-AIP-I (21 nM). Using this AgrC-I binding assay in conjunction with the other assays described in *Section 3.2*, we imagined that it should be possible to tease apart AIP analogs that bind AgrC and solicit a functional output (agonism) versus those that bind but do not effect signal transduction. As detailed below, these binding studies were entirely consistent with the results from both the cell-based and AgrC biochemical activity assays.

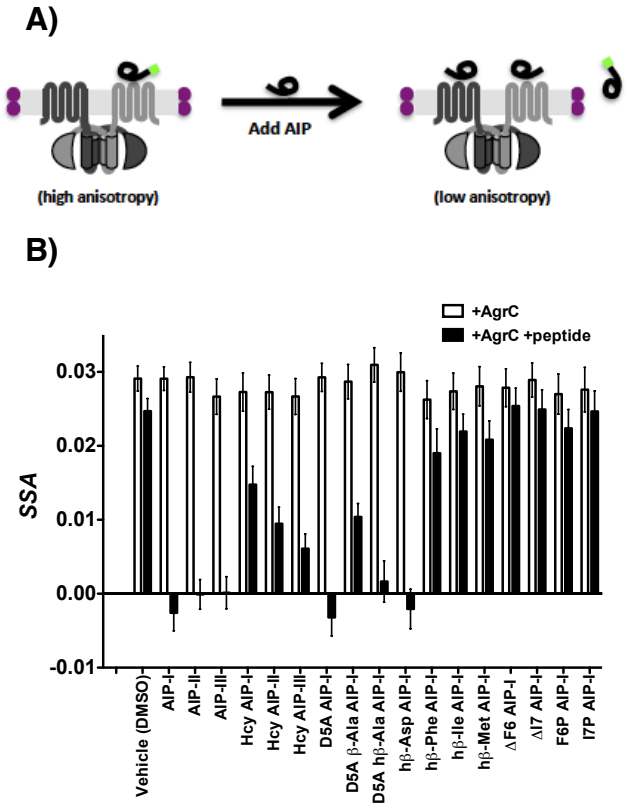

Figure 46. Binding of AIP analogs to AgrC-I

A) Schematic of the AgrC-I binding assay. A cross-section of the AgrC-I nanodisc assembly is shown, where AgrC-I is initially bound to FAM-labeled AIP-I. Upon adding unlabeled AIP-I or any other AIP in excess, the FAM-labeled AIP-I will be displaced resulting in low anisotropy, which indicates binding of the unlabeled AIP. **B)** The AIP analogs were tested using an *in vitro* assay that measures the change in steady-state anisotropy (SSA) that occurs upon competitive displace of a fluorescein-linked AIP-I (FAM-AIP-I) from AgrC-I nanodiscs. Open and solid bars correspond to the SSA before and after addition of the indicated AIP analog (10 μM). Errors; SD (n = 3).

In general, replacement of the endocyclic residues in AIP-I with the corresponding L-β-homo-amino acids led to a total loss of AgrC-I binding (Table 11, Figure 46B). As expected, AIP-I, -II and -III all bind tightly to AgrC-I, which validates the use of AgrC-I nanodiscs for measuring AIP binding affinity. Predictably, the hβ-Asp analog of AIP-I was able to bind tightly to the receptor, reflecting its stimulatory activity (Table 11, Figure 46B). Binding was abolished for those AIP analogs containing amino acid deletions as well as those containing proline. The homocysteine containing AIP analogs appear to have reduced affinity for the AgrC-I receptor as indicated by a partial displacement of FAM-AIP-I at the high concentration of AIP analogs employed. Consequently, the Hcy AIP-I is not an AgrC-I agonist and the cross group Hcy AIP analogs (II and III) do not inhibit AgrC-I. However, with respect to group II antagonism, the cross group Hcy AIP analogs (I and III) do have a strong inhibitory effect on AgrC-II as discussed in *Section 3.2.2*. Not surprisingly, the antagonist-turned-agonist D5A hβ-Ala AIP-I analog also binds tightly to the AgrC-I receptor; while the D5A β-Ala AIP-I analog only weakly interacts with the AgrC-I receptor (Table 11, Figure 46B). Clearly, insertion of a single methylene group at most positions in the AIP macrocycle backbone has catastrophic effects on ArgC receptor binding.

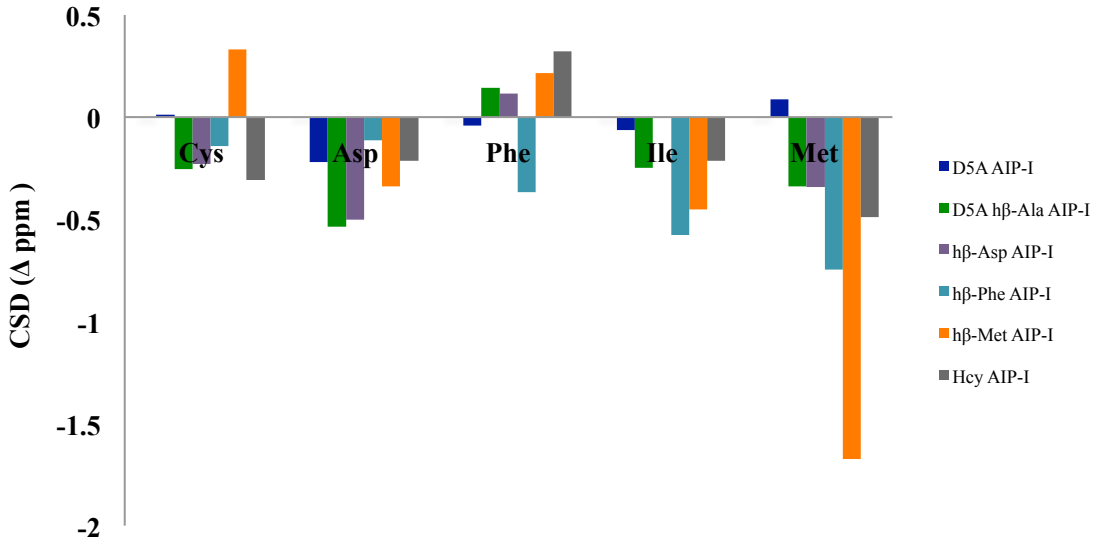

Figure 47. Solution NMR analysis of selected AIP-I analogs

Change in backbone amide ^{1}H chemical shift differences (CSDs) within the macrocycle of indicated analogs relative to native AIP-I normalized to zero (performed in DMSO-d6 at 298 K). Position 2 (Asp) includes CSDs for the D5A AIP-I analogs, where Ala or hβ-Ala is substituted for Asp.

4.3.2 NMR Analysis of AIP-I Analogs

From the cell-based and AgrC-I binding assay data, it was apparent that hβ-AAs replacement within the AIP macrocycle for the most part disrupts the interaction between the AIP and the AgrC receptor. We wanted to investigate whether these non-binding, enlarged AIP-I analogs induced major structural changes within the AIP macrocycle, which might impede the interaction with the AgrC-I receptor. To interrogate the lack of binding among some of the hβ-AA AIP-I analogs, two-dimensional NMR studies of hβ-Asp, hβ-Phe, hβ-Met, Hcy, D5A hβ-Ala and D5A AIP-I analogs were performed (See Appendix for each analogs 2D NMR assignments). Figure 47 shows a comparison of the chemical shift differences (CSDs) of the macrocycle backbone amide protons within these six AIP-I analogs (determined in DMSO-d6 at 298 K) relative to the AIP-I amide protons at the same position.

In every instance, the hβ-AA substitution strongly affects the amide proton at that native position, which indicates a perturbation within the AIP-I macrocyle and is consistent with our 2σ analysis of the CSD data (Figure 48). In the two analogs where the hydrophobic "knob" was perturbed (Phe-6 and Met-8),[59, 86] the perturbation was not only observed at the site of hβ-AA substitution but also propagated along the backbone to neighboring residues (Figure 48, Ile-7 and Met-8 in the hβ-Phe AIP-I analog, Ile-7 and Cys-4 in the hβ-Met AIP-I analog). Replacing Cys-4 with Hcy in AIP-I also caused a major perturbation at the Phe residue of Hcy AIP-I (Figure 48), which might disrupt AgrC-I binding as seen in the binding assay (Figure 48). In contrast, this residue specific 2σ analysis indicates that none of the substitutions at macrocycle position 2 in the enlarged AIP-I analogs propagate significant CSDs throughout the AIP macrocycle.

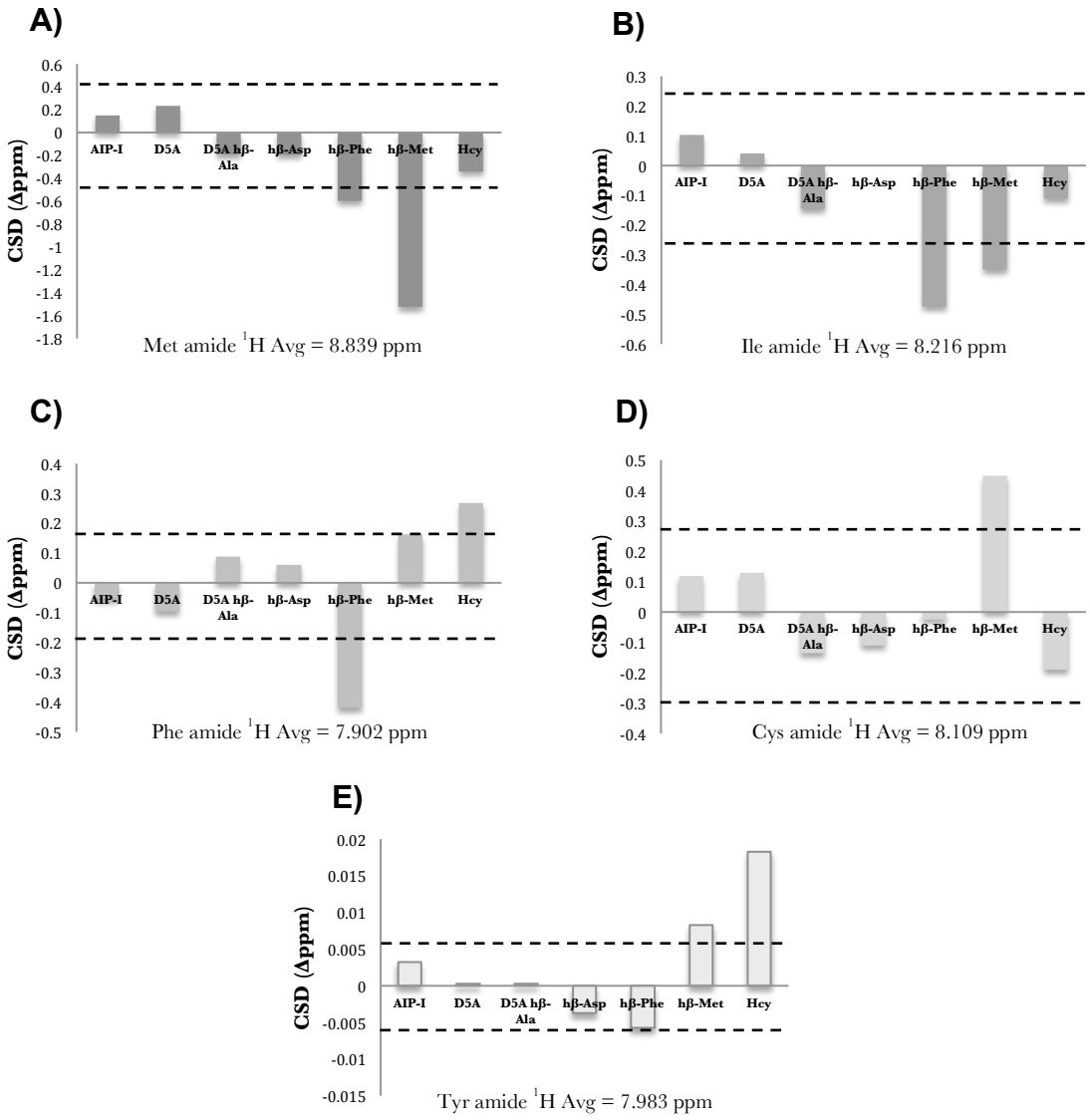

Figure 48. 2σ Analysis of Amide ^{1}H Residue-specific CSDs for Selected Enlarged AIP Analogs Indicates Which CSDs Significantly Affect AIP Binding of AgrC

Amide ^{1}H CSDs for the AIP-I analogs investigated with 2-D NMR (performed in DMSO-d6 at 298 K) are plotted according to each endocyclic position in the AIP macrocycle relative to a corresponding average CSD from the four AIP-I analogs (hβ-Asp AIP-I, D5A hβ-Ala AIP-I, D5A AIP-I and the native AIP-I) that bind AgrC-I (Figure 43B), which was normalized to zero. Using this average, a CSD standard deviation (σ) was calculated and plotted as dotted lines equal to ± 2σ. If a residue-specific CSD lies outside the ± 2σ zone, it is considered a significant CSD within that AIP-I analog. A) Met, B) Ile, C) Phe, D) Cys and E) Tyr, which provides a comparison from an AIP tail residue.

4.4 Conclusion

In this chapter, we investigated the effect of altering AIP macrocycle size and conformation on *agr* activation and inhibition. Our data support and extend the current understanding of the key features in the AIP required for receptor engagement. In general, we found that changing the chemical structure of the AIP-I macrocycle has a catastrophic effect on the ability of the peptide to bind and activate the AgrC-I receptor. The sole exception to this broad sensitivity is the second endocyclic position (Asp-5 in primary sequence) where ring expansion is permitted. Solution NMR studies suggest that this position is more tolerant of backbone changes relative to other positions in the macrocycle. This study underlines the key importance of the second endocyclic position in AIP-I for canonical receptor activation. Surprisingly, we found that incorporation of hβ-Ala at this position yields an activator of AgC-I even though the corresponding L-Ala analog is an inhibitor (at least at physiologically relevant concentrations), which suggests that the hβ-Ala analog can penetrate sufficiently into the relevant receptor pocket so as to trigger activation. Interestingly, we also found that, in terms of inhibition, methylene insertion is acceptable on one side of the thiolactone linkage (Hcy) but not on the other (hβ-Met). This indicates that receptor engagement is highly sensitive to the separation between the thioester and the Met sidechain. Collectively, our data suggests that there are three discrete regions in the AIP macrocycle that must cooperatively engage the receptor for activation to occur: the hydrophobic patch defined by C-terminus of the peptide,[59, 86] the thiolactone linkage (which must be appropriately juxtaposed to that patch), and the second endocyclic position, which must have a certain amount of steric bulk.

Chapter 5. Discussion and Future Directions

5.1 Discussion and Implications of This Work

5.1.1 AIP Secretion Does Not Require AgrB

In *Chapter 2*, we investigated the possible role of AgrB in AIP secretion. At the start of this study, it was necessary to develop an assay that could be used to investigate AIP secretion in the absence of AgrB. Thoendel *et al*. were able to demonstrate that AIP production was disrupted by non-catalytic point mutantions in AgrB, but they were unable to determine whether the lack of secretion or hydrolysis of the acyl-enzyme thioester intermediate stopped AIP production.[72] One strategy to resolve this issue would involve removing AgrB from the system. However, this experimental strategy would require replacing its enzymatic activity *in vivo* to form the AgrD(1-32)-thiolactone. The solution presented in this study uses intein chemistry to form the AgrD(1-32)-thiolactone. The newly engineered *S. aureus* cells reported in this study express AgrD(1-32)-intein^{Npu} and AgrD(1-32)-intein^{Ssp} proteins (Figure 18) and secrete AIP-I into the extracellular environment (Figure 19). To our knowledge, these *S. aureus* cells are the first to produce AIP in an AgrB-independent manner. More importantly, these AgrD(1-32)-intein-expressing cells produce functional AIP, which stimulates AgrC-I to induce β-lactamase activity (Figure 20). We also demonstrated that controlling the observed activity in the assay can be regulated by expressing a D29A AgrD(1-32)-intein construct, which produces the known D5A AIP-I inhibitor of AgrC-I (Figure 21).[63, 80] Collectively, these data indicate that we developed a biological assay to investigate AIP secretion.

For this assay to correctly function, presumably, the AgrD(1-32)-I-thiolactone embeds itself into the membrane, crosses the membrane in either an active or passive manner and is then processed to release AIP-I outside of the cell. Understandably, one concern for this assay then is cellular lysis, which would bypass the correct secretion pathway but still result in AIP-I in the extracellular milieu—especially if AIP-I were to build up in the cytoplasm of our new assay cells. Using a controlled cell lysis experiment, the AgrD(1-32)-intein^{Ssp} cells approach cellular lysis of ~40% (Table 4) but AIP-induced β-lactamase activity remains statistically the same (Figure 22). These data indicate that AIP does not accumulate in the cytoplasm of the cell, since cell lysis does not directly increase AgrC activation and β-lactamase activity. Furthermore, the Western blot analysis of controlled cell lysis indicates that AgrD(1-32)-intein protein is present in both of the cell-free lysates tested (Figure 22), but it again does not cause increased AIP-induced β-lactamase activity, which would suggest that the AgrD(1-32)-intein protein is unlikely to be further processed into AIP-I even if the intein-mediated formation of the AgrD(1-32)-I-thiolactone occurs in the cell culture supernatant. Taken together, the controlled cell lysis data suggests that the AIP-I produced by the AgrD-fused split intein expressing cells is likely secreted across the membrane.

Having developed and characterized this new AIP secretion assay, we could investigate what role AgrB-I might have in AIP secretion. To accomplish this, we engineered a new set of cells that express the AgrD-fused split intein construct along with AgrB-I as well as mutants thereof, namely C84A (catalytically dead), C84A and K129E, or C84A and K131E (Figure 23). Based on the observations of Thoendel *et al*., who

supposed that mutations in the lysine (K129-131) patch might inhibit AIP secretion,[72] we anticipated that C84A AgrB might increase AIP-induced β-lactamase activity, while the C84A and K129E or K131E AgrB-I mutants would not. Unexpectedly, the C84A AgrB-I mutants did not cause an increase in AIP-induced β-lactamase activity when compared to non-AgrB expressing cells (Figures 24 and 25). We had confirmed AgrB expression in the cells via Western blot analysis (Figure 23), so we were confident that AgrB-I mutants were expressed. Conceivably the C84A mutation might affect the putative secretion function of AgrB-I, hence we also expressed WT AgrB-I in the presence of the AgrD-intein. However, it also did not increase AIP-induced β-lactamase activity above the non-AgrB expressing cells (Figures 24 and 25). The data suggest that AgrB does not facilitate AIP secretion, since its effect on AIP-induced β-lactamase activity was inconsequential. Furthermore, the results with cells containing AgrB-I suggest that secretion of AgrD(1-32)-I-thiolactone is not coupled to the enzymatic processing of AgrD. In our cells, the WT AgrB-I could have formed the acyl-enzyme thioester intermediate and then re-catalyzed formation of AgrD(1-32)-I-thiolactone, which should induce the necessary structural changes to facilitate secretion, if AIP secretion were coupled to AgrB cleavage of AgrD. While the absence of any structural characterization of the AgrB-AgrD thioester intermediate limits our ability to explain how AgrB may interact with AgrD in the membrane, our data nonetheless suggests that AgrB does not facilitate secretion of the AgrD(1-32)-I-thiolactone.

With no apparent AgrB-mediated increase of AIP activity, we wanted to develop a working hypothesis to guide future experiments. In order to help formulate this

hypothesis, we investigated some of the physicochemical properties of AgrD. As expected, AgrD(1-32)-I-thiolactone is slightly lipophilic (Table 5), which likely promotes membrane association similar to that seen with the N-terminus of full-length AgrD.[64] Using the AgrD(1-32)-intein platform, we designed another construct to confirm the chemical characteristics of the SID sequence. If this sequence does inhibit secretion in the full-length AgrD, it should also inhibit AIP secretion if inserted into the AgrD(1-32) domain of the AgrD(1-32)-intein^{Npu} and AgrD(1-32)-intein^{Npu} constructs. As expected, inserting the 15-residue SID sequence of AgrD-II into the AgrD(1-32) domain to make the chimera AgrD-intein^{Ssp} led to inhibition of AIP secretion as measured by β-lactamase assay activity (Figure 26). This insertion into the MAD sequence of AgrD suggests that the SID sequence does not contain the necessary physicochemical properties to maintain and promote membrane association, since AIP activity was not detected in the cell culture supernatants. This finding corroborates the only known role of AgrB: SID removal to form the AIP macrocycle, which can facilitate secretion.[57]

Based on our findings, our current working model of AIP secretion begins with AgrB-mediated removal of the SID to form AgrD(1-32)-thiolactone (Figure 39). This lipophilic molecule remains associated with the membrane, awaiting secretion. Recent research has reported the presence of the MAD sequence of AgrD incorporated into amyloid fibrils of *S. aureus* biofilms,[66] strongly suggesting that both the AIP and the MAD can be secreted. Our finding that AgrB does not facilitate AIP secretion suggests either 1) another unknown, non-*agr* protein is involved in transporting AgrD(1-32)-thiolactone across the membrane or 2) AgrD(1-32)-thiolactone has intrinsic properties

that facilitate "self-secretion" of diffusion across the membrane. The former secretion pathway would make AIP biosynthesis dependent on two non-*agr* proteins. The latter "self-secretion" mechanism requires only one non-*agr* protein to produce AIP, and in the absence of a clear AgrD transporter, it is possible for AgrD(1-32)-thiolactone to partition the membrane and access the outer leaflet, where SpsB, for example, can cleave it. Membrane partitioning of AgrD(1-32)-thiolactone would be consistent with recent research, describing the cytolytic properties of the AgrD MAD sequence, which suggests the MAD can form pores in a membrane.[66, 67] It is also curious that AIP biosynthesis can be replicated in *E. coli* by only expressing AgrB and AgrD,[57, 72] so if a transporter were involved, *E. coli* cells would also have to express a transpoter analogous to the *S. aureus* one. While this seems unlikely, given that Gram-negative and Gram-positive bacteria employ very different quorum sensing systems, the data so far cannot completely rule this out. Whatever the mechanism, the AgrD(1-32)-thiolactone must access the outer leaflet of the membrane for further processing (Figure 49).

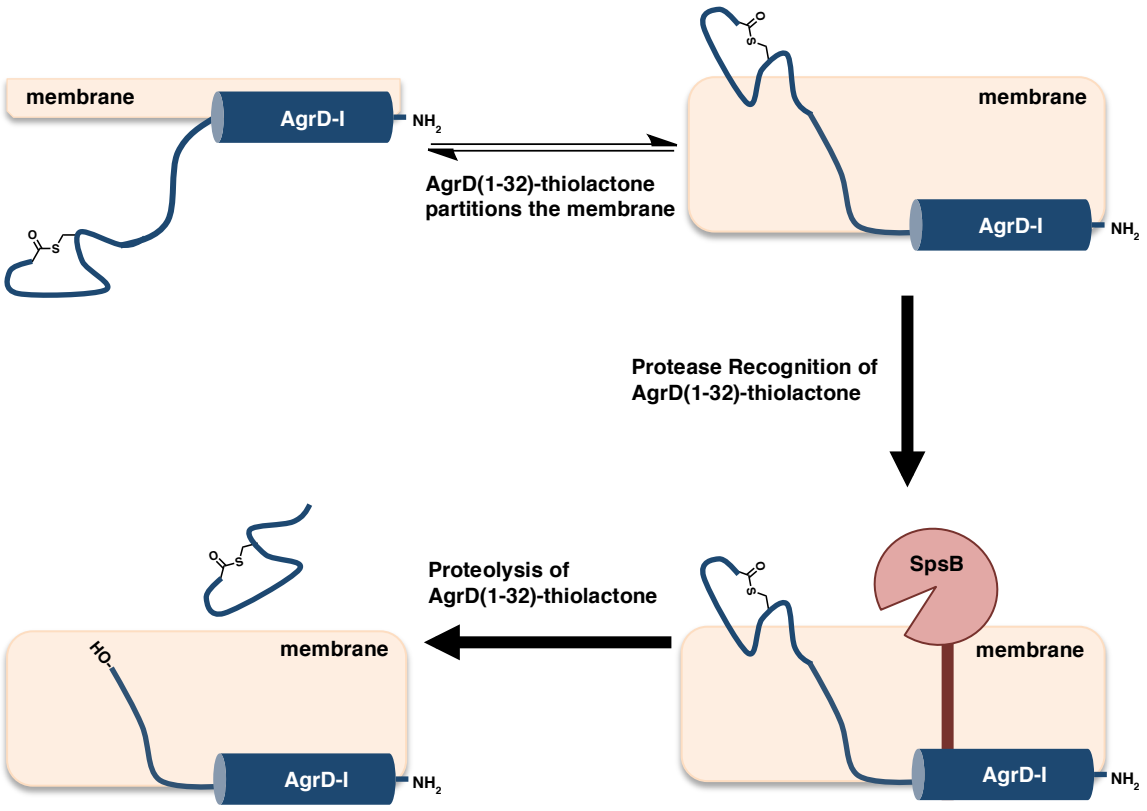

Figure 49. Proposed AIP Secretion Model

Using AIP-I biosynthesis as an example, we propose a secretion model for the AgrD(1-32)-thiolactone. Once AgrB-I has removed the SID of AgrD-I, the resulting lipophilic AgrD(1-32)-I-thiolactone remains associated with the membrane. The AIP-I precursor then partitions the membrane to access the outer leaflet, where SpsB can recognize and cleave the MAD of AgrD-I, releasing AIP-I to the extracellular environment. Although not depicted, an unknown protein could facilitate AgrD(1-32)-thiolactone secretion, and based on the results of AgrD-II cleavage study, there are likely other proteases besides SpsB that cleave the MAD of AgrD.

5.1.2 SpsB Can Only Cleave AgrD(1-32)-I-thiolactone

In chapter 3, we investigated the role of SpsB in AIP biosynthesis. SpsB is a non-*agr* regulated type I signal protease that has previously been shown to cleave an AgrD-I derived peptide.[58] Attempting to elaborate on this initial finding, we tried to characterize the SpsB catalysis of several AgrD derived peptides. While we were successful in purifying and characterizing SpsB, it would only cleave a fluorescein labeled AgrD derived peptide *in vitro* (Table 7, Figure 29), which was the only peptide Kavanaugh *et al*. had tested.[58] Even inclusion of the conserved IG sequence motif of AgrD (Figure 5A), which could help determine where a type I signal peptidase cleaves,[65] did not promote SpsB cleavage (Table 7, Figure 30B). Using a cell-based assay, however, did produce correct cleavage of the IG-AIP-I peptide, although other non-specific cleavage products were detected in IG-AIP-I and IG-AIP-III (Table 8). If SpsB catalyzed the correct cleavage of the IG-AIP-I peptide, it seemed to do so only in the context of a cell membrane (Table 8, Figure 30B).

To investigate the role of the membrane, we reconstituted SpsB and several variants of AgrD into proteoliposomes (vesicles), and in some instances, we also included AgrB. SDS-PAGE analysis of the vesicles indicated that SpsB can cleave AgrD-I and AgrD-II (Figure 33, lanes 2 and 6). However, it provided little molecular characterization of those cleavage products, and when group-specific AgrB was included in the vesicles, reconstituting the whole AIP biosynthetic pathway, SDS-PAGE provided even less resolution among the possible products. For further characterization of the vesicle cleavage products, we employed RP-HPLC and ESI-MS analysis. We confirmed the

correct SpsB and AgrB cleavages of AgrD-I (Table 8, rxns 1-4), which is the first direct evidence that two proteases are indeed needed for AIP biosynthesis. The AgrD(1-32)-I-thiolactone was also detected (Table 8, rxn 2), which was significant since AIP-I was undetected. Taken together, these data suggest a role for SpsB in AIP-I biosynthesis.

While initial attempts to detect AIP production by the AIP biosynthesis vesicles were inconclusive, we detected AIP activity using the β-lactamase reporter assay when SpsB and the AgrD(1-32)-I-thiolactone were reconstituted into vesicles (Figure 34). Subsequent RP-HPLC-MS analysis of these same vesicles confirmed AIP production (Figure 35). To our knowledge, this data provides the first direct evidence of *in vitro* AIP production, but more importantly, it argues strongly for the role of SpsB in AIP-I biosynthesis.

Having studied the role of SpsB in AIP-I biosynthesis, we turned our attention to AIP-II biosynthesis. While the SDS-PAGE analysis indicated SpsB cleaves AgrD-II (Figure 33, lane 6), the RP-HPLC and ESI-MS analysis detected only non-specific cleavage products (Table 8, rxns 5 and 6), and importantly this non-specific cleavage would actually produce a known antagonist of AgrC-II.[62, 83] The correct AgrB-II cleavage of AgrD-II was detected (Table 8, rxn 6), although it was the hydrolyzed product, not the thiolactone. To further explore the role, if any, of SpsB in AIP-II biosynthesis, we reconstituted the full-length protease and AgrD(1-32)-II-thiolactone into vesicles. These vesicles should represent the final two components necessary for AIP-II production, and in the case of AIP-I biosynthesis, these two protein components were

sufficient (Figures 33 and 34). However, using the β-lactamase reporter assay, we were unable to detect AIP-II activity from these vesicles or from vesicles also incorporating SpsA as a potential binding partner for SpsB or AgrD(1-32)-II-thiolactone (Figure 36). We thought SpsA might help guide SpsB to the correct cleavage site, but it played no such role in our reconstituted system. To test the idea that a larger protein complex consisting of AgrB-II, SpsB and SpsA or some combination thereof might be required for the final cleavage step in AIP-II production, all four components were reconstituted into vesicles. However, we again failed to detect any AIP-II activity in the coupled cellular assay (Figure 38). Thus, collectiviely our biochemical data argue against a role for SpsB in the biosynthesis of AIP-II.

While it is unclear what protein cleaves the AgrD(1-32)-II-thiolactone, cleavage does occur at the membrane (Figure 39). Specifically, AIP-II was detected in a cell culture supernatant from *agr-II* null cells (RN9120) incubated with the AgrD(1-32)-II-thiolactone. However, AIP-II was not detected in a pre-grown RN9120 culture filtered and then incubated with the group II thiolactone. Taken together, these data suggest that AIP-II production occurs at or near the membrane, because no secreted *S. aureus* factor cleaved the AgrD(1-32)-II-thiolactone to produce AIP-II. Furthermore, our data suggest that the processing step likely occurs at the outer leaflet of the membrane, because cleavage at the inner leaflet would lead to AIP-II accumulation in the cytoplasm, trapping the hydrophilic AIP-II molecule inside the cell unless a peptide pump or transporter were involved (Table 5, AIP-II $LogD_{5.9}$ value). While a transporter may be involved in AIP-II biosynthesis, our data discussed in *Section 5.1.1* suggests a model where that transporter,

if necessary, would likely transport the AgrD(1-32)-II-thiolactone to the outer leaflet for further processing (Figure 49).

5.1.3 AIP-I Activation of AgrC-I Requires Three Distinct Interactions Within the AIP Macrocycle

In *Chapter 4*, we investigated the effect of altering AIP macrocycle size and conformation on *agr* activation and inhibition. As can be seen from the SAR data summarized in Table 11, activation of the *agr* response is extremely sensitive to perturbations in the AIP macrocycle. Indeed, we found only one position that tolerated any change, namely Asp-5 of AIP-I corresponding to the second endocyclic position. In contrast, replacement of the other endocyclic residues in AIP-I with the corresponding L-β-homo-amino acids led to a total loss of cellular and biochemical activity (Table 11, Figures 42A and 46B). This was also true for those AIP analogs containing amino acid deletions, as well as those containing the proline and Hcy substitutions (Table 11, Figures 42, 43 and 46B). Collectively these data indicate that even relatively subtle changes in the macrocycle, for instance the insertion of a single methylene group at most positions in the ring, can have catastrophic effects on agonism of the ArgC receptor. Comparing the backbone amide ^{1}H chemical shifts of the inactive ring-expanded analogs indicated that methylene insertion affects the overall structure of the AIP-I macrocycle, presumably leading to a lack of receptor binding (Figures 46 and 47). By contrast, the active hβ-Asp analog had a more modest difference on backbone amide ^{1}H chemical shifts compared to native AIP-I, particularly at two hydrophobic sites (Phe, Met) which are known to be critical for receptor binding.[59, 86] The overall sensitivity to change in the macrocycle size

is broadly consistent with the many previous SAR studies on the *agr* system, which have converged on the idea that agonism is largely intolerant to changes in AIP structure.[45, 59, 63, 80, 83-86]

Previous work suggests that AIP has a hydrophobic patch or "knob" essential for AgrC binding.[59, 86] In addition, McDowell *et al*. reported that D-Met and D-Phe could be substituted into the hydrophobic knob of AIP-I and still stimulate AgrC-I.[80] There was some surprise then that the enlarged AIP analogs within this region were not only inactive (Table 11) but also incapable of binding AgrC (Figure 46B). We hypothesized that the AIP binding pocket in AgrC might be able to accommodate a small perturbation such as methylene insertion as opposed to removing large hydrophobic sidechains using alanine substitution. Our results clearly indicate that AgrC-I cannot tolerate even small perturbations to the AIP hydrophobic patch. Our solution NMR work provides some clarification as to why AgrC-I cannot bind these enlarged AIP-I analogs. The large CSD values produced by replacing Met with hβ-Met or Phe with hβ-Phe were indicative of major structural changes within the local environment of these AIP-I analogs (Figure 47). Since AIP-I is such a small peptide that doesn't exhibit traditional secondary structure, the resulting amide CSD at endocyclic position 5 of hβ-Met AIP-I, for example, does not describe a change in secondary structure, but rather suggests that the macrocycle backbone has repositioned, which likely explains the lack of binding in this AIP-I analog. Furthermore, the 2σ analysis of the CSD data suggests that inserting a methylene group at Phe-6 or Met-8 does not only directly affect the AIP macrocycle at that position but the perturbation is propagated through the macrocycle, affecting neighboring residues within

the AIP macrocycle (Figure 45). By drastically perturbing the hydrophobic knob of the AIP macrocycle with hβ-AAs, AIP binding of AgrC was abolished, explaining why most of the enlarged AIP analogs were inactive. Conversely, while inserting a methylene group at endocyclic position 2 of AIP-I did produce some large CSD values at that position, the structural effect was not further propagated throughout the AIP macrocycle (Figure 48). Consequently, the hβ-Asp and D5A hβ-Ala AIP-I analogs were able to bind AgrC-I, enabling activation.

In our attempts to characterize the biologically active AIP analogs featuring enlarged macrocycles with biochemical assays, the *in vitro* activation of AgrC-I by D5A AIP-I was surprising. There is no doubt that D5A AIP-I is an inhibitor of AgrC-I in a cellular context; this has been reported previously and was confirmed in the current study (Table 11).[63, 80] We performed several biochemical studies to try and understand the basis of the observed *in vitro* activation. We showed that the D5A AIP-I analog does not inhibit the phospho-relay between AgrC and AgrA, ruling this out as a possible explanation for the *in vivo versus in vitro* observations (Figure 44). In the AgrC-I autokinase activity assays, every control indicated that the AgrC-I nanodiscs behaved according to previously reported *in vivo* findings for AIP-I, -II and -III (Figure 43).[45, 59, 63, 80, 83-86] Finally, dose-response AgrC-I autokinase activity assays indicated that D5A AIP-I activation appeared to be delayed until two ligands had bound the AgrC-I nanodiscs (Figure 45). Since D5A AIP-I competes with FAM-AIP-I to bind the orthosteric site of AgrC-I (Figure 46B) and AIP-I binds AgrC-I in a 2:2 stoichiometry,[88] our dose-response curves would indicate that D5A AIP-I stimulation of AgrC-I occurs

after the canonical binding site of AgrC-I is occupied. Collectively, the *in vitro* and *in vivo* data point to their being multiple AgrC-I binding sites for the D5A AIP-I analog. At low concentrations the analog binds to the 'high-affinity' binding site on the receptor where it inhibits activation through competitive antagonism, whereas at elevated concentrations it binds to a putative second 'low-affinity' site where it can somehow activate the receptor. The location of this possible 'low-affinity' site is unclear, and we cannot rule out that this site might reside somewhere on the 'intracellular side' of the AgrC-I nanodiscs (i.e. in the cytoplasmic domain which would of course be accessible in the reconstituted system). Therefore, we surmise that only the 'high affinity' site is physiologically relevant, thereby accounting for the behavior of the D5A AIP-I analog on cells.

In contrast to activation of the *agr* response, antagonism of the AgrC receptor is more resilient to changes in the AIP macrocycle.[45, 62, 63, 79, 80, 83] While some trends observed for activation of the response were also seen for inhibition (e.g. among the L-β-homo-amino acid substitutions only the hβ-Asp analog retained measureable, albeit weakened, activity), a few of the analogs that were inactive as agonists were active as antagonists (Table 11). Specifically, the homocysteine containing AIP analogs all had the expected cross-group inhibitory activity (Table 11, Figure 42B). Thus, antagonism of the *agr* response does seem to be a little more tolerant to changes in the macrocycle; for example a methylene group insertion is acceptable in two positions within AIP-I. With regard to AgrC-I antagonism, it appears that replacing Cys with Hcy in AIP-II disrupted its mode of inhibition. Hcy AIP-II is no longer an inverse agonist like AIP-II, but it may

act as a very weak neutral antagonist, since it does not activate AgrC-I above basal levels (Figure 43) and it weakly binds AgrC-I (Figure 46B). Interestingly, group II cells seem to be more susceptible to inhibition by the relevant Hcy analogs than group I cells; the Hcy analog of AIP-III was a relatively potent inhibitor of AgrC-II (only ~40-fold less than wild-type AIP-III), but a weak inhibitor of AgC-I. While the absence of structural information on any AgrC sensor domain limits our ability to explain such differential effects in molecular terms, the data nonetheless highlight the fact that the molecular recognition mechanisms employed by the different AgrC receptors are far from identical.

While AIP-I endocyclic position 2 (Asp-5) was previously known to be essential to AgrC-I activation,[63, 80] the pivotal finding of this SAR study was the conversion of the known global inhibitor D5A AIP-I into an agonist of AgrC-I by replacing Ala with hβ-Ala. Furthermore, the loss of activity observed in the D5A β-Ala AIP-I analog provided another key insight. Collectively, these data highlight the importance of the second endocyclic position in AIP-I for receptor agonism. Thus, reduction in the size of the sidechain (Asp to Ala) converts the peptide into an antagonist, addition of a backbone methylene (Ala to hβ-Ala) flips it back to being an agonist, while removal of the sidechain in the expanded ring context (hβ-Ala to β-Ala) essentially removes all activity. In trying to interpret these observations, we were cognizant of previous SAR studies that indicate Asp-5 of AIP-I can be replaced with Asn, Phe or Tyr without losing the ability to activate AgrC-I.[63] Together, our SAR data is consistent with a model in which the AgrC receptor is switched on when it senses sufficient steric bulk (rather than a specific functional group, per se) at the second endocyclic position in AIP-I. This requirement is

not fulfilled by an Ala (at least not at physiologically meaningful concentrations, vide supra), but apparently is by hβ-Ala. We postulate that the added methylene group in the hβ-Ala AIP-I analog allows the sidechain methyl to extend further into the critical binding pocket in the receptor, triggering activation. Presumably, the β-Ala AIP-I analog, by lacking the sidechain, cannot extend far enough into this receptor pocket to fulfill this steric requirement.

Collectively, the available SAR data on the group I *agr* system points to three discrete regions in the AIP macrocycle that must cooperatively engage the receptor for activation to occur (Figure 50). These features are the hydrophobic patch defined by the C-terminus of the peptide,[59, 86] the thiolactone linkage (which must be appropriately juxtaposed to that patch), and the second endocyclic position, which must have a certain amount of steric bulk. Altering any one of these three features is sufficient to eliminate receptor agonism. However, it appears that maintaining the native structure of the hydrophobic patch is the only feature that absolutely must be retained for cross-group inhibition.[45, 59, 62, 63, 79, 80, 83, 84, 86] It is likely that this binding model will be a useful guide for the design of additional AIP analogs for probing the receptor interaction using biochemical methods that exploit the reconstituted AgrC nanodisc system.

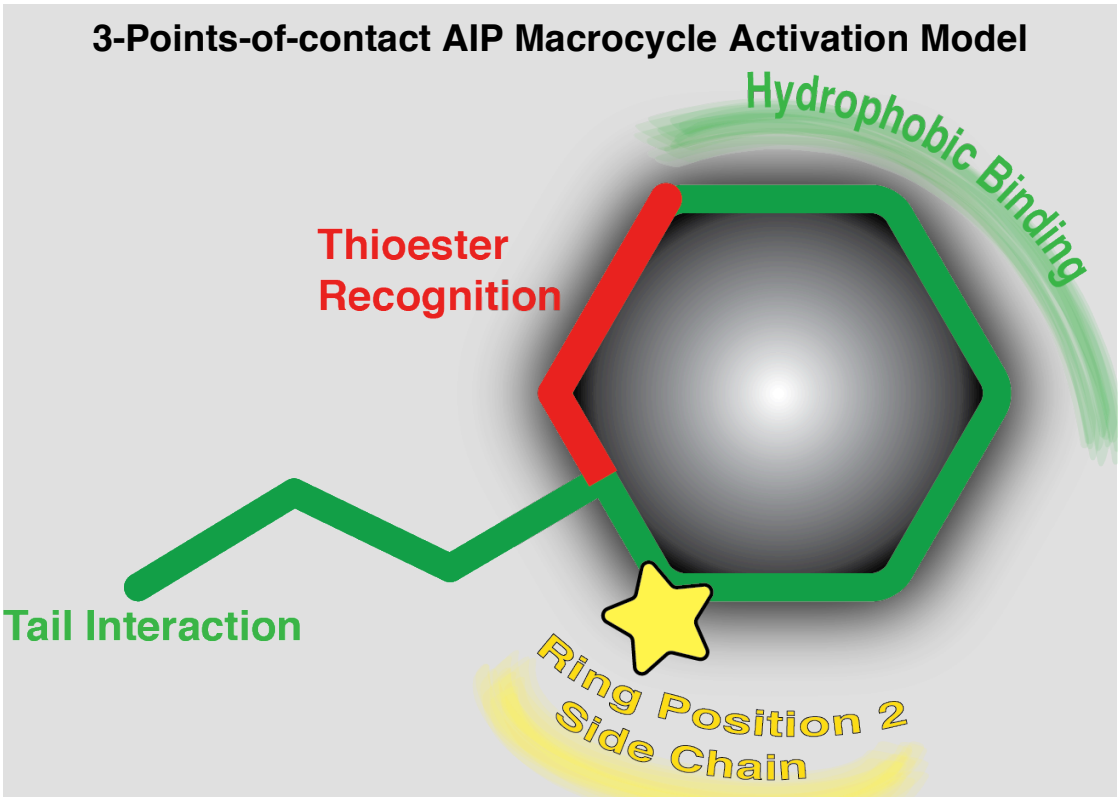

Figure 50. Proposed Role of AIP Macrocycle in *agr* Activation

Schematic illustrating the three key regions of the AIP-I macrocycle required for AgrC receptor activation. In our model, all three of these interactions must be satisfied before receptor activation ensues.

5.2 Future Directions

5.2.1. Future Directions for AIP Secretion and Biosynthesis

Develop an AgrD(1-32)-thiolactone Membrane Crossing Assay

To test our hypothesis that AgrD(1-32)-thiolactone can partition and cross the membrane, we have recently endeavored to develop an AgrD(1-32)-thiolactone vesicle crossing assay. Our initial attempts at developing a vesicle-based assay have been unsuccessful. Briefly, lipid vesicles were formed using a reverse-phase evaporation method.[145] Lipid is dissolved in diethyl ether and then aqueous buffer is added. This solution is then sonicated to form an emulsion, and the ether is removed *in vacuo*, forming vesicles of ~150 nM. The vesicle suspension is then diluted with more aqueous buffer. As part of the aqueous buffer, we tried incorporating a Cys-FLAG peptide (sequence: H-CGGDYKDDDDKK-OH), L-cysteine or cysteamine into the lumen of the lipid vesicles. These small molecules could react with the thiolactone, leading to C-terminal ligation and increasing the molecular weight of the AgrD(1-32)-thiolactone peptide, which we monitored via RP-HPLC and ESI-MS analysis. In all of the assays, the vesicles were washed with buffer to remove any thiol-containing small molecule from the outside of the vesicles. The AgrD(1-32)-II-thiolactone was then added to the outside of the vesicles. Presumably, if a reaction is detected via RP-HPLC and ESI-MS analysis, then AgrD(1-32)-II-thiolactone must have crossed the membrane to react with the thiol-containing molecules in the vesicle lumen. However, we have not detected the elongated AgrD peptide in washed vesicles. In controls, where the washed vesicles are lysed with detergent after 2-3 hours of incubation with the AgrD(1-32)-II-thiolactone and the reaction continues for 2-3 hours post-lysis, the reaction is also not detected. If any of the

thiol-containing molecules are added to the outer solution around the vesicles, however, the reaction can be detected. More effort is need to optimize this assay.

While a version of this vesicle-crossing assay may potentially work after optimization, it might be necessary to consider an alternative route. Recently, Schwartz *et al*.[66] developed two assays to determine the cytolytic properties of the AgrD-I MAD sequence (Figure 5A). One assay measured the hemolysis of human red blood cells, and the other assay measured lysis of human neutrophils. Employing these assays with AgrD-I(1-32)-thiolactone and AgrD(1-32)-II-thiolactone could provide similar insights into the ability of the AIP precursor to partition and cross the membrane as the vesicle-crossing assay. Additionally, Schwartz *et al*. provide an independent dataset to compare the AgrD(1-32)-thiolactone activity in these assays with the MAD of AgrD.

Develop a Crosslinking Strategy to Find Proteins That Interact With the AgrD(1-32)-thiolactone

In the event that the AgrD(1-32)-thiolactone cannot cross a membrane on its own, it will be necessary to identify the protein that facilitates AIP secretion. One way in which to accomplish this would be with a crosslinking strategy. Using *S. aureus* protoplasts, or whole membrane fractions, membrane proteins would be accessible to react with exogenously added peptides. Incorporating a combination of amino acids such as *p*-benzoyl-L-phenylalanine (Bpa), L-photo-methionine (photo-Met), and/or L-photo-leucine (photo-Leu) into AgrD(1-32)-I-thiolactone peptide (e.g. 2 Met, 5 Phe and 3 Leu residues in group I) would cover the whole length of the peptide sequence and increase

possible crosslinking with potential AgrD(1-32)-thiolactone binding partners. N-terminal biotinylation of the AgrD thiolactone would provide an excellent handle to recover any crosslinked protein complexes involving the AgrD(1-32)-thiolactone for further analysis via SDS-PAGE and/or mass spectrometry.

Synthesize the AgrD(1-32)-III-thiolactone for Biochemical Assays

There is currently no study investigating the cleavage of AgrD(1-32)-III-thiolactone. Since the peptide is only 32 residues, it is synthetically accessible. The synthetic strategy would employ the same general approach to synthesize AgrD(1-32)-I-thiolactone and AgrD(1-32)-II-thiolactone, where the linear peptide α-thioester is generated by SPPS employing a Boc-N^{α} protection logic and using a 3-mercaptopropionamide-based linker system. Upon forming the C-terminal thiolactone macrocycle via an intramolecular trans-thioesterification reaction, the peptide can be purified using RP-HPLC.

With the peptide in hand, it would then be possible to investigate whether it can be cleaved by fl-SpsB. In this study, we found that fl-SpsB cannot correctly cleave AgrD-II. Instead, it cleaved AgrD-II at a position that would actually produce an inhibitor of AgrC-II.[62, 83] Likewise, for AIP-III biosynthesis, it is critical that the protease responsible for cleaving AgrD(1-32)-III-thiolactone be very specific in its cleavage. Therefore, the initial investigation of the AgrD(1-32)-III-thiolactone should try to determine whether fl-SpsB is responsible for its cleavage. Further characterization may suggest that fl-SpsB does not process the AgrD(1-32)-III-thiolactone into AIP-III. At which point, it would be

necessary to identify the protein necessary to cleave and remove the MAD of AgrD-III for successful production of AIP-III.

Generate the AgrD(1-32)-II-thiolactone and/or AgrD(1-32)-III-thiolactone Using the Fused Split Intein System

One goal of this study was a proof of principle that an AgrD(1-32)-thiolactone could be produced *in vivo* in the absence of AgrB. Having accomplished that, it would be worthwhile to replicate our findings with another *agr* specificity groups, confirming the observation that AIP is secreted through a non-AgrB pathway. All of the necessary analytical tools are available for studying secretion of AgrD(1-32)-II-thiolactone. In order to study the secretion of the AgrD(1-32)-III-thiolactone, it would be necessary to engineer a better β-lactamase reporter gene assay strain (RN9537), because in our hands, the current strain is not as sensitive to AIP-III agonism and does not produce as reliable data as the group I or group II β-lactamase reporter gene assay strains. If necessary, it might be possible to obtain or engineer the group III GFP reporter gene assay strain used by Tal-Gan *et al*.[84]

Identify the Protease Responsible for Cleaving and Removing the MAD of AgrD-II

In *Section 3.5.2*, we present data suggesting a membrane-bound or peptidoglycan-associated protease cleaves AgrD(1-32)-II-thiolactone. In order to identify the protein responsible for this cleavage, the first step could be membrane fractionation of group II cell membranes—a classical, biochemical technique. Since synthesis and purification of the AgrD(1-32)-II-thiolactone has fairly low-yields because of its hydrophobicity, there

are several preliminary experiments to try. First, synthesize a peptide similar to the IG-AIP-I substrate peptide that is derived from the AgrD-II sequence and then digest this new group II derived peptide with the RN9120 cells (*agr-II* null). If the peptide were correctly cleaved, it would be a better substrate peptide, with which to test each of the membrane fractions. Once activity is detected within a fraction, characterization of the proteins within that fraction will provide possible candidates as the protease responsible for AgrD-II cleavage. These candidate membrane proteins could be expressed, purified, and incorporated into proteoliposomes for further biochemical analysis. Similar work could be done to find the protease that cleaves AgrD-III.

This membrane fractionation approach could also be validated using group I derived peptides, especially if amino acid residues such as Bpa, Photo-Met, and/or Photo-Leu were incorporated into them. These chemical handles could be used to crosslink with any proteins that interact with AgrD-I. Presumably, these group I, crosslinking peptides would at least identify SpsB as one of the proteins that bind and cleave AgrD-I within the membrane fractions.

5.2.2 Future Directions to Further Study AIP Macrocycle Size

Enlarging the Macrocycle of AIP-III

This work provides further support that the sidechain of the residue at endocyclic position 2 of AIP-I helps to stimulate AgrC-I. Interestingly, AIP-III has a native Asp residue at this position, making it identical to AIP-I; and recently, a potent, global inhibitor analog of AIP-III was reported at this same position.[84] A similar SAR study to enlarge the AIP-

III macrocycle would not only provide interesting insight into the binding pocket of AgrC-III but also reveal a possible trend within AgrC-I, -III and -IV activation. Namely, AgrC-III may require a similar stimulatory effect to AIP-III, which could be satisfied with a D4A hβ-Ala AIP-III analog.

Activity of a D5G AIP-I analog

With regards to the results presented in *Section 3.2.2*, replacing Asp-5 with Gly would produce another AIP-I analog to test. Since D5A AIP-I inhibits AgrC-I activation in a cellular context, it would be interesting to see if a D5G AIP-I analog activates or inhibits AgrC-I or if it has no activity. Our current model suggests it would likely be an inhibitor, since it has no sidechain and should still bind AgrC-I. This same experiment could be repeated with AIP-III, replacing Asp-4 with Gly, and included in an SAR study of the enlarged macrocycle of AIP-III.

Enlarging the Macrocycle of AIP-II

Enlarging the macrocycle of AIP-II is another SAR study worth pursuing. Recently, AgrC-II nanodiscs were prepared in our lab, and this biochemical tool may be very useful, since the AIP-II alanine scan indicated that alanine substitution at endocyclic position 2 only reduces activation of AgrC-II.[45] Furthermore, replacing Ser-7 with Ala made the resulting AIP-II analog more active than the native AIP-II. Thus, there are two potential endocyclic positions within AIP-II that may tolerate methylene insertion. This previous result also suggests AIP-II not only has a smaller hydrophobic patch than AIP-I and AIP-III but also indicates activation of AgrC-II likely entails a different molecular

interaction with the AIP-II macrocycle. An SAR study enlarging the AIP-II macrocycle may provide greater insight into the stimulating interaction of group II.

Structural Characterization of AgrC-I

Using AgrC-I nanodiscs, some recent work has attempted to locate the binding pocket by crosslinking a photoactive AIP-I analog to AgrC-I.[147] As this investigation continues, a photoactive analog, like p-benzoyl-L-phenylalanine (Bpa), at endocyclic position 2 might identify some of the residues responsible for AgrC activation. Making the Bpa-5 AIP-I analog might be possible, since the D5F AIP-I analog activates AgrC-I.[63] Of course, the best insight into the AgrC binding pocket would come from a crystal structure of the receptor, which would be a challenging endeavor to undertake.

5.3 Conclusion

The work presented here elucidated several mechanistic features of the AIP biosynthetic pathway and AgrC-I activation. This study provides insight into the defined roles of both AgrB and SpsB in AIP-I biosynthesis. The finding that AgrB does not facilitate secretion is the first such evidence that AIP secretion may not be mediated by a protein or requires an unidentified, as of yet, protein transporter. The investigation of SpsB cleavage found that it correctly cleaves AgrD-I and did not correctly cleave AgrD-II. This finding indicates that all the essential proteins for group-specific AIP biosynthesis may not yet be identified. In the final portion of this study, the conversion of a known, global inhibitory peptide (D5A AIP-I) into a self-activator using L-β-homoalanine provided a key insight into AgrC activation. Namely, that the sidechain at the second endocyclic position in AIP-I plays an important role in AgrC-I activation. Indeed, this study builds on the current understanding of agr activation by proposing three distinct interactions between the AIP macrocycle and AgrC. The development of several new technologies to investigate AIP biosynthesis can aid future studies into AIP-II and AIP-III biosynthesis. The cell-based secretion assay is the first instance of AIP-I production in the absence of AgrB-I and can be replicated for the other *S. aureus* specificity groups. The vesicle assays employed to investigate SpsB cleavage of AgrD lay a foundation for further characterization of the final cleavage step in AIP biosynthetic pathway. Intriguing future directions for investigation of *agr* include developing an assay to determine whether the AgrD(1-32)-thiolactone can intrinsically cross a membrane, identifying the proteases responsible for cleaving the AIP-II and AIP-III precursor peptides, and using crosslinking studies to find potential binding partners for the AgrD(1-32)-thiolactone.

Whether *agr* proves to be therapeutically relevant, a deeper understanding of the mechanisms that contribute to virulence will increase knowledge of *S. aureus* infections and provide the foundation for new discoveries and eventual advances in treatment. The insights described in this work will hopefully be applicable to other autoinducer peptide biosynthetic pathways and serve to build connections between the molecular mechanisms involved in AgrD-thiolactone formation, secretion, and cleavage among the staphylococci and other Gram-positive bacteria.

Chapter 6. Materials and Methods

Materials. All buffering reagents, salts, glucose and 2,2,2-Trifluoroethanol (TFE) were purchased from Fisher Scientific (Pittsburgh, PA). Bacto™ Casamino acids and Yeast Extract along with Tryptic Soy Agar were purchased from BD Biosciences (San Jose, CA). β-Glycerophosphate, Disodium Salt, Pentahydrate was purchased from EMD-Millipore (Darmstadt, Germany). Tryptic Soy Broth, Acetonitrile, S-trityl mercaptopropionic acid, N,N-diisopropylethylamine (DIPEA), Coomassie brilliant blue, N,N-dimethylformamide, (DMF), triisopropylsilane (TIPS), N,N'-diisopropylcarbodiimide (DIC) and 1,1,1,3,3,3-Hexafluoro-2-propanol (HFIP) were purchased from Sigma-Aldrich (St. Louis, MO). Tris(2-carboxyethyl)phosphine hydrochloride (TCEP) was purchased from Thermo Scientific (Rockford, IL). Standard N^{α}-Fmoc protected amino acids and N^{α}-Boc protected amino acids were purchased from Novabiochem (Läufelfingen, Switzerland). The N^{α}-BOC protected L-β-homo-amino acid derivatives, N^{α}-BOC protected β-alanine and 2-(1H-Benzotriazole-1-yl)-1,1,3,3-tetramethyluronium hexafluorophosphate (HBTU) were purchased from AnaSpec (Fremont, Ca). Trifluoroacetic acid (TFA) was purchased from Halocarbon (North Augusta, SC). Nitrocefin was purchased from TOKU-E USA (Bellingham, WA). DMSO-d6 was purchased from Cambridge Isotope Laboratories (Andover, MA). All denaturing SDS-PAGE gels were purchased from Bio-Rad (Hercules, CA). [γ-32P]-Adenosine triphosphate and Ultima Gold Cocktail was from PerkinElmer (Waltham, MA). All lipids were purchased from Avanti Polar lipids (Alabaster, AL). All detergents were purchased from Anatrace (Maumee, OH).

Reversed-Phase HPLC and Mass Spectrometry. Analytical and semi-preparative RP-HPLC were performed on Hewlett-Packard 1100 and 1200 series instruments equipped with a C18 Vydac column (5 μm, 4.6 x 150 mm) at a flow rate of 1 mL/min or a C18 Vydac 218TP152010 column (15-20 μm; 10 x 250 mm) at a flow rate of 4 mL/min. All runs were carried out employing gradients of solvent A (0.1% TFA in water) and solvent B (90% acetonitrile in water with 0.1% TFA). For semi-preparative HPLC runs, an initial five-minute isocratic period in initial conditions was followed by a 40-minute linear gradient with increasing solvent B concentration. For analytical HPLC runs of the AIP analogs, there was a two-minute isocratic period in initial conditions followed by a 20-minute 0-73% linear gradient with increasing solvent B concentration. Once the AIP analogs were purified and in a DMSO stock, analytical HPLC runs included an initial five-minute isocratic period in 100% solvent A followed by a 20-minute 0-73% linear gradient with increasing solvent B concentration. For analytical HPLC runs of the in vitro tr-SpsB assays, there was a two-minute isocratic period in initial conditions followed by a 30-minute 0-73% linear gradient with increasing solvent B concentration. For analytical HPLC runs of any AgrD-containing reactions, there was a five-minute isocratic period in initial conditions followed by a 20-minute 0-90% linear gradient with increasing solvent B concentration. The solvent gradients are specified in each HPLC experiment when necessary. Electrospray ionization mass spectrometric analysis (ESI-MS) was performed on all peptides and proteins by direct infusion on a Bruker Daltonics MicrOTOF-Q II mass spectrometer. For large peptides and proteins, the mass observed is reported as a deconvoluted mass obtained from Bruker software using the following parameters: Maximum Entropy, a molecular weight range at least twice the size of the

expected mass, and 20000 resolving power. MS/MS analysis was performed using Bruker Daltonics BioTools 3.2 software (Bruker Daltonics Inc., Billerica, MA).

General Methods. Coomassie stained gels were imaged on a LI-COR Odyssey Infrared Imager. The β-lactamase activation and inhibition assays were recorded on a Molecular Devices Spectramax M3 micro plate reader with absorbance measurements at 490 and 650 nm. Electroporation was accomplished using a Biorad MicroPulser™ Electroporator.

***S. aureus* Growth Conditions.** When used for any assay in this study, the *S. aureus* cells were grown in CY-GP broth (Casamino acids, 10 g/L; yeast extract, 10 g/L; glucose, 5 g/L; NaCl, 5.9 g/L; and 1.5 M β-Glycerophosphate 40 mL/L added after autoclaving) with shaking at 37°C.[148] Cell growth was monitored at OD_{540} over time. Overnight *S. aureus* cultures in tryptic soy medium were routinely used as inocula, and the cultures were prepared from bacteria grown on tryptic soy agar plates containing erythromycin (10 μg/mL) and/or chloramphenicol (10 μg/mL).

Protein Sequence Information. Amino acid sequences of full-length AgrB-I (1-189), AgrD-I (1-46), AgrB-II (1-187), AgrD-II (1-47), SpsB (1-191) and SpsA (1-174) were obtained from the NCBI protein database (Refseq accession: YP_001332977.1, YP_001332978.1, NP_372560.1, NP_372561.1, WP_000711486, and WP_000758209, respectively). *E. coli*-codon[149] optimized cDNA synthesis was purchased from Genewiz and received in pUC57 vectors. See Table A for protein sequences of fused Npu and Ssp.

Table 12. Amino Acid Sequence of Fused Split Inteins*

NpuNC-fused split intein sequence	**C**LSYETEILTVEYGLLPIGKIVEKRIECTVYSVDNNGNIYTQPVAQWHDR GEQEVFEYCLEDGSLIRATKDHKFMTVDGQMLPIDEIFERELDLMRVDN LPNIKIATRKYLGKQNVYDIGVERDHNFALKNGFIASA**AFN**HHHHHH
C1A NpuNC-fused split intein sequence **(used in the JJSA130 C33A mutants)**	**A**LSYETEILTVEYGLLPIGKIVEKRIECTVYSVDNNGNIYTQPVAQWHDR GEQEVFEYCLEDGSLIRATKDHKFMTVDGQMLPIDEIFERELDLMRVDN LPNIKIATRKYLGKQNVYDIGVERDHNFALKNGFIASA**AFN**HHHHHH
SspNC-fused split intein sequence	**C**LSFGTEILTVEYGPLPIGKIVSEEINCSVYSVDPEGRVYTQAIAQWHDR GEQEVLEYELEDGSVIRATSDHRFLTTDYQLLAIEEIFARQLDLLTLENIK QTEEALDNHRLPFPLLDAGTIKVKVIGRRSLGVQRIFDIGLPQDHNFLLA NGAIAAA**AFN**HHHHHH
C1A SspNC-fused split intein sequence **(used in the JJSA131 C33A mutants)**	**A**LSFGTEILTVEYGPLPIGKIVSEEINCSVYSVDPEGRVYTQAIAQWHDR GEQEVLEYELEDGSVIRATSDHRFLTTDYQLLAIEEIFARQLDLLTLENIK QTEEALDNHRLPFPLLDAGTIKVKVIGRRSLGVQRIFDIGLPQDHNFLLA NGAIAAA**AFN**HHHHHH

*Important residues are in boldface. The His_6-tag is underlined. cDNA synthesis was purchased from Genewiz and was codon optimized for *S. aureus* expression.[150]

Table 13. Cell Strains and Plasmids Used in This Study

Strain or Plasmid	Genotype or Description	Reference
S. aureus strains		
RN4220	Restriction-deficient mutant of strain 8325-4	[151]
RN6734	Group I strain, ϕ-13 lysogen of 6390b	[62]
RN9120	*agr*::*tetM* derivative of RN9130	[62, 151]
RN9222	RN6911 (*agr::tetM* replacement RN6734) containing pRN7062 (P2-*agrCA-I*; P3-*blaZ*), Group I β-lactamase reporter strain	[62]
RN9367	RN7206 (*agr::tetM* replacement in *agr*-I strain) containing pRN7105 (P2-*agrCA-II* and P3::*blaZ)*	[62]
RN9532	RN6911 (*agr::tetM* replacement in *agr*-I strain) containing pRN7131 (P2-*agrCA-III* and P3::*blaZ)*	[63]
RN10306	RN6911 Δ*spa::cadC*	unpublished
AgrD(1-32)-intein^{Npu}	RN10306 with *pJJSA130*	This study
D29A AgrD(1-32)-intein^{Npu}	RN10306 with $pJJSA130_{D29A}$	This study
C33A AgrD(1-32)-intein^{Npu}	RN10306 with $pJJSA130_{C33A}$	This study
AgrD(1-32)-intein^{Ssp}	RN10306 with *pJJSA131*	This study
D29A AgrD(1-32)-intein^{Ssp}	RN10306 with $pJJSA131_{D29A}$	This study
C33A AgrD(1-32)-intein^{Ssp}	RN10306 with $pJJSA131_{C33A}$	This study
Intein^{Npu}	RN10306 with *pJJSA132*	This study
Intein^{Ssp}	RN10306 with *pJJSA133*	This study
chimera AgrD(1-32)-intein^{Npu}	RN10306 with *pJJSA134*	This study
chimera AgrD(1-32)-intein^{Ssp}	RN10306 with *pJJSA135*	This study
AgrB+ AgrD(1-32)-intein^{Npu}	RN10306 with *pJJSA130* and $pJJSA140_{WT}$	This study
C84A AgrB+AgrD(1-32)-intein^{Npu}	RN10306 with *pJJSA130* and $pJJSA140_{C84A}$	This study
K129E AgrB+AgrD(1-32)-intein^{Npu}	RN10306 with *pJJSA130* and $pJJSA140_{C84A,K129E}$	This study
K131E AgrB+AgrD(1-32)-intein^{Npu}	RN10306 with *pJJSA130* and $pJJSA140_{C84A,K131E}$	This study
AgrB+AgrD(1-32)-intein^{Ssp}	RN10306 with *pJJSA131* and $pJJSA140_{WT}$	This study
C84A AgrB+ AgrD(1-32)-intein^{Ssp}	RN10306 with *pJJSA131* and $pJJSA140_{C84A}$	This study
K129E AgrB+ AgrD(1-32)-intein^{Ssp}	RN10306 with *pJJSA131* and $pJJSA140_{C84A,K129E}$	This study
K131E AgrB+ AgrD(1-32)-intein^{Ssp}	RN10306 with *pJJSA131* and $pJJSA140_{C84A,K131E}$	This study
E. coli strains		
DH5α	Chemically competent cells, Standard recipient for plasmid cloning	Promega
XL10-Gold	Supercompetent cells	Stratagene
BL-21(DE3)	Standard *E. coli* protein expression strain, *E. coli* B strain with DE3, a λ prophage carrying the T7 RNA polymerase gene and lacI^{q}	
OverExpress™ C43(DE3)	OverExpress *E. coli* strain for toxic proteins, F^{-} *ompT* gal dcm $hsdS_B(r_B^- m_B^-)$(DE3)	Lucigen
tr-SpsB	BL-21(DE3) strain containing *pJJ59*	This study
fl-SpsB	BL-21(DE3) strain containing *pJJ60*	This study
SpsA	BL-21(DE3) strain containing *pJJ70*	This study
AgrB-I	C43(DE3) cells containing *pBW-B1-2*	[152]

AgrB-II	C43(DE3) cells containing *pBW-B2-2*	[152]
AgrD-I	BL-21(DE3) strain containing *pBW-D1-1*	[152]
FLAG-AgrD-I	BL-21(DE3) strain containing *pBW-D1-7*	[152]
FLAG-AgrD-II	BL-21(DE3) strain containing *pBW-D2-7*	[152]
Plasmids		
pCN51	Shuttle vector with pT181*cop-wt repC* replicon, P_{cad}-*cadC* promoter, *ermC* (erythromycin selection), and *amp* ColE1ori (E. coli replication and selection) and Transcription terminator sequence	[140]
pJC1361	Shuttle vector with the *pE194* replicon, P_{cad}-*cadC* promoter, *cat194* (chloramphenicol selection), *amp* ColE1ori (E. coli replication and selection) and Transcription terminator sequence	unpublished
pET-15b TEV	Plasmid derived from pET-15b (Novagen) with the thrombin cleavage sequence has been mutated to the TEV cleavage sequence	This study
pET-24b $GST_{C\text{-}term}$	Plasmid derived from pET-24b (Novagen) with the GST-tag cloned to be C-terminal of the protein to be expressed.	[152]
pJJSA130	pCN51 with *agrD-I Δ33-46-npuCN-*His_6	This study
$pJJSA130_{D29A}$	pCN51 with *agrD-I Δ33-46 (D29A)-npuCN-*His_6	This study
$pJJSA130_{C33A}$	pCN51 with *agrD-I Δ33-46-npuCN-(C33A)-*His_6	This study
pJJSA131	pCN51 with *agrD-I Δ33-46-sspCN-*His_6	This study
$pJJSA131_{D29A}$	pCN51 with *agrD-I Δ33-46 (D29A)-sspCN-*His_6	This study
$pJJSA131_{C33A}$	pCN51 with *agrD-I Δ33-46-sspCN-(C33A)-*His_6	This study
pJJSA132	pCN51 with *npuCN-*His_6	This study
pJJSA133	pCN51 with *sspCN-*His_6	This study
pJJSA134	pCN51 with *agrD-I (Δ3-17::agrD-II 33-47)-npuCN-*His_6	This study
pJJSA135	pCN51 with *agrD-I (Δ3-17::agrD-II 33-47)-sspCN-*His_6	This study
$pJJSA140_{WT}$	pJC1361 with *agrB-I-FLAG*	This study
$pJJSA140_{C84A}$	pJC1361 with *agrB-I (C84A)-FLAG*	This study
$pJJSA140_{C84A,K129E}$	pJC1361 with *agrB-I (C84A, K129E)-FLAG*	This study
$pJJSA140_{C84A,K131E}$	pJC1361 with *agrB-I (C84A, K131E)-FLAG*	This study
pJJ59	pET-15b TEV with *spsB Δ1-22*	This study
pJJ60	pET-15b TEV with *spsB*	This study
pJJ70	pET-15b TEV with *spsA*	This study
pBW-B1-2	pET-24b $GST_{c\text{-}term}$ with *agrB-I-*His_6	[152]
pBW-B2-2	pET-24b $GST_{c\text{-}term}$ with *agrB-II-*His_6	[152]
pBW-D1-1	pET-24b with *agrD-I-gyrA-*His_7	[152]
pBW-D1-7	pET-24b $GST_{c\text{-}term}$ with *FLAG-*His_6*-agrD-I*	[152]
pBW-D2-7	pET-24b $GST_{c\text{-}term}$ with *FLAG-*His_6*-agrD-II*	[152]

Plasmid Construction. To generate plasmids (Table 13), target genes were amplified using primers (Table 14) and inserted into vectors via the overlap extension PCR method.[153] Plasmids pCN51 or pJC1361 were obtained from the Novick lab and were used as the backbone vectors for the fused split intein constructs or AgrB point mutants, respectively. The *agrD(1-32)-npuNC*, *agrD(1-32)-sspNC* were inserted into pCN51 and the *agrB* gene was inserted into pJC1361. The genes for the chimera *agrD(1-32)-npuNC* and *agrD(1-32)-sspNC* were synthesized by Genewiz and then inserted into the backbone vector pCN51. Various point mutations in AgrD, the AgrD(1-32)-intein constructs or AgrB were introduced via the QuikChange method (Stratagene). The pET-15b TEV plasmid was used as the backbone vector for *spsB* and *spsA*. The full-length *spsB* was constructed using multiple primers annealed together and cloned using PCR to make a large primer for insertion into pJJ59 using overlap extension PCR. Clones for all of these constructs were sequenced by Genewiz. All BW-B/D#-# cell strains and plasmids were designed and generously provided by Boyuan Wang, a graduate student in the lab.

Table 14. Oligonucleotide Primers Used in This Study

Primer	Sequence (5'-3')
QC 15b TEV for	CATCATCACAGCAGCGGC*GAGAACCTGTATTTTCAGGGC*CATATGCTCGAGGATCCG
QC 15b TEV rev	CGGATCCTCGAGCATATGGCCCTGAAAATACAGGTTCTCGCCGCTGCTGTGATGATG
SpsBΔ1-22overhang for	CAGCGGCGAGAACCTGTATTTTCAGGGCAAATTCATCGTTACCCCGTACACCATCAAAG
SpsBΔ1-22overhang rev	TGCTAGTTATTGCTCAGCGGTGGCAGCTTAATTTTTAGTATTTTCAGGATTGAAATTATG
SpsA overhang for	GGCGAGAACCTGTATTTTCAGGGCATGAAAAAAGTTGTTAAATACCTGATCTCTC
SpsA overhang rev	GTTTAGAGGCCCCAAGGGGTTATGCTAGTTAAGATTTGAACTGGATGGTCCATTTAGAG
SpsB piece1 for	AGCAGCGGCGAGAACCTGTATTTTCAGGGCATGAAAAAAGAAATCCTGGAA
SpsB piece2 rev	GAACGCAACCGCGATAGAGATGATCCATTCCAGGATTTCTTTTTTCATGCC
SpsB piece3 for	GATCATCTCTATCGCGGTTGCGTTCGTTATCCTGTTCATCGTTGGTAAATTC
SpsB piece4 rev	TTTGATGGTGTACGGGGTAACGATGAATTTACCAACGATGAACAGGATAAC
AgrD-intein overhang for	GAAAGAAGTGAAGGTCAATGTCTGAAC<u>CTGCAG</u>ATTAAGGAGGACTTAAAATGAATACAT
AgrD-intein overhang rev	TCAGTATTTATTATGCATTAGAATAGGCGCGCCTTAATGATGATGATGATGATGATTGAA
Npu 132 for	GAAC<u>CTGCAG</u>ATTAAGGAGGACTTAAAATGTGTTTATCATATGAAACAGAAATTTTAACA
Npu 132 rev	TGTTAAAATTTCTGTTTCATATGATAAACACATTTTAAGTCCTCCTTAATCTGCAGGTTC
Ssp 133 for	GAAC<u>CTGCAG</u>ATTAAGGAGGACTTAAAATGTGTTTATCATTCGGTACAGAAATTTTAACA
Ssp 133 rev	TGTTAAAATTTCTGTACCGAATGATAAACACATTTTAAGTCCTCCTTAATCTGCAGGTTC
QC 130 D29A for	GGTAACATCGCAGCTTATAGTACTTGTGCTTTCATAATGTGTTTATCATATGAAACA
QC 130 D29A rev	TGTTTCATATGATAAACACATTATGAAAGCACAAGTACTATAAGCTGCGATGTTACC
QC 131 D29A for	GGTAACATCGCAGCTTATAGTACTTGTGCTTTCATAATGTGTTTATCATTCGGTACA
QC 131 D29A rev	TGTACCGAATGATAAACACATTATGAAAGCACAAGTACTATAAGCTGCGATGTTACC
QC 130 C33A for	AGTACTTGTGACTTCATAATGGCATTATCATATGAAACAGAA
QC 130 C33A rev	TTCTGTTTCATATGATAATGCCATTATGAAGTCACAAGTACT
QC 131 C33A for	AGTACTTGTGACTTCATAATGGCATTATCATTCGGTACAGAA
QC 131 C33A rev	TTCTGTACCGAATGATAATGCCATTATGAAGTCACAAGTACT
134/135 overhang for	GAAAGAAGTGAAGGTCAATGTCTGAAC<u>CTGCAG</u>ATTAAGGAGGACTTAAAATGAATACAT
pCAD overhang for	CTTTGAGTGAGCTGGCGGCCGCTGCATGCGCACTTATTCAAGTGTATTTTTTAATAAAT
AgrB overhang for	GCCAAGCTCGGCGCGCCATTGGGATGGAACGCATGCGCACTTATTCAAGTGTATTTT
AgrB overhang rev	TTTTACACCACTCTCCTCACTGTTCATGTCGACCTGCAGGTTCAGACATTGACC
QC AgrB C84A for	CATGCACCTTCTTCTTTTTGGGCATATGTAGAAAGTATTATACTA
QC AgrB C84A rev	TAGTATAATACTTTCTACATATGCCCAAAAAGAAGAAGGTGCATG
QC AgrB C129E for	GTATATGCTCCTGCAGCAACTGAGAAGAAGCCCATTCCTGTGCGA
QC AgrB C129E rev	TCGCACAGGAATGGGCTTCTTCTCAGTTGCTGCAGGAGCATATAC
QC AgrB C131E for	GCTCCTGCAGCAACTAAAAAGGAGCCCATTCCTGTGCGACTTATT
QC AgrB C131E rev	AATAAGTCGCACAGGAATGGGCTCCTTTTTAGTTGCTGCAGGAGC

for = forward primer sequence, rev = reverse primer sequence

<u>PstI sequences are underlined</u>. While endonucleases were not used to insert genes, PstI was included in the overhang primer design for pCN51 inserts in case restriction digest was necessary to remove the P_{cad}-*cadC* promoter cassette or the gene to be expressed.

Western blot analysis of cell cultures. Uninduced and induced cell cultures were grown for a total of 8 hrs. Cells were harvested via centrifugation and frozen. Upon thawing the cells on ice, lysostaphin digestion of the peptidoglycan was carried out in the lysostaphin digest buffer (20 mM Tris-HCl (pH 8), 100 mM NaCl, 20 mM MgCl2, and 27% (w/v) sucrose) with lysostaphin at 50 or 100 μg/mL. Cells from either a 2- or 5-mL cell growth were resuspended in 0.3 or 0.5 mL, respectively, digest buffer and incubated at 37°C for ~30 minutes. Lysostaphin digest of the peptidoglycan was monitored by adding a small amount of the digest to 20% SDS in PBS to see if the solution would clarify indicating solubilization of the formed protoplasts. After the digest, the protoplasts were incubated in PBS with protease inhibitors (Roche) on ice for 15 minutes and then sonicated. Cell debris was pelleted via centrifugation. The whole cell lysates were analyzed via SDS-PAGE and Western blot. For cell culture supernatants, the supernatant was directly analyzed using SDS-PAGE. For Western blot analysis of the AgrD(1-32)-intein constructs the nitrocellulose membrane was probed with a α-His_6 antibody (Waters). AgrB constructs were probed using a α-FLAG antibody. Images were taken with a LI-COR Odyssey Infrared Imager (GE Healthsystems).

HPLC-MS Analysis of Cell Culture Supernatants. Initial purification of the AgrD(1-32)-intein^{Npu}, AgrD(1-32)-intein^{Ssp} or group I WT cell culture supernatants was performed using a 5-g C18 SPE cartridge. Prior to use, each cartridge was activated by flowing through HPLC buffer B, followed by 25 mL of HPLC buffer A. Cell culture supernatants were acidified to 1% (v/v) neat TFA prior to loading onto the column. Columns were washed twice under gravity flow with HPLC buffer A; peptides were then eluted from the column by elutions of 20% buffer B, 50% buffer B, and 70% buffer B (2x 500 μL). The

elutions were lyophilized and then resuspended in methanol (HPLC grade) for submission for analysis at the Mass Spectrometry Facility in the Princeton University Molecular Biology Department. Analysis of these samples was performed on an LTQ-XL platform (Thermo Fisher Scientific) using RP-HPLC-MS. RP-HPLC Analysis was run on an Agilent 1100 series HPLC using a 1 mM Jupiter 5µ C4 300A column. HPLC runs employed a 5-75% B linear gradient over 80 minutes (Buffer A, 0.02% TFA, 0.5% formic acid, 0.1% acetic acid, 3% acetonitrile and 97% H_2O; Buffer B, 0.02% TFA, 0.5% formic acid, 0.1% acetic acid, and 99.5% acetonitrile). SPE samples were compared to growth media from RN6734 prepared under the same protocol to provide a positive control for AIP-I detection.

Expression and Purification of tr-SpsB. The JJ59 expression strain was grown at 37°C in 1-L cultures of LB broth containing ampicillin at a concentration of 0.1 mg/mL. When the OD_{600} reached 0.6, expression was induced by the addition of 1 mM IPTG. Cells were harvested 3 hours post-induction and centrifuged at 6000 g for 15 minutes and the cell pellets were resuspended in 20 mL of urea lysis buffer (50 mM pH 7.6 phosphate, 6 M urea, 300 mM NaCl, 10 mM imidazole). The cells were then lysed by 3-4 repeated passages through a French press homogenizer. The cell-wall debris was removed by centrifugation at 40000 g for 30 minutes at 4°C. Supernatant was then purified by affinity purification using Ni-NTA resin (Qiagen). Ni-NTA columns were equilibrated with 5 column volumes (CV) of urea lysis buffer. The protein was then loaded onto the column and incubated on a nutating mixer at 4°C for 1 hour. The column was first washed with 3 CV of urea lysis buffer and 5 CV of wash buffer (lysis buffer and 25 mM imidazole). The protein was then eluted with elution buffer (lysis buffer with 300 mM imidazole) in three

fractions of 3 mL each. Urea removal via dialysis was carried out in a step-wise manner from 6 M urea to 4 M to 2 M and no urea. The dialyzed supernatant was concentrated and purified via S75 size-exclusion chromatography (CV = 25 mL), and the protein was eluted in degassed FPLC buffer (50 mM phosphate (pH 7.5), 150 mM NaCl) over a volume of 40 mL. Fractions collected near the peak of interest were analyzed by SDS-PAGE using a 15% Bis-Tris gel. The final product ~95% pure by SDS-PAGE analysis was concentrated to ~40 μM and frozen in liquid nitrogen for storage at -80°C. Protein concentration was determined using UV-Vis spectroscopy. tr-SpsB was also analyzed via RP-HPLC and ESI-MS.

Expression and Purification of SpsB and SpsA. fl-SpsB or SpsA expression strains were grown at 37°C in 1-L cultures of LB broth containing ampicillin at a concentration of 0.1 mg/mL. When the OD_{600} reached 0.6, expression was induced by addition of 1 mM IPTG. Cells were harvested 3 hours post-induction via centrifugation at 6000 g for 15 minutes and the cell pellets were resuspended in 20 mL of lysis buffer (50 mM pH 7.6 phosphate, 300 mM NaCl, 10 mM imidazole). Protease Inhibitor Cocktail (Roche, Penzberg, Germany) was then added to the cell suspension, and the cells were then lysed by 3-4 repeated passages through a French press homogenizer. The cell-wall debris was removed by centrifugation at 40000 g for 30 minutes at 4°C, and the membrane vesicles were pelleted by ultracentrifugation at 90000 g for 1 hour at 4°C. The membrane fraction was extracted using 20 mL of lysis buffer with 0.05% (w/v) DDM overnight at 4 °C. After another ultracentrifugation step at 50000 g for 30 mins, supernatant from the extraction was then purified by affinity purification using TALON Co-NTA resin (Clontech Technologies, Mountain View CA). Co-NTA columns were equilibrated with

incubated on a nutating mixer at room temperature for 2 hours. The columns were first washed with 3 CV of wash buffer 1 (lysis buffer and 0.05% DDM) and 2 CV of wash buffer 2 (lysis buffer and 0.05% DDM with 30 mM imidazole). The protein was then eluted with elution buffer (lysis buffer with addition of 300 mM imidazole and 0.05% DDM) in three fractions of 3 mL each. The elution fractions were concentrated to about 1.5 mL in 10 kDa MWCO concentrators. The concentrate was then purified via S200 size-exclusion chromatography (CV = 25 mL), and the protein was eluted in degassed FPLC buffer (50 mM phosphate (pH 7.5), 150 mM NaCl, 0.05% DDM) over a volume of 40 mL. Fractions collected near the peak of interest were analyzed by SDS-PAGE using a 15% Bis-Tris gel. The most concentrated fractions were then combined and concentrated to ~40 μM, and aliquots of the purified protein were frozen in liquid nitrogen and stored at -80 °C. Protein concentration was determined using UV-Vis spectroscopy.

Expression and Purification of AgrB-I and AgrB-II. *E. coli* C43(DE3) cells transformed with the appropriate AgrB expression plasmids were grown at 37 °C in one liter of LB medium containing 50 μg/mL kanamycin. When the OD_{600} reached 0.8, the medium was cooled down to 22°C and overnight expression was induced by addition of 0.4 mM IPTG. Cells were harvested at 6000 g for 20 minutes and the cell pellets were resuspended in 18 mL of lysis buffer (20 mM sodium phosphate, 100 mM NaCl and 1mM PMSF, pH 7.5). Cells were lysed by four passages through a French-press homogenizer. Cell-wall debris was spun down at 15000 g for 10 minutes and removed. Cell-membrane vesicles were then pelleted by ultracentrifugation at 200,000 g for 1 hour. The membrane fraction was extracted using 5 mL of buffer containing 20 mM Phosphate pH 7.5, 100 mM NaCl, 2% (w/v) DDM for 3 hours at 4 °C. After another

ultracentrifugation step at 100,000 g for 20 min, supernatant from each liter of expression culture was loaded to 2.5 mL of Talon cobalt resin. After incubation at 4 °C for 60 minutes, the resin was repacked in a 25-mL Bio-Rad disposable plastic column. The flow-through was discarded and the column was washed with 20CV of wash buffer (20 mM sodium phosphate, 100 mM NaCl, 5mM β-mercaptoethanol, 0.1% (w/v) fos-choline-12 (FC-12) and 25 mM imidazole, pH 7.5). Bound protein was eluted with 3CV of elution buffer (wash buffer with 500 mM imidazole). The elution was concentrated to 1 mL and further purified on Superdex 200 size-exclusion chromatography with running buffer (20 mM phosphate, 100 mM NaCl, 0.14% (w/v) FC-12, 1mM TECP, pH 7.0), from which the desired peak fractions were collected.

Expression and Purification of Full-length AgrD-I. Full-length, non-tagged AgrD-I was expressed as an N-terminal fusion to a GyrA-His_7 intein protein in *E. coli* BL21(DE3) strain. Expression strain harboring the appropriate expression vector was grown at 37ºC to OD_{600} = 0.6 and then induced by addition of IPTG to 1.0 mM. The culture was shaken at 37ºC for 4 additional hours post-induction and cells were collected through centrifugation. Cells were resuspended in PBS (20 mM Phosphate (pH 7.5), 100 mM NaCl). PMSF (100 mM stock in ethanol) was added to the cell suspension immediately prior to lysis at a final concentration of 1mM. Cells were disrupted by four French-Press passages. The lysate was spun at 30000 g for 1 hour. Supernatant was decanted and discarded. The pellet was resuspended in a buffer containing 7.5M GuHCl, 50mM Phosphate buffer pH = 7.5 and 2mM TCEP. The suspension was homogenized, gently shaken at 4ºC for 1hr and then spun at 30000 g for 1 hour. Supernatant from the cleared GuHCl extract was loaded to a column packed with Ni-NTA resin (Qiagen), and

the resin was washed with buffer containing 25mM imidazole and 6M GuHCl and eluted using a buffer containing 300mM imidazole, 7.2M urea and 0.05% (w/v) DDM. The eluted protein was immediately chilled and refolded through dialysis against a series of phosphate buffer with decreasing urea concentrations at 4°C.

Upon dialysis, the full-length AgrD-intein-His_7 construct was cleaved by 50 mM DTT and 5 mM TCEP with the presence of 0.1% (w/v) DDM under argon atmosphere at RT for 12 hours. Free intein released from DTT treatment as well as uncleaved fusion protein was removed in a reverse-Ni-NTA affinity process. The combined flow-through and wash fractions containing predominantly full-length AgrD-DTT esters were then supplemented by 0.1% FC-12. Residual amount of urea in this solution was removed through two concentration-dilution cycles. In each cycle, the solution was concentrated to 10% of its original volume and then diluted back using a buffer containing 50 mM phosphate (pH 7.5), 50 mM DTT and 0.07% FC-12. The solution after the second dilution was concentrated to <5 mL, to which equal weight of GuHCl was added to make a concentration of 6 M. EDTA was added at 10 mM and NaOH was used to basify the solution to pH 9.5. The solution was incubated under argon atmosphere at 37°C for 4 hours for complete saponification of full-length AgrD-DTT esters, acidified to pH < 2 using neat TFA, filtered, and submitted to C4 semi-prep HPLC for final purification.

Expression and Purification of the Full-length FlagHis_6-AgrD-I and FlagHis_6-AgrD-II. Both constructs were expressed as C-terminal GST fusion proteins in *E. coli* BL21(DE3) host cells. The expression culture was grown at 37°C to OD_{600} = 0.6 and then was cooled down to 16°C prior to induction by addition of 0.4 mM IPTG. After overnight incubation, cells were isolated from the culture medium, resuspended in lysis buffer (20

mM sodium phosphate, 100 mM NaCl, pH 7.5), and lysed by four passages through a French-press homogenizer. After centrifugation at 30000g for 30min, the cleared lysate was supplemented with 0.1% (v/v) DDM and then incubated with GS4FF resin in a plastic column at 4 °C for 60 minutes. The lysate was then drained, and the resin was washed by 20 CV of lysis buffer, resupsended in 2 CV of lysis buffer, and treated with 10 units thrombin or 0.2 mg/mL PreScission protease at room temperature with gentle shaking for 3 hours. The released full-length FlagHis$_6$-AgrD product was collected and allowed to flow through a 4-mL bed packed with Ni-NTA resin. The Ni-NTA bed was washed with 10 CV of lysis buffer with 15 mM imidazole, 10 CV of 6 M GuHCl buffered by Na-phosphate (pH 7.5) and eluted with 3 CV of elution buffer (6 M Guanidinium chloride, 0.2M acetic acid). Elution was treated with TCEP (5mM, final concentration) and then purified over a semiprep-scale C18 HPLC column.

***in vitro* tr-SpsB assays.** Assays for all AgrD derived substrate peptides were carried out in two different buffer conditions. Glycerol conditions[58] (similar to those used by Kavanaugh *et al*.) were 25 mM Tris-HCl (pH 8), 50 mM NaCl, and 20% Glycerol. Triton conditions[143] (similar to those used by Rao *et al*.) were 50 mM Tris-HCl (pH 8), 150 mM NaCl, and 0.5% Triton X-100. All assays contained 10 μM tr-SpsB and 150 or 200 μM substrate peptide. AH or IG-AIP1 inhibition assays were under Triton assay conditions and contained 150 μM substrate peptide with 150 μM control peptide. Experiments to determine whether there is a concentration-dependence for SpsB cleavage of AH or IG-AIP1 were under Trition conditions and varied AH and IG-AIP1 peptide concentration up to 400 μM or 1 mM, respectively. Assays were incubated at room temperature for 12

hours unless otherwise indicated. At the end of the incubation time, samples were acidified with HPLC buffer A and then analyzed via RP-HPLC and ESI-MS.

β-lactamase Cell Culture Supernatant Assays. Cell cultures containing a cell strain of interest were grown in CY-GP growth medium for ~2 hours (strains expressing various AgrD(1-32)-intein proteins and RN6734) until OD_{540} ~0.2-0.3. When necessary, protein expression was induced with 10 μM Cd^{2+} followed by a 6-hour induced growth period unless specified. RN9120 cell cultures were grown for 3-4 hours after adding AgrD(1-32)-II-thiolactone. Cell density (OD_{540}) measurements were taken at the end of the growth period to normalize all of the cultures. Cells were removed via centrifugation 4500 g for 10 minutes after which cell culture supernatants were sterilized using syringe-filtration (0.2 μm filter). Sterilized cell culture supernatants were then aliquoted and frozen at -80°C.

Thawed cell culture supernatants were normalized to cell density readings of original cell cultures by diluting with CY-GP broth, when necessary. Each supernatant was then buffered with 1 M MES buffer (pH 5.9) for analysis with the β-lactamase reporter gene assay. Cell culture supernatants were incubated with reporter gene strains for 1 hour with shaking at 37°C in a Spectramax M3 micro plate reader (Molecular Devices). Cell density was monitored by OD_{650} readings taken every 2 minutes. Immediately following Nitrocefin addition, an initial OD_{490} and OD_{650} reading was taken and then β-lactam hydrolysis was monitored by OD_{490} readings taken every 45 s over 15 minutes. Once saturation of OD_{490} for one of the cell culture supernatants in the assay was detected, the assay was stopped and a final OD_{490} and OD_{650} measurement was taken. The initial and final OD_{490} readings were normalized to cell density (OD_{650}) and the ΔOD_{490}

readings were calculated by subtracting the normalized initial OD_{490} from the normalized final OD_{490} reading. Each cell culture supernatant was assayed in triplicate at least two times. Error bars represent the standard deviation from the mean.

Proteoliposome Cleavage Assays. A lipid mixture of 75% POPC and 25% POPG (w/w) was prepared in an aqueous stock solution containing 1% (w/v) total lipid and solubilized in 4% n-dodecylphosphocholine (FC-12). Reconstitution experiments were prepared as a 100-µL volume containing 1 µM of each protein, 10 µM of D-TL (or AIP), 2.5 mg of lipid, and 30 mM Tris-HCl (pH 8.0). After mixing the samples, polystyrene beads (Bio-Beads, Bio-Rad) were added to achieve a Bio-Beads to detergent (w/w) ratio of 30:1, respectively. The reaction was mixed for 2 hours on a nutator. The polystyrene beads were removed via centrifugation at 5100g for 20 seconds. The reconstituted liposome mixture was then incubated at room temperature (25 °C) for 12 hours. After the 12-hour incubation period, the liposome mixture was acidified slightly by the addition of 1 M MES (pH 5.9) buffer. This proteoliposome mixture was then directly used in the β-lactamase reporter assay or SPE extraction.

SPE extraction was performed using 200-mg C2 SPE cartridges. The cartridge was activated with HPLC buffer B and equilibrated with HPLC buffer A. The buffered vesicle solution was then added to the column and washed with buffer A. Elutions with 20%, 50% and 70% buffer B were collected and lyophilized. Analysis of lyophilized elutions was performed on an Orbitrap XL platform (Thermo Fisher Scientific) using reversed-phase nano-UPLC-MS at the Mass Spectrometry Facility in the Princeton University Molecular Biology Department. SPE samples were compared to an AIP-I standard to identify the presence of AIP.

β-lactamase Activation and Inhibition Activity Assays. The activation and inhibitory activities of the AIP analogs were analyzed using an established a β-lactamase reporter assay.[10,23-25,27,31] Briefly, cell cultures of *agr*-null cell lines RN9222 (CA1-I), RN9367 (CA2-II) and RN9537 (CA3-III) with plasmids containing agrCA and agr-P3::blaZ were grown in CYGP growth media to exponential phase growth (OD_{650} ≈ 0.30-0.6). For activation assays, 90 μL aliquots of cells were treated with varying concentrations of AIP analogs or buffer for 60 mins (RN9222) or 80 mins (RN9367 and RN9537) with shaking at 37°C in a Spectramax M3 micro plate reader (Molecular Devices). For inhibition assays, 80 μL aliquots of cells were treated with 125 nM agonist AIP and varying concentrations of AIP analogs or buffer for 60 mins (RN9222) or 80 mins (RN9367) with shaking at 37°C in a micro plate reader. Cell density was monitored by OD_{650} readings taken every 2 mins. Immediately following Nitrocefin addition, β-lactam hydrolysis was monitored by OD_{490} readings taken every 45 s over 20 min. Assay data were collected as initial β-lactamase hydrolysis velocity. The values obtained for initial velocity were then normalized to cell density and percent maximal activation, plotted as percent maximal activation versus log peptide concentration, and fit to a sigmoidal dose response curve using the PRISM 5.0 package (GraphPad Software, San Diego, CA), which fits individual dose-response curves via nonlinear regression to the following four-parameter logistic equation:

$$E = \text{basal} + \frac{E_{\max} - \text{basal}}{1 + 10^{\log EC_{50} - \log[A] n_H}}$$

in which E denotes effect, [A] denotes the agonist concentration, η_H denotes the midpoint slope, EC_{50} denotes the midpoint location parameter, and E_{max} and basal denote the upper and lower asymptotes, respectively. For inhibition curves, the midpoint location

parameter from the above equation reflects the IC_{50}. Each AIP analog was assayed in triplicate at least two times. Error bars represent the standard deviation from the mean.

Fluorescent anisotropy measurements. Fluorescence measurements were performed on a Fluorolog-3 instrument (HORIBA Jobin Yvon) equipped with automated dual polarizers and using a Semi-Micro Fluorometer Cell (Starna Cells) with a 10-mm path length. The measurement chamber was held at a constant temperature of 30.0°C by an Advanced Series AC200 thermostat (Thermo Scientific) connected to an Arctic series refrigerated circulating water bath (Thermo Scientific). The excitation wavelength was 490 nm and emission wavelength was recorded at 520 nM, both with a bandwidth of 5 nm. Ten measurements were taken per titration point with an integration time of 0.5 sec for V/V, V/H, H/H and H/V polarizer settings (excitation/emission, V: vertical polarization, H: horizontal polarization). The final anisotropy, *r,* was calculated from $r = (I_{VV} - G \times I_{VH})/(I_{VV} + 2 \times G \times I_{VH})$, with $G = I_{HV}/I_{HH}$.

In a typical experiment, 700 μL of measurement buffer (20 mM HEPES, pH 7.0, 100 mM NaCl, 1 mM TCEP, 2 μM BSA and 100 nM of empty nanodiscs) containing 21 nM FAM-AIP-I was transferred to the cuvette and the fluorescent anisotropy was measured as a reference. AgrC-I nanodiscs (4.2 μM, 26.8 μL) were then added for a final concentration of 150 nM, and the mixture allowed to equilibrate for 3 minutes before taking the pre-competition anisotropy measurement. Finally, the competitor AIP or AIP analog (500μM, 15μL in 50% DMSO) was mixed in for a final concentration of 10 μM and the post-competition anisotropy was measured following 3-minute incubation. Three individual competitions were performed for each compound. The averaged, reference-subtracted anisotropy measured both pre- and post-competition were plotted for each

compound as shown in Figure 5. SSA (y-axis) is calculated by subtracting the SSA value at the starting stage (free FAM-AIP-I, before the addition of AgrC-I discs) from the SSA values measured before or after competition.

AgrC Autophosphorylation Assay. All autokinase reactions were performed in reaction buffer containing 50 mM Tris-HCl, 15 mM HEPES-Na pH 7.8, 100 mM NaCl, 10 mM $MgCl_2$ and 1 mM TCEP. AIPs were included as indicated (from DMSO stocks), and DMSO was added to make the overall DMSO concentration up to 2.7% (v/v). Typically, an autokinase reaction contained 20 μM [γ-^{32}P]-ATP (1Ci/mmol) and 1.4 μM AgrC-I discs. After incubation at 37 °C for 40 minutes, the reaction was either spotted on nitrocellulose membrane (5μL/spot in triplicate) or mixed with 4x SDS sample buffer (1x concentration: 50 mM Tris-HCl pH 8.0, 2 % (w/v) SDS, 10 (v/v) % glycerol, 10 mM dithiothreitol and 0.01 (w/v) % bromophenol blue). Samples spotted on nitrocellulose membrane were analyzed with scintillation counting. Samples from a mock reaction (in the absence of AgrC-I) under the same conditions were also included as the background. All samples were air-dried and then washed 3x5min with TBST buffer (50mM Tris pH 8.5, 150 mM NaCl and 0.1% (v/v) Tween-20) and air-dried again. Each piece of membrane was subsequently transferred to a 4mL counting vial containing 3.5mL of Ultima Gold™ Cocktails (Perkin Elmer) and luminescence from the vial was quantified in a scintillation counter. Background-corrected count numbers (in *c*ount *p*er *m*inute, CPM) of each reaction was normalized to the AIP-free reaction and plotted. Dose-response plots were prepared from several AgrC autophosphorylation assays with varying concentrations of AIP-I or D5A AIP-I. Samples mixed with SDS-PAGE loading buffer were immediately resolved on a 15% Tris-HCl SDS-polyacrylamide gel. The gel was

then dried, and incubated with Eastman Kodak BIOMAX MR film for 5 hrs at RT. After development, the autoradiogram (film) was scanned using ImageQuant LAS 4000 (GE).

Phospho-relay from AgrC-I to AgrA Assay. AgrC-I discs (4.0 μM) were phosphorylated in the absence of AIP with 50 μM [γ-^{32}P]-ATP at 37ºC for 120 min, and subsequently exchanged into an ATP-free reaction buffer (50 mM Tris-HCl, 15 mM HEPES-Na pH 7.8, 10mM $MgCl_2$, 100 mM NaCl and 1 mM TCEP) using Bio-Rad Micro Bio-Spin™ P-6 Gel Columns. The stock was equally divided into four portions, to which was added 10 μM (final concentration) D5A AIP-I, AIP-I, AIP-II or vehicle (DMSO). These pre-phosphorylated AgrC-I stocks (50 μL) were mixed with 10 μL AgrA protein (50 μM stock in 50 mM Tris-HCl pH 8.0, 100 mM NaCl , 5 mM TCEP in 20% (v/v) glycerol) to initiate the phospho-relay. The AgrA buffer was used to mix with AgrC-I samples in mock reactions. All reactions were incubated at 30ºC from which 10-μL samples were withdrawn at indicated time points, mixed with 4x SDS sample buffer and chilled on ice. All samples were resolved on a 15% Tris-HCl SDS-polyacrylamide gel and detected through autoradiography as described in the *Autophosphorylation Assay* secton of this chapter.

Fmoc-SPPS of SpsB Substrate Peptides. AgrD derived substrate peptides were synthesized manually or with a Liberty microwave-assisted automated peptide synthesizer (CEM). All peptides were synthesized on a rink amide resin (Novabiochem). Chain assembly was carried out with HBTU (4.9 eqv. to resin) and HOBt (4.9 eqv. to resin) activation using a 5-fold excess of standard N^{α}-Fmoc protected amino acid over the resin in DMF (dimethylformamide) with DIEA (N,N-diisopropylethylamine, 8 eqv. to resin). The Fmoc protecting group was removed with 20% piperidine in DMF. Peptides

were acetylated at the N-terminus with a solution (20:40 eqv. to resin) of acetic anhydride/DIPEA in DMF for 10 minutes. Peptides were cleaved from the resin using the standard TFA cleavage cocktail (95% (v/v) TFA, 2.5% (v/v) triisopropylsilane (TIS) and 2.5% (v/v) H_2O). Crude peptide products were precipitated and washed with cold Et_2O, dissolved in solvent A with a minimal amount of solvent B and then purified by RP-HPLC and characterized by ESI-MS.

Boc-SPPS of the AIP Analogs Featuring Enlarged, Reduced or Constrained Macrocycles and the AgrD-I-thiolactone and AgrD-II-thiolactone peptides. AIP analogs used in this study are listed in Table 10. All AIP analogs and the AgrD-I-thiolactone and AgrD-II-thiolactone peptides were chemically synthesized using standard solid-phase approaches with 4-methylbenzhydrylamine-copoly(styrene-1% DVB) (MBHA resin) as a support.[63, 141] S-trityl mercaptopropionic acid was coupled to the MBHA resin to form a thioester linker before peptide elongation using standard Boc-SPPS with in situ neutralization/HBTU activation. The 3-thiopropionic acid linker on MBHA resin is labile to HF cleavage conditions, thereby releasing linear α-thioester peptides upon global deprotection with anhydrous HF. Following removal of HF, the crude peptide product was precipitated using cold ethyl ether, washed thoroughly with ethyl ether, and then dissolved in 50% HPLC solvent B for the AIPs and AIP analogs or 50% TFE for the AgrD(1-32)-thiolactone peptides.

After lyophilization, AIP linear α-thioester peptides were dissolved in 50% HPLC solvent B and cyclized in solution by the addition of 1 equivalent volume of 0.2 M phosphate buffer at pH 7 (proline substitution and deletion AIP analogs) or 7.2 (enlarged AIP analogs). For the constrained and deletion AIP analogs, the cyclization reaction

required ~4 hours and was monitored by analytical RP-HPLC. For the enlarged AIP analogs, the cyclization reaction was allowed to proceed overnight (~16 hours) and was monitored by analytical RP-HPLC. During the overnight cyclization reactions, the solution was brought up to 10 mM TCEP incrementally. After the AIP cyclization, the AIP and AIP analog peptides were purified by semi-preparative RP-HPLC and characterized by analytical RP-HPLC, mass spectrometry and NMR spectroscopy. The concentrations of stock solutions for AIPs and AIP analogs were calculated on the basis of amino acid analysis (New England Peptide, Gardner, MA), with the peptides dissolved in 50% DMSO. Frozen peptide stocks were kept in 50% DMSO after amino acid analysis and serially diluted into an assay buffer of 20% propylene glycol and 100 mM phosphate, pH 5.9, which was also used for assays with cells.

For cyclization of the D(1-32)-thiolactone peptides, the lyophilized crude α-thioester was dissolved in a solution of 60% acetonitrile and 40% water, with 50 mM HEPES (pH 7) and 2.5 mM TCEP. During the overnight cyclization reactions, the solution was brought up to 10 mM TCEP incrementally. The reaction mixture was injected directly into the HPLC and purified on a protein C4 semi-preparative column (Vydac, Deerfield, IL) using a gradient of 50-90% solvent B over 30 minutes. Peaks were collected in fractions; fractions were analyzed by C4 analytical RP-HPLC and MS to assess purity. All pure fractions were combined and lyophilized. The AgrD(1-32)-II-thiolactone and AgrD(1-32)-I-thiolactone frozen stocks were kept in 100% DMSO.

Data for Control Peptide. ESI-MS *m/z* calculated for $C_{42}H_{73}N_{15}O_{15}$ 1027.54, found 1028.5 ($[M + H]^+$).

Data for Fl-AH Peptide. ESI-MS *m/z* calculated for $C_{53}H_{61}N_9O_{17}$ 1095.42, found 1096.4 ($[M + H]^+$).

Data for AH Peptide. ESI-MS *m/z* calculated for $C_{34}H_{53}N_9O_{12}$ 779.38, found 780.4 ($[M + H]^+$).

Data for IG-AIP1. ESI-MS *m/z* calculated for $C_{52}H_{85}N_{15}O_{17}$ 1191.62, found 1192.6 ($[M + H]^+$).

Data for IG-AIP3. ESI-MS *m/z* calculated for $C_{57}H_{87}N_{17}O_{17}$ 1281.65, found 1282.6 ($[M + H]^+$).

Data for Hcy AIP-I. ^{1}H NMR (500 MHz, DMSO-d6) δ 8.74 (d, 1H J = 7.63 Hz), δ 8.52 (d, 1H, J = 7.86), δ 8.20 (d, 1H J = 8.26 Hz), δ 8.13 (d, 1H, J = 8.04 Hz), δ 8.01 (m, 3H), δ 7.92 (d, 1H, J = 7.91), δ 7.29 (t, 2H, J = 7.39 Hz), δ 7.22 (m, 3H), δ 7.06 (d, 2H, J = 8.11 Hz), δ 6.69 (d, 2H, J = 7.88 Hz), δ 5.21 (m 1H), δ 4.87 (d, 1H J = 4.22), δ 4.56 (m, 2H), δ 4.34 (m, 2H), δ 4.23 (dd, 1H), δ 4.09 (m, 1H), δ 4.02 (m, 1H), δ 3.75 (t, 1H, J = 8.025 Hz), δ 3.67 (m, 2H), δ 3.60 (m 2H), δ 3.48 (m, 1H), δ 3.07 (m, 2H), δ 3.02 (m, 2H), δ 2.95 (m, 1H), δ 2.79 (m, 2H), δ 2.67 (m, 2H), δ 2.06 (s, 3H), δ 1.99 (m, 3H), δ 1.77 (m, 1H), δ 1.64 (m, 1H), δ 1.56 (m, 1H), δ 1.24 (d, 3H), δ 1.06 (d, 2H, J = 6.15 Hz), δ 0.88 (m, 2H), δ 0.80 (d, 2H, J = 6.69 Hz), δ 0.77 (t, 3H, J = 7.225 Hz); ESI-MS *m/z* calculated for $C_{44}H_{62}N_8O_{13}S_2$ 974.39, found 975.4 ($[M + H^+]$).

Data for Hcy AIP-II. ^{1}H NMR (500 MHz, DMSO-d6) δ 8.39 (d, 1H, J = 9.06 Hz), δ 8.32 (d, 1H, J = 7.36 Hz)), δ 8.19 (d, 1H, J = 8.92 Hz), δ 8.09 (d, 1H, J = 9.07 Hz), δ 8.01 (d, 1H, J = 8.21 Hz), δ 7.98 (d, 1H, J = 6.23 Hz), δ 7.86 (m, 3H), δ 7.80 (d, 1H, J =7.08 Hz), δ 7.31 (s, 1H), δ 7.26 (d, 1H, J = 7.93 Hz), δ 7.20 (m, 2H), δ 7.13 (m, 3H), δ 6.85 (s, 1H), δ 5.26 (m, 1H), δ 4.95 (m, 1H), δ 4.54 (m, 1H), δ 4.48 (m, 1H), δ 4.34 (m,

1H), δ 4.26 (m, 2H), δ 4.18 (m, 2H), δ 3.87 (m, 2H), δ 3.63 (m, 1H), δ 3.55 (m, 2H), δ 3.25 (m, 1H), δ 2.90 (m, 1H), δ 2.81 (m, 1H), δ 2.57 (m, 1H), δ 2.51 (d, 1H), δ 2.48, (d, 1H), δ 2.30 (m, 1H), δ 1.90 (m, 2H), δ 1.75 (m, 1H), δ 1.40 (m, 1H), δ 1.35 (m, 1H), δ 1.24 (m, 1H), δ 1.12 (d, 3H, J = 6.80 Hz), δ 0.80 (d, 3H, J = 6.79 Hz), δ 0.75 (t, 6H, J = 6.375 Hz), δ 0.68 (d, 3H, J = 6.52 Hz); ESI-MS *m/z* calculated for $C_{39}H_{60}N_{10}O_{12}S$ 892.41, found 893.4 ([M + H^+]).

Data for Hcy AIP-III. ^{1}H NMR (500 MHz, DMSO-d6) δ 8.55 (d, 1H, J = 7.22 Hz), δ 8.18 (t, 2H, J = 7.76 Hz), δ 8.11 (d, 1H, J = 7.44 Hz), δ 8.05 (m, 2H), δ 7.99 (s, 2H), δ 7.34 (s, 1H), δ 7.21 (t, 2H, J = 7.33 Hz), δ 7.13 (m, 3H), δ 6.91 (s, 1H), δ 5.12 (t, 1H, J = 4.95 Hz), δ 4.52 (m, 2H), δ 4.26 (m, 1H), δ 4.19 (m, 1H), δ 4.15 (m, 1H), δ 3.86 (m, 1H), δ 3.56 (s, 1H), δ 3.41 (d, 2H, J = 4.85 Hz), δ 3.07 (m, 1H), δ 2.93 (m, 1H), δ 2.80 (m, 1H), δ 2.58 (m, 2H), δ 2.50 (d, 1H), δ 2.39 (d, 1H, J = 5.17 Hz), δ 2.35 (m, 1H), δ 2.32 (m, 1H), δ 1.98 (m, 1H), δ 1.65 (m, 3H), δ 1.48 (m, 2H), δ 1.40 (m, 2H), δ 1.32 (m, 1H), δ 1.05 (m, 1H), δ 0.84 (m, 6H), δ 0.78 (m, 6H), δ 0.73 (d, 3H, J = 6.47 Hz); ESI-MS *m/z* calculated for $C_{39}H_{60}N_8O_{10}S$ 832.42, found 833.4 ([M + H^+]).

Data for hβ-Met AIP-I. ^{1}H NMR (500 MHz, DMSO-d6) δ 8.75 (d, 1H, J = 7.9 Hz), δ 8.57 (d, 1H, J = 7.05 Hz), δ 8.08 (d, 1H, J = 6.83 Hz), δ 7.99 (m, 4H), δ 7.88 (m, 2H), δ 7.30 (m, 2H), δ 7.24 (m, 3H), δ 7.07 (d, 2H, J = 8.21 Hz), δ 6.69 (d, 2H, J = 8.34), δ 5.17 (t, 1H, J = 5.18 Hz), δ 4.97 (d, 1H, J = 4.76 Hz), δ 4.55 (m, 1H), δ 4.45 (m, 1H), δ 4.37 (m, 1H), δ 4.30 (dd, 1H, J = 3.21 Hz), δ 4.24 (m, 1H), δ 4.09 (m, 2H), δ 4.02 (m, 1H), δ 3.68 (m, 3H), δ 3.61 (m, 2H), δ 3.18 (m, 1H), δ 3.10 (m 1H), δ 3.08 (m, 1H), δ 3.04 (m, 1H), δ 2.79 (m, 1H), δ 2.69 (m, 1H), δ 2.65 (m, 1H), δ 2.61 (m, 1H), δ 2.57 (m, 1H), δ 2.43 (m, 2H), δ 2.03 (s, 3H), δ 1.90 (m, 1H), δ 1.75 (m, 2H), δ 1.32 (m, 1H), δ 1.24 (s,

1H), δ 1.05 (d, 2H, J = 6.19 Hz), δ 0.96 (m, 1H), δ 0.85 (d, 3H, J = 6.79 Hz), δ 0.78 (t, 3H, J = 7.21 Hz); ESI-MS *m/z* calculated for $C_{44}H_{62}N_8O_{13}S_2$ 974.39, found 975.4 ([M + H^+]).

Data for hβ-Ile AIP-I. ^{1}H NMR (500 MHz, DMSO-d6) δ 9.27 (s, 1H), δ 8.68 (d, 1H, J = 7.71 Hz), δ 8.42 (d, 1H, J = 7.41 Hz), δ 8.37 (d, 1H, J = 7.42 Hz), δ 7.93 (m, 2H), δ 7.85 (d, 1H, J = 8.31 Hz), δ 7.62 (d, 1H, J = 7.12 Hz), δ 7.42 (d, 1H, J = 8.16 Hz), δ 7.20 (m, 2H), δ 7.12 (m, 3H), δ 7.00 (d, 2H, J = 8.3 Hz), δ 6.62 (d, 2H, J = 8.31 Hz), δ 5.07 (m, 1H), δ 4.76 (m, 1H), δ 4.47 (m, 2H), δ 4.34 (m, 2H), δ 4.26 (m, 1H), δ 4.17 (dd, 1H, J = 3.57), δ 3.97 (m, 2H), δ 3.61 (m, 1H), δ 3.55 (m, 1H), δ 3.45 (m, 3H), δ 3.12 (m, 2H), δ 3.00 (m, 2H), δ 2.87 (m, 2H), δ 2.80 (m, 2H), δ 2.72 (m, 2H), δ 2.37 (m, 2H) δ 2.22 (m, 1H), δ 1.96 (s, 3H), δ 1.89 (m, 1H), δ 1.75 (m, 1H), δ 1.69 (m, 1H), δ 1.18 (m, 1H), δ 0.98 (d, 2H, J = 6.38 Hz), δ 0.86 (m, 1H), δ 0.70 (m, 6H); ESI-MS *m/z* calculated for $C_{44}H_{62}N_8O_{13}S_2$ 974.39, found 975.4 ([M + H^+]).

Data for hβ-Phe AIP-I. ^{1}H NMR (500 MHz, DMSO-d6) δ 9.27 (s, 1H), δ 8.68 (d, 1H, J = 7.98 Hz), δ 8.18 (m, 1H), δ 8.03 (m, 2H), δ 7.92 (m, 3H), δ 7.69 (d, 1H, J = 9.9 Hz), δ 7.43 (d, 1H, J = 7.33 Hz), δ 7.25 (t, 2H, J = 7.43 Hz), δ 7.16 (d, 3H, J = 7.33 Hz), δ 7.00 (d, 2H, J = 8.19 Hz), δ 6.62 (d, 2H J = 8.19 Hz), δ 5.13 (m, 1H), δ 4.85 (m, 1H), δ 4.46 (m, 2H), δ 4.37 (m, 1H), δ 4.28 (m, 1H), δ 4.15 (m, 2H), δ 4.04 (m, 1H), δ 3.96 (m, 2H), δ 3.60 (m, 1H), δ 3.53 (m, 1H), δ 2.97 (m, 4H), δ 2.84 (m, 1H), δ 2.73 (m, 1H), δ 2.57 (m, 4H), δ 2.33 (m, 2H), δ 2.20 (m, 1H), δ 2.07 (m, 1H), δ 1.96 (s, 3H), δ 1.83 (m, 1H), δ 1.66 (m, 1H), δ 1.27 (m, 1H), δ 1.17 (s, 1H), δ 0.97 (d, 3H, J = 6.25 Hz), δ 0.73 (m, 6H); ESI-MS *m/z* calculated for $C_{44}H_{62}N_8O_{13}S_2$ 974.39, found 975.4 ([M + H^+]).

Data for hβ-Asp AIP-I. ^{1}H NMR (500 MHz, DMSO-d6) δ 9.26 (s, 1H), δ 8.67(d, 1H, J = 7.57 Hz), δ 8.58 (m, 1H), δ 7.91 (m, 5H), δ 7.66 (d, 1H, J = 9.14 Hz), δ 7.21 (m, 2H), δ 7.15 (d, 3H, J = 7.32 Hz), δ 7.00 (d, 2H, J = 8.36 Hz), δ 6.62 (d, 2H, J = 8.36 Hz), δ 5.18 (m, 1H), δ 4.81 (m, 1H), δ 4.48 (m, 2H), δ 4.38 (m, 1H), δ 4.24 (m, 1H), δ 4.18 (dd, 1H, J = 3.28 Hz), δ 4.12 (m, 1H), δ 4.02 (m, 1H), δ 3.95 (m, 1H), δ 3.89 (m, 1H), δ 3.81 (m, 1H), δ 3.62 (m, 2H), δ 3.53 (m, 2H), δ 3.00 (m, 1H), δ 2.95 (m, 2H) δ 2.74 (m, 2H), δ 2.57 (m, 2H), δ 2.39 (m, 1H), δ 2.30 (m, 1H), δ 2.23 (m, 2H), δ 2.16 (m, 1H), δ 2.01 (s, 1H), δ 1.99 (s, 3H), δ 1.90 (m, 2H), δ 1.30 (m, 1H), δ 1.17 (s, 1H), δ 0.97 (d, 3H, J = 6.24 Hz), δ 0.75 (m, 6H); ESI-MS *m/z* calculated for $C_{44}H_{62}N_8O_{13}S_2$ 974.39, found 975.4 ([M + H^+]).

Data for D5A β-Ala AIP-I. ^{1}H NMR (500 MHz, DMSO-d6) δ 9.29 (s, 1H), δ 8.84 (d, 1H, J = 7.62 Hz), δ 8.33 (d, 1H, J = 6.88 Hz), δ 8.27 (d, 1H, J = 8.18 Hz), δ 8.18 (d, 1H, J = 8.18 Hz), δ 7.97 (m, 2H), δ 7.83 (m, 2H), δ 7.22 (m, 2H), δ 7.17 (m, 3H), δ 6.96 (d, 2H, J = 8.74), δ 6.62 (d, 2H, J = 8.18 Hz), δ 4.94 (s, 1H), δ 4.76 (m, 1H), δ 4.39 (m, 1H), δ 4.31 (m, 1H), δ 4.24 (m, 2H), δ 4.12 (m, 2H), δ 4.04 (m, 1H), δ 3.97 (m, 1H), δ 3.09 (m, 1H), δ 2.97 (m, 1H), δ 2.91 (m, 1H), δ 2.80 (m, 1H), δ 2.71 (m, 4H), δ 2.39 (t, 2H, J = 7.91 Hz), δ 2.23 (m, 2H), δ 2.10 (m, 2H), δ 1.96 (s, 3H), δ 1.85 (m, 2H), δ 1.72 (m, 2H), δ 1.39 (m, 1H), δ 1.02 (d, 3H, J = 6.51 Hz), δ 0.79 (m, 7H); ESI-MS *m/z* calculated for $C_{42}H_{60}N_8O_{11}S_2$ 916.38, found 917.4 ([M + H^+]).

Data for D5A hβ-Ala AIP-I. ^{1}H NMR (500 MHz, DMSO-d6) δ 9.27(s, 1H), δ 8.68 (d, 1H, J = 7.85 Hz), δ 8.58 (d, 1H, J = 8.11), δ 7.99 (m, 1H), δ 7.92 (m, 4H), δ 7.62 (d, 1H, J = 9.36 Hz), δ 7.21 (m, 2H), δ 7.15 (d, 3H, J = 7.41 Hz), δ 6.99 (d, 2H, J = 8.54 Hz), δ 6.61 (d, 2H J = 8.39), δ 5.18 (s, 1H), δ 4.83 (s, 1H), δ 4.48 (m, 2H), δ 4.26 (m, 1H), δ

4.18 (dd, 2H, J = 3.08 Hz), δ 4.02 (m, 1H), δ 3.95 (m, 1H), δ 3.89 (m, 1H), δ 3.82 (m, 1H), δ 3.61 (m, 1H), δ 3.54 (m, 1H), δ 3.02 (m, 1H), δ 2.95 (m, 2H), δ 2.74, (m, 2H), δ 2.57 (m, 1H), δ 2.39 (m, 1H), δ 2.32 (m, 1H), δ 2.30 (m, 1H), δ 2.03 (m, 1H), δ 1.99 (s, 3H), δ 1.92 (m, 3H), δ 1.31 (m, 1H), δ 1.17 (s, 2H), δ 0.97 (d, 3H, J = 6.54 Hz), δ 0.91 (d, 3H, J = 6.66 Hz), δ 0.79 (d, 1H), δ 0.75 (m, 6H); ESI-MS *m/z* calculated for $C_{43}H_{62}N_8O_{11}S_2$ 930.4, found 931.2 ([M + H^+]).

Data for F6P AIP-I. ^{1}H NMR (500 MHz, DMSO-d6) δ 9.50 (s, 1H), δ 9.33 (d, 1H, J = 6.58 Hz), δ 8.72 (d, 1H, J = 7.95 Hz), δ 8.34 (d, 1H, J = 7.72 Hz), δ 8.02 (m, 2H), δ 7.93 (d, 1H, J = 8.62 Hz), δ 7.49 (d, 1H, J = 6.35 Hz), δ 7.05 (d, 2H, J = 7.53 Hz), δ 6.68 (d, 2H, J = 8.67 Hz), δ 4.74 (m, 1H), δ 4.54 (m, 2H), δ 4.33 (m, 1H), δ 4.24 (m, 1H), δ 4.14 (m, 1H), δ 3.04 (m, 2H), δ 2.87 (m, 1H), δ 2.82 (m, 1H), δ 2.39 (m, 3H), δ 2.13 (m, 1H), δ 2.04 (m, 2H), δ 1.98 (s, 3H), δ 1.92 (m, 2H), δ 1.71 (m, 1H), δ 1.30 (m, 1H), δ 1.22 (m, 1H), δ 1.05 (d, 3H, J = 6.36 Hz), δ 0.95 (m, 1H), δ 0.80 (m, 7H); ESI-MS *m/z* calculated for $C_{39}H_{58}N_8O_{13}S_2$ 910.36, found 911.4 ([M + H^+]).

Data for I7P AIP-I. ^{1}H NMR (500 MHz, DMSO-d6) δ 9.28 (s, 1H), δ 8.70 (m, 3H), δ 8.43 (d, 1H, J = 7.72 Hz), δ 7.91 (m, 4H), δ 7.28 (t, 2H, J = 7.21 Hz), δ 7.23 (t, 1H, J = 7.31 Hz), δ 7.14 (d, 2H, J = 7.1 Hz), δ 7.00 (d, 2H, J = 7.93 Hz), δ 6.62 (d, 2H, J = 8.36 Hz), δ 5.15 (m, 1H), δ 4.93 (d, 1H, J = 4.81), δ 4.59 (m, 1H), δ 4.47 (m, 2H), δ 4.36 (m, 1H), δ 4.20 (dd, 1H, J = 2.79 Hz), δ 4.10 (m, 1H), δ 4.03 (m, 1H), δ 3.95 (m, 1H), δ 3.58 (m, 2H), δ 3.16 (m, 1H), δ 3.11 (m, 1H), δ 2.98 (m, 2H), δ 2.76 (m, 3H), δ 2.37 (m, 1H), δ 2.23 (m, 1H), δ 2.00 (m, 2H), δ 1.94 (s, 3H), δ 1.78 (m, 1H), δ 1.54 (m, 1H), δ 1.25 (m, 1H), δ 1.17 (s, 1H), δ 0.97 (d, 3H, J = 6.52 Hz), δ 0.84 (m, 1H); ESI-MS *m/z* calculated for $C_{42}H_{56}N_8O_{13}S_2$ 944.34, found 945.3 ([M + H^+]).

Data for ΔF6 AIP-I. ^{1}H NMR (500 MHz, DMSO-d6) δ 9.37 (s, 1H), δ 8.73 (d, 1H, J = 7.14 Hz), δ 8.38 (d, 1H, J = 9.22 Hz), δ 8.31 (d, 1H, J = 9.22 Hz), δ 8.19 (d, 1H, J = 8.53 Hz), δ 7.95 (d, 1H, J = 8.76 Hz), δ 7.55 (d, 1H, J = 8.53 Hz), δ 7.06 (d, 2H, J = 8.53 Hz), δ 6.69 (d, 2H, J = 8.53 Hz), δ 4.56 (m, 2H), δ 4.45 (m, 1H), δ 4.36 (m, 1H), δ 4.22 (m, 2H), δ 4.10 (m, 1H), δ 3.94 (m, 2H), δ 3.21 (m, 1H), δ 3.02 (m, 2H), δ 2.75 (m, 4H), δ 2.59 (m, 2H), δ 2.41 (m, 3H), δ 2.07 (m, 1H), δ 2.03 (s, 3H), δ 1.88 (m, 1H), δ 1.73 (m, 1H), δ 1.45 (m, 1H), δ 1.24 (s, 1H), δ 1.08 (m, 1H), δ 1.04 (d, 3H, J = 6.46 Hz), δ 0.83 (m, 7H); ESI-MS *m/z* calculated for $C_{34}H_{51}N_7O_{12}S_2$ 813.3, found 814.3 ([M + H^+]).

Data for ΔI7 AIP-I. ^{1}H NMR (500 MHz, DMSO-d6) δ 9.27 (s, 1H), δ 8.68 (d, 1H, J = 7.82 Hz), δ 8.41 (d, 1H, J = 8.49 Hz), δ 8.34 (d, 1H, J = 9.84 Hz), δ 8.12 (d, 1H, J = 8.27 Hz), δ 7.92 (s, 1H), δ 7.88 (d, 1H), δ 7.59 (d, 1H, J = 8.26 Hz), δ 7.21 (m, 2H), δ 7.14 (m, 4H), δ 6.99 (d, 2H, J = 8.49 Hz), δ 6.62 (d, 2H, J = 8.50 Hz), δ 5.21 (m, 1H), δ 4.87 (d, 1H, J = 4.92 Hz), δ 4.50 (m, 2H), δ 4.31 (m, 4H), δ 4.16 (dd, 1H, J = 3.25 Hz), δ 4.03 (m, 1H), δ 3.94 (m, 1H), δ 3.62 (m, 1H), δ 3.52 (m, 1H), δ 3.13 (m, 1H), δ 2.95 (m, 1H), δ 2.88 (d, 2H, J = 7.61 Hz), δ 2.73 (m, 3H), δ 2.59 (m, 2H), δ 2.26 (m, 1H), δ 2.19 (m, 1H), δ 1.98 (m, 1H), δ 1.94 (s, 3H), δ 1.80 (m, 1H), δ 0.96 (d, 3H, J = 6.09 Hz); ESI-MS *m/z* calculated for $C_{37}H_{49}N_7O_{12}S_2$ 847.29, found 848.3 ([M + H^+]).

Data for AIP-I. ESI-MS *m/z* calculated for $C_{43}H_{60}N_8O_{13}S_2$ 960.4, found 961.4 ([M + H^+]). (See *Appendix* for 2-D NMR data as well.)

Data for Ac-AIP-I. ESI-MS *m/z* calculated for $C_{45}H_{62}N_8O_{14}S_2$ 1002.4, found 1003.4 ([M + H^+]).

Data for AIP-II. ESI-MS *m/z* calculated for $C_{38}H_{58}N_{10}O_{12}S$ 878.4, found 879.4 ([M + H^+]).

Data for Ac-AIP-II. ESI-MS *m/z* calculated for $C_{40}H_{60}N_{10}O_{13}S$ 920.4, found 921.4 ([M + H^+]).

Data for AgrD(1-32)-I-thiolactone. ESI-MS *m/z* calculated for $C_{170}H_{253}N_{37}O_{45}S_3$ 3631.24, found 3630.8 ([M + H^+]).

Data for AgrD(1-32)-II-thiolactone. ESI-MS *m/z* calculated for $C_{159}H_{251}N_{37}O_{40}S_3$ 3417.14, found 3417.09 ([M + H^+]).

NMR Spectroscopy. Lyophilized AIP analogs were dissolved in 100% DMSO-d6 (Cambridge Isotope Laboratories). ^{1}H NMR spectra were recorded on a Bruker 500 Avance-III equipped with a Cryo-QNP probe (Bruker BioSpin, Billerica, MA). ^{1}H NMR chemical shifts are reported in parts per million (ppm) and referenced relative to the residual solvent proton signal for DMSO-d6 at 2.50 ppm. One hundred and twenty-eight scans were recorded for each AIP analog ^{1}H NMR experiment. ^{1}H NMR analysis yielded complete assignments for all synthetic peptides. Two-dimensional TOCSY (70 ms mixing time) and NOESY experiments (500 ms mixing time) for certain AIP-I analogs were performed on an Avance III spectrometer operating at a ^{1}H Larmor frequency of 800 MHz and equipped with a TCI cryoprobe (Bruker BioSpin, Billerca, MA). Spectra were acquired at 25°C, with acquisition times of 393 ms (8192 points) and 32 ms (512 points) in the direct and indirect dimensions, respectively. 16 scans per point (TOCSY) and 16 to 64 scans per point (NOESY) were acquired for different samples. Data were processed with the NMRPipe software[154] and visualized in Sparky.[155] Two-dimensional NMR experiments characterized several enlarged AIP-I analogs. See the Appendix for 2-D NMR data tables.

Appendix.

Schematic of Various Samples Added to β-lactamase Reporter Gene Assay Cells

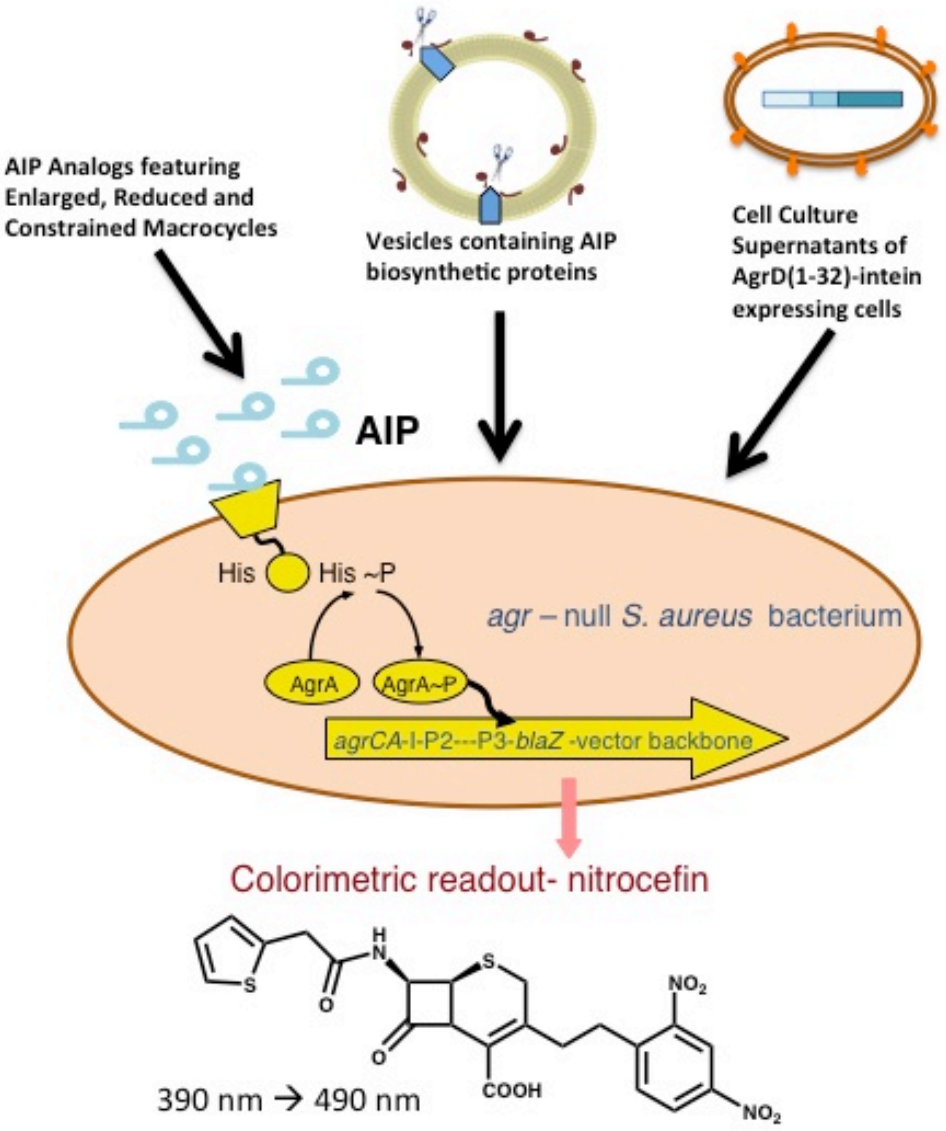

2D-NMR Chemical Shift Assignments for AIP-I, D5A AIP-I and the Enlarged AIP-I Analogs

AIP-I	HN	Hα	Hβ	Hγ	Other
Met	8.988	4.275	2.184	2.442	1.942, Hε
Ile	8.320	3.732	1.933	1.134, 1.107, 0.7594	0.7192, Hδ
Phe	7.848	4.477	2.978	--	7.194, HAr
Asp	8.217	4.415	2.483, 2.373	--	--
Cys	8.227	4.361	3.182, 2.915	--	--
Thr	7.953	4.244	4.061	1.038	--
Ser	8.739	4.555	3.689, 3.593	--	5.22, HO
Tyr	7.986	4.027	3.037, 2.796	--	7.075, HAr

D5A AIP-I	HN	Hα	Hβ	Hγ	Other
Met	9.074	4.243	2.188	--	1.95, Hε
Ile	8.257	3.771	--	1.163, 0.7755	--
Phe	7.806	4.493	2.963	--	7.271, 7.195, HAr
Ala	7.996	4.283	1.034	--	--
Cys	8.238	4.278	3.183, 2.889	--	--
Thr	7.966	4.258	4.089	1.046	--
Ser	8.726	4.556	3.683, 3.57	--	--
Tyr	7.983	4.022	3.027, 2.791	--	7.068, HAr

hβ-Asp AIP-I	HN	Hα	Hβ	Hγ	Other
Met	8.645	4.31	2.124	2.575	1.969, Hε
Ile	--	3.883	--	1.379, 1.015, 0.8119	--
Phe	7.963	4.562	3.021, 2.832	--	7.225, HAr
hβ-Asp	7.716	2.479	4.455*	2.306, 2.231	--
Cys	7.999	3.971	3.084, 2.656	--	--
Thr	7.951	4.251	4.096	1.045	--
Ser	8.73	4.551	3.692, 3.612	--	5.238, HO
Tyr	7.979	4.025	3.028, 2.795	--	7.07, HAr

D5A hβ-Ala AIP-I	HN	Hα	Hβ	Hγ	Other
Met	8.648	4.328	2.116	2.584	1.986, Hε
Ile	8.071	3.891	--	1.387, 0.8115	--
Phe	7.991	4.559	--	--	7.219, HAr
hβ-Ala	7.679	2.396, 2.086	4.24*	0.9817	--
Cys	7.973	3.978	3.089, 2.643	--	--
Thr	7.948	4.253	4.098	1.044	--
Ser	8.733	4.548	3.687, 3.611	--	5.234, HO
Tyr	7.983	4.026	3.029, 2.795	--	7.069, HAr

hβ-Phe AIP-I	HN	Hα	Hβ	Hγ	Other
Met	8.241	4.354	2.146	2.41	1.901, Hε
Ile	7.743	4.215	1.734	1.342, 1.068, 0.7927	--
hβ-Phe	7.482	2.272	4.116*	2.915, 2.631	7.31, 7.233, HAr
Asp	8.103	4.528	2.543, 2.507	--	--
Cys	8.086	4.451	3.087, 3.029	--	--
Ser	8.731	4.544	3.679, 3.598	--	5.183, HO
Thr	7.934	4.232	4.043	1.042	--
Tyr	7.977	4.023	3.034, 2.793	--	7.07, 6.693, HAr

hβ-Met AIP-I	HN	Hα	Hβ	Hγ	Other
hβ-Met	7.313	--	4.077*	2.438	2.688, Hδ 1.743, Hε
Ile	7.867	3.683	1.899	1.316, 0.956, 0.8415	0.7772, Hδ
Phe	8.064	4.443	3.308, 3.147	--	7.294, 7.238, HAr
Asp	7.878	4.25	3.19, 3.083	--	--
Cys	8.557	4.367	2.582, 2.417	--	--
Thr	7.96	4.294	4.096	1.046	--
Ser	8.729	4.546	3.669, 3.613	--	5.174, HO
Tyr	7.991	4.016	3.029, 2.797	--	7.065, 6.689, HAr

Hcy AIP-I	HN	Hα	Hβ	Hγ	Other
Met	8.499	4.324	2.056	2.537, 2.446	1.958, Hε
Ile	8.105	3.745	1.972	1.212, 0.881	0.7823, Hδ
Phe	8.17	4.537	2.977	--	7.278, 7.207, HAr
Asp	8.002	4.333	2.482	--	--
Hcy	7.919	4.317	2.939, 2.673	2.018, 1.764	--
Thr	7.967	4.209	4.09	1.047	--
Ser	8.701	4.54	3.661 3.608	--	5.252, HO
Tyr	8.001	4.008	3.018, 2.798	--	7.052, 6.682, HAr

References

1. Gordon, R.J. and F.D. Lowy, *Pathogenesis of methicillin-resistant Staphylococcus aureus infection*. Clin Infect Dis, 2008. **46 Suppl 5**: p. S350-9.

2. Lowy, F.D., *Staphylococcus aureus Infections*. The New England Journal of Medicine, 1998. **339**(8): p. 520-532.

3. Chambers, H.F. and F.R. Deleo, *Waves of resistance: Staphylococcus aureus in the antibiotic era*. Nat Rev Microbiol, 2009. **7**(9): p. 629-41.

4. Wisplinghoff, H., et al., *Nosocomial bloodstream infections in US hospitals: analysis of 24,179 cases from a prospective nationwide surveillance study*. Clin Infect Dis, 2004. **39**(3): p. 309-17.

5. Thompson, D.S. and R. Workman, *Hospital-wide infection control practice and Meticillin-resistant Staphylococcus aureus (MRSA) in the intensive care unit (ICU): an observational study*. JRSM Open, 2014. **5**(10): p. 2054270414547145.

6. Klevens, R.M., et al., *Invasive methicillin-resistant Staphylococcus aureus infections in the United States*. JAMA, 2007. **298**(15): p. 1763-71.

7. Pappano, D.A., *MRSA Infections in 2009*. Pediatric Emergency Medicine Reports, 2009(July): p. 1-21.

8. Kirby, W.M., *Extraction of a Highly Potent Penicillin Inactivator from Penicillin Resistant Staphylococci*. Science, 1944. **99**(2579): p. 452-3.

9. Novick, R.P., *Staphylococcal penicillinase and the new penicillins*. Biochem J, 1962. **83**: p. 229-35.

10. Grundmann, H., et al., *Emergence and resurgence of meticillin-resistant Staphylococcus aureus as a public-health threat*. Lancet, 2006. **368**(9538): p. 874-85.

11. Jancin, B., *Majority of MRSA is now community acquired*. Pediatric News, 2010. **44**(6).

12. Deurenberg, R.H. and E.E. Stobberingh, *The evolution of Staphylococcus aureus*. Infect Genet Evol, 2008. **8**(6): p. 747-63.

13. Deurenberg, R.H. and E.E. Stobberingh, *The molecular evolution of hospital- and community-associated methicillin-resistant Staphylococcus aureus*. Curr Mol Med, 2009. **9**(2): p. 100-15.

14. Smith, T.L., et al., *Emergence of vancomycin resistance in Staphylococcus aureus. Glycopeptide-Intermediate Staphylococcus aureus Working Group*. N Engl J Med, 1999. **340**(7): p. 493-501.

15. Sieradzki, K., et al., *The development of vancomycin resistance in a patient with methicillin-resistant Staphylococcus aureus infection*. N Engl J Med, 1999. **340**(7): p. 517-23.

16. Holmes, N.E., P.D. Johnson, and B.P. Howden, *Relationship between vancomycin-resistant Staphylococcus aureus, vancomycin-intermediate S. aureus, high vancomycin MIC, and outcome in serious S. aureus infections*. J Clin Microbiol, 2012. **50**(8): p. 2548-52.

17. Gardete, S. and A. Tomasz, *Mechanisms of vancomycin resistance in Staphylococcus aureus*. J Clin Invest, 2014. **124**(7): p. 2836-40.

18. Fisher, J.F., S.O. Meroueh, and S. Mobashery, *Bacterial resistance to beta-lactam antibiotics: compelling opportunism, compelling opportunity*. Chem Rev, 2005. **105**(2): p. 395-424.

19. Xie, J., et al., *A redesigned vancomycin engineered for dual D-Ala-D-ala And D-Ala-D-Lac binding exhibits potent antimicrobial activity against vancomycin-resistant bacteria*. J Am Chem Soc, 2011. **133**(35): p. 13946-9.

20. Fuqua, C., S.C. Winans, and E.P. Greenberg, *Census and consensus in bacterial ecosystems: the LuxR-LuxI family of quorum-sensing transcriptional regulators*. Annu Rev Microbiol, 1996. **50**: p. 727-51.

21. Novick, R.P. and E. Geisinger, *Quorum Sensing in Staphylococci*. Annu Rev Genet, 2008. **42**: p. 541-64.

22. Taga, M.E. and B.L. Bassler, *Chemical communication among bacteria*. Proc Natl Acad Sci U S A, 2003. **100 Suppl 2**: p. 14549-54.

23. George, E.A. and T.W. Muir, *Molecular mechanisms of agr quorum sensing in virulent staphylococci*. Chembiochem, 2007. **8**(8): p. 847-55.

24. Engebrecht, J., K. Nealson, and M. Silverman, *Bacterial bioluminescence: isolation and genetic analysis of functions from Vibrio fischeri*. Cell, 1983. **32**(3): p. 773-81.

25. Novick, R.P., et al., *The agr P2 operon: an autocatalytic sensory transduction system in Staphylococcus aureus*. Mol Gen Genet, 1995. **248**(4): p. 446-58.

26. Mascher, T., J.D. Helmann, and G. Unden, *Stimulus perception in bacterial signal-transducing histidine kinases*. Microbiol Mol Biol Rev, 2006. **70**(4): p. 910-38.

27. Dutta, R., L. Qin, and M. Inouye, *Histidine kinases: diversity of domain organization*. Mol Microbiol, 1999. **34**(4): p. 633-40.

28. Casino, P., V. Rubio, and A. Marina, *The mechanism of signal transduction by two-component systems*. Curr Opin Struct Biol, 2010. **20**(6): p. 763-71.

29. Capra, E.J. and M.T. Laub, *Evolution of Two-Component Signal Transduction Systems*. Annu Rev Microbiol, 2012. **66**: p. 325-347.

30. Recsei, P., et al., *Regulation of exoprotein gene expression in Staphylococcus aureus by agar*. Mol Gen Genet, 1986. **202**(1): p. 58-61.

31. Ji, G., R.C. Beavis, and R.P. Novick, *Cell density control of staphylococcal virulence mediated by an octapeptide pheromone*. Proc Natl Acad Sci U S A, 1995. **92**(26): p. 12055-9.

32. Honeyman, A., H. Friedman, and M. Bendinelli, *Staphylococcus aureus infection and disease*. 2001, New York: Kluwer Academic/Plenum Publishers.

33. Dufour, P., et al., *High genetic variability of the agr locus in Staphylococcus species*. J Bacteriol, 2002. **184**(4): p. 1180-6.

34. Wuster, A. and M.M. Babu, *Conservation and evolutionary dynamics of the agr cell-to-cell communication system across firmicutes*. J Bacteriol, 2008. **190**(2): p. 743-6.

35. Nishiguchi, K., et al., *Structure-activity relationship of gelatinase biosynthesis-activating pheromone of Enterococcus faecalis*. J Bacteriol, 2009. **191**(2): p. 641-50.

36. Riedel, C.U., et al., *AgrD-dependent quorum sensing affects biofilm formation, invasion, virulence and global gene expression profiles in Listeria monocytogenes*. Mol Microbiol, 2009. **71**(5): p. 1177-89.

37. Ohtani, K., et al., *Virulence gene regulation by the agr system in Clostridium perfringens*. J Bacteriol, 2009. **191**(12): p. 3919-27.

38. Cooksley, C.M., et al., *Regulation of neurotoxin production and sporulation by a Putative agrBD signaling system in proteolytic Clostridium botulinum*. Appl Environ Microbiol, 2010. **76**(13): p. 4448-60.

39. Bronner, S., H. Monteil, and G. Prevost, *Regulation of virulence determinants in Staphylococcus aureus: complexity and applications*. FEMS Microbiol Rev, 2004. **28**(2): p. 183-200.

40. Novick, R.P., *Autoinduction and signal transduction in the regulation of staphylococcal virulence*. Mol Microbiol, 2003. **48**(6): p. 1429-49.

41. Pragman, A.A. and P.M. Schlievert, *Virulence regulation in Staphylococcus aureus: the need for in vivo analysis of virulence factor regulation*. FEMS Immunol Med Microbiol, 2004. **42**(2): p. 147-54.

42. Cheung, A.L., et al., *Regulation of virulence determinants in vitro and in vivo in Staphylococcus aureus*. FEMS Immunol Med Microbiol, 2004. **40**(1): p. 1-9.

43. Cheung, A.L., et al., *Diminished virulence of a sar-/agr- mutant of Staphylococcus aureus in the rabbit model of endocarditis*. J Clin Invest, 1994. **94**(5): p. 1815-22.

44. Giese, M.J., et al., *A comparison of the early inflammatory effects of an agr-/sar- versus a wild type strain of Staphylococcus aureus in a rat model of endophthalmitis*. Curr Eye Res, 1999. **18**(3): p. 177-85.

45. Mayville, P., et al., *Structure-activity analysis of synthetic autoinducing thiolactone peptides from Staphylococcus aureus responsible for virulence*. Proc Natl Acad Sci U S A, 1999. **96**(4): p. 1218-23.

46. Blevins, J.S., et al., *Role of sarA in the pathogenesis of Staphylococcus aureus musculoskeletal infection*. Infect Immun, 2003. **71**(1): p. 516-23.

47. Reyes, D., et al., *Coordinated regulation by AgrA, SarA, and SarR to control agr expression in Staphylococcus aureus*. J Bacteriol, 2011. **193**(21): p. 6020-31.

48. Luong, T.T., et al., *Transcription Profiling of the mgrA Regulon in Staphylococcus aureus*. J Bacteriol, 2006. **188**(5): p. 1899-910.

49. Giraudo, A.T., et al., *Characterization of a Tn551-mutant of Staphylococcus aureus defective in the production of several exoproteins*. Can J Microbiol, 1994. **40**(8): p. 677-81.

50. Novick, R.P. and D. Jiang, *The staphylococcal saeRS system coordinates environmental signals with agr quorum sensing*. Microbiology, 2003. **149**(Pt 10): p. 2709-17.

51. Pragman, A.A., et al., *Characterization of virulence factor regulation by SrrAB, a two-component system in Staphylococcus aureus*. J Bacteriol, 2004. **186**(8): p. 2430-8.

52. Said-Salim, B., et al., *Global regulation of Staphylococcus aureus genes by Rot*. J Bacteriol, 2003. **185**(2): p. 610-9.

53. Geisinger, E., et al., *Inhibition of rot translation by RNAIII, a key feature of agr function*. Mol Microbiol, 2006. **61**(4): p. 1038-48.

54. McNamara, P.J., et al., *Identification, cloning, and initial characterization of rot, a locus encoding a regulator of virulence factor expression in Staphylococcus aureus*. J Bacteriol, 2000. **182**(11): p. 3197-203.

55. Thoendel, M., et al., *Peptide signaling in the staphylococci*. Chem Rev, 2011. **111**(1): p. 117-51.

56. Zhang, L., et al., *Transmembrane topology of AgrB, the protein involved in the post-translational modification of AgrD in Staphylococcus aureus*. J Biol Chem, 2002. **277**(38): p. 34736-42.

57. Thoendel, M. and A.R. Horswill, *Identification of Staphylococcus aureus AgrD residues required for autoinducing peptide biosynthesis*. J Biol Chem, 2009. **284**(33): p. 21828-38.

58. Kavanaugh, J.S., M. Thoendel, and A.R. Horswill, *A role for type I signal peptidase in Staphylococcus aureus quorum sensing*. Mol Microbiol, 2007. **65**(3): p. 780-98.

59. Wright, J.S., 3rd, et al., *Hydrophobic interactions drive ligand-receptor recognition for activation and inhibition of staphylococcal quorum sensing*. Proc Natl Acad Sci U S A, 2004. **101**(46): p. 16168-73.

60. Novick, R.P., et al., *Synthesis of staphylococcal virulence factors is controlled by a regulatory RNA molecule*. EMBO J, 1993. **12**(10): p. 3967-75.

61. Ji, G., R. Beavis, and R.P. Novick, *Bacterial interference caused by autoinducing peptide variants*. Science, 1997. **276**(5321): p. 2027-30.

62. Lyon, G.J., et al., *Rational design of a global inhibitor of the virulence response in Staphylococcus aureus, based in part on localization of the site of inhibition to the receptor-histidine kinase, AgrC*. Proc Natl Acad Sci U S A, 2000. **97**(24): p. 13330-5.

63. Lyon, G.J., et al., *Key determinants of receptor activation in the agr autoinducing peptides of Staphylococcus aureus*. Biochemistry, 2002. **41**(31): p. 10095-104.

64. Zhang, L., J. Lin, and G. Ji, *Membrane anchoring of the AgrD N-terminal amphipathic region is required for its processing to produce a quorum-sensing pheromone in Staphylococcus aureus*. J Biol Chem, 2004. **279**(19): p. 19448-56.

65. Roosmalen, M.L.v., et al., *Type I signal peptidases of Gram-positive bacteria*. Biochim Biophys Acta, 2004. **1694**: p. 279-297.

66. Schwartz, K., et al., *The AgrD N-terminal leader peptide of Staphylococcus aureus has cytolytic and amyloidogenic properties*. Infect Immun, 2014. **82**(9): p. 3837-44.

67. Gonzalez, D.J., et al., *N-Terminal AgrD Peptides from the Classical Staphylococcus aureus Agr System Have Cytotoxic and Proinflammatory Activities*. Chem Biol, 2014. **21**: p. 1-6.

68. Peschel, A. and M. Otto, *Phenol-soluble modulins and staphylococcal infection*. Nat Rev Microbiol, 2013. **11**(10): p. 667-73.

69. Petersen, T.N., et al., *SignalP 4.0: discriminating signal peptides from transmembrane regions*. Nat Methods, 2011. **8**(10): p. 785-6.

70. Qiu, R., et al., *Identification of the putative staphylococcal AgrB catalytic residues involving the proteolytic cleavage of AgrD to generate autoinducing peptide*. J Biol Chem, 2005. **280**(17): p. 16695-704.

71. Zhang, L. and G. Ji, *Identification of a staphylococcal AgrB segment(s) responsible for group-specific processing of AgrD by gene swapping*. J Bacteriol, 2004. **186**(20): p. 6706-13.

72. Thoendel, M. and A.R. Horswill, *Random mutagenesis and topology analysis of the autoinducing peptide biosynthesis proteins in Staphylococcus aureus*. Mol Microbiol, 2013. **87**(2): p. 318-37.

73. Cregg, K.M., I. Wilding, and M.T. Black, *Molecular cloning and expression of the spsB gene encoding an essential type I signal peptidase from Staphylococcus aureus*. J Bacteriol, 1996. **178**(19): p. 5712-8.

74. Paetzel, M., R.E. Dalbey, and N.C. Strynadka, *Crystal structure of a bacterial signal peptidase apoenzyme: implications for signal peptide binding and the Ser-Lys dyad mechanism*. J Biol Chem, 2002. **277**(11): p. 9512-9.

75. Saenz, H.L., et al., *Inducible expression and cellular location of AgrB, a protein involved in the maturation of the staphylococcal quorum-sensing pheromone*. Arch Microbiol, 2000. **174**(6): p. 452-5.

76. Paetzel, M., et al., *Signal peptidases*. Chem Rev, 2002. **102**(12): p. 4549-80.

77. Paetzel, M. and N.C. Strynadka, *Common protein architecture and binding sites in proteases utilizing a Ser/Lys dyad mechanism*. Protein Sci, 1999. **8**(11): p. 2533-6.

78. Paetzel, M., R.E. Dalbey, and N.C. Strynadka, *The structure and mechanism of bacterial type I signal peptidases. A novel antibiotic target*. Pharmacol Ther, 2000. **87**(1): p. 27-49.

79. Lyon, G.J., et al., *Reversible and specific extracellular antagonism of receptor-histidine kinase signaling*. J Biol Chem, 2002. **277**(8): p. 6247-53.

80. McDowell, P., et al., *Structure, activity and evolution of the group I thiolactone peptide quorum-sensing system of Stapylococcus aureus*. Mol Microbiol, 2001. **41**(2): p. 503-512.

81. Scott, R.J., et al., *Side-chain-to-tail thiolactone peptide inhibitors of the staphylococcal quorum-sensing system*. Bioorg Med Chem Lett, 2003. **13**(15): p. 2449-53.

82. Geisinger, E., et al., *Identification of ligand specificity determinants in AgrC, the Staphylococcus aureus quorum-sensing receptor*. J Biol Chem, 2008. **283**(14): p. 8930-8.

83. George, E.A., R.P. Novick, and T.W. Muir, *Cyclic peptide inhibitors of staphylococcal virulence prepared by Fmoc-based thiolactone peptide synthesis*. J Am Chem Soc, 2008. **130**(14): p. 4914-24.

84. Tal-Gan, Y., et al., *Highly potent inhibitors of quorum sensing in Staphylococcus aureus revealed through a systematic synthetic study of the group-III autoinducing peptide*. J Am Chem Soc, 2013. **135**(21): p. 7869-82.

85. Tal-Gan, Y., D.M. Stacy, and H.E. Blackwell, *N-Methyl and peptoid scans of an autoinducing peptide reveal new structural features required for inhibition and activation of AgrC quorum sensing receptors in Staphylococcus aureus*. Chem Commun (Camb), 2014. **50**(23): p. 3000-3.

86. Tal-Gan, Y., et al., *Structural characterization of native autoinducing peptides and abiotic analogues reveals key features essential for activation and inhibition of an AgrC quorum sensing receptor in Staphylococcus aureus*. J Am Chem Soc, 2013. **135**(49): p. 18436-44.

87. Geisinger, E., T.W. Muir, and R.P. Novick, *agr receptor mutants reveal distinct modes of inhibition by staphylococcal autoinducing peptides*. Proc Natl Acad Sci U S A, 2009. **106**(4): p. 1216-21.

88. Wang, B., et al., *Activation and inhibition of the receptor histidine kinase AgrC occurs through opposite helical transduction motions*. Mol Cell, 2014. **53**(6): p. 929-40.

89. Grebe, T.W. and J.B. Stock, *The histidine protein kinase superfamily*. Adv Microb Physiol, 1999. **41**: p. 139-227.

90. George-Cisar, E.A., et al., *Symmetric signalling within asymmetric dimers of the Staphylococcus aureus receptor histidine kinase AgrC*. Mol Microbiol, 2009. **74**(1): p. 44-57.

91. Wolanin, P.M., P.A. Thomason, and J.B. Stock, *Histidine protein kinases: key signal transducers outside the animal kingdom*. Genome Biol, 2002. **3**(10): p. REVIEWS3013.

92. Jones, D.T., *Improving the accuracy of transmembrane protein topology prediction using evolutionary information*. Bioinformatics, 2007. **23**(5): p. 538-44.

93. Bernsel, A., et al., *TOPCONS: consensus prediction of membrane protein topology*. Nucleic Acids Res, 2009. **37**(Web Server issue): p. W465-8.

94. Lina, G., et al., *Transmembrane topology and histidine protein kinase activity of AgrC, the agr signal receptor in Staphylococcus aureus*. Mol Microbiol, 1998. **28**(3): p. 655-62.

95. Wang, L., et al., *New insight into transmembrane topology of Staphylococcus aureus histidine kinase AgrC*. Biochim Biophys Acta, 2014. **1838**(3): p. 988-93.

96. Havarstein, L.S., et al., *Identification of the streptococcal competence-pheromone receptor*. Mol Microbiol, 1996. **21**(4): p. 863-9.

97. Johnsborg, O., D.B. Diep, and I.F. Nes, *Structural analysis of the peptide pheromone receptor PlnB, a histidine protein kinase from Lactobacillus plantarum*. J Bacteriol, 2003. **185**(23): p. 6913-20.

98. Koenig, R.L., et al., *Staphylococcus aureus AgrA binding to the RNAIII-agr regulatory region*. J Bacteriol, 2004. **186**(22): p. 7549-55.

99. Nikolskaya, A.N. and M.Y. Galperin, *A novel type of conserved DNA-binding domain in the transcriptional regulators of the AlgR/AgrA/LytR family*. Nucleic Acids Res, 2002. **30**(11): p. 2453-9.

100. Sidote, D.J., et al., *Structure of the Staphylococcus aureus AgrA LytTR domain bound to DNA reveals a beta fold with an unusual mode of binding*. Structure, 2008. **16**(5): p. 727-35.

101. Traber, K. and R. Novick, *A slipped-mispairing mutation in AgrA of laboratory strains and clinical isolates results in delayed activation of agr and failure to translate delta- and alpha-haemolysins*. Mol Microbiol, 2006. **59**(5): p. 1519-30.

102. Benito, Y., et al., *Probing the structure of RNAIII, the Staphylococcus aureus agr regulatory RNA, and identification of the RNA domain involved in repression of protein A expression*. RNA, 2000. **6**(5): p. 668-79.

103. Huntzinger, E., et al., *Staphylococcus aureus RNAIII and the endoribonuclease III coordinately regulate spa gene expression*. EMBO J, 2005. **24**(4): p. 824-35.

104. Janzon, L. and S. Arvidson, *The role of the delta-lysin gene (hld) in the regulation of virulence genes by the accessory gene regulator (agr) in Staphylococcus aureus*. EMBO J, 1990. **9**(5): p. 1391-9.

105. Verdon, J., et al., *delta-hemolysin, an update on a membrane-interacting peptide*. Peptides, 2009. **30**(4): p. 817-23.

106. Balaban, N. and R.P. Novick, *Translation of RNAIII, the Staphylococcus aureus agr regulatory RNA molecule, can be activated by a 3'-end deletion*. FEMS Microbiol Lett, 1995. **133**(1-2): p. 155-61.

107. Morfeldt, E., et al., *Activation of alpha-toxin translation in Staphylococcus aureus by the trans-encoded antisense RNA, RNAIII*. EMBO J, 1995. **14**(18): p. 4569-77.

108. Boisset, S., et al., *Staphylococcus aureus RNAIII coordinately represses the synthesis of virulence factors and the transcription regulator Rot by an antisense mechanism*. Genes Dev, 2007. **21**(11): p. 1353-66.

109. Chevalier, C., et al., *Staphylococcus aureus RNAIII binds to two distant regions of coa mRNA to arrest translation and promote mRNA degradation*. PLoS Pathog, 2010. **6**(3): p. e1000809.

110. Reed, S.B., et al., *Molecular characterization of a novel Staphylococcus aureus serine protease operon*. Infect Immun, 2001. **69**(3): p. 1521-7.

111. Shaw, L., et al., *The role and regulation of the extracellular proteases of Staphylococcus aureus*. Microbiology, 2004. **150**(Pt 1): p. 217-28.

112. Oscarsson, J., K. Tegmark-Wisell, and S. Arvidson, *Coordinated and differential control of aureolysin (aur) and serine protease (sspA) transcription in Staphylococcus aureus by sarA, rot and agr (RNAIII)*. Int J Med Microbiol, 2006. **296**(6): p. 365-80.

113. Daugherty, S. and M.G. Low, *Cloning, expression, and mutagenesis of phosphatidylinositol-specific phospholipase C from Staphylococcus aureus: a potential staphylococcal virulence factor*. Infect Immun, 1993. **61**(12): p. 5078-89.

114. Chamberlain, N.R. and B. Imanoel, *Genetic regulation of fatty acid modifying enzyme from Staphylococcus aureus*. J Med Microbiol, 1996. **44**(2): p. 125-9.

115. Janzon, L., S. Lofdahl, and S. Arvidson, *Identification and nucleotide sequence of the delta-lysin gene, hld, adjacent to the accessory gene regulator (agr) of Staphylococcus aureus*. Mol Gen Genet, 1989. **219**(3): p. 480-5.

116. Bronner, S., et al., *Variable expressions of Staphylococcus aureus bicomponent leucotoxins semiquantified by competitive reverse transcription-PCR*. Appl Environ Microbiol, 2000. **66**(9): p. 3931-8.

117. Gaskill, M.E. and S.A. Khan, *Regulation of the enterotoxin B gene in Staphylococcus aureus*. J Biol Chem, 1988. **263**(13): p. 6276-80.

118. Tseng, C.W. and G.C. Stewart, *Rot repression of enterotoxin B expression in Staphylococcus aureus*. J Bacteriol, 2005. **187**(15): p. 5301-9.

119. Regassa, L.B., J.L. Couch, and M.J. Betley, *Steady-state staphylococcal enterotoxin type C mRNA is affected by a product of the accessory gene regulator (agr) and by glucose*. Infect Immun, 1991. **59**(3): p. 955-62.

120. Bayles, K.W. and J.J. Iandolo, *Genetic and molecular analyses of the gene encoding staphylococcal enterotoxin D*. J Bacteriol, 1989. **171**(9): p. 4799-806.

121. O'Toole, P.W. and T.J. Foster, *Molecular cloning and expression of the epidermolytic toxin A gene of Staphylococcus aureus*. Microb Pathog, 1986. **1**(6): p. 583-94.

122. Sheehan, B.J., et al., *Osmotic and growth-phase dependent regulation of the eta gene of Staphylococcus aureus: a role for DNA supercoiling*. Mol Gen Genet, 1992. **232**(1): p. 49-57.

123. Queck, S.Y., et al., *RNAIII-independent target gene control by the agr quorum-sensing system: insight into the evolution of virulence regulation in Staphylococcus aureus*. Mol Cell, 2008. **32**(1): p. 150-8.

124. Geissmann, T., et al., *A search for small noncoding RNAs in Staphylococcus aureus reveals a conserved sequence motif for regulation*. Nucleic Acids Res, 2009. **37**(21): p. 7239-57.

125. Dassy, B., et al., *Involvement of the accessory gene regulator (agr) in expression of type 5 capsular polysaccharide by Staphylococcus aureus*. J Gen Microbiol, 1993. **139 Pt 6**: p. 1301-6.

126. Luong, T., et al., *Regulation of Staphylococcus aureus capsular polysaccharide expression by agr and sarA*. Infect Immun, 2002. **70**(2): p. 444-50.

127. Saravia-Otten, P., H.P. Muller, and S. Arvidson, *Transcription of Staphylococcus aureus fibronectin binding protein genes is negatively regulated by agr and an agr-independent mechanism*. J Bacteriol, 1997. **179**(17): p. 5259-63.

128. Lebeau, C., et al., *Coagulase expression in Staphylococcus aureus is positively and negatively modulated by an agr-dependent mechanism*. J Bacteriol, 1994. **176**(17): p. 5534-6.

129. Pantrangi, M., et al., *Staphylococcal superantigen-like genes, ssl5 and ssl8, are positively regulated by Sae and negatively by Agr in the Newman strain*. FEMS Microbiol Lett, 2010. **308**(2): p. 175-84.

130. Dunman, P.M., et al., *Transcription profiling-based identification of Staphylococcus aureus genes regulated by the agr and/or sarA loci*. J Bacteriol, 2001. **183**(24): p. 7341-53.

131. Villaruz, A.E., et al., *A point mutation in the agr locus rather than expression of the Panton-Valentine leukocidin caused previously reported phenotypes in Staphylococcus aureus pneumonia and gene regulation*. J Infect Dis, 2009. **200**(5): p. 724-34.

132. Ziebandt, A.K., et al., *The influence of agr and sigmaB in growth phase dependent regulation of virulence factors in Staphylococcus aureus*. Proteomics, 2004. **4**(10): p. 3034-47.

133. Tjalsma, H., et al., *Proteomics of protein secretion by Bacillus subtilis: separating the "secrets" of the secretome*. Microbiol Mol Biol Rev, 2004. **68**(2): p. 207-33.

134. Vila-Perello, M. and T.W. Muir, *Biological applications of protein splicing*. Cell, 2010. **143**(2): p. 191-200.

135. Shah, N.H. and T.W. Muir, *Inteins: Nature's Gift to Protein Chemists*. Chem Sci, 2014. **5**(1): p. 446-461.

136. Camarero, J.A., et al., *Peptide chemical ligation inside living cells: in vivo generation of a circular protein domain*. Bioorg Med Chem, 2001. **9**(9): p. 2479-84.

137. Kalkum, M., G.J. Lyon, and B.T. Chait, *Detection of secreted peptides by using hypothesis-driven multistage mass spectrometry*. Proc Natl Acad Sci U S A, 2003. **100**(5): p. 2795-800.

138. Shah, N.H., et al., *Ultrafast protein splicing is common among cyanobacterial split inteins: implications for protein engineering*. J Am Chem Soc, 2012. **134**(28): p. 11338-41.

139. Giriat, I. and T.W. Muir, *Protein semi-synthesis in living cells*. J Am Chem Soc, 2003. **125**(24): p. 7180-1.

140. Charpentier, E., et al., *Novel cassette-based shuttle vector system for gram-positive bacteria*. Appl Environ Microbiol, 2004. **70**(10): p. 6076-85.

141. Schnolzer, M., et al., *In situ neutralization in Boc-chemistry solid phase peptide synthesis. Rapid, high yield assembly of difficult sequences*. Int J Pept Protein Res, 1992. **40**(3-4): p. 180-93.

142. Kerns, E. and L. Di, *Drug-like Properties: Concepts, Structure Design and Methods*. 1st ed. 2008, USA: Academic Press.

143. Rao, S., et al., *Enzymatic investigation of the Staphylococcus aureus type I signal peptidase SpsB - implications for the search for novel antibiotics*. FEBS J, 2009. **276**(12): p. 3222-34.

144. Lloyd-Wiliams, P., F. Alberico, and E. Giralt, *Chemical Approaches to the Synthesis of Peptides and Proteins*. 1st Edition ed. 1997, New York: CRC Press.

145. Rigaud, J.L. and D. Levy, *Reconstitution of membrane proteins into liposomes*. Methods Enzymol, 2003. **372**: p. 65-86.

146. Murray, E.J., et al., *Targeting Staphylococcus aureus quorum sensing with nonpeptidic small molecule inhibitors*. J Med Chem, 2014. **57**(6): p. 2813-9.

147. Zhao, A. and T.W. Muir, *unpublished work*. 2015.

148. Novick, R.P., *Genetic systems in staphylococci*. Methods Enzymol, 1991. **204**: p. 587-636.

149. Grote, A., et al., *JCat: a novel tool to adapt codon usage of a target gene to its potential expression host*. Nucleic Acids Res, 2005. **33**(Web Server issue): p. W526-31.

150. Puigbo, P., et al., *OPTIMZER: A web server for optimizing the codon usage of DNA sequences*. Nucleic Acids Res, 2007. **35**: p. W126-W131.

151. Wright, J.S., 3rd, R. Jin, and R.P. Novick, *Transient interference with staphylococcal quorum sensing blocks abscess formation*. Proc Natl Acad Sci U S A, 2005. **102**(5): p. 1691-6.

152. Wang, B. and T.W. Muir, *unpublished work*. 2015.

153. Bryksin, A.V. and I. Matsumura, *Overlap extension PCR cloning: a simple and reliable way to create recombinant plasmids*. Biotechniques, 2010. **48**(6): p. 463-5.

154. Delaglio, F., et al., *NMRPipe: a multidimensional spectral processing system based on UNIX pipes*. J Biomol NMR, 1995. **6**(3): p. 277-93.

155. Goddard, T. and D.G. Kneller, *Sparky 3*. University of California, San Francisco.